

https://dspace.org/

An in vitro study investigating the effects of functional groups on the toxicity of gold nanoparticles

Tlotleng, Nonhlanhla

2017
https://hdl.handle.net/10539/24803

Downloaded from a DSpace repository. https://dspace.org/

AN *IN VITRO* STUDY INVESTIGATING THE EFFECTS OF FUNCTIONAL GROUPS ON THE TOXICITY OF GOLD NANOPARTICLES

Nonhlanhla Tlotleng

A thesis submitted to the faculty of Health Science, University of the Witwatersrand, Johannesburg, in fulfilment of the requirement for the degree of **Doctor of Philosophy**.

Johannesburg, 2017

Professor Lisa Claire du Toit

Department of Pharmacy and Pharmacology

Dr Robert Tshikhudo

Materials Science and Manufacturing: Light Metals

Council for Scientific and Industrial Research

DECLARATION

I, Nonhlanhla Tlotleng declare that this thesis is my own work. It is being submitted for the degree of Doctor of Philosophy in the University of the Witwatersrand, Johannesburg. It has not been submitted before for any degree or examination at this or any other university.

……..

…….day of …….

To my precious daughter

Usiphile Palesa Tlotleng

Publications arising from the study

- **Melissa A Vetten**, **Nonhlanhla Tlotleng**, **Delia Tanner Rascher**, **Amanda Skepu**, **Frankline K Keter**, **Kailen Boodhia**, **Leigh-Anne Koekemoer**, **Charlene Andraos**, **Robert Tshikhudo** and **Mary Gulumian.** Label-free *in vitro* toxicity and uptake assessment of citrate stabilized gold nanoparticles in three cell lines. *Particle and Fibre Toxicology,* 2013, 10: 50.

- **Nonhlanhla Tlotleng, Melissa A Vetten, Pam Sharp, Frankline Keter, Amanda Skepu Robert Tshikhudo and Mary Gulumian.** Cytotoxicity, intracellular localization and exocytosis of citrate capped and PEG coated gold nanoparticles in human hepatocytes and kidney cells. *Cell biology and Toxicology,* 2016, 32 (4): 305-21.

- **Mary Gulumian, Melissa A Vetten, Kailen Boodhia, and Nonhlanhla Tlotleng.** Toxicity assessment and intracellular uptake of gold nanoparticles: Effect of ligands, functional groups and cell type. *Toxicology Letters*, 2016, 259.S186. http://dx.doi.org/10.1016/j.toxlet.2016.07.444.

- **Nonhlanhla Tlotleng, Mangethe Zwane, Robert Tshikhudo and Lisa Claire du Toit**. Generation of hydroxyl radicals in the presence of hydrogen peroxide and gold nanoparticles: Effect of concentration, size and surface functional groups. **(*manuscript to be submitted to Journal of Nanoparticle Research*)**

- **Nonhlanhla Tlotleng, Robert Tshikhudo and Lisa Claire du Toit**. ICP-MS analysis of intracellular gold nanoparticles and toxicity in cultured human cells. **(*manuscript to be submitted to Cell biology and Toxicology*)**

Conference Presentations

- **Nonhlanhla Tlotleng**, Robert Tshikhudo and Mary Gulumian*. An in vitro study investigating the effects of functional groups on the toxicity of gold nanoparticles*. Gold nanoparticles symposium, MINTEK, South Africa, 28 August 2012 (**oral presentation**).

- **Nonhlanhla Tlotleng**, Mary Gulumian and Robert Tshikhudo. *In vitro* toxicity assessment of gold nanoparticles in human embryonic kidney cell line. The 6th International conference on nanotoxicology, Beijing China, 4- 7 September 2012 (**poster presentation**).

- **Nonhlanhla Tlotleng**, Robert Tshikhudo and Mary Gulumian*. Cellular uptake and toxicity assessment of citrate stabilized and monolayer protected gold nanoparticles in human embryonic kidney cell line.* The 4th Annual Gauteng's Nanoscience young researcher's symposium, University of the Witwatersrand, School of Chemistry, Johannesburg South Africa, 7 September 2012 (**oral presentation**).

- Mary Gulumian, Melissa Vetten, **Nonhlanhla Tlotleng** and Robert Tshikhudo. *Toxicity testing and intracellular uptake.* The 8th congress of toxicology in developing countries (8CTD), Bangkok, Thailand, 10- 13 September 2012 (**poster presentation**).

- **Nonhlanhla Tlotleng**, Robert Tshikhudo and Mary Gulumian. *In-vitro toxicity assessment of citrate stabilized and PEG functionalized gold nanoparticles in human embryonic kidney cell line.* The 46th Annual Congress of the SASBCP in association with the Dept. of Family Medicine (UP) and TOXSA, Pretoria, South Africa, 29 September – 2 October 2012 **(oral presentation).**

- Thingahangwi Madzivhandila, **Nonhlanhla Tlotleng**, Xolani Masoka, Sekobe Gopolang and Mary Gulumian. *The analysis of functional groups and quantification of*

individual ligands from the surface of multi-functionalized gold nanoparticle using Fourier transform infrared spectroscopy (FTIR). The 46th Annual Congress of the SASBCP in association with the Dept. of Family Medicine (UP) and TOXSA, Pretoria, South Africa, 29- 2 October 2012 **(poster presentation)**.

- **Nonhlanhla Tlotleng**, Robert Tshikhudo and Mary Gulumian. *Toxicity response and uptake of gold nanoparticles in human embryonic kidney cells.* The 2nd Consortium for advanced research training in Africa (CARTA) public health conference, University of the Witwatersrand, Johannesburg, South Africa, 27 November 2012 (**poster presentation**).

- **Nonhlanhla Tlotleng**, Robert Tshikhudo and Mary Gulumian*. Cytotoxicity and uptake of citrate stabilized gold nanoparticles in human cell lines.* The 12th International chemistry conference in Africa, Pretoria, South Africa, 5- 12 July 2013 **(oral presentation)**.

- Thingahangwi Madzivhandila, **Nonhlanhla Tlotleng**, Xolani Masoka, Sekobe Gopolang and Mary Gulumian. *The analysis of selected functional groups and identification of individual ligands attached to gold nanoparticles using Fourier transform infrared spectroscopy (FTIR)-ATR.* The 12th International chemistry conference in Africa, Pretoria, South Africa, 5- 12 July 2013 **(oral presentation)**.

- **Nonhlanhla Tlotleng**, Robert Tshikhudo and Mary Gulumian*. Effect of surface coating on the interaction and cytotoxicity of gold nanoparticles in human liver hepatocellular (HepG 2) and human embryonic kidney (HEK 293) cells.* The 5th cross faculty graduate symposium, University of the Witwatersrand, Johannesburg, South Africa, 1- 2 August 2013 **(oral presentation)**.

- Thingahangwi Madzivhandila, **Nonhlanhla Tlotleng**, Xolani Masoka, Sekobe Gopolang and Mary Gulumian. *Analysis of functional groups and quantification of*

individual ligands from the surface of multi-functionalized gold nanoparticles using Fourier Transform Infrared Spectroscopy. 6th International Symposium on Nanotechnology, Occupational and Environmental Health (NanOEH), Nagoya, Japan, 28- 31 October 2013, (**poster presentation**).

- **Nonhlanhla Tlotleng**, Robert Tshikhudo and Mary Gulumian*. A comparative transmission electron microscopy study on the uptake of gold nanoparticles in human kidney and liver cell lines.* The 5th Annual Gauteng's Nanoscience young researcher's symposium, CSIR NCNSM, Pretoria, South Africa, 8 November 2013 (**oral presentation**).

- **Nonhlanhla Tlotleng**, Robert Tshikhudo and Mary Gulumian. *Uptake and localization of gold nanoparticles in cultured cells assessed by transmission electron microscopy.* 51st Annual conference of the Microscopy Society of Southern Africa, Farm Inn, Pretoria, South Africa, 3- 6 December 2013 (**oral presentation**).

- **Nonhlanhla Tlotleng**, Robert Tshikhudo and Mary Gulumian. *Cytotoxicity induced by gold nanoparticles on cultured human cells*. 5th International Conference on Nanoscience and Nanotechnology, Vaal university of technology, Vanderbijlpark, South Africa, 30 March- 02 April 2014 (**oral presentation**).

- **Nonhlanhla Tlotleng**, Robert Tshikhudo and Mary Gulumian. Exocytosis of gold nanoparticles in cultured cells. 7th International symposium on Nanotechnology, Occupational and Environmental Health, Limpopo, South Africa, 18- 22 October 2015 (**poster presentation)**.

ABSTRACT

AN *IN VITRO* STUDY INVESTIGATING THE EFFECTS OF FUNCTIONAL GROUPS ON THE TOXICITY OF GOLD NANOPARTICLES

The thesis provides a comprehensive investigation on the interaction and toxicity effects of newly synthesized gold nanoparticles in human embryonic kidney (HEK 293) and human hepatocellular carcinoma (HepG2) cell lines. The citrate stabilized AuNPs with increasing diameter and polyethylene glycol modified AuNPs presenting various functional groups were synthesized. The synthesis of AuNPs was achieved using the citrate reduction and the Brust–Schiffrin methods. The AuNPs were further characterized in cell growth medium using TEM, UV-vis, Zetasizer and FTIR. Cellular uptake and sub-cellular localization of AuNPs was studied with dark field microscopy and field emission electron microscope fitted with an energy dispersive X-ray spectrometer. TEM was further used to show the exocytosis of the AuNPs following long term exposure. Cytotoxicity of AuNPs was assessed using real-time cell analyzer impedance technology to monitor cell viability and cell proliferation. Furthermore, the genotoxicity, cytokine induction and the effect of AuNPs on the generation of free radicals was investigated using chromosome aberration test; flow cytometer and electron spin resonance. TEM micrographs confirmed that AuNPs were taken up by the cells. The AuNPs were deposited in the cytoplasm and in endosomal and lysosomal vesicles of cells. Furthermore, TEM revealed that AuNPs are depleted from cells after 4 weeks of culture through excretion of the nanoparticles filled vesicles to the medium. AuNPs deposited in the cell cytoplasm are removed by diffusion through the plasma membrane. Quantification of intracellular AuNPs revealed a high uptake of citrate stabilized AuNPs in the two cell lines when compared to the PEG-coated AuNPs. The cytotoxicity profiles of the nanoparticles revealed a size and surface chemistry dependent effect on cells, with HEK 293 cells as the most sensitive cell type. AuNPs with the azide, nitriloacetic acid, carboxyl, biotin, hydroxyl, and the methoxy functional groups showed genotoxicity effects in HEK 293 cells. In addition, the carboxyl and the nitriloacetic acid functionalized AuNPs showed catalytic activity in free radical generation. In conclusion, the functional groups on AuNPs surface may induce adverse effects in cells through interaction with cellular components. The results will have implication in hazard identification of newly synthesized AuNPs and safety evaluation of AuNPs in future studies.

Acknowledgements

I send my special gratitude to my Heavenly Father, for the strength, faith, grace, and inspiration throughout this work. It wouldn't have been possible or done without him. Furthermore, I would like to thank the following people and institutes:

My supervisor Prof Lisa Claire du Toit and co-supervisors Dr Robert Tshikhudo and Prof Mariam Gulumian for the guidance and continued academic support.

The National Research Foundation (NRF) and the University of the Witwatersrand for financial assistance.

The Toxicology and Biochemistry Department of the National Health Laboratory Services for supporting the study.

Dr Melissa Chengalroyen (NHLS, TB Research Unit), Mrs. Pam Sharp (Microscopy Unit, University of the Witwatersrand), Dr Darin Reddy (Microscopy Unit, University of the Witwatersrand), and Prof Jim Phillips (NIOH, Pathology) for assistance and guidance with the TEM work.

Mr Poobie Poobalan (Analytical Services Department, NIOH) for assistance with the ICP-MS.

The **Occupational Hygiene Department** at the NIOH for assistance with the FTIR works.

The **Immunology and Microbiology Department** of the NIOH for continuous testing of the gold nanoparticles samples for bacterial and fungal contamination.

Mr Mangethe Zwane for assistance with the ESR study.

My friends and colleagues, Millicent Magogotya, Dr Wells Utembe, and Dr Puleng Matatiele for moral and academic support

A special gratitude to a colleague and a special friend Mrs Jiya Miriam John, for the immense support and strength provided throughout this work.

My family for keeping me in their prayers and for their love.

Special thanks to Prof Kogie Moodley for the support, inspiration and encouragement.

TABLE OF CONTENTS

DECLARATION ii

ABSTRACT viii

Acknowledgements ix

List of figures xvi

List of tables xxii

List of Abbreviations xxiii

Preface 1

Motivation for the Study 2

Aims for the work 2

THESIS LAYOUT 4

CHAPTER 1: Introduction 8

1.1 Literature Review 8

1.1.1 Nanoparticles and nanomaterials: A general overview 8

1.1.2 Introduction to Gold nanoparticles 10

1.1.3 Applications and uses of gold nanoparticles in medical technology 11

1.1.4 Common approaches used for the synthesis of gold nanoparticles 13

1.1.5 Surface coatings for functionalization of gold nanoparticles 14

1.1.6 Rationale for introducing functional groups to gold nanoparticles surfaces 18

1.1.6.1 Selective targeting and enhanced cellular delivery 18

1.1.6.2 A prolonged circulating period *in vivo* and reduced non-specific adsorption by macrophages 19

1.1.6.3 Increased solubility and enhanced stability of the nanoparticles 20

1.1.6.4 Reduce toxicity of the nanoparticles 21

1.2 Interface of gold nanoparticles with cells 22

1.2.1 Fate of nanoparticles (*in vivo* studies) 22

1.2.3 Physico-chemical properties of gold nanoparticles influencing cellular toxicity 26

1.2.3.1 Size 26

1.2.3.2 Shape 28
1.2.3.3 Surface Chemistry 29
1.2.4 Possible mechanisms of gold nanoparticle toxicity 37
1.2.4.1 Induction of inflammatory cytokines 37
1.2.4.2 Free radical generation and oxidative stress 38
1.2.4.3 DNA damage as a mechanism of nanoparticle toxicity 41
1.2.4.4 Apoptosis as a model of cell injury 43
References 45
CHAPTER 2 56
Physico-chemical characterization of citrate stabilized and alkylthiolated PEG-gold nanoparticles in cell growth medium 56
2.1 Introduction 56
2.2 Experimental methods 60
2.2.1 Instrumentation used in the study to assess physico-chemical properties of AuNPs 60
2.2.1.1 Transmission electron microscopy 60
2.2.1.2 UV-Vis spectrophotometer 60
2.2.1.4 Fourier Transform Infrared spectroscopy 61
2.2.1.5 Zeta potential measurement of gold nanoparticles 61
2.2.2 Synthesis of citrate stabilized and functionalized gold nanoparticles 62
2.2.3 Preparation of AuNPs in cell growth medium and physico-chemical characterization 67
2.3 Results and discussion 67
2.4 Summary and Conclusions 78
2.5 References 79
CHAPTER 3 82
Cellular uptake, intracellular localization and exocytosis of gold nanoparticles 82
3.1 Introduction 82
3.2 Experimental methods 84

3.2.1 Culturing and maintenance of cell lines 84
3.2.2 Determination of cell viability by the trypan blue exclusion assay 85
3.2.3 Cellular uptake of AuNPs using dark field imaging microscopy 86
3.2.4 Uptake, localization and distribution of AuNPs in cells using TEM 87
3.2.5 Quantification of intracellular AuNPs by ICP-MS 88
3.3 Results and Discussion 89
3.3.1 Cellular uptake of AuNPs assessed by dark field microscopy 90
3.3.2 Intracellular localization and distribution of AuNPs in cells via TEM analysis . 97
3.3.3 Quantitative analysis of intracellular gold nanoparticle concentrations with ICP-MS 106
3.4 Summary and Conclusion 113
3.5 References 114
CHAPTER 4 118
In vitro assessment of cytotoxicity of gold nanoparticles in human liver and kidney cells .. 118
4.1 Introduction 118
4.2 Experimental methods 120
4.2.1 Cell culturing for cytotoxicity studies 120
4.2.2 Testing of different cell densities for determining the optimal growth curve for HepG2 cells 121
4.2.3 Testing of different coating conditions for HepG2 cells 121
4.2.4 Testing of different cell seeding densities for determining the optimal growth curve for HEK 293 cells 122
4.2.5 Cytotoxicity of AuNPs using real-time impedance measurement 122
4.2.6 Instrumentation and software used for cytotoxicity measurement 123
4.2.6.1 XCELLigence RTCA system 123
4.2.7 Statistical analysis for cytotoxicity studies 124
4.3 Results and Discussion 124
4.3.1 Real time impedance measurement of cytotoxicity of gold nanoparticles in HepG2 cells 127

4.3.2 Real time impedance measurement of cytotoxicity of gold nanoparticles in HEK 293 cells 139

4.4 Summary and Conclusions 150

4.5 References 152

CHAPTER 5 155

Mechanisms of gold nanoparticles toxicity 155

5.1 Introduction 155

5.1.1 Pro-inflammatory release in response to cell-nanoparticle interaction 156

5.1.2 DNA damage as a mechanism of nanoparticle toxicity 156

5.1.3 Free radical generation 156

5.2 Experimental Procedures 157

5.2.1 Determination of pro-inflammatory cytokines after gold nanoparticle exposure 157

5.2.2 Chromosome aberration test for genotoxicty testing 158

5.2.3 Free radical generation using electron spin resonance 159

5.2.3.1 Preparation of reagents and reaction medium 159

5.2.3.2 Preparation of 4-hydroxyl Tempol (4-OH Tempol) ESR standard 160

5.2.3.3 Measurement of free radicals using ESR 161

5.3 Results and Discussion 162

5.3.1 Determination of pro- inflammatory cytokines following gold nanoparticle exposure 162

5.3.2 Chromosome aberration test for genotoxicty testing 168

5.3.3 Free radical generation using electron spin resonance 170

5.4. Summary and Conclusion 188

5.5 References 192

CHAPTER 6 195

Conclusions and Future outlook 195

Recommendations for future studies 198

Appendices 199

Appendix 1 199
Appendix 2 202
Appendix 3 205
Appendix 4 206
Appendix 5 207
Appendix 6 208

List of figures

Figure 1.1: Schematic diagram of a typical nanoparticle.....…...9

Figure 1.2: TEM images showing gold nanoparticles with various shapes. (a) gold nanospheres (b) gold nanorods and (c) gold nanocubes…….…….....11

Figure 1.3: A schematic diagram of thiol functionalized gold nanoparticles or AuMPCs….15

Figure 1.4: Folic acid functionalized AuNPs for cancer cell detection…….....19

Figure 1.5: Different pathways that are utilized by cells to take up nanomaterials…….….24

Figure 1.6: Diagram of the different pathways by which nanoparticles can induce oxidative stress…….....…….....39

Figure 1.7: Pathway of ROS production and removal……...…...40

Figure 1.8: Diagram of the different mechanisms by which NPs can induce genotoxic effects or affect intracellular signaling pathways……..…….……...…..42

Figure 1.9: Morphological changes in cells undergoing apoptosis and necrosis…..…….44

Figure 2.1: A plot of zeta potential vs. pH showing values where nanoparticle would be expected to be stable……...…....….57

Figure 2.2: Monolayer protected clusters and mixed monolayer protected clusters used in the study…….62

Figure 2.3: TEM micrograph of 14, 20 and 40nm citrate stabilized AuNPs in RPMI-1640 and EMEM medium supplemented with 10% FBS. The optical absorption spectra of the AuNPs …….……..……..……..……67

Figure 2.4: TEM micrograph of 14 nm azide-PEG MMPCs, biotin-PEG MMPCs, methoxy-PEG MPCs, hydroxyl-PEG MPCs, carboxyl-PEG MPCs and NTA-PEG MMPCs in RPMI-1640 and EMEM growth medium…….……..69

Figure 2.5: Particle size distribution of azide-PEG MMPCs, biotin-PEG MMPCs, methoxy-PEG MPCs, hydroxyl-PEG MPCs, carboxyl-PEG MPCs and NTA-PEG MMPCs…….70

Figure 2.6: UV-vis spectra of 14 nm azide-PEG-OH, biotin-PEG-OH, methoxy-PEG, hydroxyl-PEG, carboxyl-PEG and NTA-PEG-OH AuNPs in RPMI-1640 and EMEM growth medium.71

Figure 3.1: Schematic diagram of ICP- MS sample introduction, ion formation and analysis……..83

Figure 3.2: Dark field images of liver carcinoma HepG2 and kidney HEK 293 cells without AuNPs…….…..…89

Figure 3.3: Dark field images of HepG2 cells incubated with citrate stabilized AuNPs of increasing diameter for 4, 6 and 24 hrs…….…..……..90

Figure 3.4: HepG2 cells incubated with azide-PEG, NTA-PEG, biotin-PEG, carboxyl-PEG, hydroxyl-PEG and methoxy-PEG coated AuNPs for 4, 6 and 24 hrs……..……..92

Figure 3.5: HEK 293 cells incubated with citrate AuNPs stabilized AuNPs of increasing diameter for 4, 6 and 24 hrs ……..……..….93

Figure 3.6: HEK 293 cells incubated with azide-PEG, NTA-PEG, biotin-PEG, carboxyl-PEG, hydroxyl-PEG and methoxy-PEG coated AuNPs for 4, 6 and 24 hrs……..……..95

Figure 3.7: HepG2 cells incubated with AuNPs for 24 hrs. TEM images of 14, 20 and 40 nm citrate stabilized AuNPs and EDX analysis confirming the elemental Au in cell sections ……97

Figure 3.8: TEM images of HepG2 cells treated with azide-PEG, NTA-PEG, biotin-PEG, carboxyl-PEG, hydroxyl-PEG and methoxy-PEG AuNPs for 24 hrs……...98

Figure 3.9: TEM image showing nuclear region of HepG2 cells…….……100

Figure 3.10: HEK 293 cells incubated with AuNPs for 24 hrs. Cells were treated with 14, 20 and 40 nm citrate stabilized AuNPs……..……....101

Figure 3.11: TEM images of HEK 293 cells incubated with azide-PEG, NTA-PEG, biotin-PEG, carboxyl-PEG; hydroxyl-PEG and methoxy-PEG AuNPs for 24 hrs…….102

Figure 3.12: TEM image of HepG2 cells incubated with 14 nm citrate AuNPs for 3 and 4 weeks…….……103

Figure 3.13: HepG2 cells incubated with 40 nm citrate stabilized AuNPs. Excreted vesicles with AuNPs were seen as early as 1 week after incubation. Intracellular AuNPs were located in endo-lysosomal vesicle two weeks after incubation……..……104

Figure 3.14: TEM sections of cells exposed to carboxyl-PEG coated AuNPs 1 week, 2 weeks, 3 week and 4 weeks…….……105

Figure 3.15: Quantification by ICP-MS showing the mean concentrations (in µg/L) of Au in HepG2 cells after 1, 4 and 24 hr incubation with citrate stabilized and PEG coated gold nanoparticles……..……..……107

Figure 3.16: Quantification by ICP-MS showing the concentration (in µg/L) of Au element HEK 293 cells 1, 4 and 24 hr incubation with citrate stabilized and PEG coated AuNPs at 1nM concentration……...……....108

Figure 4.1: Schematic diagram of impedance measurement.....119

Figure 4.2: HepG2 cells seeded at different densities on non-coated E- plates…..……..124

Figure 4.3: Growth curves of HepG2 cells seeded on collagen coated E-plate.....125

Figure 4.4: HepG2 cells seeded on Poly-L- lysine coated E plate at 10 000 cells/well…..127

Figure 4.5: Growth Curve of HepG2 cells seeded at 10000 cells/well in a Poly-L-lysine (150 ug/mL) coated E- plates…….……...128

Figure 4.6: Impedence monitoring of proliferation and viability of HepG2 cells following incubation with 14 nm citrate stabilized AuNPs at concentrations of 5, 2, 1; and 0.5 nM…129

Figure 4.7: Impedence monitoring of proliferation and viability of HepG2 cells following incubation with 20 nm citrate stabilized AuNPs at concentrations of 5, 2, 1; and 0.5 nM..131

Figure 4.8: Impedence monitoring of proliferation and viability of HepG2 cells following incubation with 40 nm citrate stabilized AuNPs at concentrations of 5, 2, 1; and 0.5 nM…132

Figure 4.9: Impedence monitoring of proliferation and viability of HepG2 cells following incubation with azide-PEG coated AuNPs at concentrations of 5, 2, 1; and 0.5 nM……..…134

Figure 4.10: Impedence monitoring of proliferation and viability of HepG2 cells following incubation with nitriloacetic acid-PEG coated AuNPs at concentrations of 5, 2, 1; and 0.5 nM……..…135
Figure 4.11: Impedence monitoring of proliferation and viability of HepG2 cells following incubation with carboxyl-PEG coated AuNPs at concentrations of 5, 2, 1; and 0.5 nM.....136

Figure 4.12: Impedence monitoring of proliferation and viability of HepG2 cells following incubation with biotin-PEG coated AuNPs at concentrations of 5, 2, 1; and 0.5 nM…….137

Figure 4.13: Impedence monitoring of proliferation and viability of HepG2 cells following incubation with hydroxyl-PEG coated AuNPs at concentrations of 5, 2, 1; and 0.5 nM…..138

Figure 4.14: Impedence monitoring of proliferation and viability of HepG2 cells following incubation with methoxy-PEG coated AuNPs at concentrations of 5, 2, 1; and 0.5 nM…..139

Figure 4.15: HEK293 cells growth curve at cell density of 50 000 cells.....140

Figure 4.16: Impedence monitoring of proliferation and viability of HEK 293 cells following incubation with 14 nm citrate stabilized AuNPs……..…….....141

Figure 4.17: Impedence monitoring of proliferation and viability of HEK 293 cells following incubation with 20 nm citrate stabilized AuNPs……...142

Figure 4.18: Impedence monitoring of proliferation and viability of HEK 293 cells following incubation with 40 nm citrate stabilized AuNPs…….……..…143

Figure 4.19: Impedence monitoring of proliferation and viability of HEK 293 cells following incubation with azide-PEG gold nanoparticles at concentrations of 5, 2, 1; and 0.5 nM.....144

Figure 4.20: Impedence monitoring of proliferation and viability of HEK 293 cells following incubation with nitriloacetic acid-PEG AuNPs……...…145

Figure 4.21: Impedence monitoring of proliferation and viability of HEK 293 cells following incubation with carboxyl-PEG gold nanoparticles at concentrations of 5, 2, 1; and 0.5 nM146

Figure 4.22: Impedence monitoring of proliferation and viability of HEK 293 cells following incubation with biotin-PEG AuNPs…….……..…148

Figure 4.23: Impedence monitoring of proliferation and viability of HEK 293 cells following incubation with hydroxyl-PEG gold nanoparticles at concentrations of 5, 2, 1; and 0.5 nM ……..……..149
Figure 4.24: Impedence monitoring of proliferation and viability of HEK 293 cells following incubation with methoxy-PEG gold nanoparticles at concentrations of 5, 2, 1; and 0.5 nM ……...150
Figure 5.1: Some of the hypothesized mechanisms by which nanomaterials can induce cellular toxicity……..156
Figure 5.2: Calibration of the ESR instrument using the spin probe 4-hydroxyl Tempol…162
Figure 5.3: Concentration of IL-6 and TNF-α in cell culture medium of HepG2 cells exposed to AuNPs for 4 and 24 hrs…….....….165
Figure 5.4: Concentration of IL-6 and TNF-α in cell cultre medium of HEK 293 cells exposed to AuNPs for 4 and 24 hrs……...…....167
Figure 5.5: Percent chromosome abberation in HepG2 cells incubated with AuNPs for 24hrs…….……..…...170
Figure 5.6: Percent chromosome abberation in HEK 293 cells incubated with AuNPs for 24 hrs……...…….…...…....171
Figure 5.7: ESR signal intensity of H_2O_2 decomposition in the presence of Fe^{2+}……....173
Figure 5.8: ESR signal intensity in the reaction of hydrogen peroxide and 14nm citrate stabilized AuNPs.....175
Figure 5.9: ESR signal intensity in the reaction of hydrogen peroxide and 20nm citrate stabilized ……..……..176
Figure 5.10: ESR signal intensity in the reaction of hydrogen peroxide and 40nm citrate stabilized.....…...177
Figure 5.11: ESR signal intensity in the reaction of hydrogen peroxide and azide-PEG AuNPs ……..…....178
Figure 5.12: ESR signal intensity in the reaction of hydrogen peroxide and of NTA-PEG AuNPs ……..…..…...179
Figure 5.13: ESR signal intensity in the reaction of hydrogen peroxide and carboxyl-PEG ……...…180

Figure 5.14: ESR signal intensity in the reaction of hydrogen peroxide and biotin-PEG AuNPs ……..……..……..…181

Figure 5.15: ESR signal intensity in the reaction of hydrogen peroxide and hydroxyl-PEG AuNPs ……..……..……...182

Figure 5.16: ESR signal intensity in the reaction of hydrogen peroxide and methoxy-PEG AuNPs …….183

Figure 5.17: Decomposition of hydrogen peroxide at pH 3.6 by AuNPs…….…..184

Figure 5.18: ESR signal intensity showing the effect of 14, 20 and 40nm citrate stabilized AuNPs on the generation of ·OH at pH 4.6……...…....185

Figure 5.19: ESR signal intensity showing the effect of azide-PEG, NTA-PEG and carboxyl-PEG AuNPs on the generation of ·OH at pH 4.6……..187

Figure 5.20: ESR signal intensity showing the effect of biotin-PEG and hydroxyl-PEG on the generation of •OH at pH 4.6……..……..……...188

Figure 5.21: ESR signal intensity showing the effect of methoxy-PEG AuNPs on the generation of ·OH at pH 4.6……..……..189

List of tables

Table 1.1: Functional groups that are generally attached on gold nanoparticle surfaces….17

Table 1.2: Summary of selected *in vitro* cytotoxicity studies in gold nanoparticles ……..…..30

Table 1.3: Summary of selected *in vivo* cytotoxicity studies in gold nanoparticles..…..……..34

Table 2.1: Specification of gold nanoparticles used in this study…….……..…...64

Table 2.2: Summary of SPR band of AuNPs in water/buffer and in cell growth medium…..72

Table 2.3: Zeta potential (mV) and pH of gold nanoparticles suspended in Milli-Q water…75

Table 2.4: Zeta potential (mV) of gold nanoparticles suspendend in growth medium……..76

Table 3.1: Cell lines used in the study…….....84

Table 3.2: List of the investigated gold nanoparticles…….....88

Table 3.3: Concentration of AuNPs in HepG2 and HEK 293 cells.……..……...109

Table 3.4: Comparison of median concentration of AuNPs in HepG2 and HEK 293 cells following incubation for 1, 4 and 24 hrs……111

Table 5.1: Comparison of concentrations (pg/mL) of IL-6 and TNF-α released in HepG2 and HEK 293 cells after treatment with AuNPs…….…...168

Table 5.2: Signal intensity of DMPO/•OH in reaction medium pH 6.5……..……..…190

List of Abbreviations

AFM	=	Atomic force microscopy
ATP	=	Adenosine triphosphate
AuMMPCs	=	gold mixed monolayer protected clusters
AuMPCs	=	gold monolayer protected clusters
AuNPs	=	Gold nanoparticles
CAT	=	Catalase
CBA	=	Cytometric Bead Array
CI	=	Cell-index
CTAB	=	Cetyltrimethylammonium bromide
DLS	=	Dynamic light scattering
DMPO	=	5, 5 dimethyl N-oxide pyrroline
DTS	=	Dispersion Technology Software
EDS	=	Energy dispersive X-ray spectrometer
EMEM	=	Essential minimum eagle medium
ENPs	=	Engineered nanoparticles
ESR	=	Electron spin resonance
FBS	=	Fetal calf serum
FTIR	=	Fourier transform infrared spectroscopy
GPX	=	Glutathione peroxidase
HCl	=	Hydrochloric acid
HEK 293	=	Human embryonic kidney cells
HepG2	=	Human liver hepatocytes cells
ICP-MS	=	Inductive coupled plasma-mass spectroscopy
IL	=	Interleukin
KCl	=	Potassium chloride

LDH	=	Lactate dehydrogenase
MMPCs	=	Mixed-monolayer protected clusters
MPCs	=	Monolayer protected clusters
MTT	=	3-(4, 5-dimethylthiazol-2-yl)-2, 5-diphenyltetrazolium bromide
NaOH	=	Sodium hydroxide
Nm	=	Nanometer
NMR	=	Nuclear magnetic resonance
NPs	=	Nanoparticles
NTA	=	Nitriloacetic acid
PB	=	Phosphate buffer
PBS	=	Phosphate Buffered Saline
PC	=	Phosphatidylcholine
PEG	=	Poly-ethylene glycol
PSD	=	Particle size distribution
ROS	=	Reactive oxygen species
RPMI	=	Roswell park memorial institute
RTCA	=	Real time cell analyzer
SEM	=	Scanning electron microscopy
SOD	=	Superoxide dismutase
SPR	=	Surface plasmon resonance
TEM	=	Transmission electron microscopy
TNF-α	=	Tumor necrosis factor alpha
TPP	=	Triphenylphosphine
UV-Vis	=	Ultraviolet-Visible

PREFACE

Established studies on incidental particles have shown that nanomaterials contribute to the onset of chronic diseases (Oberdörster *et al*., 2005). The toxicity of engineered nanoparticles (≤ 100nm) on the other hand is poorly understood. However, due to their small size, nanoparticles have the ability to enter cells, translocate to major organelles and interrupt cell functions to influence basic processes of cell functioning (Buzea *et al.,* 2007; Dechent and Simon, 2008). Nanoparticles can hinder cellular functions to influence basic processes such as cell growth, metabolic rate, and apoptosis or programmed cell death. Thus, many diseases, such as cancer results in uncontrolled cells proliferation and have been associated with dysfunction of cellular processes (Buzea *et al.,* 2007). On the other hand, the physico-chemical properties of nanomaterials, including diameter or size, surface chemistry, and surface plasmon resonance have been shown to be beneficial in cancer therapy, drug delivery and bio-imaging (Buzea *et al.,* 2007).

MOTIVATION FOR THE STUDY

The demand for gold nanoparticles (AuNPs) in life science applications has necessitated an extensive investigation on the safety of these nanomaterials. Although investigators have presented the toxicity of citrate stabilized and ligand coated AuNPs, the choice of ligands, specific functional groups and experimental conditions remain the choice of an individual researcher. Hence, the level of toxicity investigated for the AuNPs presented in the literature may not represent the level of toxicity of the gold nanomaterials developed in South Africa. In this study, detailed toxicity effects of various ligands stabilized and functionalized AuNPs are undertaken. By elucidating toxicity effects that occur upon interaction of the functional groups with the cell surface or cellular components, this study facilitated hazard identification of newly synthesized AuNPs. The findings encouraged the development of proper protocols for manufacturing safer gold nanoparticles. The study provides an insight on the effect and the possible roles of different functional groups used in surface coatings of AuNPs in cellular toxicity. This work offers a point of reference for future studies investigating the potential toxicity of functionalized AuNPs.

Aims for the work

1. Evaluating the physico-chemical properties of the citrate stabilized and thioalkylated Polyethylene glycol (PEG)-AuNPs in cell growth medium

1.1. To assess the physico-chemical properties of AuNPs in cell growth medium using the UV-Vis spectrophotometer, dynamic light scattering (DLS) technique for zeta potential and size measurement and transmission electron microscopy (TEM).

1.2. To determine the stability of the AuNPs in cell growth medium prior exposure to cells for toxicity studies.

1.3. To confirm the presence of functional groups on AuNPs surfaces, using Fourier transform infrared spectroscopy (FTIR).

2. *In vitro* cellular interaction of AuNPs with the selected human cell lines

2.1. To introduce AuNPs to human embryonic kidney cells (HEK 293) and the human liver hepatocytes (Hep G2) cells.

2.2. To assess the cellular uptake of the AuNPs in human cell lines using the CytoViva® dark field imaging technology and transmission electron microscopy.

2.3. To assess sub-cellular distribution of intracellular AuNPs with the TEM.

2.4. To assess the fate of the AuNPs in cells.

2.5. To quantify the intracellular concentration of AuNPs with inductively coupled plasma- mass spectroscopy (ICP-MS).

3. Assessment of cytotoxicity effects of the AuNPs

3.1. To determine viability and proliferations of cells after treatment with various concentrations of AuNPs.

3.2. Determine non-cytotoxic concentrations of AuNPs in HEK 293 cells and Hep G2 cells for further toxicity measurements.

4. Investigation of the mechanism of toxicity of AuNPs

4.1. Quantify the release of pro-inflammatory cytokines (Interleukin IL-6 and Tumour necrosis factor- α) in cell culture medium of treated cells.

4.2. Assess the genotoxicity in cells using chromosome aberration test.

4.3. Assess the ability of AuNPs to generate free radicals.

5. Determine the properties of functional groups responsible for cellular toxicity

5.1. Elucidate the effect of functional groups in AuNPs toxicity.

THESIS LAYOUT

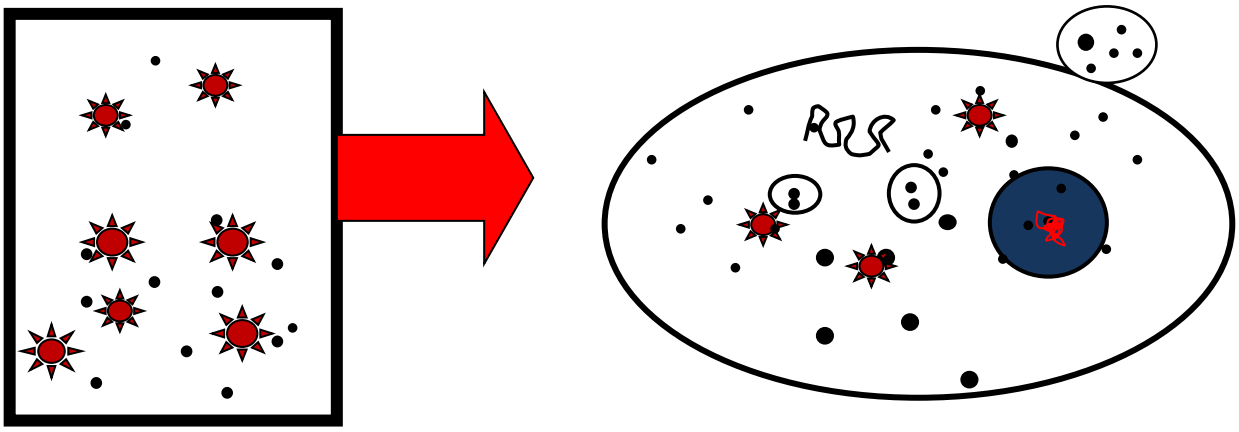
Executive summary

Introduction and literature review

Physico-chemical characterization of AuNPs in medium

AuNPs uptake and sub cellular localization

Exocytosis



Interaction of AuNPs with cellular components and mechanisms of cellular toxicity

Conclusion and future outlook

Chapter 1 Introduction and Literature review

Chapter one delivers the introduction on various aspects of nanomaterials that are responsible for toxicity in cells. A brief review on the synthesis techniques of AuNPs, their unique optical and structural properties, and their medical applications is outlined. The importance of functionalizing AuNPs surfaces with various functional groups is emphasized. Furthermore, emphasis on the role of the other physical and chemical properties of AuNPs, including size, shape, and surface charge in cellular toxicity is outlined. A literature survey on *in vitro* and *in vivo* models showing toxicity effects associated with AuNPs in relation to the physico-chemical properties on various cellular models and animals are outlined.

Chapter 2 Assessment of the physico-chemical properties of the citrate stabilized and alkylthiolated PEG- gold nanoparticles in cell growth medium.

In this chapter, various techniques for characterizing the physico-chemical properties of nanomaterials are introduced. These techniques were employed to confirm surface functional groups on monolayer protected gold clusters and to evaluate the hydrodynamic size, shape, morphology and the surface charge of AuNPs in cell growth medium. The results indicated an overall stability of the AuNPs in the respective medium prior to exposure to cells.

Chapter 3 In vitro cellular interactions, uptake and localization of gold nanoparticles in human cell lines

Citrate stabilized AuNPs of various sizes (14, 20 and 40nm) and MPCs presenting various functional groups are exposed to HEK 293 and the HepG2 cells. Cellular uptake and localization of AuNPs in sub cellular organelles are assessed. Furthermore, studies showing the fate of the AuNPs in the two cell lines were conducted. Intracellular nanoparticles were further quantified by ICP-MS technique, and the differences in the uptake between the two cell lines and the respective nanoparticles are compared.

Chapter 4 Real time measurement of cell viability and proliferation

The cytotoxicity of the AuNPs at various concentrations is assessed using real time, label free impedance technology. The effect of the AuNPs at each concentration on cell viability and cell proliferation over time is presented.

Chapter 5 Mechanisms of gold nanoparticles toxicity

In this chapter various toxicity endpoint are conducted. Induction of pro-inflammatory cytokines in supernatant of treated cells was assessed with flow cytometer techniques. Structural chromosomal aberration as a form of DNA damage is assessed after treatment of cells with AuNPs. Finally, to elucidate the role of AuNPs in cellular toxicity, the study intended to examine the effect of AuNPs on generation of reactive oxygen species (ROS). The chemical reactions were conducted in a cell free system, in the presence of hydrogen peroxide (H_2O_2), representing a constituent present in cells in steady state concentrations.

The reactions were conducted over a wide range of physiologically relevant pH, representing conditions within sub-cellular compartments.

Chapter 6 Conclusions and future outlook

A summary of the results from the previous chapters is presented. A conclusion on AuNPs toxicity in relation to the different functionalization and size is outlined. Furthermore, possible outcomes on AuNPs toxicity in cells are presented. Finally, future studies on the topic are presented.

CHAPTER 1: INTRODUCTION

1.1 LITERATURE REVIEW

1.1.1 Nanoparticles and nanomaterials: A general overview

The last decade has seen an increase in nanotechnology and nanoscience research with the development of nanomaterials for a wide range of applications. Nanomaterials are commonly denoted as nanoparticles (NPs) and are characterized by a physical diameter of 1-100 nanometer (nm) (Baptista *et al.*, 2008). Three forms of nanoparticles exist: 1) incidental or anthropogenic nanoparticles, 2) natural nanoparticles, and 3) engineered or manufactured nanoparticles (ENPs). Incidental nanoparticles are produced from occupational activities such as sandblasting and metal working. Natural nanoparticles are the results of natural occurrences such as forest fires, smoke and volcanic ashes. The first two do not have a pre-determined size, shape or surface chemistry. ENPs are intentionally manufactured with very specific physical and chemical properties (Medina *et al.,* 2007). The tailor made physico-chemical (size, surface chemistry, shape) properties of the ENPs make them desirable for commercial purpose.

Generally, engineered nanoparticles consist of a core and an outer organic layer (Salata, 2004). The core can either be a metal or a non-metal compound that dictates the optical and electrical properties of the nanoparticles. The outer layer prevents contact between the particles and hence prevents agglomeration of the nanoparticles during synthesis. A schematic diagram of typical nanoparticles is presented in Figure 1.1.

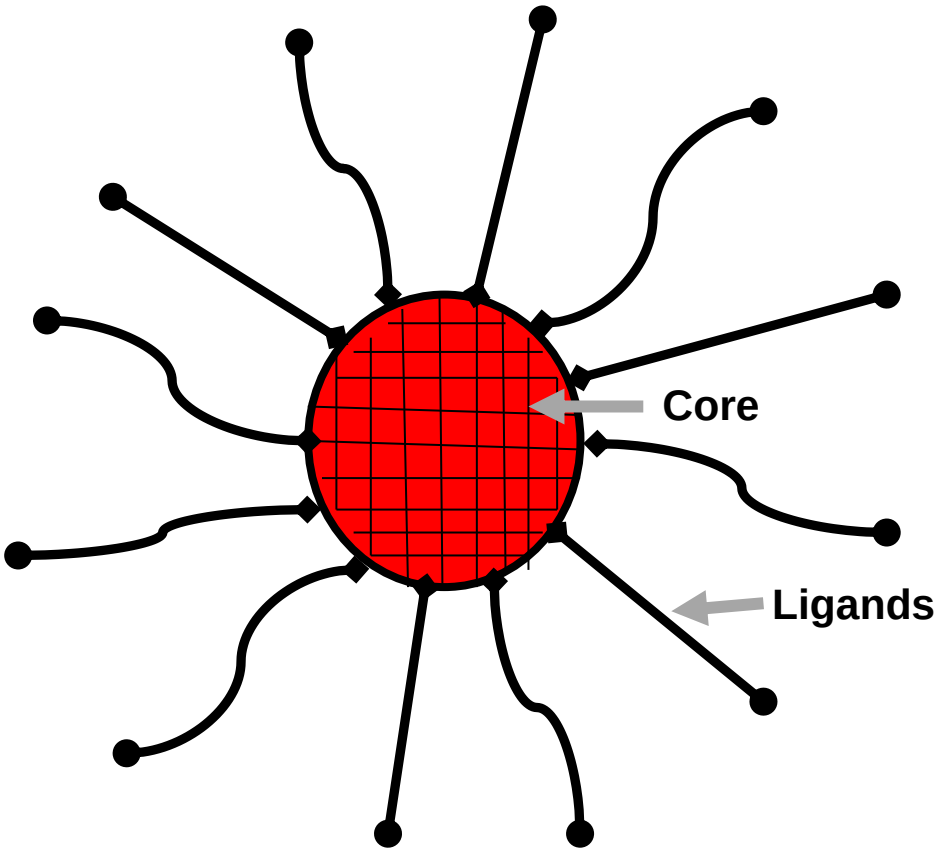


Figure 1.1: Schematic diagram of a typical nanoparticle

Engineered nanoparticles (ENPs) have a long history. Metal and metal oxide ENPs are the most frequently studied nanomaterials. These include titanium dioxide (TiO_2), cadmium (Cd) complexes, gold (Au), cerium dioxide (CeO_2), nickel (Ni), silver (Ag), aluminium oxide (Al_2O_3), silicon dioxide (SiO_2), and zinc oxide (ZnO) (Tiwari *et al.,* 2011). One type of ENPs that has gained popularity in life science applications are AuNPs and is discussed further in the following section.

1.1.2 Introduction to Gold nanoparticles

Gold (Au) is one of the most stable and inert chemical compound (Tiwari *et al.,* 2011). Au exists in three chemical states, Au (0), Au (I) and Au (III). The chemical reduction of Au (III) is used for the synthesis of colloidal gold or AuNPs. AuNPs have been developed as promising delivery system for pharmaceutical product into diverse cell types (Rana *et al.,* 2011). This is due to the small size-large surface area, shape, electrical and optical properties and their chemical stability (Jennings and Strouse, 2007; Oh *et al.,* 2011).

The increasing demand of AuNPs application has also been attributed to the stability of the colloids at high temperatures and ease of uptake by different cell types (Tiwari *et al.,* 2011). One challenge of using AuNPs as a delivery system into cells is the high reactivity of the AuNPs with any cell type. To obviate this problem, attempts are made to conjugate the nanoparticles with various biomolecules and ligands, to control their interactions with specific cells. For this purpose, citrate-, amines, proteins, antibodies and nuclear motifs, amongst others have been attached to AuNPs surfaces to control their interaction with target cells.

In addition to AuNPs compatibility with cells, several reasons make AuNPs preferred materials for use in nanomedicine, namely (i) they are easily prepared and reliable methods for synthesis are available (Ghosh *et al.,* 2008, Kim *et al.,* 2009; Liang *et al.,* 2010); (ii) a variety of nanoparticles sizes (2-100nm) with diverse morphologies (spheres, rods, tubes, wires, ribbons, plate, hexagonal, triangular and cubic) can be prepared by varying the reaction parameters during synthesis (Figure 1.2) (Ghosh *et al.,* 2008, Liang *et al.,* 2010); (iii) they are soluble in most organic solvents and (iv) a variety of coatings, presenting different functional groups can be introduced on the nanoparticles surface for novel application (Patra *et al.,* 2010; Zhang *et al.,* 2010a).

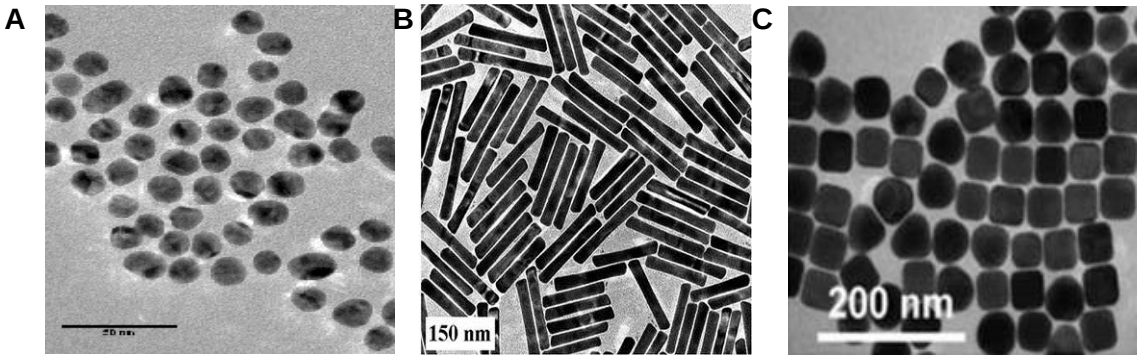


Figure 1.2: TEM micrographs showing gold nanoparticles with various shapes. (a) gold nanospheres (courtesy of MINTEK); (b) gold nanorods(AuNRs) (Vigderman and Zubarev, 2013) and (c) gold nanocubes (Miranda *et al.,* 2011).

1.1.3 Applications and uses of gold nanoparticles in medical technology

The medical application of gold can historically be traced back to the 1920s, where metallic gold and gold derivatives were used to alleviate tuberculosis and rheumatic diseases (Merchant *et al.,* 1998; Fadeel *et al.,* 2010). The most recent application of AuNPs covers the area of microbial diagnostics (Baptista *et al.,* 2008), pathogen control (Pissuwan *et al.,* 2010), drug delivery (Pissuwan *et al.,* 2009), cancer detection (Sarah, 2010), cancer treatment (Chen *et al.,* 2008; Chithrani *et al.,* 2009) and gene therapy (Rosi *et al.,* 2006). For example, to improve on the application of AuNPs in cancer therapy, antibodies have been attached to the AuNPs surfaces (Mukherjee *et al.,* 2007). This increased the efficacy of the antibodies in the treatment of B-Chronic Lymphocytic Leukemia (CLL). In human immunodeficiency virus (HIV) therapy, AuNPs functionalized with ligands containing sulfate terminal groups were attached to the HIV envelope glycoprotein gp120 to inhibit infection of

T-cells (Gianvincenzo *et al.,* 2010). The results of this study showed the possibility of tailored AuNPs-sulfate ligands as an anti-HIV molecule (Gianvincenzo *et al.,* 2010).

Delivery of drug molecules to the infected and tumor cells is the most popular application for AuNPs mediated cancer therapy and pathogenic control. For example, Gu *et al.* (2003) have used vancomycin conjugated to AuNPs to destroy the antibiotic resistant bacterium *Enterococcus faecium* and *Enterococcus faecalis.* The authors of this study were able to show that the activity of vancomycin was increased as the result of its conjugation to the nanoparticles (Gu *et al.,* 2003). Compared to the direct drug targeting methods, AuNPs mediated drug delivery to cells minimizes adverse effects in healthy cells (Shenoy *et al.,* 2006).

The optical properties of AuNPs makes these materials hold great promise in optical and imaging applications. These properties of gold arise from their surface plasmon resonance (SPR), which provides easy detection of the nanoparticles within cells (Levy *et al.,* 2010). Gold nanorods are especially useful within this area, as a result of their absorption and scattering of electromagnetic radiation in the near infrared (NIR) region, where the optical absorption in tissues is optimal (Tong *et al.,* 2010). In this process, photons that are absorbed by nanoparticles are converted to heat. The nanoparticles have found application in thermal cancer therapy. For example, a report by Zhang *et al.* (2010b) showed the three-dimensional X-ray imaging of damaged bone tissues using AuNPs *in vivo,* emphasizing the importance of AuNPs in bio-imaging (Zhang *et al.,* 2010b).

1.1.4 Common approaches used for the synthesis of gold nanoparticles

Various methods exist for the production of AuNPs. The most popular being the reduction of tetrachloroauric acid ($AuCl_4^-$) to metallic gold in the presence of stabilizing agents such as sodium citrate or sodium borohydrate (Zhou *et al.,* 2006; Low and Bansal, 2010). The stabilizing agent binds to the nanoparticles surfaces to constrain synthesis to the intended size range and to stabilize the colloids (Baptista *et al.,* 2008). The original method to prepare AuNPs was developed by Turkevich *et al.* (1951) to produce dispersed nanoparticles with average size of 20nm.

Synthesized AuNPs produced by the Turkevich method differ in several forms; some exist as branched nanocrystals with varying shapes of monopod, bipod, tripod, and tetrapod structures (Wu *et al.,* 2006). Following this development, attempts were made to design methods that allowed a controlled synthesis of AuNPs with pre-chosen sizes. The different sizes ranging from 10-150nm can be obtained by varying the reducing agents and gold salts (Frens *et al.,* 1973). Improvements to this method have afforded the synthesis of nanoparticles with increased stability. Additional stabilization of nanoparticles is conferred by functionalizing with organic ligands such as peptides, proteins, fungus (Mukherjee *et al.,* 2001) and large polymers such as poly-ethylene glycol (PEG) (Lu *et al.,* 2008; Pillay *et al.,* 2010).

A method of synthesizing AuNPs that possess robust and stable surface functionalities was first proposed by the Brust-Schiffrin group (Brust *et al.,* 1994). In a reaction of a reducing agent and a thiol ligand, the Brust-Schiffrin method allows the formation of thiol stabilized

AuNPs with different sizes (Daniel and Astruc, 2004). To date, this method is effective for the synthesis of AuNPs stabilized by a variety of functionalized ligands, referred to as monolayer- protected clusters (MPCs) (Templeton *et al.,* 2000; Drechsler *et al.,* 2004).

Thiol-functionalized nanoparticles produced by the Brust-Schiffrin method provide large quantities of nanoparticles. These nanoparticles are stable at ambient conditions (air, humidity, room temperature), and can be cycled between the solid state and the dissolved state without changing their composition (Murphy *et al.,* 2007). Developments to these methods have allowed the incorporation of multiple functionalities to MPCs to form mixed-monolayer protected clusters (MMPCs) (Liu *et al.,* 2007).

1.1.5 Surface coatings for functionalization of gold nanoparticles

Surface functional groups have been explored to develop ENPs as effective carriers for delivery of drug molecules (De Jong and Borm, 2008). The introduction of functional groups on nanoparticles surfaces presents an avenue of increasing their availability for biological applications (Basiruddin *et al.,* 2010). In addition, surface modifications can prolong the circulation period of the nanoparticles in blood during *in vivo* application, enhance uptake of the nanoparticles at a target site, reduce adverse effect of the drug to non-target organs, and alter excretion (De Jong and Borm, 2008).

Different strategies exist for synthesizing AuMPCs and AuMMPCs, including ligand exchange reactions with functionalized alkanethiolates (Templeton *et al.,* 1999). In ligand exchange reactions, a thiolate (SH) group is incorporated onto AuNPs surface, a cluster monolayer is formed by mixing the thiol group and the ligand group in solution (Hostetler *et al.,* 1999). This reaction allows an opportunity to present a selection of terminal groups or

functional groups to the nanoparticles surface (Ostuni *et al.,* 1999). MMPCs have also been prepared via the sequential addition of a ligand followed by a target group such as a proteins or antibodies (Liu *et al.,* 2007). These particles or clusters were found to be stable than particles prepared by simultaneous co- adsorption of surface coatings (Liu *et al.,* 2007).

Polymers, polypeptide, sugars, oligonucleotides and proteins are amongst others commonly used as coating agents to present functional groups to the nanoparticles surfaces (Basiruddin *et al.,* 2010; Tiwari *et al.,* 2011). These molecules are known as bi-functional ligands. They play a significant role in studying the interaction of the nanoparticles with its surrounding environment (Grubbs *et al.,* 2007). Bi-functional ligands are attached to the gold surface exposing a secondary group to the exterior of the particle (Ghosh *et al.,* 2008). Figure 1.3 shows a diagram of how surface coatings and functional groups are presented on nanoparticles surfaces. In Figure 1.3, the thiol- group is covalently bonded to the Au core. The ligand attached to the metal core and act as spacer, offering flexibility of the nanoparticles.

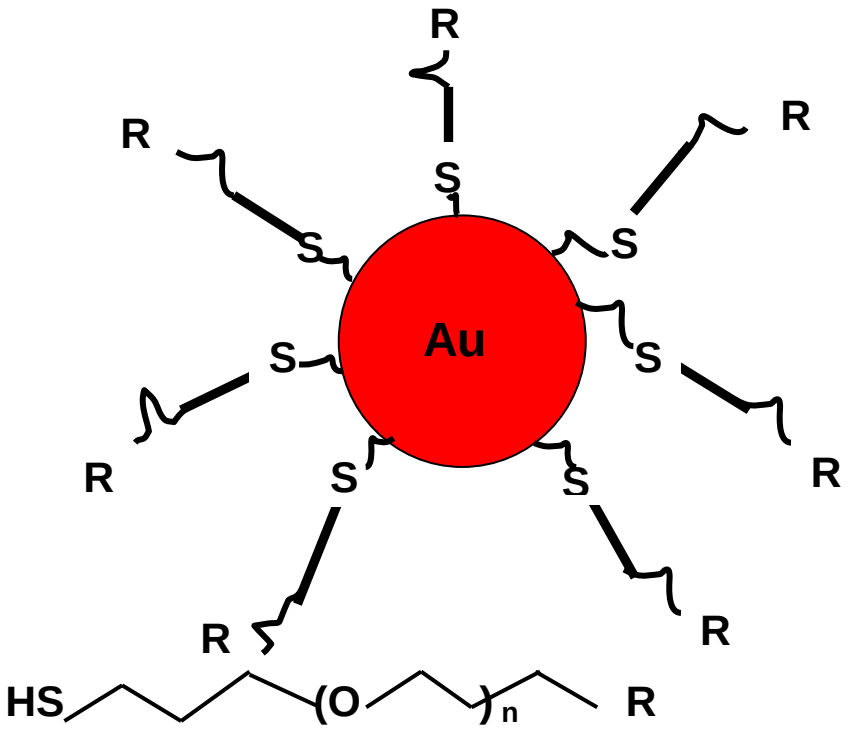


Figure 1.3: A diagram of thiol functionalized gold nanoparticles or AuMPCs

Several research groups have highlighted the attractive use of polymers as functional ligands. Poly-ethylene glycol (PEG), poly-D-L-lactic-co-glycolic acid (PLGA), poly-L-lysine (PLL) and their co-polymers have successfully been applied to AuNPs surfaces (Prencipe *et al.,* 2009; Raja *et al.,* 2010). A conventional PEG molecule consists of a linear or a branched structure with hydroxyl functional groups at both ends ($HO\text{-}(CH_2CH_2O)_n\text{-}CH_2CH_2\text{-}OH$, where n=2, 3 and 4). The presence of both hydrophilic and hydrophobic groups in an alkylated PEG molecule has made it a popular ligand for green synthesis. The oxidation of the terminal hydroxyl group of PEG provides an opportunity to incorporate the PEG ligand with other end groups and to adsorb larger molecules, such as drug derivatives.

In addition to its low toxicity to cells, PEG molecule is stable against oxidation-reduction reactions and disintegration by acids and bases. Low molecular PEG is soluble in water and in many biological medium (Pissuwan *et al.,* 2009; Shenoy *et al.,* 2006; Shukla *et al.,* 2006). High molecular weight PEG imparts more stability to the nanoparticles (Tiwari *et al.,* 2011; Otsuka *et al.,* 2003), short-chain low molecular weight PEG (1500-5000 Daltons) are preferred as they offer sufficient surface coverage on the nanoparticles surface and improved aqueous solubility. The AuNPs used in this study were therefore stabilized with low molecular weight thioalkylated PEG as shown in Figure 1.3.

The preferred terminal functional groups for AuNPs include the nitriloacetic acid [NTA], carboxylic acids, hydroxyl group, biotin and the methoxy functional groups (Grubbs *et al.,* 2007). The applications of these functional groups are summarized in Table 1.1. Chemical synthesis methods, such as the ligand exchange reactions are used to introduce functional groups of choice on the nanoparticles (Pan *et al.,* 2007; Simpson *et al.,* 2010).

Table 1.1: Functional groups that are generally attached on gold nanoparticles surfaces

Functional group	***Application***	***References***
Carboxyl (-COOH)	Site specific binding of biomolecules, cell specific targeting and efficient delivery of molecules	Zhang *et al.,* 2010; Hong *et al.,* 2006
Azide ($-N_3^-$)	Bio-molecule conjugation and cell specific targeting of NPs	Basiruddin *et al.,* 2010
Methyl/methoxy ($-OCH_3$)	Attachment of biological receptors for biosensing. Reduce non- specific binding of proteins	Shenoy *et al.,* 2006
Hydroxyl (-OH)	Biomolecules conjugation	Zhang *et al.,* 2010
Amine ($-NH_2$)	Conjugation of DNA, proteins; drug delivery	Basiruddin *et al.,* 2010

The carboxyl, NTA and biotin terminal groups on the nanoparticles surface allow further conjugation of a variety of biomolecules. For example, the biotin is useful in the Streptavidin-biotin interaction, which is currently applied in many commercial diagnostics (Aslan *et al.,* 2004). Another example is the Ni (II)-NTA-conjugate that has been used for the adsorption of hexahistidine-tagged (6xHis) recombinant proteins; for analytical and drug delivery applications (Huang *et al.,* 2006; Li *et al.,* 2007). Besides the adsorption of the common functional groups that are stated, compounds with a higher molecular weight such as maleimide and vinylsulfone have been incorporated as terminal functional groups on the surface. For examples, Shenoy *et al.* (2006) used coumarin carbamate-PEG AuNPs for intracellular tracking of the nanoparticles on human breast carcinoma cells.

1.1.6 Rationale for introducing functional groups to gold nanoparticles surfaces

1.1.6.1 Selective targeting and enhanced cellular delivery

Some functional groups are attached for the selective interaction and targeting of the particles with specific cell types and organelles (Hong *et al.,* 2006; Patra *et al.,* 2007). The interaction of the nanoparticles with the cell surface is facilitated by the electrical surface charge on the functional groups. For example, cationic amino acid functionalized AuNPs were shown to provide an effective platform for DNA and RNA delivery into cells (Han *et al.,* 2006; Noh *et al.,* 2007; Lee *et al.,* 2009). The modified AuNPs showed an efficient delivery of the oligonucleotides in gene therapeutics than commercially available delivery agents (Lee *et al.,* 2009). Brown *et al.* (2010) also demonstrated the effective delivery of the anticancer drug (oxaliplatin) to lung cancer cells using PEG coated AuNPs with carboxyl group on the nanoparticles surfaces. Similarly, Zhang *et al.* (2010b) reported a high affinity of folic acid-glutathione conjugated gold nanoparticles (FA-GSH-AuNPs) to the cell surface receptors of various human cancer cells. In this study, AuNPs were stabilized by a thiol group on the glutathione molecule; with a carboxyl and amino functional groups (Figure 1.4).

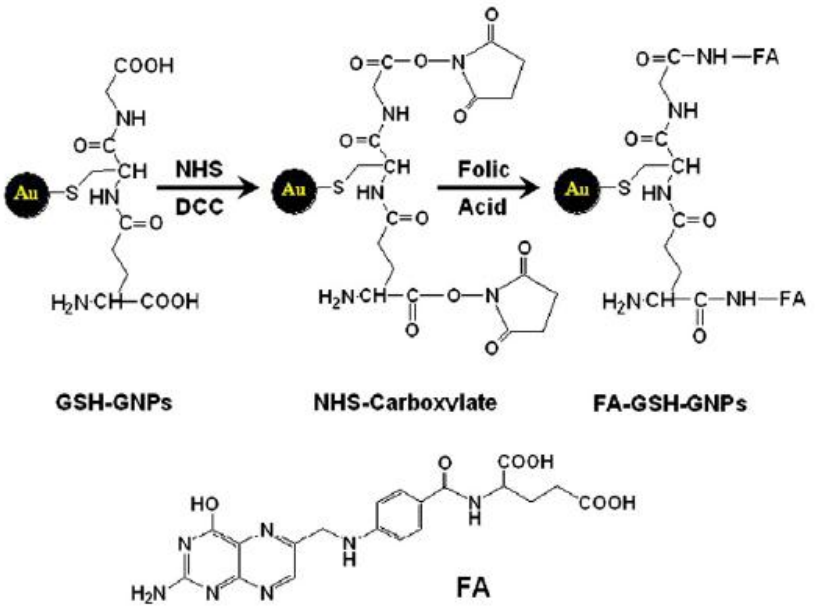


Figure 1.4: Folic acid functionalized AuNPs for cancer cell detection (Zhang et al., 2010b)

The conjugated folic acid on the nanoparticles surface was shown to represent a useful target for receptor mediated delivery of AuNPs to tumor cells as a result of the high expression of folate receptors on cancer cells (Zhang *et al.,* 2010b). Conjugation of the folic acid is distinctive for increasing the selective targeting and specific delivery of drug compounds by the nanoparticles. Drug induced side effects are minimized by targeting the nanoparticles directly to the 'infected' or tumor site.

1.1.6.2 A prolonged circulating period *in vivo* and reduced non-specific adsorption by macrophages

Functionalizing nanoparticles preserve their lifetime as a carrier and ensure that the target molecule carries out its intended function (Liang *et al.,* 2010). Thus, with the view to improve the bioavailability, modification of nanoparticle surfaces is frequently used to improve nanoparticles dispersibility and decrease opsonization. Studies comparing the bio-

distribution of PEG-coated and non-PEGylated gold nanorods in animals reported that a larger percentage of PEGylated AuNPs remained in the bloodstream half an hour longer following intravenous injection of the particles (Niidome *et al.,* 2006). In contrast, the uncoated particles were shown to have accumulated in the liver.

Functionalization of the nanoparticles surface was also shown to reduce the nonspecific adsorption and interactions with resident macrophages (Shenoy *et al.,* 2006). For example, Simpson *et al.* (2010) reported that PEG-AuNPs can elicit an immune response in animals, generating anti-PEG- antibodies. This reaction prevents clearance of the nanoparticles in the blood stream. In a similar study, PEG coating was shown to reduce nonspecific uptake of iron nanoparticles by macrophage cells (Xie *et al.,* 2006). The length of PEG chain and the reactive group on the chain terminus is thought to be responsible in determining the circulating time of the nanoparticles (Simpson *et al.,* 2010). A longer alkyl chain with an alcohol terminus has been shown to promote the circulation time of the nanoparticles in the injected test animal (Hainfield *et al.,* 2006).

1.1.6.3 Increased solubility and enhanced stability of the nanoparticles

The addition of surface coatings on nanoparticles surfaces improves the stability of the nanoparticles in many biological fluids. The surface coating maintains the integrity of the colloidal nanoparticles over a wide range of pH and ionic strength solutions and at elevated temperatures (Simpson *et al.,* 2010). For example, Prencipe *et al.* (2009) reported the enhanced stability of gold nanospheres and gold nanorods functionalized with PEG. For example, AuNPs (with average size 1 and 50nm) coated with PEG have been shown to be stable for nine months (Otsuka *et al.,* 2003). The stability was shown to be due to the covalent interaction between the thiol groups on the PEG molecule and the nanoparticles

core. The covalent bonding provided long-term colloidal stability and resistance to denaturation (Bhattacharya *et al.,* 2009). The findings were reported by Otsuka *et al.* (2003); where a higher stability of 50nm *ω*-mercapto and *α*-acetal PEG coated gold nanoparticles was evident in various buffers and in serum containing medium.

A similar study reported that DNA covalently bound to the amine functional group on PEG functionalized AuNPs was more stable compared to the non-covalently bound DNA (Kawano *et al.,* 2006). Enhanced solubility of gold nanoparticles in biological solutions and in organic solvents was achieved by PEGylation of the nanoparticles (Otsuka *et al.,* 2003). These findings emphasize the importance of coating nanoparticles for *in vitro* and *in vivo* applications. The solubility of the drug agent is also enhanced by using ligand coated nanoparticles.

1.1.6.4 Reduce toxicity of the nanoparticles

Chemical surfactants are used as stabilizing agents in nanoparticles synthesis and can contribute to cellular toxicity (Chithrani *et al.,* 2006; Khan *et al.,* 2007). However, the attachment of ligands to nanoparticles surface can reduce the possible toxicity of the particles (Alkilany *et al.,* 2009). Qui *et al.* (2010) demonstrated that gold nanoparticles coated with cetyltrimethylammonium bromide (CTAB) induced apoptosis on K562 leukemia cell line *in vitro*. The authors of these studies suggested that toxicity was related to the positive charge on the quaternary ammonium species on the CTAB molecule (Qui *et al.,* 2010). The toxicity of gold nanorods has been reduced by substituting the CTAB molecule with less toxic agents. Takahashi *et al.* (2006) reported that replacing the CTAB on the AuNRs solution with phosphatidylcholine (PC) as a stabilizing agent can reduce the toxicity associated with gold nanorods. The cytotoxicity results of PC-AuNRs on HeLa cells indicated 85 % cell viability.

1.2 Interface of gold nanoparticles with cells

1.2.1 Fate of nanoparticles (*in vivo* studies)

The effectiveness and safe use of nanomaterials for medical applications must be studied. The interaction between the nanoparticles and the cells provides a starting point to evaluate the safe use of nanomaterials (Nahiidi *et al.,* 2013). *In vitro and in vivo* studies on the distribution and biological effects of AuNPs can provide a basis for assessing long and short term health impact of these particles. *In vivo* studies have shown that the liver, spleen, brain, lungs, lymph nodes and the kidney are major organs where nanoparticles, including gold accumulate (Li *et al.,* 2008). For example, Kumar *et al.* (2010) reported the accumulation of silica nanoparticles in the liver. Similarly, Yu *et al.* (2007) found that AuNPs between 30 and 110nm when exposed to rats for up to 15 days accumulated in the lungs, olfactory bulb, spleen, esophagus, tongue, kidney, aorta, heart and in the blood. The results were similar to those earlier reported by Takenaka *et al.* (2006) when they injected engineered gold nanomaterials (5-8nm) into rats and found their retention in the lungs to be less than 30 minutes. The nanoparticles were later translocated through the blood system into other tissues after 30 minutes of instillation.

Nanoparticle size and surface coating play a major role in determining the fate of the nanoparticles in the body and in cells (Shukla *et al.,* 2006, Buzea *et al.,* 2007). This was shown in a study by Sadauskas *et al.* (2009) demonstrating the effect of 2nm, 40nm and 100nm AuNPs in mice. In the study, the liver was shown as the main site of accumulation of the NPs with only a small fraction of the AuNPs being translocated into the blood circulation. Hirn *et al.* (2011) also reported on the accumulation of 18nm mono-sulfonated

triphenylphosphine (TPPMS) stabilized AuNPs in the kupffer cells, endothelial cells and hepatocytes of the liver following intravenous injection in mice. In the study, the carboxyl and amine coated AuNPs (2.8nm) were shown to accumulate in the kidney (Hirn *et al.,* 2011).

Lasagna-Reeves *et al.* (2010) also observed a significant amount of AuNPs in the liver, blood, brain, kidney, spleen, and lungs. Based on these reports, AuNPs with a size range of 10-240nm were confirmed to accumulate in the liver and the kidney. Therefore, the human embryonic kidney cell line (HEK 293) and the human liver carcinoma cell line (HepG2) were selected in this study as representive models for toxicological research in investigating AuNPs interactions and effects.

1.2.2 Cellular interaction and uptake of nanoparticles by cells (*in vitro* and *in vivo* studies)

Cells use endocytosis for uptake of nutrients and any foreign substances presented to the cell plasma membrane. This mechanism is divided into different pathways, as shown in Figure 1.5. Briefly, the uptake of molecules in cells is based on the engulfing of the foreign molecule by protrusions on the plasma membrane and thereafter, direct penetration of the membrane-filled vesicle into the cell.

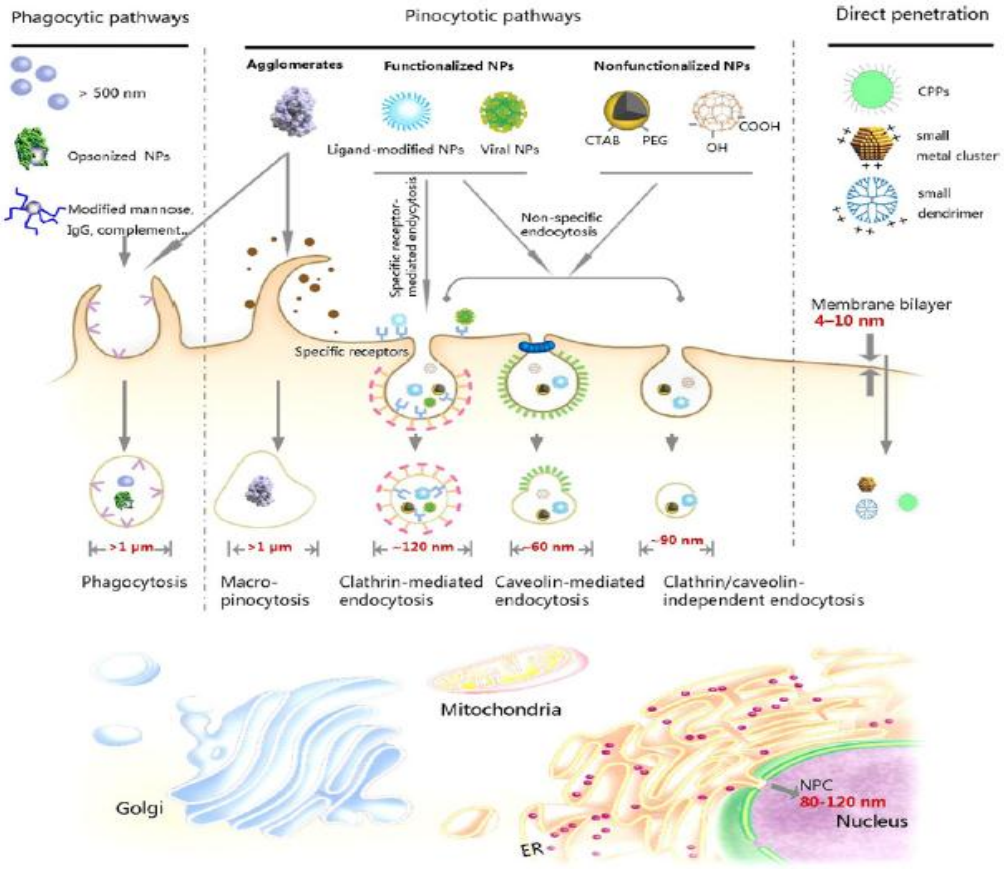


Figure 1.5: Different pathways that are utilized by cells to take up nanomaterials (Zhu et al., 2012).

Once inside the cells, the engulfed molecules, including nanoparticles get trapped into vesicles of different sizes, which may be formed from the plasma membrane (Zhu *et al.,* 2012). The sizes of the vesicle within the cell depend on the size of the material initially taken in by the cell. Thus, nanoparticles sizes have a major role in influencing which pathway the cell use during uptake (Khlebtsov and Dykman, 2011). Surface chemistry also detects the pathway which the cell will use for uptake, with the surface charge playing a critical role in cellular interaction (Goodman *et al.,* 2004).

Phagocytosis is a pathway commonly observed in macrophages. The pathway is used for the uptake of larger particles with size exceeding 0.5μm, such as bacteria (Dobrovolskaia and McNeil, 2007). Pinocytosis on the other hand, is used for the uptake of materials in the size range of approximately 100nm. The pinocytotic pathway is further divided into micro-pinocytosis, clathrin, caveolin, and clathrin/caveolin mediated endocytosis (Shukla *et al.,* 2006). From the literature, clathrin mediated endocytosis facilitated by membrane bound vesicles with diameter of 120nm have been shown to be the typical route for ligand-modified nanoparticles (Shukla *et al.,* 2006).

Nanoparticles uptake by cultured cells are enclosed within vesicle like structures of the endosomes, phagosomes or macropinosomes (Dobrovolskaia and McNeil, 2007). These vesicles mature to become the lysosomal vesicles, multivesicular bodies or late endosomes (Dobrovolskaia and McNeil, 2007). The lysosomes are the last compartment of endocytocised particles and contain proteases and other enzymes that degrade most foreign material (Dobrovolskaia and McNeil, 2007).

In the acidic compartments of cellular lysosomes (pH 4.0- 5.5) and endosomes (pH 6.0), other metal nanoparticles such as silver may be degraded (Panariti *et al.,* 2012). However non-degradable particles, such as gold may have their surface coatings removed, resulting in a reaction of the metal ion with cell components. Panariti *et al.* (2012) suggested the release of free ions from metal nanoparticles degraded in the lysosomes and endosomal vesicles may generate harmful radicals that can affect cell homeostasis.

Nanoparticles escaping the endosomal pathways can translocate in the cytoplasm and accumulate in other organelles within the cell (Buzea *et al.,* 2007; Oh *et al.,* 2011). The mitochondria, nucleus, and the endoplasmic reticulum are also critical compartments of endocytocised nanoparticles (Chithrani *et al.,* 2009; Su *et al.,* 2011). However, nanoparticles uptake within these compartments depends on nanoparticles size, with nanoparticles <5nm generally localizing in the nucleus (Buzea *et al.,* 2007). A study by Shukla *et al.* (2006), determining the intracellular fate of 3 and 8nm poly-L-lysine functionalized AuNPs confirmed internalization of the nanoparticles in the nucleus and lysosomal bodies of RAW264.7 mouse macrophage cells (Shukla *et al.,* 2006).

While the process of endocytosis is important, the exocytosis of the nanoparticles is equally important and must be understood. The nanoparticles remaining in the cell for a longer period after exposure increases the possibility of unintended chronic toxicity (Oh and Park, 2014). Thus, it is important to not only study uptake but also the exocytosis of the internalized nanoparticles from cells, to decisively confirm their long term safety.

1.2.3 Physico-chemical properties of gold nanoparticles influencing cellular toxicity

1.2.3.1 Size

Nanoparticles size does not only control endocytosis portals in cells but can be expected to influence cytotoxicity (Buzea *et al.,* 2007). Generally, small sized nanoparticles can easily transverse through tissues and cellular organelles, hence are thought to be most harmful as a result of their likelihood to penetrate nuclear cell membrane. The increased toxicity effect of smaller nanoparticles is also attributed to the high surface to volume ratios (Fadeel *et al.,*

2010; Nel *et al.,* 2006). In contrast, large nanoparticles are recognized by cells as foreign and are rapidly cleared from the blood stream (Simpson *et al.,* 2010). These studies have shown that large nanoparticles are unable to enter major organelles with the cells (Fadeel *et al.,* 2010; Nel *et al.,* 2006).

Nanoparticles with increasing diameter of over 40nm results in reduced translocation efficiency and a less pronounced cytotoxic effect (Simpson *et al.,* 2010). To examine the size dependent cytotoxicity of AuNPs, Pan *et al.* (2009) investigated the toxicity of triphenylphosphine (TPP) stabilized AuNPs with hydrodynamic size of 1.2nm, 1.4nm and 1.8nm; and 15nm in fibroblast (L929), epithelial (HeLa), macrophages (J774A1) and melanoma cell lines (SK- Mel-28). According to the toxicity data generated from this study, AuNPs with sizes of 1.4nm were the most cytotoxic, resulting in excessive necrotic cell death (Pan *et al.,* 2009). AuNPs with size of 15nm were shown to be non-toxic, even when the dose was increased 100-fold higher than the lethal dose (LC_{50}) of the small clusters (Pan *et al.,* 2009).

In another study, human bone marrow mesenchymal stem cells (hBMSCs) and hepatoma cells (HuH-7) were incubated with 5 and 30nm AuNPs, where more than 80% of cell survival was reported for the 30nm nanoparticles (Fan *et al.,* 2008). The cell viability was decreased to less than 60% after incubation with 5nm nanoparticles for 5 days (Fan *et al.,* 2008). Similarly, the size dependent toxicity of larger nanoparticles has also been investigated (Chen *et al.,* 2009). Gold nanoparticles of 20 and 100nm in diameters were shown not to have an effect on the viability of human retina microvascular endothelial cells (HRMECs) *in vitro* (Kim *et al.,* 2009); suggesting that nanoparticles with larger sizes may be non-toxic when tested *in vitro.* Even at high concentrations, nanoparticles with large sizes were reported to be non-toxic to cultured cells (Pan *et al.,* 2009). Even though further studies are

desirable, the results of these studies indicated that NPs with diameters of 10-30nm may be ideal for medical applications.

Whereas the concept of small particles being more toxic and large particles less toxic have been confirmed by most studies, opposite results have been reported. For example, AuNPs with a hydrodynamic size of 3–8nm were shown to not be cytotoxic, and reduced free radical species generation in macrophage cells (Alkilany and Murphy, 2010). Another study on embryonic lung fibroblasts showed significant oxidative DNA damage by 20nm AuNPs (Li *et al.,* 2009). In the study, a decrease in expression of DNA repair genes and cell cycle genes was also evident. Even though conflicting results have been reported on cytotoxicity of AuNPs of different diameters, most authors agree that aggregated particles are unable to cause adverse effect on cells (Dechnent and Simon, 2008).

1.2.3.2 Shape

The conception that shape may influence AuNPs toxicity has been attributed to the chemical molecules that are used to stabilize nanoparticles during synthesis (Simpson *et al.,* 2010). AuNRs for example have been shown to be toxic to human keratinocyte cells (HaCaT) than spherical gold nanomaterials (Chithrani *et al.,* 2009). Similarly AuNRs were reported to induce a loss of mitochondrial integrity on human breast adenocarcinoma cell line (MCF- 7) (Qiu *et al.,* 2010). The replacement of the CTAB molecule, a stabilizing agent used in the synthesis of AuNRs (gold nanorods), with ligands such as phosphatidyl choline was shown to reduce the toxicity of the nanorods.

1.2.3.3 Surface Chemistry

The surface chemistry does not only influence the interaction of the nanoparticles to the cells, but has been shown to be accountable for toxicity effects observed in nanoparticles toxicity. For example, Goodman *et al.* (2004) have shown that 2nm spherical AuNPs capped with quaternary amines as functional groups were moderately toxic to Cos-1 cells. The positively charged CTAB coated AuNPs in a study by Goodman *et al.* (2004) were found to be cytotoxic. Based on this reports, cationic or positively charged particles were shown to exert the highest cytotoxic effects upon interaction with cells than negatively charged particles (Oberdorster *et al.,* 2005). Selected *in vitro* and *in vivo* studies on gold nanoparticles uptake and their toxicity are summarized in Table 1.2 and 1.3.

Table 1.2: Summary of selected in vitro cytotoxicity studies in gold nanoparticles

Study	**Type of cell line**	**Shape, size and surface chemistry of AuNPs**	**Dose**	**Cytotoxicity test**	**Duration of exposure**	**Results**	**Reference**
Gold nanoparticles are taken up by human cells but do not cause acute cytotoxicity	Human leukemia cells (K562)	4, 12, or 18nm Citrate AuNPs	25mM - 250mM	3-(4,5-dimethylthiazol-2-yl)-2,5-diphenyltetrazolium bromide (MTT) assay	15 min, 1-24 h	Non-toxic to K562 cells	Connor *et al.,* 2005
The influence of polycaprolactone (PCL) coating on the internalization and cytotoxicity of gold nanoparticles	The human umbilical vein endothelial (ECV-304) cells	100nm Spherical non-coated and PCL-coated AuNPs	20µL	Microtubule staining	48h	The both AuNPs were found in the endosomes or lysosomes, cytoplasm, nucleic envelope, and nucleus. Bare were slightly toxic while PCL coated had no effect	Mao *et al.,* 2007
Disruption of HepG2 cell adhesion by gold nanoparticle and Paclitaxel disclosed by *in situ* QCM measurement	Human hepatocellular carcinoma (HepG2) cells	25±3.5 nm, spherical AuNPs	1.0nmol/L AuNPs,	MTT, quartz crystal microbalance (QCM) and flow cytometer assay	24 hrs	AuNPs show low cytotoxicity but can disrupt adhesion and enhance apoptosis of HepG2 cell.	Wei *et al.,* 2007

						Paclitaxel plus AuNPs inhibits the growth of HepG2 cell more effectively than Paclitaxel alone	
Gold nanoparticles and oxidative stress in *Mytilus edulis*	*Mytilus edulis*	13nm citrate stabilized AuNPs	1mM	Oxidative stress, Catalase activity, neutral red retention time assay, 2DE gels	24 hrs	AuNPs induced oxidative Stress in bivalves, especially in digestive gland	Tedesco *et al.,* 2008
Challenge in understanding size and shape dependent toxicity of gold nanomaterials in human skin keratinocytes	Human skin cell line HaCaT keratinocytes	1.5nm diameter CTAB coated AuNRs and citrate stabilized Spherical AuNPs	10 µL	MTT	24 hrs	Spherical AuNPs were non-toxic. AuNPs Nanorods were highly toxic due to presence of CTAB coat layer used for the synthesis of nanorods.	Wang *et al.,* 2008
Aqueous synthesis of gold nanoparticles and their cytotoxicity in human dermal fibroblast – fetal cells	Human dermal fibroblast-fetal cells	10-50nm Citrate coated spherical AuNPs	10, 50, 100, 200, 300µM	MTT	72 hrs	20nm were non-toxic even at 300µM	Qu and Lu, 2009.

Cellular uptake and toxicity of gold nanoparticles in prostate cancer cells: a comparative study of rods and spheres	Human prostate carcinoma PC-3 cells	30-90nm spherical AuNPs	1.5nM	MTT and lactate dehydrogenase (LDH) assay	88 hrs	No LDH leakage observed up to 34 nM. Plain spherical 50 and 90 nm in diameter induced the proliferation of PC cells	Arnida *et al.,* 2010
Pancreatic carcinoma cells are susceptible to noninvasive radio frequency fields after treatment with targeted gold nanoparticles	Pancreatic carcinoma cell line (EGFR-1, Panc-1, and Cama-1)	20nm spherical Spherical L cetuximab-conjugated AuNPs (L C225-AuNP)	100-nmol	Flow cytometer	36 hrs	Panc-1 showed 46% cell viability, Cama-1 cell had a viability of 92%.	Glazer *et al.,* 2010
Autophagy and oxidative stress associated with gold nanoparticles	MRC-5 human lung fibroblasts	20nm FBS coated AuNPs	1nM	Oxidative stress polymerase chain reaction (PCR) array, Lipid hydroperoxide assay, Western blotting	72 hrs	Oxidative damage, induced up regulation of antioxidants, stress response genes and protein expression	Li *et al.,* 2010
In vitro toxicity studies of polymer-coated gold nanorods	Mammary adenocarcinoma (SKBR3), Human	Length = 44.8±2.8nm and 41.8± 3.3nm	20uL	MTT assay		PEGylated particles did not induce	Raja *et al.,* 2010

	leukemia cells (HL60)	Width = 18.5 ±1.6nm and 11.7 ±1.4nm PEG coated nanorod and PSS-coated nanorods				toxicity to all the cells tested. PEGylated gold nanorods also exhibited better dispersion stability, PSS-coated rods tended to flocculate or cluster with induced toxicity	
Effects and uptake of gold nanoparticles deposited at the air–liquid interface of a human epithelial airway model	A549 cells, a human alveolar epithelial-like cell	15nm	200–2000µg	PCR, (ELISA)	4 and 24 hrs	No adverse effects from AuNPs were observed.	Brandenberger *et al.,* 2010

Table 1.3: Summary of selected in vivo cytotoxicity studies in gold nanoparticles

Study	**Study population**	**Size, shape and surfaces chemistry of AuNPs**	**Route of exposure**	**Dose**	**Cytotoxicity tests**	**Duration of exposure**	**Outcome**	**Reference**
Particle size-dependent organ distribution of gold nanoparticles after intravenous administration	Male WU Wistar-derived rats	10, 50, 100 and 250nm spherical AuNPs	Intravenously	1mL	Organ Index	24 hrs	The AUNPs were found in the liver and spleen. 10nm was present in all blood, liver, spleen, kidney, testis, thymus, heart, lung and brain. Larger particles were only detected in blood, liver and spleen.	De Jong *et al.,* 2008
Assessment of the *in Vivo* toxicity of Gold Nanoparticles	BALB/C Mice	3 to 100nm Non0coated AuNPs	Intraperitoneal	8 mg/kg/week	Physical and behavioral examination	21 days	AuNPs of 8,12,17, 37nm induced fatigue, loss of appetite, change of fur color, and weight loss. Most died within 21 days. 3-5 nm did not induce sickness.	Chen *et al.,* 2009
Biodistribution of gold nanoparticles	Female mice	2, 40 and 100 nm Negatively	Intratracheal	1.4-1.6 mg/kg	Organ index (liver)	1 day, 1-3 months and 6 months	AuNPs found in the liver and macrophages	Sadauskas *et al.,* 2009

in mouse lung following intratracheal instillation		charged spherical AuNPs-						
Toxicological effects of gold nanoparticles *in vivo* by different administration routes	Mice	13.5nm Spherical citrate-coated AuNPs	Oral, intraperitoneal routes and the tail vein intravenous injection	137.5–2200 µg/kg	Animal survival, weight, hematology, morphology, and organ index	14–28 days	AuNPs induced decrease in body weight, red blood cells, and hematocrit. No adverse effects were observed at low concentration of AuNPs. Oral admin caused a significant decrease in body weight, spleen index, and red blood cells.	Zhang *et al.,* 2010
Biodistribution of gold nanoparticles and gene expression changes in the liver and spleen after intravenous administration in rats.	Male Wistar rats	20nm	Tail-vein intravenous injection	0.2mL (0.01 mg/kg)	Organ index	1 day, 1 week, 1 and 2 month	AuNPs accumulated and persisted in the liver and spleen than other organs.	Balasubramanian *et al.,* 2010
Bioaccumulation and toxicity of gold	Male Mice C57/BL6	12.5 ± 1.7nm citrate	Intraperitoneal	40–400 µg/kg/day	Animal survival, weight,	8 days	The AuNPs were able to cross the brain	Lasagna-Reeves *et al.,*2010

nanoparticles after repeated administration in mice.		stabilized AuNPs			hematology, morphology, and organ index		barrier and accumulate in neural tissues but No toxicity was evident. But there was uptake in the spleen, kidney and liver	
Functionalized gold nanoparticles: a detailed *in vivo* multimodal microscopic brain distribution study	Male CD1 mice	15±1nm human serum albumin (HSA), polyallylamine hydrochloride, polystyrene-4-sulfonate coated AuNPs	Tail vein intravenous injection	150–200 µL	Organ index	0-7days	Functionalized AuNPs accumulate in the hippocampus, thalamus, hypothalamus, and the cerebral cortex.	Sousa *et al.,* 2010
Unexpected Toxicity of Monolayer Protected Gold Clusters Eliminated by PEG-Thiol Place Exchange Reactions	BALBc/c female mice	2.5±1.0nm PEG-coated AuNPs	Subcutaneous injection	200µL	Organ index	4 weeks	100 % survival at all the different concentrations of PEG-coated AuNPs. AuNPs present in the organs	Simpson *et al.,* 2010

1.2.4 Possible mechanisms of gold nanoparticle toxicity

1.2.4.1 Induction of inflammatory cytokines

Inflammatory and pro-inflammatory cytokines are released by cells as a late response to nanoparticles stimuli (Jeng and Swanson, 2006; Nel *et al.,* 2006). Cytokines are characterized by a group of signaling proteins that have specific function in cells, including communication, immune response and cell division (Jeng and Swanson, 2006; Nel *et al.,* 2006). These signaling classes of proteins are produced by different cells in the body, particularly epithelial, endothelial and macrophage cells following exposure to foreign substances. Interleukin 1 (IL-1), interleukin 6 (IL-6) and tumor necrosis factor α (TNF-α) are the commonly secreted cytokines across the different cell types. IL-6 for example is produced during acute phase response in cells (Jeng and Swanson, 2006; Nel *et al.,* 2006).

TNF-α is produced to increase the responsiveness of the cells to growth factors and to encourage signaling pathways that lead to cell proliferation. Cytokine release by cells exposed to AuNPs and other nanoparticles has been reported *in vitro* and in *in vivo* studies (Monteiro-Riviere *et al.,* 2005). For example, *in vitro* studies assessing the toxicity of single walled carbon nanotubes (SWCNT) and multi walled carbon nanotubes (MWCNT) in cultured skin cells have shown that both nanotubes can trigger the secretion of pro-inflammatory cytokines resulting in cell oxidative stress, and a decrease in cell viability (Monteiro-Riviere *et al.,* 2005).

Brandenberger *et al.* (2010) further investigated the effects of 15nm AuNPs stabilized with citrate ions in cultured A549 alveolar lung epithelial cells. The study reported the release of pro

and anti-inflammatory cytokines in cells 4hrs and 24hrs after treatment with the AuNPs. The expression of mRNA for the induction of inflammatory mediators TNFα, IL-8, IL-1, IL-2, IL-4, IL-6, IL-8, IL-10 and Interferon gamma (INFy) in the Brandenberger *et al.* (2010) study were measured by real time PCR (rtPCR).

Similarly, Gosens *et al.* (2010) investigated the *in vivo* effects of agglomerated and single 50nm and 250nm citrate stabilized AuNPs by studying the production levels of TNF-α and IL-6 in bronchoalveolar lavage fluid (BALF) of rats 3 and 24hrs post nanoparticles exposure. An increase in TNF-α and IL-6 levels was reported after 24hrs for 250nm single gold particles, whilst increased levels of TNF-α was observed after 3hrs for agglomerated 50nm nanoparticles.

1.2.4.2 Free radical generation and oxidative stress

Among the possible mechanisms of nanoparticles toxicity, oxidative stress remains an important factor. The stimulation of ROS (reactive oxygen species) generation by NPs in cells may take place at several levels, including the surface reactivity of nanoparticles with cellular components (Klotz and Sies, 2009). The interaction of nanoparticles with cell structures that are involved in regulating the reduction-oxidation status of the cell such as the mitochondria can trigger free radical generation (Klotz and Sies, 2009). Similarly, a reaction on the nanoparticle surface with cell surface receptors can generate ROS (Klotz and Sies, 2009). Figure 1.6 is a representative diagram showing the different mechanisms by which nanoparticles can induce the generation of free radical species in cells.

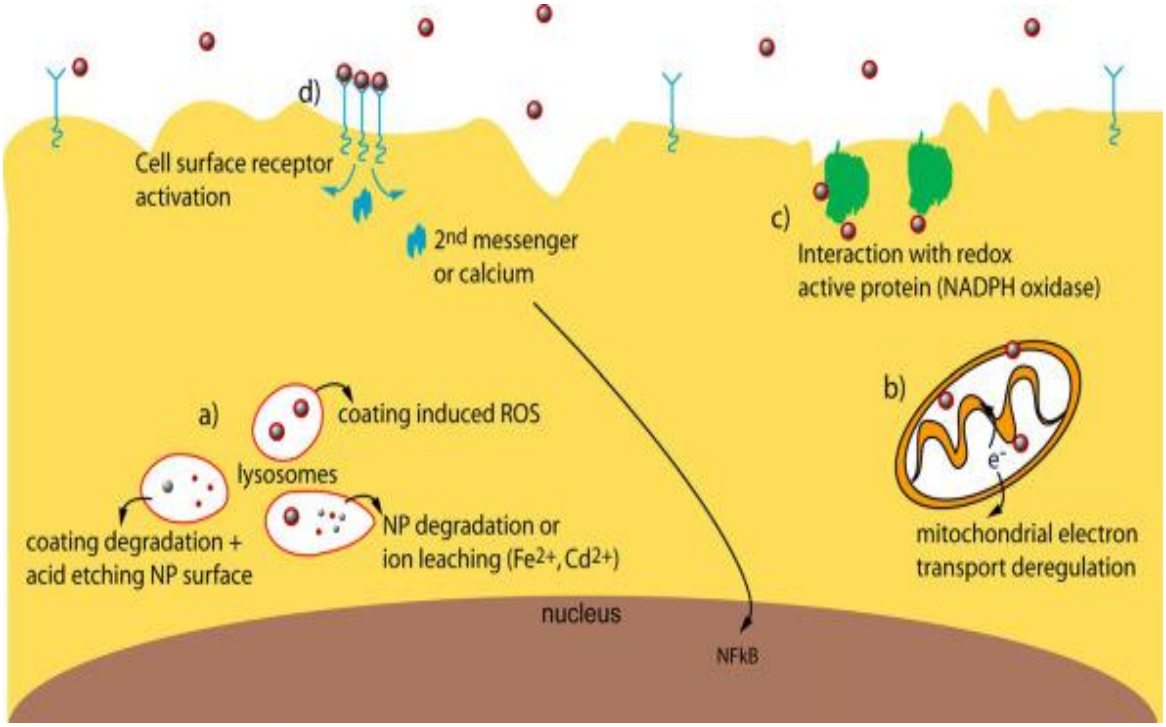


Figure 1.6: Diagram of the different pathways by which nanoparticles can induce oxidative stress (Soenen et al., 2011)

ROS species that are generated from these reactions are subdivided into two different types, including free radicals of the nitric oxide ($NO^{\cdot}$), hydroxide radicals ($^{\cdot}OH$), the superoxide anion ($O_2^{\cdot}$) and a non-radical free species of hydrogen peroxide (H_2O_2) and peroxynitrite ($ONOO^-$). The reactive groups or functional groups on the nanoparticles surfaces have been shown to produce different free radicals in cells, depending on the charge of the functional group (Schaeublin *et al.,* 2011). For example, positively charged particles containing a nitrogen atom with three reactive sites to form nitric oxide that can react further with superoxide, a by-product of the electron transport chain, to generate peroxynitrite, a powerful oxidant that is toxic to cells at elevated concentration (Schaeublin *et al.,* 2011). Thus, free radicals of $O_2^{\cdot}$, OH and non-radical species H_2O_2, are generated by cells following nanoparticles stimuli (Rahal *et al.,* 2014).

An excessive amount of free radicals in cells can damage membrane lipids, proteins and nucleic acids through lipid peroxidation, cell cycle arrest, mutagenesis and cell lysis (Hillegass *et al.,* 2010; Nel *et al.,* 2006; Lewinski *et al.,* 2008). However, biological cells possesses protective mechanisms against oxidative stress, such as the glutathione (GSH) redox system; that can neutralize excessive amount of free radical species to maintain the stability of intracellular redox status (Li *et al.,* 2008). The pathway for ROS generation in cells and the removal mechanisms are depicted in Figure 1.7.

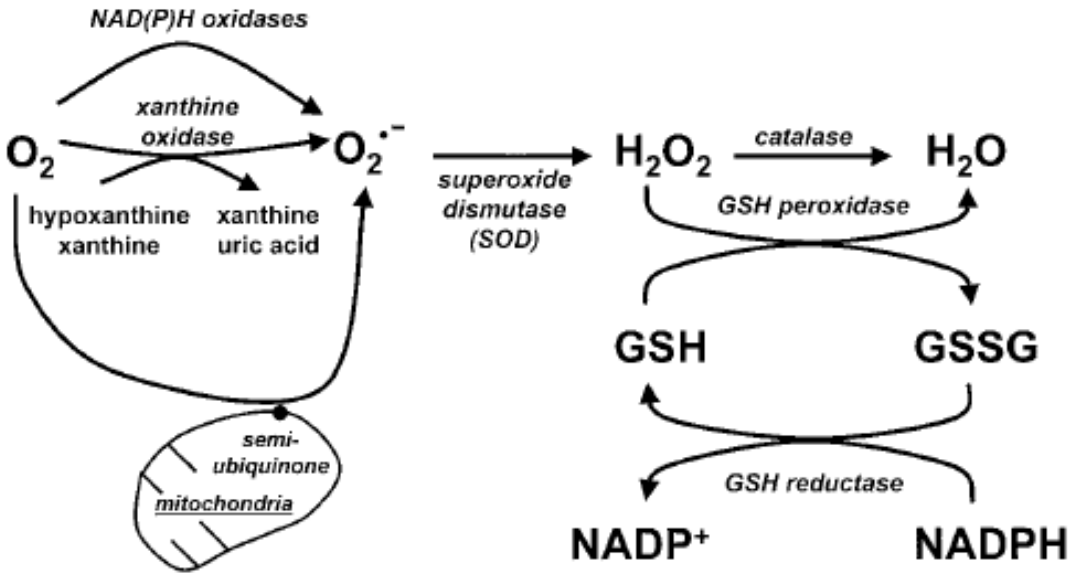


Figure 1.7: Pathway of ROS production and removal (adapted from Dröge, 2002)

Glutathione peroxidase (GPX), glutathione reductase, superoxide dismutase (SOD), and catalase (CAT) amongst others are generated when the cell undergo oxidative stress due to free radicals production (Donaldson and Stone, 2003). Besides offering protection from oxidative stress, some of these entities offer defense against DNA damage and cytotoxicity in cells (Zhang *et al.,* 2010). Oxidative stress related to AuNPs and the defense mechanisms has been elucidated in cells, including in a study by Thakor *et al. (2011)*. In the study, oxidative stress in HeLa and HepG2 cells treated with PEGylated gold nanoparticles reported a minimal toxicity to both cells. The observation was supported by the conclusion that excess ROS generation by cells was balanced by production of antioxidant enzymes in cells as a defense mechanism against oxidative stress (Thakor *et al.,* 2011).

1.2.4.3 DNA damage as a mechanism of nanoparticle toxicity

In addition to cytotoxicity, genotoxicity presents another form of injury to cells. Genotoxicity, which is the ability of an agent to cause DNA damage, can occur either indirectly via oxidative stress in cells due to elevated levels of ROS or directly when nanoparticles enter the nucleus to interact with genomic with DNA (Buzea *et al.,* 2007; Medina *et al.,* 2007; Singh *et al.,* 2009). A diagram showing the different mechanisms that nanoparticles can cause genotoxicity damage in cells is presented in Figure 1.8.

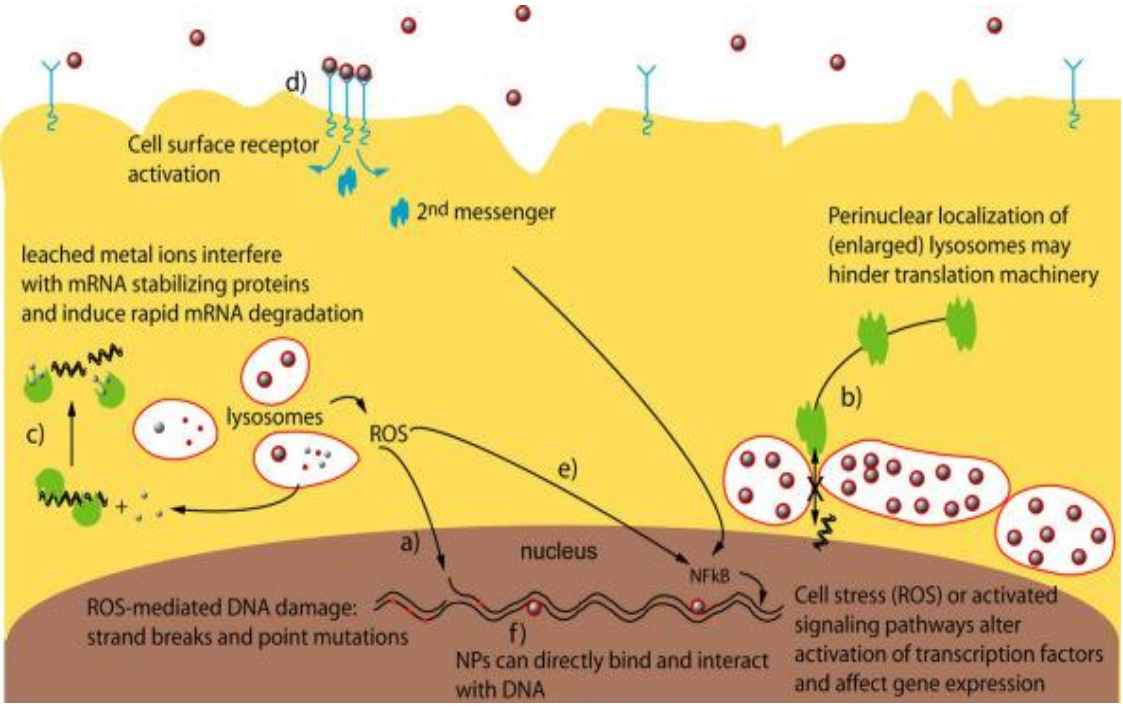


Figure 1.8: Diagram of the different mechanisms by which NPs can induce genotoxic effects or affect intracellular signaling pathways (Soenen et al., 2011)

Direct DNA damage to cell nuclear exposed to functionalized gold nanoparticles has been reported (Pan *et al.*, 2007). This was shown to depend on the diameter and surface coating of the nanoparticles. For example, Pan *et al.* (2007) revealed that 1.4nm AuNPs functionalized with triphenylphosphine (TPPMS) could enter the cells very easily and bind on double stranded DNA major grooves to disrupt cellular function. A similar study reported that AuNPs with nucleus targeting motifs can elicit significant damage of DNA and programmed cell death (Kang *et al.,* 2010). The perinuclear localization of NPs can obstruct genetic transcription and translation pathways that lead to the synthesis of proteins as shown in Figure 1.8F.

Nanoparticles localized in lysosomal compartments are likely to be degraded due to the acidic environment of these compartments. Nanoparticle contained with this compartment can escape to the cytoplasm and can interfere with surrounding proteins to induce DNA point mutations. As observed by Li and co-workers, high levels of DNA damage in cells that were treated with AuNPs were reported. In the study, the AuNPs were shown to be localized in cytoplasmic vesicles (Li *et al.,* 2008).

To ascertain if AuNPs could induce genotoxic damage to cells, several biochemical assays are used in literature, including studying the gene expression level of DNA repair genes. For example, Li *et al.* (2008) analyzed mutagenicity of DNA bases by measuring the quantity of 8-hydroxy-deoxyguanosine (8OHdG) in MRC-5 human fetal lung fibroblast cell line, after exposing the cells to different concentrations of citrate stabilized 20nm AuNPs. The down-regulation of DNA repair genes in this study suggested that AuNPs causes DNA damage. Regardless of the genetic damage caused by AuNPs as observed by Li *et al.* (2008), cytotoxicity was not observed in cell cultures. The comet assay, micronucleus assay and the chromosomal aberration test are reliable and sensitive method for quantifying and classifying DNA and structural damage in chromosomes. These techniques were utilized in this study and will be discussed in detail in the subsequent chapter.

1.2.4.4 Apoptosis as a model of cell injury

Adverse effects on cell proliferation, cytokine release, ROS and DNA damage can initiate cell injury or cell death through apoptosis (Proskuryakov *et al.,* 2003). Apoptosis, also referred to as ‘programmed cell death’ comprises of distinct morphological and biochemical changes in cells.

Apoptosis differs from necrosis (unplanned or accidental cell death) in that it may be beneficial to cells (Kruman and Mattson, 1999). The sequences of events underlying these two mechanisms are not well understood (Sun *et al.,* 2011). However, cell plasma membrane shrinkage and nucleus damage are morphological features in cells undergoing apoptosis. Cells undergoing necrosis on the other hand, are distinguished by swelling of the plasma membrane and eventual disintegration of the cell (Figure 1.9).

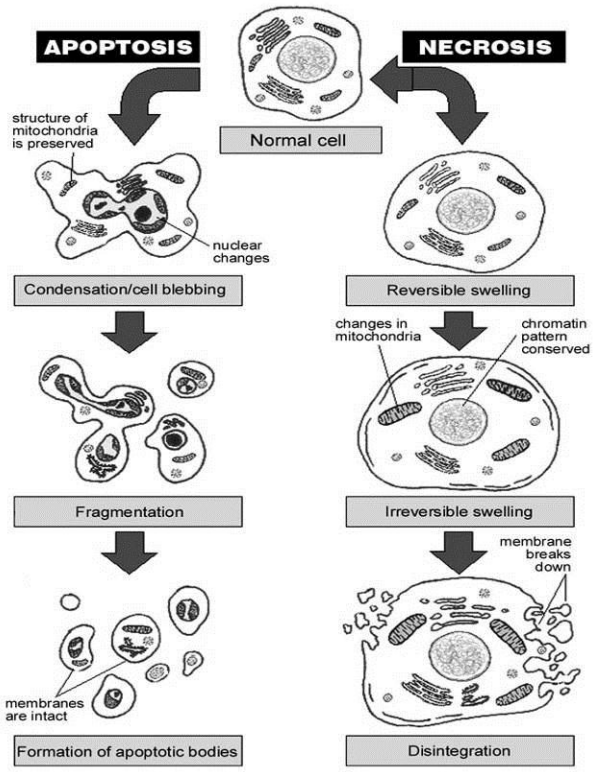


Figure 1.9: Morphological changes in cells undergoing apoptosis and necrosis (Sidnartha Ray, 2013).

Apoptosis and necrosis have been reported in cell lines that have been exposed to AuNPs. For example, Pan and co-workers found that AuNPs with 1.4nm in diameter elicited necrosis by oxidative stress and mitochondrial damage in HeLa cervix carcinoma epithelial cells (Pan *et al.,* 2009). Qui *et al.* (2010) reported on the ability of the positively charged CTAB coated AuNRs to cause apoptosis on human breast adenocarcinoma cells (MCF-7) due to an increased intracellular ROS production level on treated cells. Furthermore, Schaeublin *et al.* (2011) showed that the surface chemistry of the nanoparticles may determine whether cells die by apoptosis or necrosis. In this report, positive and negative charged AuNPs induced apoptosis through a depolarization of the mitochondrial membrane potential (MMP) and the release of intracellular calcium.

References

Alkilany AM and Murphy C. 2010. Toxicity and Cellular uptake of gold nanoparticles: What we have learned so far?. *Journal of Nanoparticle Research,* 12 (7): 2313- 2333.

Alkilany AM, Nagaria PK, Hexel CR, Shaw TJ, Murphy CJ, and Wyatt MD. 2009. Cellular Uptake and Cytotoxicity of Gold Nanorods: Molecular Origin of Cytotoxicity and Surface Effects. *Nanomedicine,* 5 (6): 701- 708.

Arnida M, and Ghandeharia H. 2010. Cellular uptake and toxicity of gold nanoparticles in prostate cancer cells: a comparative study of rods and spheres. *J. Appl. Toxicol*, 30: 212–217.

Aslan K, Luhrs CC and Perez-Luna VH. 2004. Controlled and reversible aggregation of biotinlyted gold nanoparticles with Streptavidin. *Journal Phys Chem B*, 108: 1561-15639.

Balasubramanian SK, Jittiwat J, Manikandan J, Ong CN, Yu LE, and Ong WY. 2010. Biodistribution of gold nanoparticles and gene expression changes in the liver and spleen after intravenous administration in rats. *Biomaterials,* 31:2034–2042.

Baptista P, Pereira E, Eaton P, Doria G, Miranda A, Gomes I, Quaresma P, and Franco R. 2008. Gold nanoparticles for the development of clinical diagnostics methods. *Anal. Bioanl. Chem*, 391: 943- 950.

Basiruddin SK, Saha A, and Pradhan N. 2010. Functionalized Gold Nanorod Solution via Reverse Micelle Based Polyacrylate Coating. *Langmuir*; 26: 7475-7481.

Bhattacharya R, Patra CR, Earl A, Wand S, Katarya A, Lu L, and Mukherjee P. 2007. Attaching folic acid to gold nanoparticles using non-covalent interaction via different polyethylene glycol backbones and targeting cancer cells. *Nanomedicine: Nanotechnology, Biology, and Medicine,* 3: 224–238.

Brandenberger C, Rothen- Rutishauser B, Muhfeld C., Schmid O, Ferron GA, and Maier K L. 2010. Effects and uptake of gold nanoparticles deposited at the air- liquid interface of a human epithelial airway model. *Toxicology and Applied Pharmacology,* 242: 56-65.

Brown SD, Native P, Smith J, Stirling D, Edward PR, and Venugopal B. 2010. Gold nanoparticles for the improved anticancer drug delivery of the active component of oxaliplatin. *Journal American Chemical Society,* 132: 4679- 4689.

Brust M, Walker D, Schiffin DJ, and Whyman R. 1994. Synthesis of thiol derivative gold nanoparticles in a two phase liquid-liquid system. *J. Chem. Soc. Chem. Commun,* 7 (1): 801-802.

Buzea C, Blandino IP, and Robbie K. 2007. Nanomaterials and nanoparticles: sources and toxicity. *Biointerphases,* 2 (4): MR17-MR172.

Chen PC, Mwakwari SC, and Oyelere AK. 2008. Gold nanoparticles: from medicine to nanosensing. *Nanotechnology, Science and Application*, 1: 45-66.

Chithrani BD, Steward A, Allen C, and Jaffary DA. 2009. Intracellular uptake, transport, and processing of nanostructures in cancer cells. *Nanomedicine: Nanotechnology, Biology, and Medicine,* 5: 8–127

Connor EE, Mwamuka J, Gole A, Murphy CJ, and Wyatt MD. 2005. Gold nanoparticles are taken up by the cells but do not cause acute cytotoxicity. *Small*, 1: 325- 327.

De Jong AH, and Borm PJA. 2008. Drug delivery and nanoparticles: Applications and hazards. *International Journal of Nanomedicine*, 3 (2):133-149.

Dechent JW and Simon U. 2008. Function follows form: Shape complementarity and nanoparticles toxicity. *Nanomedicine*, 3 (5): 601- 603.

Dobrovolskaia AK and McNeil SE. 2007. Characterization of nanoparticles for therapeutics. *Nanomedicine,* 2 (6): 789- 803.

Donaldson K and Stone V. 2003. Current hypothesis on the mechanisms of toxicity of ultrafine particles. *Ann Ist Super Sanità*; 39 (3): 405-410.

Drechsler U, Erdogan, and Rotello VM. 2004. Nanoparticles: Scaffolds for Molecular Recognition. *Chem. Eur. J*, 10: 5570-5579.

Dröge W. 2002. Free radicals in the physiological control of cell function. Physiological Reviews, 82 (1): 47-95.

Fadeel B and Garcia-bennet AE. 2010. Better safe than sorry: Understanding the toxicological properties of inorganic nanoparticles manufactured for biomedical applications. *Advanced Drug Delivery Reviews*, 62: 362- 374.

Fan JH, Hung WI, Li WT, and Yeh JM. 2008. Biocompatibility and study of gold nanoparticles to human cells. 13th International Conference on Biomedical Engineering ICBME 2008 (3-6 Dec) Singapore Berlin, 870- 873.

Frens G. 1973. Controlled nucleation for the regulation of the particle size in monodisperse gold suspensions. *Nature (London) Phys Sci*, 241:20–22.

Ghosh O, Han G, De M, Kim CK, and Rotello VM. 2008. Gold Nanoparticles in delivery applications. *Advanced Drug Delivery Reviews*, 60: 1307-1315.

Gianvincenzo PD, Marradi M, Martínez-Ávila OM, Bedoya LM, Alcamí J, Penadés S. 2010. Gold nanoparticles capped with sulfate-ended ligands as anti-HIV agents. *Bioorganic & Medicinal Chemistry Letters*, 20: 2718–2721.

Glazer ES, Massey KL, Zhu C, and Curleybn SA. 2010. Pancreatic carcinoma cells are susceptible to noninvasive radio frequency fields after treatment with targeted gold nanoparticles. *Surgery,* 148: 319-324.

Goodman CM, McCusker CD, Yilmaz T, and Rotello VM. 2004. Toxicity of gold nanoparticles functionalized with cationic and anionic side chains. *Bioconjugate Chem,* 15: 897- 900.

Grubbs RB. 2007. Roles of polymer ligands in nanoparticle stabilization. *Polymer Reviews,* 47 (2); 197- 215.

Gu YJ, Cheng J, Lin C, Lam YW, Cheng SH, and Wong WT. 2009. Nuclear penetration of surface functionalized gold nanoparticles. *Toxicology and Applied Pharmacology*, 237; 196-204.

Hainfeld JF, Slatkin DN, Focella TM, and Smilowitz HM. 2006. Gold nanoparticles: A new X-ray contract agent. *The British Journal of Radiology,* 79, 248–253.

Han G, Martin CT, and Rotello VM. 2006. Stability of gold nanoparticle-bound DNA toward biological, physical, and chemical agents. *Chem. Biol. Drug Des,* 67: 78–82.

Hillegass JM, Shukla A, Lathrop SA, MacPherson MB, Fukagawa NK, and Mossman BT. 2010. Assessing nanotoxicity in cells *in vitro*. *Wiley Interdiscip Rev Nanomed Nanobiotechnology*, 2 (3): 219- 231.

Hirn S, Behnke MS, Schleh C, Wenk A, Lipka J, Schäffler M, Takenaka S, Möller W, Schmidn G, Simon U, Kreyling WG. 2011. Particle size-dependent and surface charge-dependent biodistribution of gold nanoparticles after intravenous administration. *European Journal of Pharmaceutics and Biopharmaceutics*, doi:10.1016/j.ejpb.2010.12.029.

Hong R, Han G, Fernandez JM., Kim BJ, Forbes NS, and Rotello VM. 2006. Glutathione mediated release using monolayer protected nanoparticle carriers. *J. Am. Chem. Soc,* 128: 1078- 1079.

Hostetler MJ, Templeton AC, and Murray R W. 1999. Dynamics of Place Exchange Reactions on Monolayer-Protected Gold Cluster Molecules. *Langmuir*; 15: 3782-3789.

Huang Z, Park JI, Watson DS, and Szoka FC Jr. 2006. Facile synthesis of multivalent nitriloacetic acid (NTA) and NTA conjugated for analytical and drug delivery applications. *Bioconjugate chem*, 17 (6):1592-1600.

Jeng HA, and Swanson J. 2006. Toxicity of metal oxide nanoparticles in mammalian cells. *J Environ Sci Health Hazard Subst Environ Eng,* 41 (12): 2699-711.

Jennings T, and Strouse G. 2007. Past, present, and future of gold nanoparticles. *Adv. Exp. Med. Biol*. 620: 34.

Kawano T, Yamagata M, Takahashi H, Niidome Y, Yamada S, Katayama Y, and Niidome T. 2006. Stabilizing of plasmid DNA in vivo by PEG-modified cationic gold nanoparticles and the gene expression assisted with electrical pulses. *J. Control. Release,* 111: 382–389.

Khlebtsov and Dykman. 2011. Biodistribution and toxicity of gold nanoparticles: a review of in vitro and in vivo studies. *Chemical Society Reviews,* 40: 1647-1671.

Kim JH, Kim KW, Kim MH, and You YS. 2009. Intravenously administered gold nanoparticles pass through the blood- retinal barrier depending on the particle size, and induce no retinal toxicity. *Nanotechnology*, 20: 1-8.

Klotz L and Sies H. 2009. Cellular Generation of Oxidants: Relation to Oxidative Stress. Weinheim: Wiley, Chapter 3. 45-61.

Kumar SA, Peter Y-A, and Nadeau J. Biosynthesis, separation and conjugation of gold nanoparticles to doxorubicin for cellular uptake and toxicity. *Nanotechnology*. doi:10.1088/0957-4484/19/49/495101

Lasagna-Reeves C, Gonzalez-Romero D, Barria MA, Olmedo I, Clos A. Ramanujam VM S, Urayama A, Vergara L, and Soto C. 2010. Bioaccumulation and toxicity of gold nanoparticles after repeated administration in mice. *Biochem Biophys Res Commun,* 393:649–655.

Lee JS, Green JJ, Love KT, Sunshine J, Langer R, and Anderson D.G. 2009. Gold, poly (β-amino ester) nanoparticles for small interfering RNA delivery. *Nano Lett,* 9: 2402–2406.

Levy R, Shaheen U, Cesbron Y, and See V. 2010. Gold nanoparticle delivery in mammalian live cells: a critical review. *Nano Reviews*, 1: 4889- 4894.

Lewinski N, Colvin V, Drezek R. 2008. Cytotoxicity of nanoparticles. *Small*. 4 (1): 26-49.

Li JJ, Hartono D, Ong CN, Bay BH, and Yung LYL. 2008. Autophagy and oxidative stress associated with gold nanoparticles. *Biomaterials,* 31: 5996-6003.

Li JJ, Zou D, Harton CN, Ong B, and Laung-Yung Y. 2008. Gold nanoparticles induce oxidative damage in lung fibroblast *in vitro*. *Advanced Materials,* 20: 138-142.

Liang M, Lin C, Whittaker MR, Minchin RF, Montero MJ, and Toth I. 2010. Cellular Uptake of densely packed polymer coatings on gold nanoparticles. *ACS Nano*, 4 (1): 403- 413.

Liu Y, Shipton MK, Kaufman ED, and Franzen S. 2007. Synthesis, Stability and Cellular Internalization of Gold Nanoparticles Containing Mixed Peptide-Poly (ethylene glycol) Monolayers. *Anal. Chem,* 79 (6): 2221-2229.

Low A and Bansal V. 2010. A visual tutorial on the synthesis of gold nanoparticles. *Biomed Imaging Interv J 2010; 6(1):e9.*

Lu X, Tuan HY, Korgelc BA, and Xia Y. 2008. Facile Synthesis of Gold Nanoparticles with Narrow Size Distribution by Using AuCl or AuBr as the Precursor. *Chemistry*, 14(5): 1584–1591.
Mao Z, Wang B, Ma L, Gao C, and Shen J. 2007. The influence of polycaprolactone coating on the internalization and cytotoxicity of gold nanoparticles. *Nanomedicine: Nanotechnology, Biology, and Medicine,* 3: 215–223.

Medina C, Santoz- Martinez NJ, Radomski A, Corrigan OI, and Radomski MW. 2007. Nanoparticles: pharmacological and toxicological significance. *British Journal of Pharmacology*, 150: 552- 558.
Miranda A, Malheiro E, Eaton P, Carvalho PA, and Pereira E. 2011. Synthesis of gold nanocubes in aqueous solution with remarkable shape-selectivity. *Journal of Porphyrins and Phthalocyanines*, 15 (6): 441.

Monteiro-Riviere NA, Nemanich RJ, Inman AO, Wang JJ, and Riviere AE. 2005. Multi-walled carbon nanotube interactions with human epidermal keratinocytes, *Toxicology letters,* 155 (3): 377-384.

Mukherjee P, Ahmad A, Mandal D, Senapati S, Sainkar SR, Khan MI, Ramani R, Parischa R, Ajayakumar PV, Alam M, Sastry M, Kumar R. Angew. *Chem 2001; 113:3697–3700.Angew. Chem. Int*. Ed 2001; 40:3585–3588.

Murphy CJ, Gole AM., Stone JW., Sisco PN., Alkilany AM., Goldsmith EC, and Baxter S C. 2008. Gold Nanoparticle in Biology: Beyond Toxicity to cellular Imaging. *Acc. Chem. Res*, 41 (12): 1721–1730.

Nahiidi S, Jafari M, Fdalat M, Raymond K, Khademhosseini A and Chen P. 2013. Biocompatibility of engineered nanoparticles for drug delivery. *Journal of Controlled release,* 166: 182- 194.

Nel A, Xia T, Madler L, and Li N. 2006. Toxic potential of materials at the nano level. *Science,* 311: 622.

Niidome T, Yamagata M, Okamoto Y, Akiyama Y, Takahashi H, and Niidome Y. 2006. PEG-modified gold nanorods with a stealth character for in vivo applications. *Journal of Controlled Release,* 114: 343- 347.

Noh SM, Kim WK, Kim SJ, Kim JM Baek KH, and Oh YK. 2007. Enhanced cellular delivery and transfection efficiency of plasmid DNA using positively charged biocompatible colloidal gold nanoparticles. *Biochim. Biophys. Acta,* 1770, 747–752.

Oberdorster G, Oberdorster E, and Oberdorster J. 2005. Nanotoxicology: An Emerging Discipline Evolving from Studies of Ultrafine Particles. *Environ. Health Perspect*. 113: 823.

Oh E, Delehanty JB, Sapsford KE, Susumu K, Goswami R, Blanco-Canosa JB, Dawson P E, Granek J, and Medintz IL. 2011. Cellular Uptake and Fate of PEGylated Gold nanoparticles Is Dependent on Both Cell-Penetration Peptides and Particle Size. *ACS Nano*, 5 (8): 6434-6448.

Oh N and Park J. 2014. Surface chemistry of Gold nanoparticles mediates their exocytosis in macrophages. *ACS Nano*, 8 (6) 6232-6241.

Ostuni E, Yan L, and Whitesides GM. 1999. The interaction of proteins and cells with self-assembled monolayers of alkanethiolates on gold and silver. *Colloids and Surfaces B: Biointerfaces*, 15: 3-30.

Otsuka H, Nagasaki Y, and Kataoka K. 2003. PEGylated nanoparticles for biological and pharmaceutical applications. *Advanced Drug Delivery Reviews,* 55: 403- 419.

Pan Y, Neuss S, Leifert A, Fischler M, Wen F, Simon U, Schmid G, Brandau W, and Jansen Denchet W. 2007. Size-dependent cytotoxicity of gold nanoparticles. *Nanoparticle Toxicity,* 3 (11): 1941- 1949.

Panariti A, Miserochhi G, and Rivolta I. 2012. The effect of nanoparticle uptake on cellular behavior: disrupting or enabling functions? *Nanotechnology, Science and Applications*, 5: 87-100.

Patra CR, Bhattacharya R, Mukhopadhyay D, and Mukherjee P. 2010. Fabrication of gold nanoparticles for targeted therapy in pancreatic cancer. *Advanced drug delivery Reviews,* 62: 346- 361.

Patra HK, Banerjee S, Chaudhuri U, Lahiri P, and Dasgupta AK. 2007. Cell selective response to Gold Nanoparticles. *Nanomedicine,* 3: 111- 119.

Pillay J, Ozoemena KI, Tshikhudo R, and Moutloali R. 2010. Monolayer-Protected Clusters of Gold Nanoparticles: Impacts of Stabilizing Ligands on the Heterogeneous Electron Transfer Dynamics and Voltametric Detection. *Langmuir,* 26 (11): 9061–9068.

Pissuwan D, Cortie CH, Valenzuela SM, and Cortie MB. 2010. Functionalized gold nanoparticles for controlling pathogenic bacteria. *Trends Biotechnol*, 28 (4): 207-13.

Pissuwan D, Niidome T, and Cortie MB. 2009. The forth application of gold nanoparticles in drug and gene delivery systems. *Journal of Controlled Release,* 1-7.

Prencipe G, Tabakman SM, Welsher K, Liu Z, Goodwin AP, Zhang L, and Dai H. 2009. PEG branched polymer for functionalization of nanomaterials with ultra-long blood circulation. *J. Am. Chem. Soc,* 131 (13) 4783-4787.

Qiu Y, Liu Y, Wang L, Xu L, Bai R, Ji Yinglu, Wu X, Zhao Y, Li Y, and Chen C. 2010. Surface chemistry and aspect ratio mediated cellular uptake of Au nanorods. *Biomaterials,* 31: 7606-7619.

Qiu Y, Liu Y, Wang L, Xu L, Bai R, Ji Yinglu, Wu X, Zhao Y, Li Y, and Chen C. 2010. Surface chemistry and aspect ratio mediated cellular uptake of Au nanorods. *Biomaterials,* 31: 7606-7619.

Qu Y, and Lu X. 2009. Aqueous synthesis of gold nanoparticles and their cytotoxicity in human dermal fibroblast–fetal. *Biomedical Materials,* 4:025007. doi: 10.1088/1748-6041/4/2/025007.

Rahal A, Kumar A, Singh V, Yadav B, Tiwari R, Cakraborty S, and Dhama K. 2014. Oxidative stress, Prooxidants and Antioxidants: The Interplay, *Biomed Res Int.*761264.

Raja G, Rayavarapu RG, Petersen W, Hartsuiker L, Chin P, Janssen H, van Leeuwen FW B, Otto C, Manohar S, and Leeuwen TG. 2010. *In vitro* toxicity studies of polymer-coated gold nanorods. *Nanotechnology,* 21: 145-149.

Rana S, Bajaj A, Mout R, and Rotello VM. 2011. Monolayer coated gold nanoparticles for delivery applications. *Advanced Drug Delivery Reviews,* 64 (2): 200- 216

Rosi AL, Giljohann DA, Thaxton CS, Lytton-Jean AKR, Han MS, and Mirkin CA. 2006. Oligonucleatide- Modified Gold Nanoparticle for Intracellular Gene regulation. *Science*, 312: 1027-1030.

Sadauskas E, Jacobsen NR, Danscher G, Stoltenberg M, Vogel U, Larsen A, Kreyling W, and Wallin H. 2009. Biodistribution of gold nanoparticles in mouse lung following intratracheal instillation. *Chemistry Central Journal*, 3:16.

Salata OV. 2004. Applications of nanoparticles in biology and medicine. *Journal of Nanobiotechnology,* 2:3.

Sarah B. 2010. Breath test to detect cancer may be possible, say scientists. http://www.guardian.co.uk/world/2010/aug/11/breath-test-detect-cancer-scientists (Accessed 25 May 2011).

Schaeublin NM., Braydich-Stolle LK, Schrand AM, Mileer JM, Hutchison J, Schalegr JJ, and Hussain SM. 2011. Surface charge of gold nanoparticles mediates mechanism of toxicity, *Nanoscale,* 3: 410-420.

Shenoy D, Fu W, Li J, Crasto C, Jones G, DiMarzio C, Sridhar S, and Amiji M. 2006. Surface Functionalization of Gold nanoparticles using hetero- bifunctional poly (ethylene glycol) spacer for intracellular tracking and delivery. *International Journal of Nanomedicine*, 1(1): 51- 57.

Simpson CA., Huffman BJ, Gerdon AE, and Cliffel DE. 2010. Unexpected Toxicity of Monolayer Protected Gold clusters Eliminated by PEG- Thiol Place Exchange Reactions. *Chem. Res. Toxico*, A-E.

Singh N, Manshian B, Jenkins GJ, Griffiths SM, Williams PM, Mafffeis TG, Wright CJ, and Doak SH. 2009. NanoGenetoxicology: the DNA damaging potential of engineered nanomaterials. *Biomaterials*, 30: 3891- 3814.

Soenen SJ, Montenegro JM, Park WJ, De Smelt SC, and Braeckmans K. 2011. Cellular toxicity of inorganic nanoparticles: common aspect guidelines for improved nanotoxicity evaluation. *Nanotoday*, 4:446-465.

Sousa F, Mandal S, Garrovo C, Astolfo A, Bonifacio A, Latawiec D, Menk RH, Arfelli F, Huewel S, Legname G, Galla HJ, and Krol S. 2010. Functionalized gold nanoparticles: a detailed in vivo multimodal microscopic brain distribution study. *Nanoscale, 2* (12):2 826-34.

Sun L, Li Y, Liu X., Jin M, Zhang L, Du Z, Guo C, Huang P, and Sun Z. 2011. Cytotoxicity and mitochondrial damage caused by silica nanoparticles. *Toxicology in vitro,* 2011, 8:1619- 1629.

Takahashi H, Niidome Y, Niidome T, kaneko K, Kawasaki H, and Yamada S. 2006. Modification of gold nanorods Using Phosphatidylcholine to reduce cytotoxicity. *Langmuir,* 22: 2-4.

Takenaka S, Karge E, and Kreyling WG. 2006. Distribution pattern of inhaled ultrafine gold nanoparticles in the rat lung. *Inhalation Toxicology,* 18:733–40.

Templeton AC, Chen S, Gross SM, and Murray RW. 1999. Water-soluble, Isolable Gold Clusters Protected by Tiopronin and Coenzyme A Monolayer. *Langmuir*; 15: 66-76.

Templeton AC., Wuelfing WP, and Murray RW. 2000. Monolayer-Protected Cluster Molecules. *Accounts of Chemical Research*, 33 (1): 27-36.

Thakor AS, Paulmurugan R, Kempen P, Zavaleta C, Sinclair R, Tarik F. Massoud TF, and Gambhir SS. 2011. Oxidative Stress Mediates the Effects of Raman- Active Gold Nanoparticles in Human cells. *Nanoparticle Cytotoxicity*, 7 (1): 126- 136.

Tiwari PM, Vig K, Dennis VA and Singh SR. 2011. Functionalized gold nanoparticles and their biomedical applications. *Nanomaterials*, 1: 31- 63.

Tong S, Sugimoto K, Tanda K, and Earnshaw WC. 2007. Three distinct stages of apoptotic nuclear condensation revealed by time-lapse imaging, biochemical and electron microscopy analysis of cell free apoptosis. *Exp Cell Res,* 313 (16): 3635- 3644.

Turkevich J, Stevenson PC, and Hillier J. 1951. A study of the nucleation and growth processes in the synthesis of colloidal gold. *Discuss Faraday Soc*, 11:55–75.

Vigderman L and Zubarev ER. 2013. Therapeutic platforms based on gold nanoparticles and their covalent conjugates with drug molecules. *Advanced Drug Delivery Reviews*, 65: 663-676.

Wei XL, Mo ZH, Li B, and Wei JM. 2007. Disruption of HepG2 cell adhesion by gold nanoparticle and Paclitaxel disclosed by in situ QCM measurement. *Colloids and Surfaces B: Biointerfaces,* 59: 100–104.

Wu HY, Liu M, and Huang M H.2006. Direct Synthesis of Branched Gold Nanocrystals and Their Transformation into Spherical Nanoparticles. *J. Phys. Chem. B* 2006, *110,* 19291-19294.

Xie J, Peng S, Brower N, Pourmand N, Wang SX, and Sun SH. 2006. One-pot synthesis of monodisperse iron oxide nanoparticles for potential biomedical applications. *Pure and Applied Chemistry,* 78 (5):1003-1014, 2006.

Zhang XD, Wu HY, Wu D, Wang YY, Chang JH, Zhai ZB, Meng AM, Liu PX, Zhang LA, Fan FY. 2010. Toxicologic effects of gold nanoparticles in vivo by different administration routes. *International Journal of Nanomedicine,* 5: 771–781.

Zhang Z, Jia J, Lai Y, Ma Y, Weng J, and Sun L. 2010a. Conjugating folic acid to gold nanoparticles through glutathione for targeting and detecting cancer cells. *Bioorganic and Medicinal Chemistry*, 18: 5528-5534.

Zhang Z, Ross RP, and Roeder RK. 2010b. Preparation of functionalized gold nanoparticles as a targeted X- ray contrast agent for damaged bone tissue. *Nanoscale,* 2: 582.

Zhou H, Li X, Lemoh H, Zhang B, and Yan B. 2010. Structural confirmation and quantification of individual ligands from the surfaces of multi- functionalized gold nanoparticles. *Analyst*, 135: 1210-1213.

CHAPTER 2

PHYSICO-CHEMICAL CHARACTERIZATION OF CITRATE STABILIZED AND ALKYLTHIOLATED PEG-GOLD NANOPARTICLES IN CELL GROWTH MEDIUM

2.1 Introduction

The physical and chemical characteristics of nanomaterials in cell culture medium need to be assessed for *in vitro* toxicity studies (Murdock *et al.,* 2008; Warheit, 2008). The morphology, particle size, surface chemistry and the state of dispersion of the nanoparticles are important factors that need to be defined (Murdock *et al.,* 2008; Aillon *et al.,* 2009). As previously described, these characteristics provide the basis for understanding the interaction of nanomaterials with the cells and the properties that might be responsible for their biological activity or response (Powers *et al.,* 2006; Bihar *et al.,* 2008; Gosens *et al.,* 2012).

Cell culture medium consists of a variety of organic and inorganic compounds and an excessive amount of serum proteins that are required for optimal cell growth (Horie *et al.,* 2009). Nanoparticles have a high surface reactivity, and as such are prone to non-specific binding with media components to form secondary nanoparticles or aggregates (Dutta, 2007; Sun *et al.,* 2011). As such methods have been devised to characterize these nanoparticles in biological medium before exposure to cells. The most popular being the qualitative analysis of nanoparticles morphology and size by microscopic techniques such as transmission electron microscopy (TEM), scanning electron microscopy (SEM) and atomic force microscopy (AFM). Techniques such as Fourier transform infrared spectroscopy (FTIR), nuclear magnetic

resonance (NMR), gel electrophoresis, ultraviolet-Visible (UV-Vis) spectrometer and the dynamic light scattering (DLS) techniques are used to measure nanoparticles concentration, size and surface chemistry (Amendola and Meneghetti, 2009; Zhou *et al.,* 2010).

In this chapter, the physico-chemical properties of the AuNPs were assessed in RPM-1640 and EMEM cell culture medium, supplemented with 10% fetal bovine serum (FBS) using TEM for morphology and particle size distribution (PSD) analysis of the nanoparticles, UV-Vis for measuring the absorption and scattering properties of AuNPs, DLS for zeta potential measurement and the FTIR to confirm surface functional groups on the nanoparticles surfaces. The results from this study will give an indication on the dispersity of the AuNPs suspension in the two cell growth medium as well as an indication on the stability of the nanoparticles when exposed to cells. The principles of the techniques used are outlined below.

DLS has been identified as one of the most established method to assess surface characteristics of colloidal particles in the size range of 1nm to 5μm (Powers *et al.,* 2006; Mahl *et al.,* 2010). Furthermore, size distribution and zeta potential of metal nanoparticles, including gold has been evaluated by DLS measurements (Mahl *et al.,* 2010). DLS uses scattered light to measure the movement of particles in liquid environment (Jans *et al.,* 2009). This movement, referred to as the Brownian motion is proportional to the hydrodynamic size of the particles and colloids (Brar and Verma, 2011). By this technique, the zeta potential of nanoparticles, representing the chemical charge on the surface of the nanoparticles has been assessed (Powers *et al.,* 2009). The zeta potential governs the magnitude of the interaction between colloidal particles in a solution and hence gives the stability of the nanoparticles in solutions. A diagram illustrating an association between zeta potential measurement and the pH of the nanoparticles is shown in Figure 2.1.

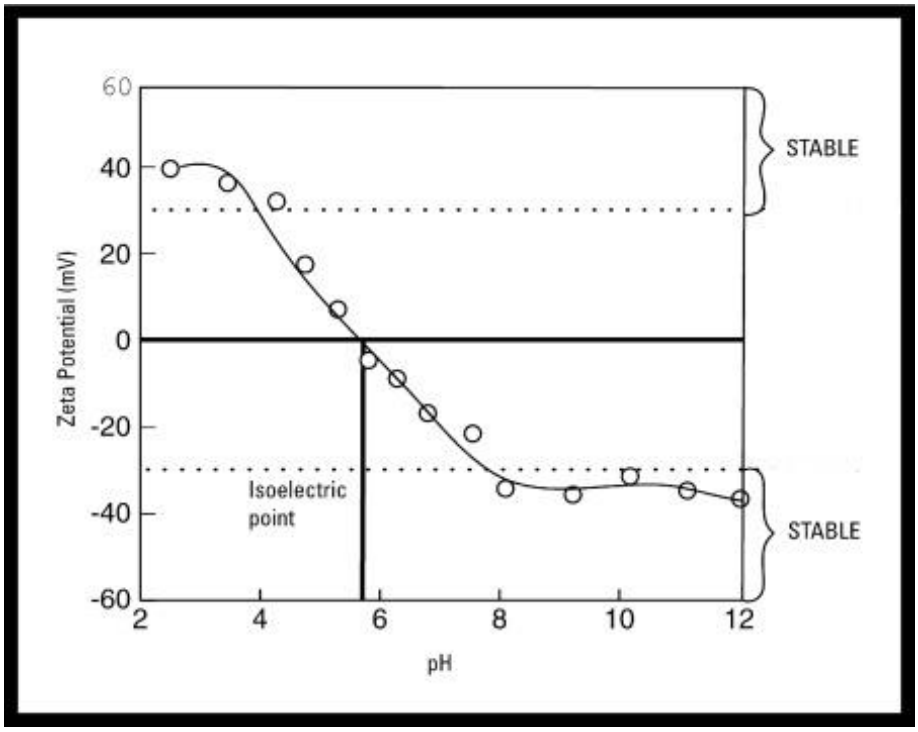


Figure 2.1: A plot of zeta potential vs. pH showing values where nanoparticle would be expected to be stable (downloaded from http://www.silver-colloids.com, accessed 25 May 2012).

As illustrated in Figure 2.1, the pH of the nanoparticles solution significantly affects the zeta potential measurements. A larger negative or positive zeta potential indicate enhanced stability of the colloidal suspension, whereas a low zeta potential value indicate a reduced stability of the particles.

The UV-Vis spectrophotometer has been a technique of choice to monitor the size, aggregation of nanoparticles, including gold in aqueous solution (Jain *et al.,* 2006; Amendola and Meneghetti, 2009). Nanoparticles size, concentration as well as composition have been evaluated by spectrophotometric analysis. UV-Vis spectroscopy utilizes electron transitions in response to optical excitation, giving a unique collected peak known as the surface plasmon

resonance (SPR) band. The absorption spectrum of metallic nanoparticles, including gold is characterized by a strong absorption band (sharp peak) in the near infra-red visible range of 400-700nm (Jain *et al.,* 2006). The band is narrow for bulk materials, including aggregates of nanoparticles (Haiss *et al*., 2007; Jans *et al.,* 2009). Hence, the intensity of SPR band of nanoparticles is strongly affected by size (Jain *et al.,* 2006). However, the shape, the composition and the refractive index of the solution in which the nanoparticles are suspended can also change the absorption spectra of the nanoparticles (Murdock *et al.,* 2008; Baptista *et al.,* 2008).

TEM has facilitated in-depth analysis of the morphology of nanomaterials (Albanese and Chen, 2011). The TEM utilizes an array of high energy electrons that are focused and transferred through a copper grid containing the sample to qualitatively analyze physical parameters (Powers *et al.,* 2006). Qualitative and quantitative information on nanoparticles dimensions such as particle size distribution, shape, crystallography, elemental composition, and the state of aggregation can be obtained with the TEM (Haiss *et al.,* 2007; Bihar *et al.,* 2008; Ng *et al.,* 2010).

FTIR is used to identify molecular structures of individual ligands on the surface of nanoparticles (Zhou *et al.,* 2010; Fadeel *et al.,* 2010). Assessing the position, shape and intensity of peaks in the spectrum reveals information on the types of the functional groups present that make up the molecules. Functional ligands of mixed monolayer protected clusters (MMPCs) have been successfully characterized with FTIR (Shakeri-Zadeh *et al*., 2010; Zhou *et al.,* 2010). An FTIR spectrum is recorded by passing a beam containing many different frequencies of light through the sample. Analysis of the transmitted light reveals the energy that is absorbed by the sample

at a range of wavelengths. The absorbed frequencies are characteristic of the structure of the ligand.

2.2 Experimental methods

2.2.1 Instrumentation used in the study to assess physico-chemical properties of AuNPs

2.2.1.1 Transmission electron microscopy

AuNPs morphology in water and in cell growth medium was assessed with TEM. The copper grids for TEM analysis were prepared by dropping a solution (100µL) containing the nanoparticles on a 400 mesh carbon-coated copper grid. The grid was allowed to dry at room temperature before analysis. TEM images were obtained using a Field emission TEM, operated at 200kV (JEOL-JEM 2100F, Tokyo, Japan), fitted with an energy dispersive X-ray spectrometer (EDS OXFORD INCA spectrometer) and a digital GATAN camera (ERLANGSHEN ES500 W). Particle size distribution was determined by analysing multiple TEM images using Image J software, to determine the mean average size as well as the maximum diameter of the nanoparticles.

2.2.1.2 UV-Vis spectrophotometer

The SPR absorption of the AuNPs in water and in cell growth medium was studied using the Perkin Elmer Lambda 20 UV-Vis spectrophotometer from Thermo scientific (USA). UV-Vis spectrophotometer reading wavelength was set to start at 300nm and end at 700nm in a quartz

cell with a path length of 1cm. The respective growth medium was used as a standard for background correction.

2.2.1.4 Fourier Transform Infrared spectroscopy

The AuNPs samples were prepared for FTIR analysis according to the method of Zhou *et al.* (2013). Briefly the concentrated AuNPs solution were centrifuged at 13 000 *X g* for 30min, the supernatant was discarded and the pellet was dried for 12 hrs in a 50°C oven to remove the excess liquid. The pellet was mounted on the sample holder of the FTIR and the spectra were recorded. The instrument was operated in the absorbance mode at a resolution of 6 cm^{-1}. To obtain a good signal to noise ratio, 64 scans were taken in the range of 450- 4500cm^{-1}.

2.2.1.5 Zeta potential measurement of gold nanoparticles

The Zetasizer was used to assess the zeta potential measurement of the AuNPs. AuNPs were diluted to a final concentration of 1nM in water and in cell growth medium. The measurements were made in triplicate, and the average value of the measurements is presented. Measurements were performed on a Malvern Zetasizer Nano-ZS instrument (ZEN3600) (Malvern Instruments Ltd, USA). Approximately 1mL of the prepared nanoparticle suspensions was transferred to a square cuvette for DLS measurements. Measurements were carried out at room temperature in triplicate, with a minimum of 10 runs and a maximum of 100 runs. The Malvern Zetasizer uses the Dispersion Technology Software (DTS) (Version 4.20) for data collection and analysis. The software collects and interprets data for the particle size and the zeta potential.

2.2.2 Synthesis of citrate stabilized and functionalized gold nanoparticles

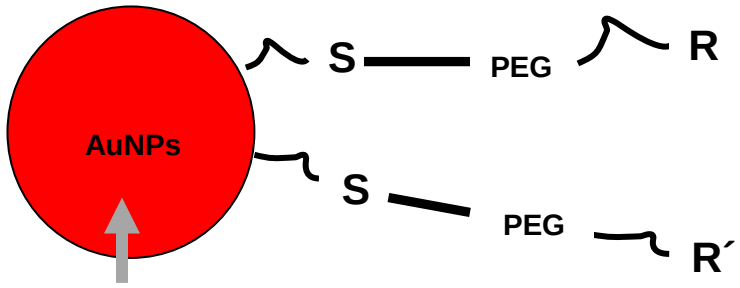
Citrate stabilized and the monolayer protected gold clusters (MPCs) were synthesized at the Advanced Materials Division (AMD) at MINTEK (Randburg, South Africa). The 14nm AuNPs were prepared using the sodium citrate as the reducing agent as previously described (Turkevich *et al.,* 1951). The Gold (III) chloride trihydrate ($HAuCl_4.3H_2O$) and trisodium citrate ($Na_3C_6H_5O_7.2H_2O$) were purchased from Sigma Aldrich and were used without further purification. Briefly, the 14nm AuNPs were prepared by adding trisodium citrate aqueous solution (10mL, 17mM) into 180mL (0.3mM) of boiling $HAuCl_4.3H_2O$ aqueous solution. The mixture was boiled under reflux for 15 minutes and the resultant suspension was allowed to cool to room temperature. The deep red citrate-stabilized gold nanoparticles suspension was further stirred overnight followed by filtration using a non-pyrogenic 0.25µm sterile filter before use.

The PEG coated AuNPs were prepared using ligand exchange procedures where the citrate was replaced with PEG molecules containing the desired functional groups. The ligand exchange experiments were left to run for about 8 hours before being purified by centrifugation. The citrate stabilized AuNPs were suspended in borate buffer, while the PEG coated AuNPs were suspended in Milli Q water. The hydroxyl group is shown as one of functional group on the PEG-biotin MMPCs, PEG-azide MMPCs, and PEG-NTA MMPCs. The methoxy groups and the carboxyl group are reactive groups on the PEG-OCH_3 and PEG-COOH.

The citrate ions are shown as reactive or functional groups on the surface of citrate stabilized AuNPs. For the purpose of this work, the citrate stabilized AuNPs will be referred to as Cit-

14nm, Cit-20nm and Cit-40nm. The citrate AuNPs were 14, 20 and 40± 2nmin size. As the study intended to compare the effects of the different functional groups on AuNPs surfaces, a pre-determined size of 14± 2nm was selected for the synthesis of PEG coated AuNPs.

The PEG-OH was used as a co-stabilizer during synthesis of the MMPCs. Figure 2.2 shows the classification of the MPCs and the MMPCs used in the study. The PEG-COOH, PEG-OH and PEG-OCH_3 were classified as the MPCs, whereas the MMPCs consisted of the PEG-biotin and PEG-OH, PEG-azide and PEG-OH, and PEG-NTA and PEG-OH. The hydroxyl group is shown as one of functional group on the PEG-biotin MMPCs, PEG-azide MMPCs, and PEG-NTA MMPCs. The methoxy groups and the carboxyl group are reactive groups on the PEG-COOH and PEG-OCH_3.



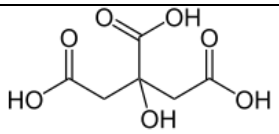
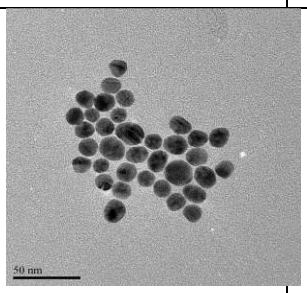
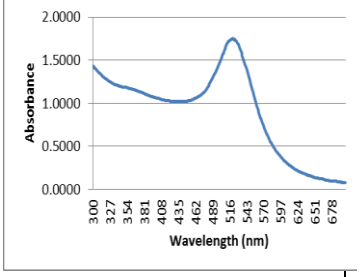
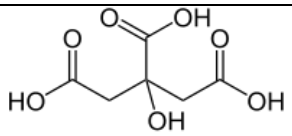
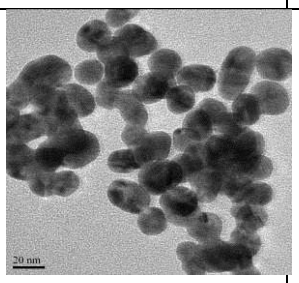
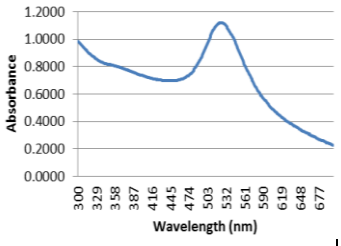
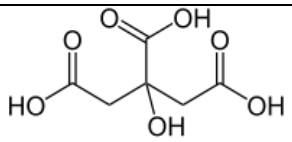
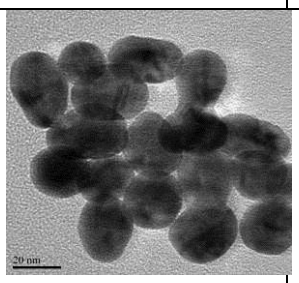
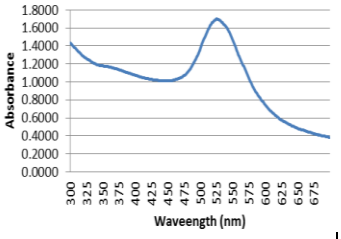
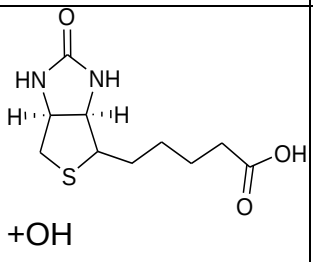
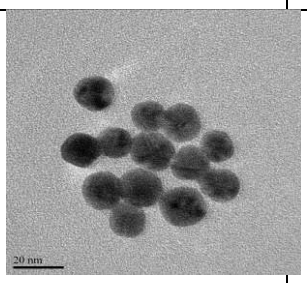
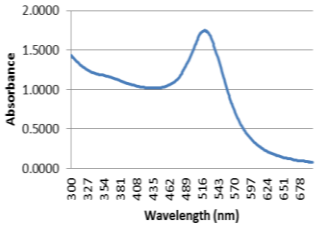
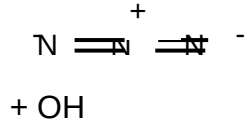
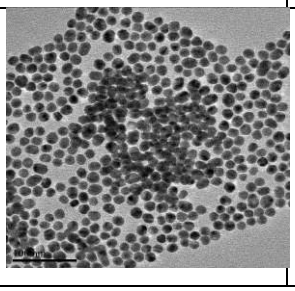
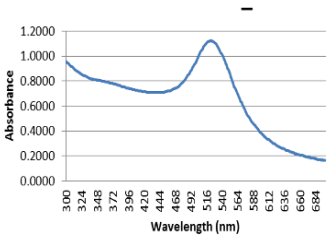
Core 14, 20, 40nm

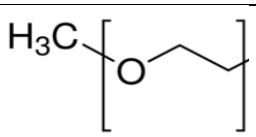
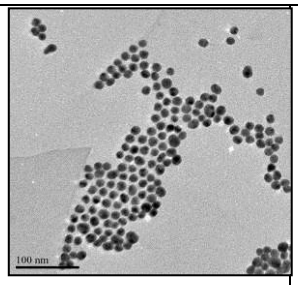
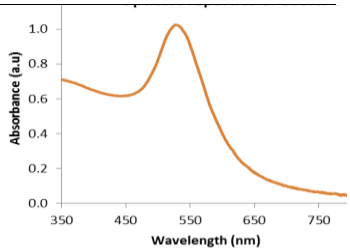
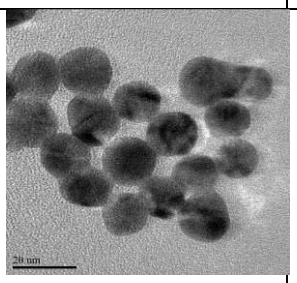
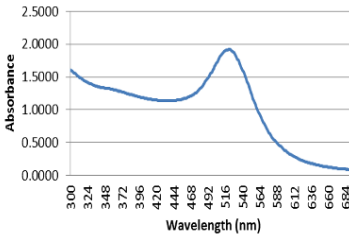
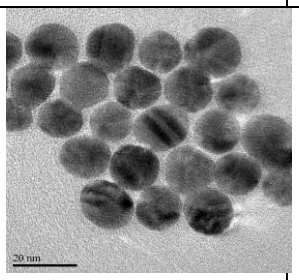
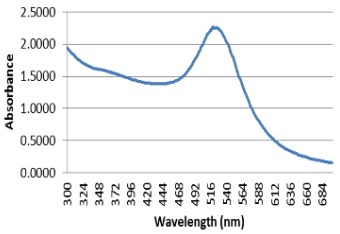
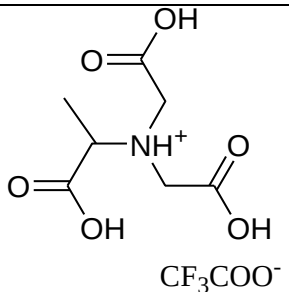
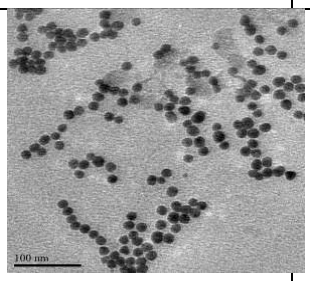
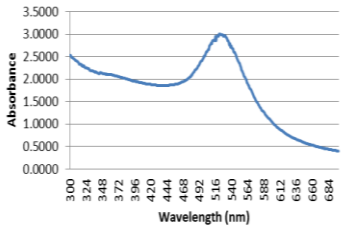
MPCs	R´=R =OH =COOH = OCH_3
MMPCs	99%; 1% R´=OH R=azide =NTA =biotin

Figure 2.2: Monolayer protected clusters and mixed monolayer protected clusters used in the study

The surface composition, morphological analysis and UV-Vis spectra of the AuNPs after synthesis are outlined in Table 2.1. The SPR band of the citrate stabilized AuNPs in buffer was 519, 530 and 532nm for the 14, 20 and the 40nm nanoparticles, respectively. The SPR of the 14nm MPCs and MMPCs in water was 520nm. The specification of the SPR absorption is in agreement with the reported absorption of nanosized AuNPs at this size range (Jain *et al.,* 2006).

Table 2.1: Specification of gold nanoparticles used in this study

AuNPs	***Surface composition***	***Reactive functional groups***	***Particle shape (TEM)***	***Optical properties (UV-Vis)***
14nm Citrate Cit-14 nm	Citrate			
20nm Citrate Cit-20 nm	Citrate			
4.nm Citrate Cit-40 nm	Citrate			
14nm Biotin-PEG	1% PEG-biotin+ 99% PEG-OH			
14nm Azide-PEG	1% PEG-azide+ 99% PEG-OH			

14nm Methoxy-PEG	100% PEG methoxy			
14nm Hydroxyl - PEG	100% PEG OH	-OH		
14nm Carboxyl - PEG	100% PEG-COOH	-COOH		
14nm NTA-PEG	1% PEG-NTA+ 99% PEG-OH	 CF_3COO^- + OH		

2.2.3 Preparation of AuNPs in cell growth medium and physico-chemical characterization

Characterization of AuNPs in cell culture medium was achieved by re-suspension of freshly synthesized batches of AuNPs in the respective cell culture medium (Roswell park memorial institute medium (RPMI)-1640 and essential minimum eagle medium (EMEM) supplemented with 10% fetal bovine serum (FBS). Briefly, the nanoparticles solutions in Milli-Q water or borate buffer were centrifuged at 13 000 x *g* for 30 min, the supernatant was discarded and the pellet was re-suspended in the respective growth medium. The AuNPs were immediately characterized with the TEM, UV-Vis spectrophotometer, FTIR and DLS techniques. The pH of the AuNPs in the growth medium was also determined.

2.3 Results and discussion

Figure 2.3 shows the TEM analysis and UV-Vis spectra of Cit-14nm, Cit-20nm and Cit-40nm AuNPs suspended in RPMI 1640 and EMEM growth media. The TEM micrographs show a noticeable dominance of spherical nanoparticles in the RPMI-1640 and EMEM growth media with maximum diameters of 16nm, 23nm and 41nm, respectively (Fig 2.3A-2.3F). There was no observable difference in the size of citrate AuNPs that were suspended in RPMI-1640 and EMEM media. The SPR spectra of the Cit-14nm, 20nm and 40nm suspended in RPMI-1640 and EMEM growth media were observed around 551nm, 554nm and 557nm (Figure 2.3G and 2.3H). The red shift as observed in the measured spectra of AuNPs in the growth medium can be attributed to the polydispersity of the nanoparticles, resulting in an increase in the size of the AuNPs.

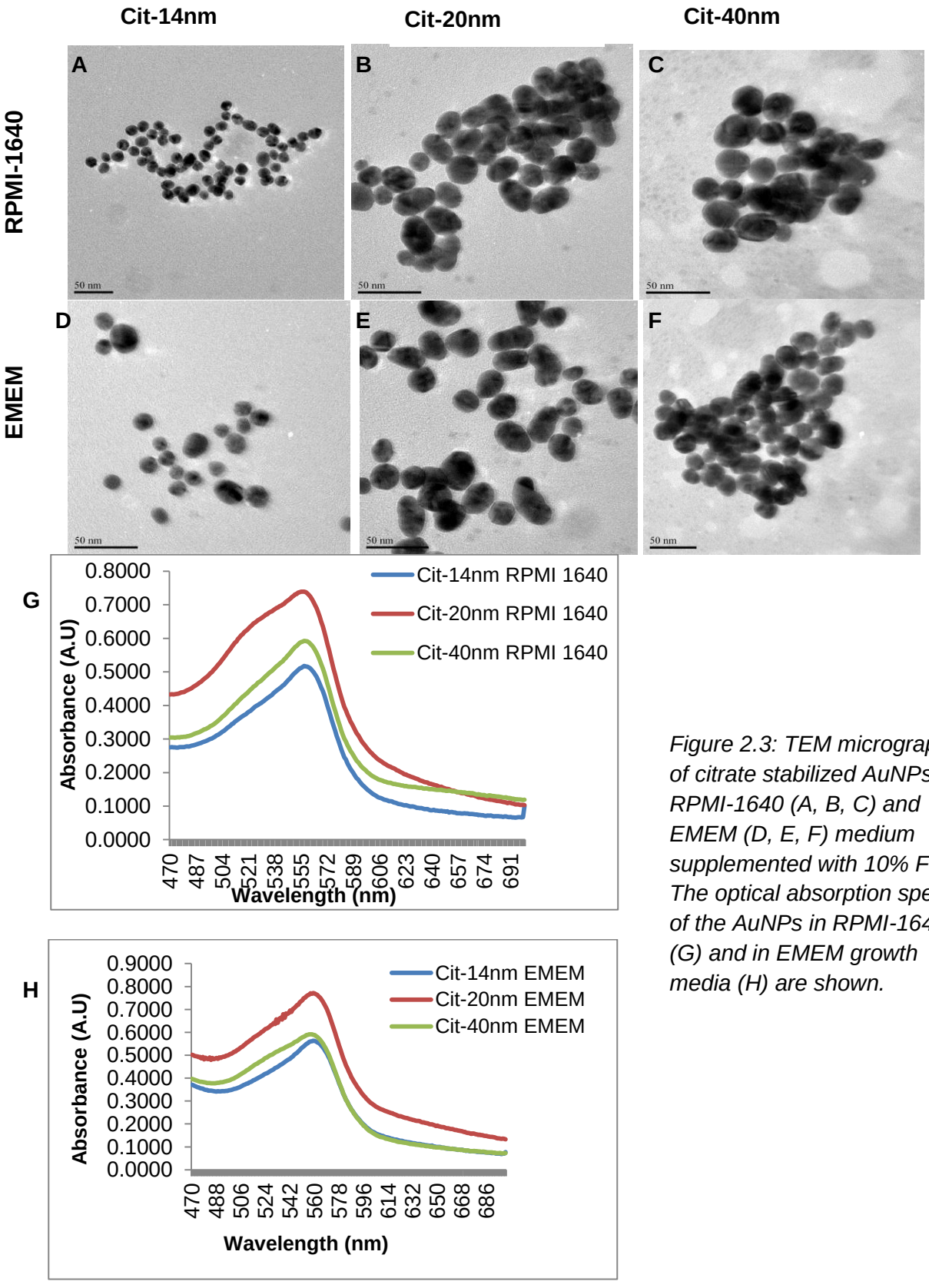


Figure 2.3: TEM micrographs of citrate stabilized AuNPs in RPMI-1640 (A, B, C) and EMEM (D, E, F) medium supplemented with 10% FBS. The optical absorption spectra of the AuNPs in RPMI-1640 (G) and in EMEM growth media (H) are shown.

Polydispersity in nanoparticles solution occurs when the attractive forces between the particles are greater that the repulsion forces produced that are intended to keep the nanoparticles surface apart (Albanese and Chen, 2011; Merhi *et al.,* 2012). The negative charges on the nanoparticles surface and the positive charges associated with the proteins in the media attached on nanoparticle surfaces may result in the nanoparticles interacting with one another.

The TEM micrographs of PEG coated AuNPs in cell growth medium is shown in Figure 2.4. Upon closer inspection of the images, AuNPs show dispersed nanoparticles with spherical morphology. A size distribution with an average diameters of 15±2nm and maximum diameters of 22nm were obtained. The particle size distribution of the MPCs and MMPCs are shown in Figure 2.5.

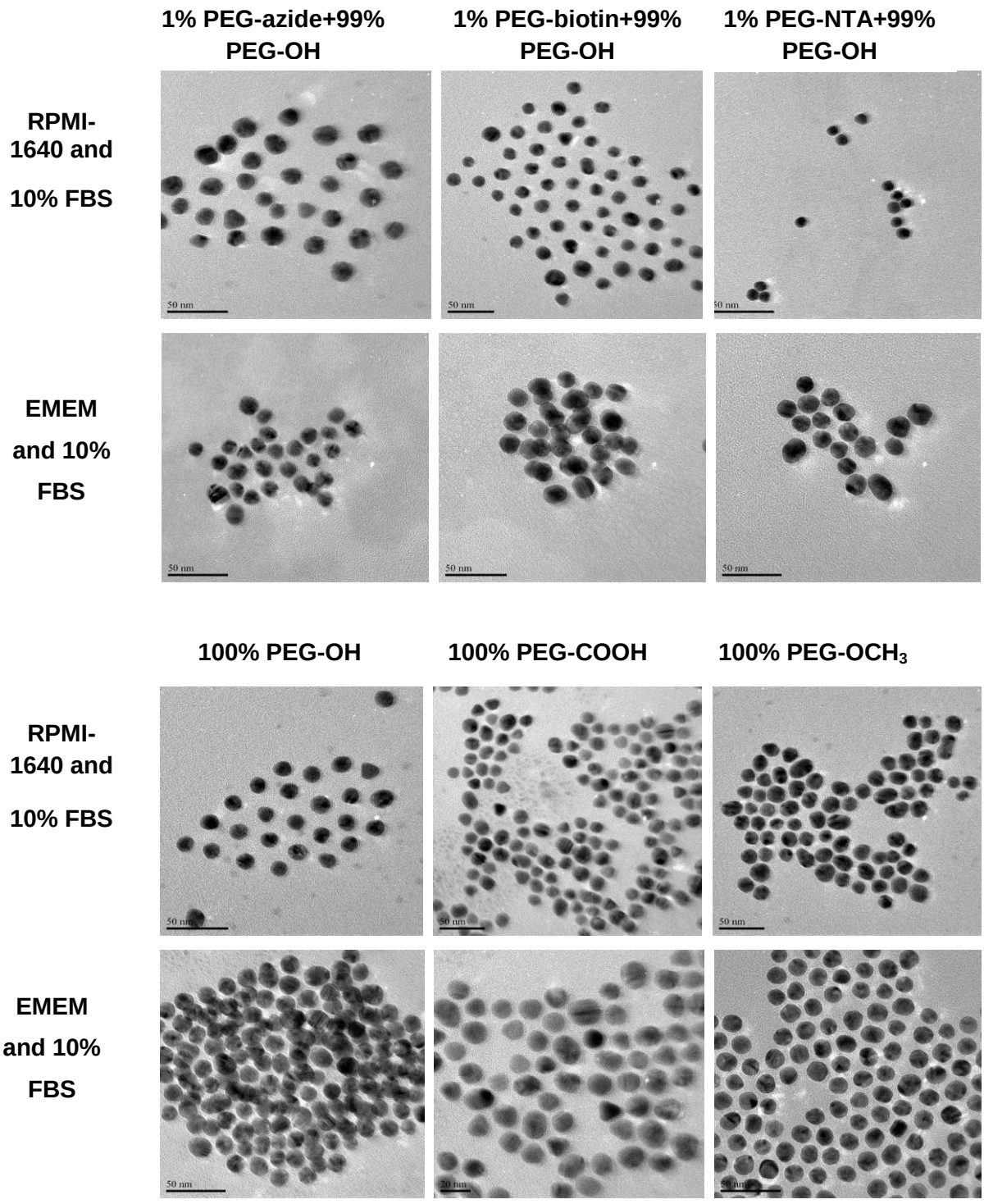


Figure 2.4: TEM micrographs of PEG-azide MMPCs, PEG-biotin MMPCs, PEG-NTA MMPCs, PEG-OH MPCs, PEG-OCH_3 MPCs and PEG-COOH MPCs in RPMI-1640 and EMEM growth medium.

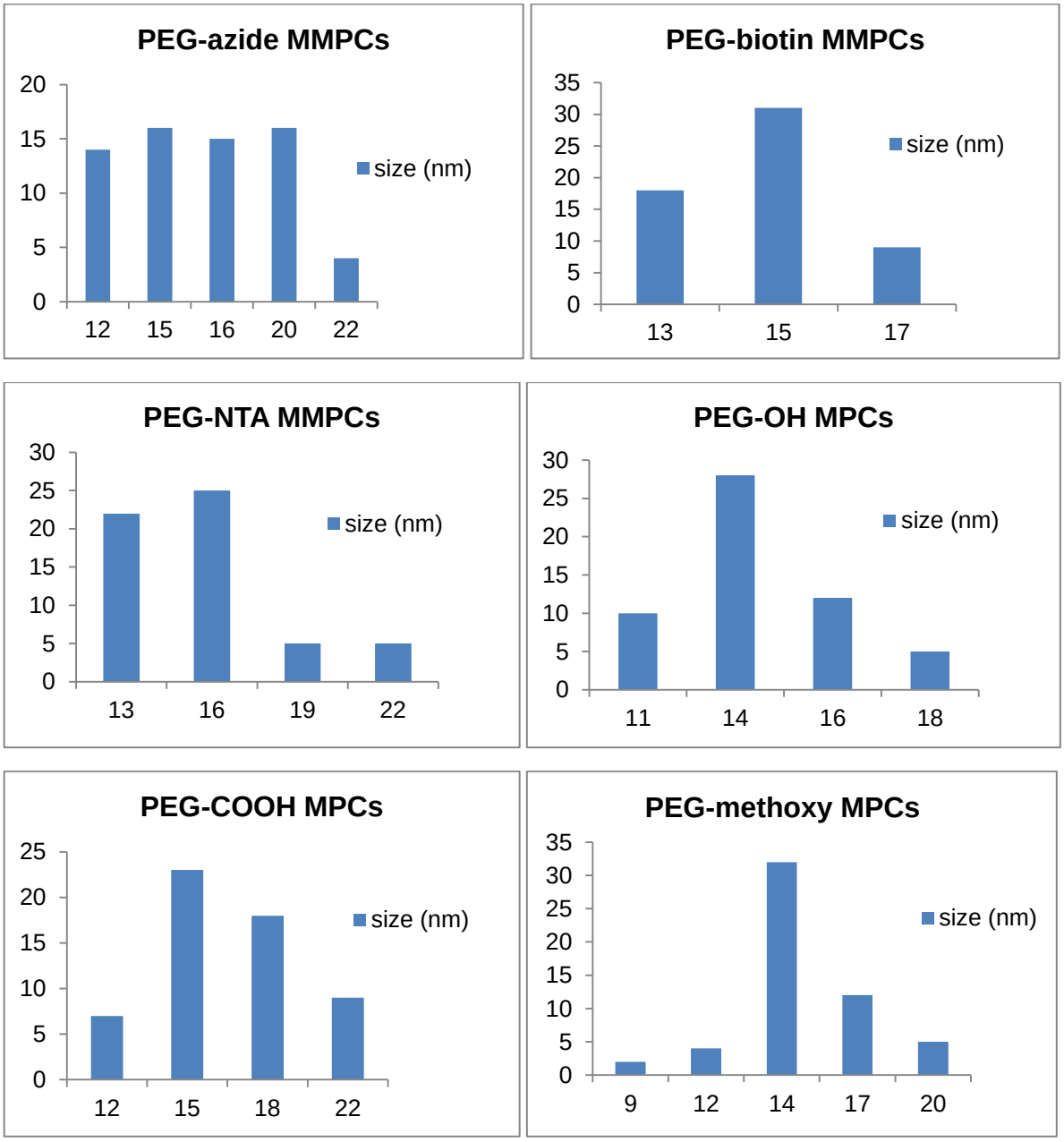


Figure 2.5 Particle size distributions of PEG-azide MMPCs, PEG-biotin MMPCs, PEG-NTA MMPCs, PEG-OH MPCs, PEG-OCH_3 MPCs and PEG-COOH MPCs.

The slight increase in size may indicate absorption of media component onto the nanoparticle surfaces (Albanese and Chan, 2011). A noticeable clumping of the nanoparticles was seen on TEM images of PEG-OH MPCs that were suspended in EMEM growth medium. Clumping of these particles may be due to the non-specific adsorption of proteins in the media to the nanoparticle surfaces. Even so, the AuNPs did maintain their spherical morphology. Figure 2.6A and 2.6B shows the SPR of PEG coated AuNPs in RPMI-1640 and EMEM growth medium.

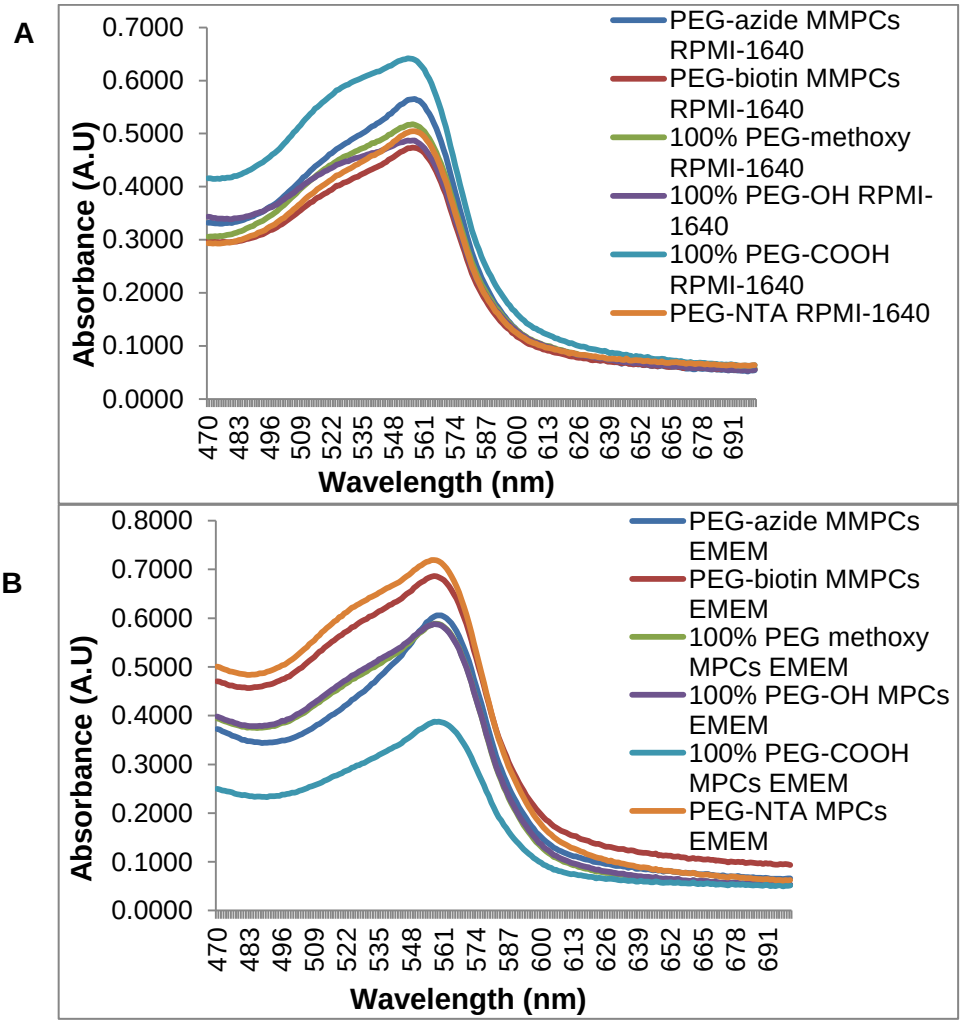


Figure 2.6: UV-Vis spectra of 14nm PEG-azide MMPCs, PEG-biotin MMPCs, PEG-NTA MMPCs, PEG-OH MPCs, PEG-OCH_3 MPCs and PEG-COOH MPCs in RPMI-1640 and EMEM growth medium.

Table 2.2 summarizes the SPR band of the AuNPs in water and in cell growth medium. AuNPs coated with PEG molecules show a SPR peak of 522nm in water. The citrate nanoparticles often form the backbone for modification of the nanoparticles surface; it was therefore expected that the SPR peak of AuNPs would shift from 519 to 522nm after modification with the PEG ligands. The absorption spectra were in agreement with surface coated AuNPs presented in the literature (Nghiem *et al.,* 2012).

Table 2.2: Summary of SPR band of AuNPs in water/buffer and in cell growth medium

AuNPs	**λ (nm) water/buffer**	**λ (nm) RPMI1640 +10% FBS**	**λ (nm) EMEM +10% FBS**
Cit-14nm	519	543	550
Cit-20nm	530	549	551
Cit-40nm	532	549	549
14nm PEG-azide MMPCs	522	546	548
14nm PEG-biotin MMPCs	522	533	546
14nm PEG-OCH3 MPCs	522	542	551
14nm PEG-OH MPCs	522	549	569
14nm PEG-COOH MPCs	522	543	546
14nm PEG-NTA MMPCs	522	537	544

A shift to the longer wavelength in the SPR spectra of the PEG coated AuNPs from 522nm in the two cell culture medium was observed. The adsorption of proteins present in the media could be the results of an increase in the size of the nanoparticles, causing a shift of the SPR band to the longer wavelength (Cui *et al.,* 2012). The shift of the SPR band of the PEG coated AuNPs could not be attributed to aggregation as dispersed nanoparticles were indicated on the TEM images. Hence, the additional surface coatings on the PEG coated AuNPs surface is applied to form an electrostatic barrier that is intended to keep the nanoparticles dispersed in biological solution and to offer additional stability to the nanoparticles solution (Mahl *et al.,* 2010).

Subsequent characterization using FTIR spectrophotometry revealed the functional groups on the AuNPs surfaces. The IR spectra of the AuNPs in RPMI-1640 and EMEM growth media revealed vibrations of the peaks at wavelength of 2300-4000cm^{-1}. The peaks were identical, irrespective of the cell culture media. The prominent peaks for the citrate stabilized AuNPs were stretching frequencies of strong vibrations around 2987, 2901cm^{-1}*(v (O-H) s)* and 1394cm^{-1}*(v (O-H) m)* characteristic of the carboxylic acid of the citrate stabilizer. Hydrogen bonding at frequencies of 3674cm^{-1} *(v (O-H) m)* was observed.

The aliphatic bands of the PEG chains on the PEG coated AuNPs were identified at wavelengths of between at 3030-2845cm^{-1}. A broad peak at 2920cm^{-1} *(v (OH) s)* indicating stretching of the hydroxyl groups was observed on the PEG-azide MMPCs, PEG-biotin MMPCs and the PEG-NTA MMPCs. The presence of an amino compound at frequencies of 3540-3200cm^{-1} was detected on the PEG-azide MMPCs. The vibration peaks at frequencies around 1649cm^{-1}, 1579cm^{-1} and 1071cm^{-1} confirmed functional groups on the biotin molecule. The peak

at 1649cm^{-1} *(v (NH) m)* and 1579cm^{-1} *(v (C=O) s)* were largely due to the carbonyls and the amine group present in the biotin molecules.

Prominent peaks indicating strong bonding frequencies at 2901cm^{-1}, 2971cm^{-1} and 1066cm^{-1} *(v (C-O) s)* were seen on the PEG-OCH_3 MPCs. The peak at around 2901cm^{-1} and 2987cm^{-1} (*v* (C-H) *m*) were due to the stretching frequencies of the methyl group. FTIR spectra revealed prominent peaks around 2973cm^{-1}*(v (O-H) s),* 2902cm^{-1}(*v* (C-H) *m*), 1394cm^{-1}*(v (O-H) s),* and 1066cm^{-1}*(v (C-O) s)* on the hydroxyl-PEG AuNPs, characteristic of the alkyl band of the PEG chain and the hydroxyl group on the nanoparticles surface.

The PEG-COOH MPCs indicated vibration frequencies around 2973cm^{-1}*(v (O-H) s),* 2908cm^{-1}*(v (C-H) m),* 1394cm^{-1}*(v (C-H) m)* and 1760cm^{-1}*(v (C=O) s)* were observed, characteristic of the carboxyl functional groups. Furthermore, FTIR analysis revealed vibration frequencies around 2921cm^{-1}(*v* (C=O) *s*), 1400cm^{-1} *(v (CO) s)* and 1077 cm^{-1} *(v (OH) m)* characteristics of carboxylic and hydroxyl groups in the NTA moiety.

The zeta potential readings of the citrate stabilized AuNPs in water and PEG coated AuNPs in buffer were measured and are presented in Table 2.3. The pH of the nanoparticles in buffer (pH 6.83) was measured as indicated in Table 2.3. The pH of the 14, 20 and 40nm citrate stabilized AuNPs was around 6, with zeta potential of -26, -32 and -56mV respectively. At this pH, a high zeta potential indicate stability of the nanoparticles. The zeta potential measurements of the MPCs and MMPCs indicated readings ranging from -23 to -56mV. Nonetheless, there was a variation in the readings for the NTA-PEG MMPCs, PEG-biotin MMPCs and the PEG-OCH_3 MPC, which can affect the final average reading presented in Table 2.3. The variation might be attributed to a number of factors, including changes in the surface chemistry of the

nanoparticles, amongst other factors. The pH of the MPCs and the MMPCs was around 6, slightly increasing for PEG-COOH MPCs and PEG-OCH_3 MPC. Nonetheless, the measurements revealed a negative charge on the nanoparticles surface, contributing to the polydispersity of the nanoparticles.

Table 2.3: Zeta potential (mV) and pH of gold nanoparticles suspended in double deionized water

AuNPs	**Average reading (mV)**	**pH of AuNPs in buffer**
Cit-14 nm	-26	6.22
Cit-20 nm	-35	6.18
Cit-40 nm	-56	6.14
14nm PEG-azide MMPCs	-56	6.73
14nm PEG-biotin MMPCs	-56	6.46
14nm PEG-OCH_3 MPCs	-34	6.86
14nm PEG-OH MPCs	-23	6.03
14nm PEG-COOH MPCs	-42	6.87
14nm PEG-NTA MMPCs	-31	6.27

Zeta potential analysis revealed a significant decrease in values after suspending the AuNPs in cell growth medium (Table 2.4). The pH of RPMI-1640 and EMEM growth media was 8.2. The zeta potential readings of -5 to -10mV were recorded for PEG coated AuNPs in RPMI-1640 and EMEM growth media. Nonetheless, the AuNPs retained their negative surface charge in the two cell growth media. The pH of the AuNPs in cell growth medium was around 8. The zeta potential of colloids has been shown to gradually decrease in physiological media, including cell growth medium (Paoli Lacerda *et al.,* 2010; Graf *et al.,* 2012; Sabuncu *et al.,* 2012). For example, Sabuncu *et al.* (2012) showed a decrease in zeta potential reading of 18 nm AuNPs from -

71.04mV to -15.75mV after suspending the nanoparticles in DMEM cell culture medium containing 10 % $^{v}/_{v}$ FCS. The decrease in zeta potential reading has been shown to be the result of increased ionic strength of the media. The polydispersity index (PDI) of the AuNPs in the media is indicated in the Table 2.4. The PDI values indicate that the AuNPs sample have a broad size distribution.

Table 2.4: Zeta potential (mV) and pH of gold nanoparticles suspendend in growth medium

AuNPs	**Cell growth medium (with 10% FBS and 1% antibiotics)**	**Average reading (mV)**	**pH of AuNPs in buffer**	**PDI**
Cit-14 nm	RPMI	-10	8.25	0.53
	EMEM	-9	8.16	0.57
Cit-20 nm	RPMI	-12	8.28	0.47
	EMEM	-10	8.24	0.55
Cit-40 nm	RPMI	-10	8.25	0.40
	EMEM	-9	8.21	0.48
14nm PEG-azide MMPCs	RPMI	-9	8.32	0.50
	EMEM	-16	8.19	0.59
14nm PEG-biotin MMPCs	RPMI	-9	8.22	0.50
	EMEM	-9	8.20	0.51
14nm PEG-OCH_3 MPCs	RPMI	-7	8.25	0.47
	EMEM	-9	8.17	0.53
14nm PEG-OH MPCs	RPMI	-9	8.35	0.48
	EMEM	-10	8.28	0.52
14nm PEG-COOH MPCs	RPMI	-7	8.39	0.48
	EMEM	-8	8.28	0.56
14nm PEG-NTA MMPCs	RPMI	-8	8.34	0.47
	EMEM	-5	8.26	0.50

2.4 Summary and Conclusions

In this chapter, the physico-chemical characteristics of citrate stabilized and PEG coated AuNPs presenting various functional groups were assessed in water or buffer and in cell growth media. The particle dispersity, size, surface chemistry, morphology and absorption spectra were explored by commonly used techniques for characterizing nanoparticles solutions.

The results indicated the successful synthesis of spherical citrate stabilized AuNPs with sizes of 14, 20 and 40nm. Using ligand exchange reactions, thioalkylated PEG coated AuNPs with the azide, biotin, hydroxyl, methoxy, carboxyl and NTA functional groups were synthesized. FTIR spectra confirmed the presence of the functional groups on the AuNPs surfaces in water and in the two cell culture media, indicating that the AuNPs retained their surface coatings in cell media. TEM images revealed spherical morphology of the AuNPs in water and in cell growth media. The UV-Vis spectra of the AuNPs indicated absorption at wavelength between 517-550nm. Due to the high reactivity of nanoparticles, specific binding of proteins present in the media to the nanoparticles surfaces was correlated to the shift in the SPR band of the AuNPs, as previously described (Menghua *et al.,* 2014). Zeta potential measurements confirmed the negative charge on the nanoparticles synthesis in water and in cell growth media. A larger zeta potential reading was obtained on AuNPs after synthesis indicated extreme stability of the AuNPs in buffer solution.

A decrease in zeta potential reading of the AuNPs in cell growth media was however not attributed to aggregation, as the negative charge on the nanoparticles surface was thought to result in the repulsion of the nanoparticles. Therefore, as indicated by TEM analysis,

polydispersed nanoparticles were seen. In conclusion, there was no observable difference in the morphology, size and zeta potential reading of the analysed AuNPs in the selected media.

2.5 References

Aillon K, Xie Y, El-Gendy, Berkland CJ, and Forrest ML. 2009. Effects of nanomaterial physicochemical properties on *in vivo* toxicity. *Advanced Drug delivery Reviews*, 61: 457-466.

Albanese A and Chan WCW. 2011. Effects of gold nanoparticle aggregation on cell Uptake and Toxicity. *ACS Nano*, 5 (7): 5478- 5489.

Amendola V and Meneghetti. 2009. Size evaluation of gold nanoparticles by UV-Vis spectroscopy. *J.Physi.Chem C,* 113:4277- 4285.

Baptista P, Pereira E, Eaton P, Doria G, Miranda A, Gomes I, Quaresma P, and Franco R. 2008. Gold nanoparticles for the development of clinical diagnostics methods. *Anal. Bioanl. Chem,* 391: 943- 950.

Bihar P, Vippola M, Schultes S, Praetner M, and Krombach F. 2008. Optimized dispersion of nanoparticles for biological *in vitro* and *in vivo* studies. *Particle and Fiber Toxicology*, 5 (14): 1-14.

Brar SK and Verma M. 2011. Measurement of nanoparticles by light-scattering techniques. *Trends in Analytical Chemistry,* 30 (1): 4-17.

Cui W, Li J, Zhang Y, and Liang L. 2012. Effects of aggregation and the surface properties of gold nanoparticles on cytotoxicity and cell growth. *Nanomedicine: Nanotechnology. Biology and medicine,* 8: 46-53.

Dutta D, Sundararam SK, Teeguarden JG, Riley BJ, and Jacobs JM. 2007. Adsorbed proteins influence the biological activity and molecular targeting of nanomaterials. *Toxicological Sciences*, 10 (1): 303- 315.

Fadeel B, and Garcia-bennet A E. 2010. Better safe than sorry: Understanding the toxicological properties of inorganic nanoparticles manufactured for biomedical applications. *Advanced Drug Delivery Reviews*, 62: 362- 374.

Gosens I, Post JA, Fonteyne LJJ, Jansen E HJM, Geus JW, and Jong WH. 2010. Impact of agglomeration state of nano-and submicron sized gold particles on pulmonary inflammation. *Particle and Fiber Toxicology*, 7 (37): 2-11.

Graf C, Gao Q, Schutz I, Noufele CN, Ruan W, and Ruhl E. 2012. Surface functionalization of silica nanoparticles supports colloidal stability in physiological media and facilitates internalization in cells. *Langmuir,* 28: 7598- 7613.

Haiss W, Thanh NTK, Aveyara J, and Fernig DG. 2007. Determination of Size and Concentration of Gold Nanoparticles from UV-Vis Spectra. *Anal. Chem,* 79: 4215- 4221.

Horie M, Nishio K, Fujita K, Endoh S, Miyauchi A, Saito Y, Iwahashi H, Yamamoto K, Murayama H, and Yoshida Y. 2009. Protein adsorption of ultrafine metal oxide and its influence on cytotoxicity toward cultured cells. *Chem Res Toxicol,* 22 (3): 543- 553.

Jain PK, Lee KS, El-Sayed IH, and El-Sayed MA. 2006. Calculated Absorption and scattering properties of gold nanoparticles of different size, shape, and composition: Applications in biological imaging and biomedicine. *J.Physi.Chem B*, 110: 7238-7248.

Jans H, Liu X, Austin L, Maes G, and Huo Q. 2009. Dynamic Light Scattering as a Powerful Tool for Gold Nanoparticle Bioconjugation and Biomolecular Binding Studies Measurement of nanoparticles by light-scattering techniques. *Anal. Chem*, 81: 9425- 9432.

Mahl D, Greulich C, Meyer-Zaikaw, Koller M, and Epple M. 2010. Gold nanoparticles: dispersibility in biological media and cell- biological effect, *Journal of Material Chemistry*, 6176-6181.

Maiorano G, Sabella S, Sorce B, Brunetti V, Malvindi MA, and Pompa PP. 2010. Effects of cell culture media on the dynamic formation of protein-nanoparticle complexes and influence on the cellular response. *ACS Nano*, 4 (12): 7481-7491.

Menghua C, Liu R, Deng Z Ge G, and Xie L. 2014. Quantitative study of protein coronas on gold nanoparticles with different surface modifications. *Nano Research,* 7 (3): 345-352.

Merhi M, Domb CY, Brient A, Chang J, Plael A, and Betbeder. 2012. Study of serum interaction with cationic nanoparticles: implications for *in vitro* endocytosis, cytotoxicity and genotoxicity. *International Journal of Pharmaceutics*, 423: 37-44.

Monopoli MP, Walczy KD, Campbell A, Elia G, Lynch I, and Dawson KA. 2011. Physical-Chemical aspects of protein corona: Relevance to in vitro and in vivo biological impacts of nanoparticles. *Journal of the American Chemical Society*, 133 (8): 2525-2534.

Murdock RC, Braydich-Stolle, Schrand AM, Schlager JJ, and Hussain SM. 2008. Characterization of nanomaterials dispersion in solution prior to *in vitro* exposure using dynamic light scattering technique. *Toxicological Sciences*, 101 (2): 239- 253.

Ng CT, Perumalsamy R, Watt F, and Yuan YL. 2010. Localizing cellular uptake of nanomaterials in vitro by transmission electron microscopy. *Microscopy: Science, technology and education. Formatted,* 316-320.

Nghiem TH, Nguyen TT, Fort E, Nguyen TP, and Tran HN. 2012. Capping and *in vivo* toxicity studies of gold nanoparticles. *Advances in natural Sciences*: *nanoscience and nanotechnology*, 3: 1-5.

Paoli Lacerda, Park JJ, Meuse C, Pristinski, Becker ML, and Douglas JF. 2010. Interaction of gold nanoparticles with common human blood proteins. *ACS Nano*, 4 (1): 365- 379.

Powers KW, Browns C, Krishna VB, Wasdo SC, and Roberts SM. 2006. Research strategies for safety evaluations of nanomaterials. Part VI. Characterization of nanoscale particles for toxicological evaluations. *Toxicological Sciences*, 90 (2): 296-303

Sabanchu AC, Grubbs J, Qian S, and Beskok A. 2012. Probing nanoparticle interactions in cell culture media*. Colloids and Surfaces B: Biointerfaces*, 95: 96-102.

Shakeri-Zadel A, Ghasemifad M, and Mansoori GA. 2010. Structural and optical characterization of folate conjugates gold-nanoparticles. Physica E, 42: 1272-1280.

Sun L, Li Y, Liu X, Jin M, Zhang L, Du Z, Guo C, Huang P, and Sun Z. 2011. Cytotoxicity and mitochondrial damage caused by silica nanoparticles. *Toxicology in vitro*, 2011, 25 (8): 1619-1629.

Warheit DB. 2008. How meaningful are the results of nanotoxicity studies in the absence of adequate material characterization? *Toxicological Sciences*, 101 (2): 182-185.

Zhou H, Li X, Lemoh H, Zhang B, and Yan B. 2010. Structural confirmation and quantification of individual ligands from the surfaces of multi- functionalized gold nanoparticles. *Analyst*, 135: 1210- 1213.

CHAPTER 3

CELLULAR UPTAKE, INTRACELLULAR LOCALIZATION AND EXOCYTOSIS OF GOLD NANOPARTICLES

3.1 Introduction

Numerous studies have examined cellular uptake of AuNPs to understand the underlying nanoparticle cell interactions (Liu *et al.,* 2013). Uptake of nanoparticles by cells has been correlated to the physico-chemical properties of the nanomaterials, in particular the size, shape as well as surface chemistries, including surface charge, surface functional groups, ligand type and the conjugate biomolecules attached to the nanoparticle surface (Oh *et al.,* 2011; Kettler *et al.,* 2014). Cellular interaction of citrate-stabilized AuNPs with various sizes and PEG-coated AuNPs presenting different functional groups will be assessed in human kidney and hepatocyte carcinoma cell lines, representing major accumulation sites of AuNPs.

Intracellular distribution and localization of AuNPs was thoroughly assessed. In addition, this study was set to quantify intracellular AuNPs in the cells, and compare the level of uptake of the nanoparticles between the two cell lines. Comparing the uptake in the two cell lines is important for toxicity studies, as the concentration of intracellular nanoparticles may influence the outcome of cytotoxicity. The difference in internalized nanoparticles based on surface chemistry of the AuNPs was also established. Lastly, the exocytosis of the AuNPs in the cells was assessed. The techniques used for the analysis are briefly discussed in the next paragraphs.

The CytoViva dark field optical microscope (CytoViva Inc., Auburn, AL, USA) provides a simple and convenient technique to assess the uptake of nanoparticles into cells (Skebo *et al.,* 2007; Rocha *et al.,* 2011). The technique utilizes the scattering properties of nanoparticles to give information on intracellular nanoparticles, and thus requires no additional staining or contrast agent to visualize the sample (Meyer *et al.,* 2010). The Uptake of nanomaterials, including silver (25, 80, 130nm); aluminum (80nm); and manganese (40nm) nanoparticles in rat liver cells (BRL 3A), rat alveolar macrophages (MACs), and rat neuro-endocrine cells (PC-12) have been visualized with the dark field illumination system (Skebo *et al.,* 2007).

TEM has been a method of choice for the intracellular detection of metal nanoparticles in cells (Muhlfeld *et al.,* 2007, Mayhew *et al.,* 2009, Brandenberger *et al.,* 2010). TEM provides good contrast visualization of metal nanoparticles inside cells as a result of the high electron density of metal nanomaterials (Brown and Hondow, 2013). As such, nanoparticles with size range of 5nm and less could easily be detected in cellular compartments (AshaRani *et al.,* 2009; Huang *et al.,* 2012). The technique was used in this study to confirm AuNPs in cells, their localization in cellular compartments as well as to study the exocytosis of the AuNPs from cells.

Inductively coupled plasma mass spectrometry (ICP-MS) has been applied for the analysis and quantification of metal nanoparticles in cells, due to the high sensitivity and low detection limits of the instruments (Zhu *et al.,* 2012; Freese *et al.,* 2012). In ICP-MS analysis, the sample often presented in liquid form, is pumped into a sample introductory system, where it is converted into aerosols. The aerosol is then transferred via a sample injector into the plasma, where it exists in ground state atoms and ions, representing the elemental composition of the sample. Figure 3.1 show a schematic diagram of working principles of the ICP-MS.

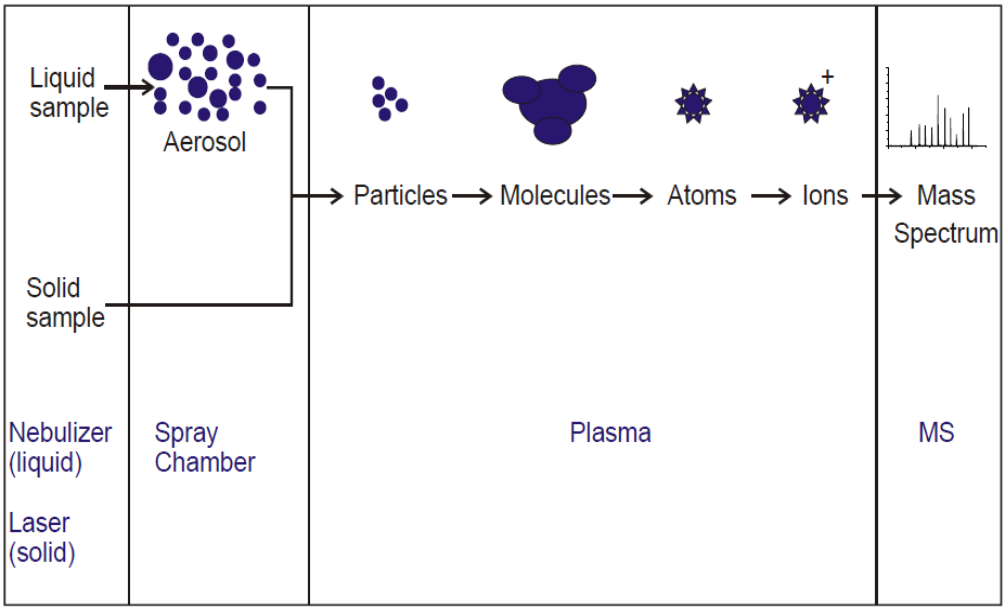


Figure 3.1: Schematic diagram of ICP- MS sample introduction, ion formation and analysis. (Ammann, 2007).

3.2 Experimental methods

3.2.1 Culturing and maintenance of cell lines

The HepG2 cell line used in the study was purchased from the European Collection of Cell Cultures (ECCAC, UK) (product number 85011430). The HEK 293 cells were generously provided by Dr Abdullah Ely from the Department of Molecular Medicine and Hematology at the University of the Witwatersrand, Johannesburg, South Africa. Cell lines were routinely cultured under standard culturing conditions (37°C and 5% CO_2 in a humidified environment). The HEK 293 cells were maintained in RPMI-1640 medium with L-glutamine, 10% heat-inactivated FBS and 1% Penicillin/Streptomycin. HepG2 were maintained in EMEM with L-glutamine, 10% heat-inactivated FBS and 1% Penicillin/Streptomycin. Cell culture reagents were purchased from

Lonza, Belgium. A summary of the cell lines, origin and the medium used for cell culture are tabulated in Table 3.1 below.

Table 3.1: Cell lines used in the study

Cell line	Origin	Media
Caucasian hepatocytes carcinoma (HepG2)	Human	EMEM
Embryonic kidney cells (HEK 293)	Human	RPMI-1640

3.2.2 Determination of cell viability by the trypan blue exclusion assay

The cells were continuously viewed under the Olympus SLX40 phase contrast microscope, at 20X magnification to assess the morphology and degree of confluency. Once the desired confluency was reached (80-90%), the spent media was discarded and the cell monolayer was washed with Phosphate Buffered Saline (PBS). The cells were detached from the flasks by a brief treatment with a warm 1X trypsin/EDTA solution. The cells were re-suspended in their respective growth medium. The cell viability was determined by the trypan blue cell viability assay and the cell number determined using a countess cell counter. The spent media recovered from cells was routinely checked for mycoplasma contamination using the Mycodetect kit® from Invitrogen, South Africa.

3.2.3 Cellular uptake of AuNPs using dark field imaging microscopy

Slide preparations for dark field imaging of cells were carried out in the biosafety cabinet. AuNPs were checked for contamination prior to exposure to cells and were used for experimentation when tested negative for bacterial and fungal contamination. The cells were grown overnight in cover slips to a 50% confluent monolayer in a 12 well cell culture plate, at a cell density of 7.4 X 10^4 cells/cm^2. The cover slips for growing HepG2 cells were pre-coated with poly-L-lysine (Sigma-Aldrich, South Africa) following the manufacturers recommendation to facilitate cell attachment. After reaching confluency, the cells were exposed to a 1nM solution of freshly prepared citrate-stabilized and PEG-coated gold nanoparticles suspended in either EMEM or RPMI-1640 growth medium.

The cells were allowed to interact with the AuNPs by further incubating for 4, 6 and 24 hrs at 37°C and 5% CO_2. Following the incubation periods, the spent media was removed and the cells were detached from the culture plate by washing with warm growth medium and PBS solution. The cells were then fixed in 4% ($^v/_v$) formaldehyde Tris/HCl solution (pH 7.5) for 15 minutes at 4ºC. After fixation, the cover slips were washed once with warm PBS and allowed to dry in the biosafety cabinet. The cover slips were glued on clean microscope slides using Kaiser's gelatin solution (Sigma Aldrich, South Africa). Nanoparticles uptake by cells were observed under a high resolution illumination microscopy system. Dark-field images were captured at 60x magnification using the CytoViva 150 Unit integrated onto the Olympus BX43 microscope.

3.2.4 Uptake, localization and distribution of AuNPs in cells using TEM

Subcellular localization and distribution of AuNPs in cells was studied with the TEM. The cells were grown in 25cm^2 flasks under standard cell culture conditions as described. At 50% confluency, cells were exposed to the AuNPs suspended in either EMEM or RPMI-1640 growth medium and further incubated for 24 hrs. Following incubation period, the cell monolayer was detached from the flasks as previously described and suspended in their respective growth medium. The cell viability was determined by the trypan blue cell viability assay.

The cell pellet was processed for electron microscopy analysis by fixing in a 1% glutaraldehyde and 4% formaldehyde solution in 0.1M Phosphate buffer (PB) (pH 7.4) at room temperature for 1 hr. The cell suspensions were centrifuged at 10000 *X g* for 10 min. The fixative solution was removed and the cell pellet was fixed in fresh fixative media overnight at room temperature. After centrifugation, the pellets was washed three times in PB and post-fixed with 1% ($^v/_v$) osmium tetroxide solution for 1 hr, at room temperature. The post-fixed pellets were dehydrated in ethanol series of 30, 50, 70, 80, 90, 95 and 100% and 100% propylene oxide before being transferred to BEEM® capsules filled with epon resin. The capsules were incubated in a 60°C oven for 48 hrs, to complete the embedding (Lu *et al.,* 2010).

Ultrathin sections (60-100nm) of the embedded cells were cut with a Reichert UItracut S microtome and transferred without further additional staining onto fomvar coated 300 mesh copper grids. The copper grids were observed with a Field emission transmission electron microscope (JEOL-JEM 2100F, Tokyo, Japan), fitted out with an energy dispersive X-ray spectrometer (EDS OXFORD INCA spectrometer) and a digital GATAN camera (ERLANGSHEN ES500 W). Energy dispersive X-ray (EDX, EDAX system) spectra were taken

at distinct points to determine the elemental composition of the internalized nanomaterials. TEM images were also captured with the JEOL 100S conventional TEM operated at 60KV.

To further assess exocytosis of the AuNPs in cells, citrate stabilized AuNPs and the PEG-coated AuNPs containing the carboxyl functional group were incubated in the respective culture medium for 24 hrs, the medium was removed and fresh medium without the AuNPs were added to the cells which were returned to the incubator for further incubation. Flasks were incubated for 24 hrs (24 hrs post treatment with AuNPs), 1 week (144 hrs post treatment with AuNPs), 2 weeks (312 hrs post treatment with AuNPs), 3 weeks (480 hrs post treatment) and 4 weeks (648 hrs post treatment with AuNPs). Following each incubation periods, the cells were processed for TEM analysis as described previously.

3.2.5 Quantification of intracellular AuNPs by ICP-MS

To measure intracellular AuNPs, the cells were seeded in a 25cm^2 flask and treated at about 50% confluency with 1nM final concentration of AuNPs. The flasks were further incubated for 1, 4 and 24 hrs. Following incubation, the cell monolayer was washed with warm growth medium and PBS solution. The spent medium (5mL) and the PBS (5mL) wash were kept at 4°C for analysis **(Appendix 2)**. The cell pellet were resuspended in their respective growth medium and the cell viability determined by the trypan blue cell viability assay. Once the cell number was determined, the cell suspension was centrifuged and the supernatant discarded. The cell pellets were prepared for analysis by digesting the pellet in 2mL of fresh aqua regia, hydrochloric acid and nitric acid (3:1 $^{v}/_{v}$) for 2 hrs at 90°C. The digest were kept in the fridge at 4°C until required for analysis. Samples were analyzed in triplicate experiments. Descriptive statistics including

summary measures were conducted for both cell types at each incubation time. Normality assumption was checked using Shapiro-Wilk test. A non-parametric Wilcoxon-rank-sum test was employed to compare statistical significance of the median concentrations of AuNPs in HepG2 and HEK 293 cells.

3.3 Results and Discussion

The AuNPs used for uptake studies were characterized in cell culture medium as described in the preceding chapters. A table summarizing the nanoparticles investigated in this study is shown in Table 3.2.

Table 3.2: List of the investigated nanoparticles

Au Core size	Surface functionalities	Abbreviated as
14nm	Citrate	14nm citrate
20nm		20nm citrate
40nm		40 nm citrate
14nm	1% azide-PEG (99% PEG-OH)	Azide-PEG
	1% NTA-PEG (99% PEG-OH)	NTA-PEG
	1% biotin-PEG (99% PEG-OH)	biotin-PEG
	100% carboxyl-PEG	carboxyl-PEG
	100% hydroxyl-PEG	hydroxyl-PEG
	100% methoxy-PEG	methoxy-PEG

3.3.1 Cellular uptake of AuNPs assessed by dark field microscopy

Dark field images of HepG2 and HEK 293 cells are presented in Figure 3.2. As shown, the control or untreated cell samples represent a monolayer of cells without AuNPs.

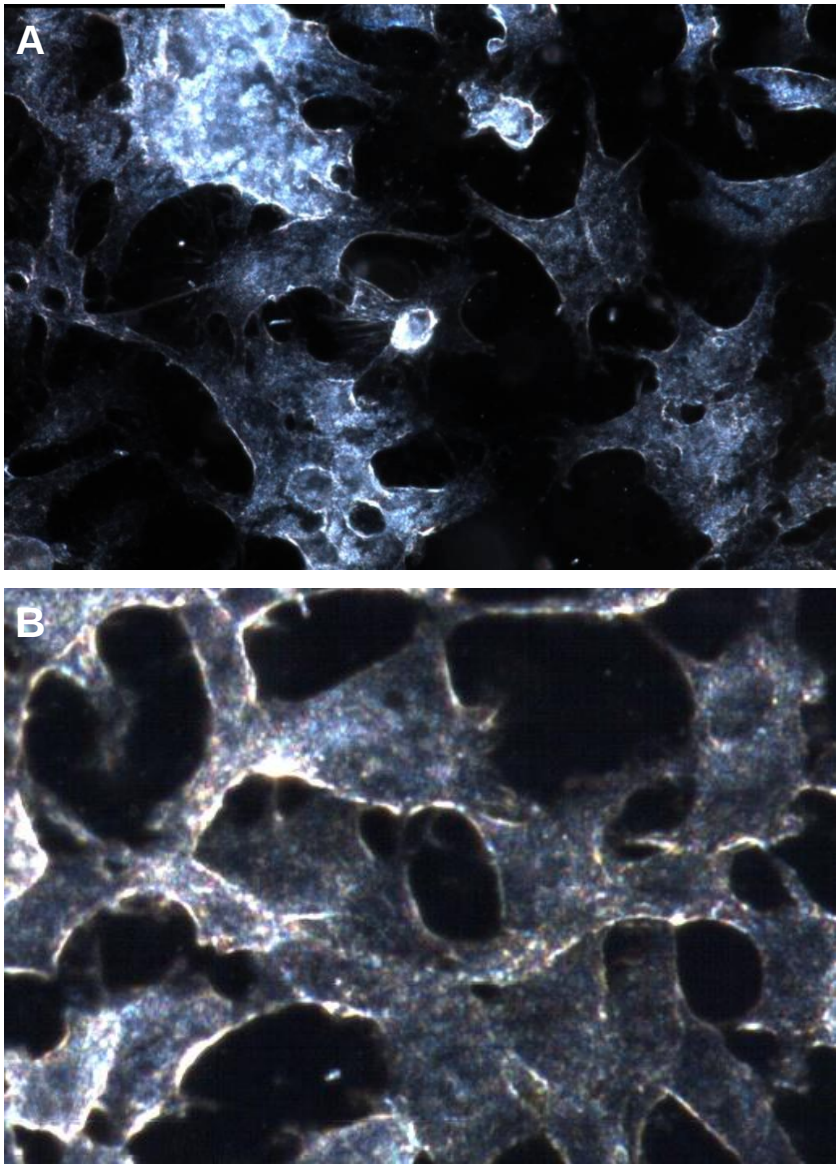


Figure 3.2: Dark field images of (A) liver carcinoma HepG2 and (B) kidney HEK 293 cells without AuNPs.

Figure 3.3 shows dark field images of HepG2 cells treated with 14, 20 and 40nm citrate AuNPs for 4, 6 and 24 hrs. The AuNPs were visible in cell surfaces as bright spots, owing to their intense optical scattering properties (Skebo *et al.,* 2007; Rocha *et al.,* 2011). All three sizes of the citrate stabilized AuNPs where internalized by cells. The images show that the nanoparticles were inside the cells as single and aggregated particles of different sizes (indicated by arrows). In addition, uptake of the citrate AuNPs in cells increased with the exposure time. Nonetheless, the quantity of intracellular AuNPs was confirmed by ICP-MS in the next section.

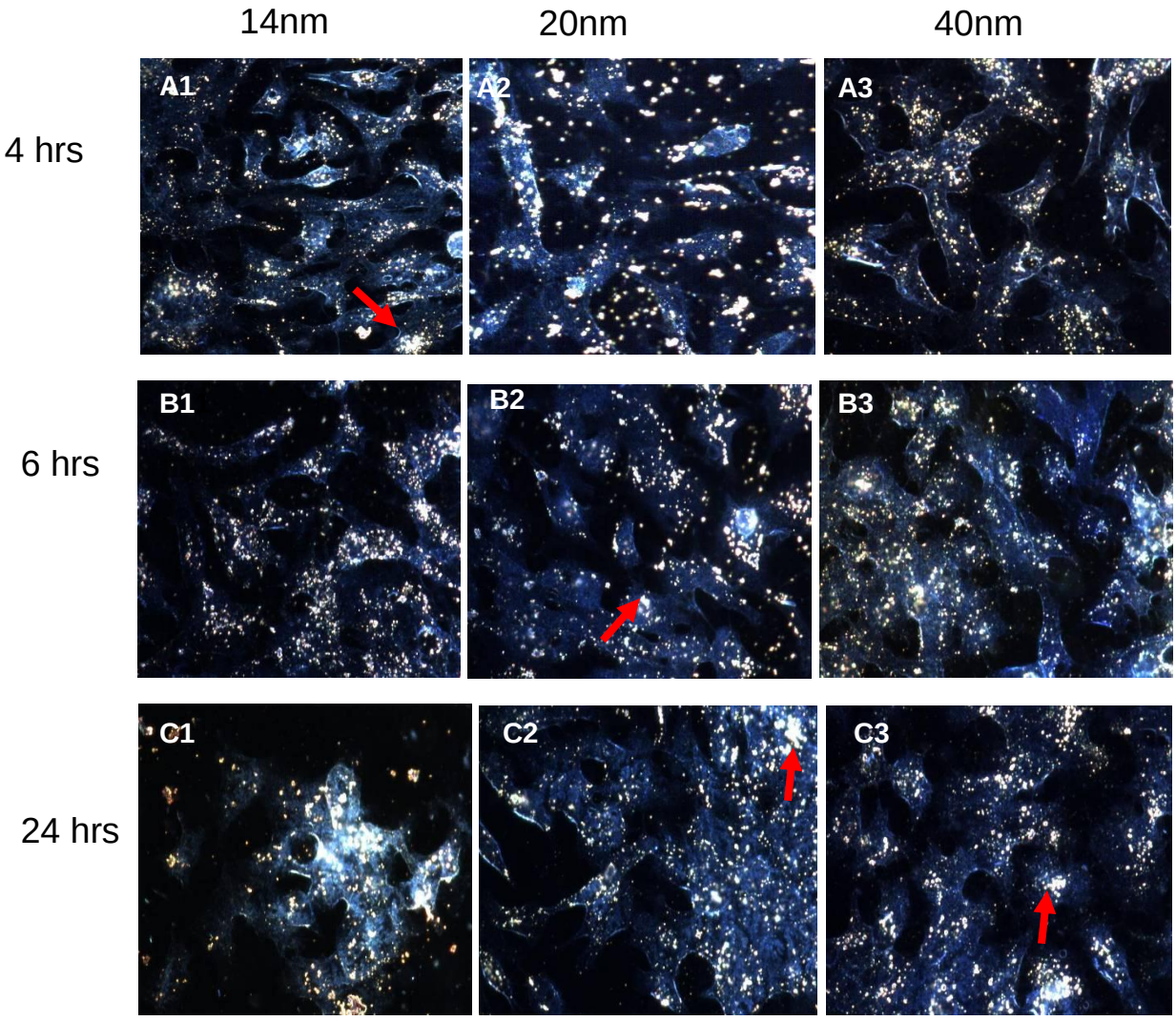


Figure 3.3: Dark field images of HepG2 cells incubated with citrate stabilized AuNPs of increasing diameter for 4 hrs (A1-A3), 6 hrs (B1-B3) and 24 hrs (C1-C3).

Uptake of PEG functionalized AuNPs in HepG2 cells visualized by dark field microscopy is shown in Figure 3.4. Internalized AuNPs were seen on the cell monolayer as shown with cells treated with the azide-PEG, NTA-PEG and biotin-PEG-coated AuNPs. Figure 3.4 reveals high interaction with cells of the AuNPs that contains the positively charged NTA groups. The AuNPs containing the negatively charged groups carboxyl and hydroxyl and the neutral group methoxy were seen in small numbers within the cell monolayer. Nonetheless, uptake of the PEG-coated AuNPs with cells was lower when compared to the cells that were treated with the citrate AuNPs. This was further confirmed by ICP-MS analysis. Aggregated nanoparticles on cell membrane were also observed in cells treated with carboxyl-PEG and hydroxyl-PEG AuNPs 4, 6 and 24 hrs after incubation. The images indicate that some of the nanoparticles are unable to enter the cell because of their larger size.

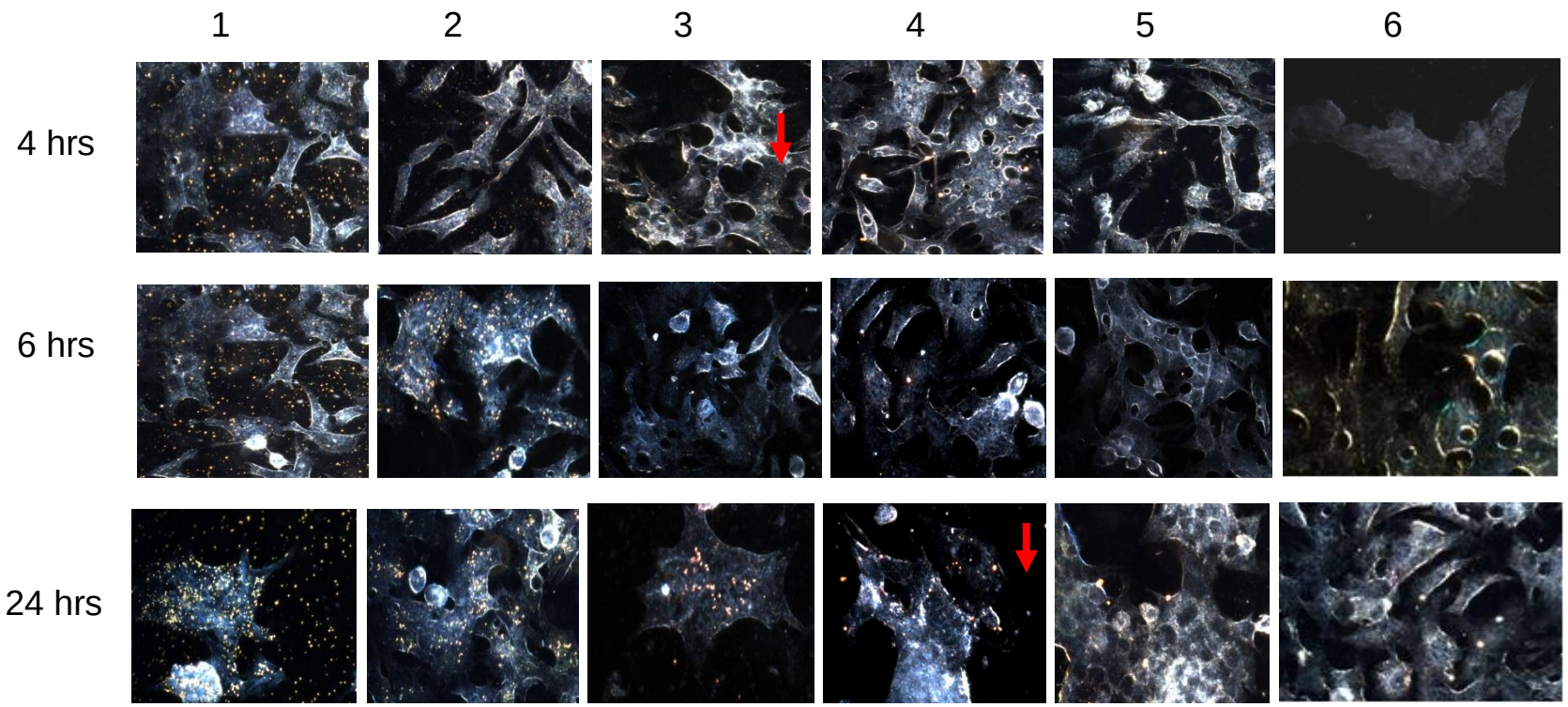


Figure 3.4: HepG2 cells incubated with (1) azide-PEG, (2) NTA-PEG, (3) biotin-PEG, (4) carboxyl-PEG, (5) hydroxyl-PEG and (6) methoxy-PEG coated AuNPs for 4, 6 and 24 hrs

AuNPs uptake in HEK 293 cells was also assessed with dark field imaging microscope. Figure 3.5 shows images of 14, 20 and 40nm citrate AuNPs incubated with cells for 4, 6 and 24 hrs. The images showed the 40nm citrate AuNPs to have the highest uptake in cells than the 14 and the 20nm particles. Nonetheless this was further confirmed by ICP-MS analysis. AuNPs were shown to be internalized by cells as clusters of different sizes. Similar to HepG2 cells, the images shows that uptake of all three citrate AuNPs to increase in cells as the incubation time was increased.

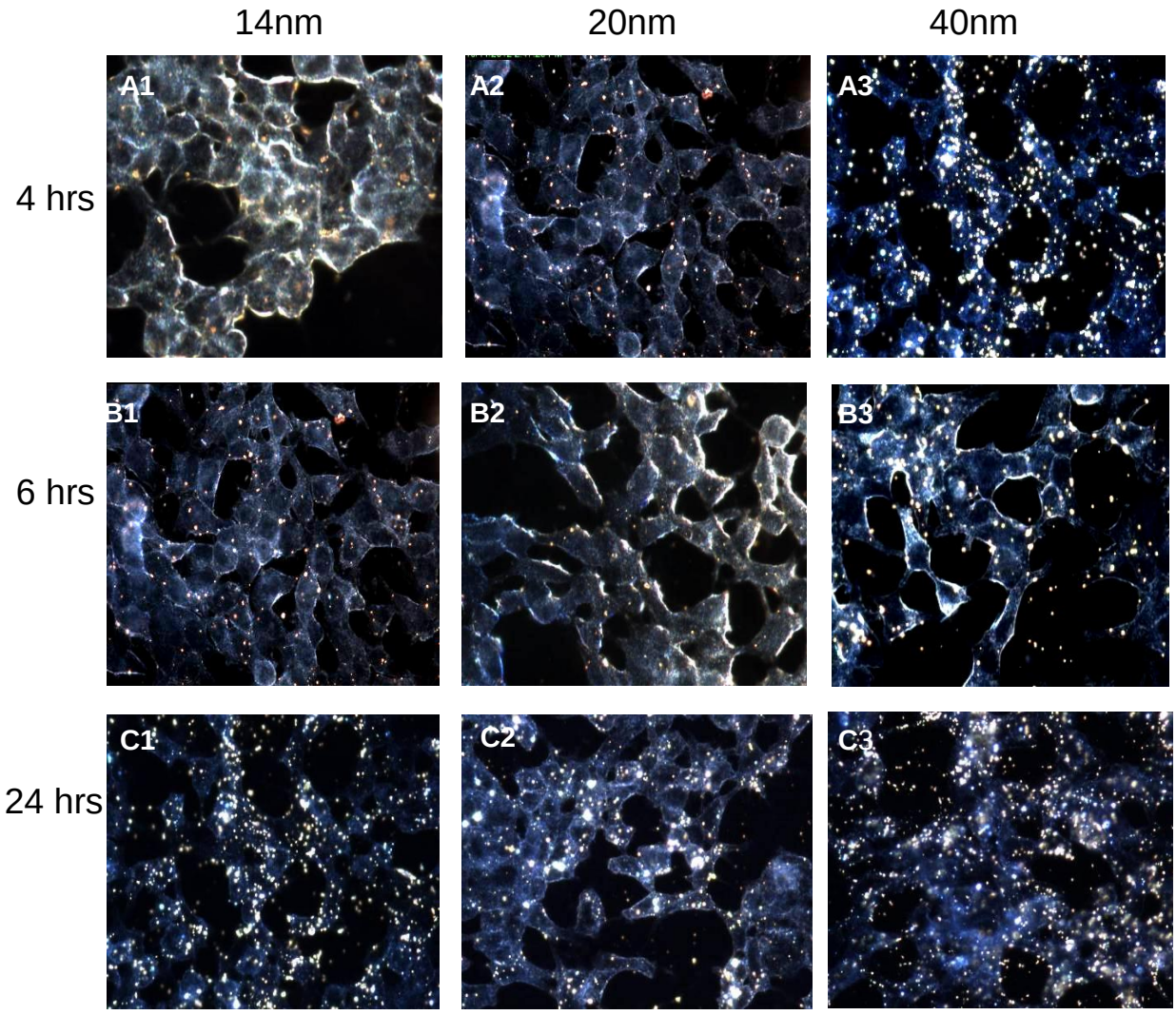


Figure 3.5: HEK 293 cells incubated with citrate stabilized AuNPs of increasing diameter. Dark field images of citrate-stabilized AuNPs for 4hrs (A1-A3), 6hrs (B1-B3) and 24 hrs (C1-C3).

Dark field images in Figure 3.6 show the uptake of PEG-coated AuNPs in HEK 293 cells after 4, 6 and 24 hrs incubation. AuNPs were internalized in cell in different sizes, with large aggregates visible on the cell surface. Similar to the citrate AuNPs, the longer the incubation time indicated high uptake of PEG-coated AuNPs by cells. Similarly, the azide-PEG AuNPs were shown to be the most interacting with the HEK 293 cells, with the methoxy-PEG AuNPs being the least found in cells. Large clusters of AuNPs on cell membrane were seen on majority of the images in cells incubated with the NTA-PEG, biotin-PEG, carboxyl-PEG, hydroxyl-PEG and the methoxy-PEG-coated AuNPs in Figure 3.6 (indicated by arrow). Attachment of AuNPs on cell membrane may be the results of the PEG coating on the AuNPs surface, resulting in minimal uptake of these nanoparticles.

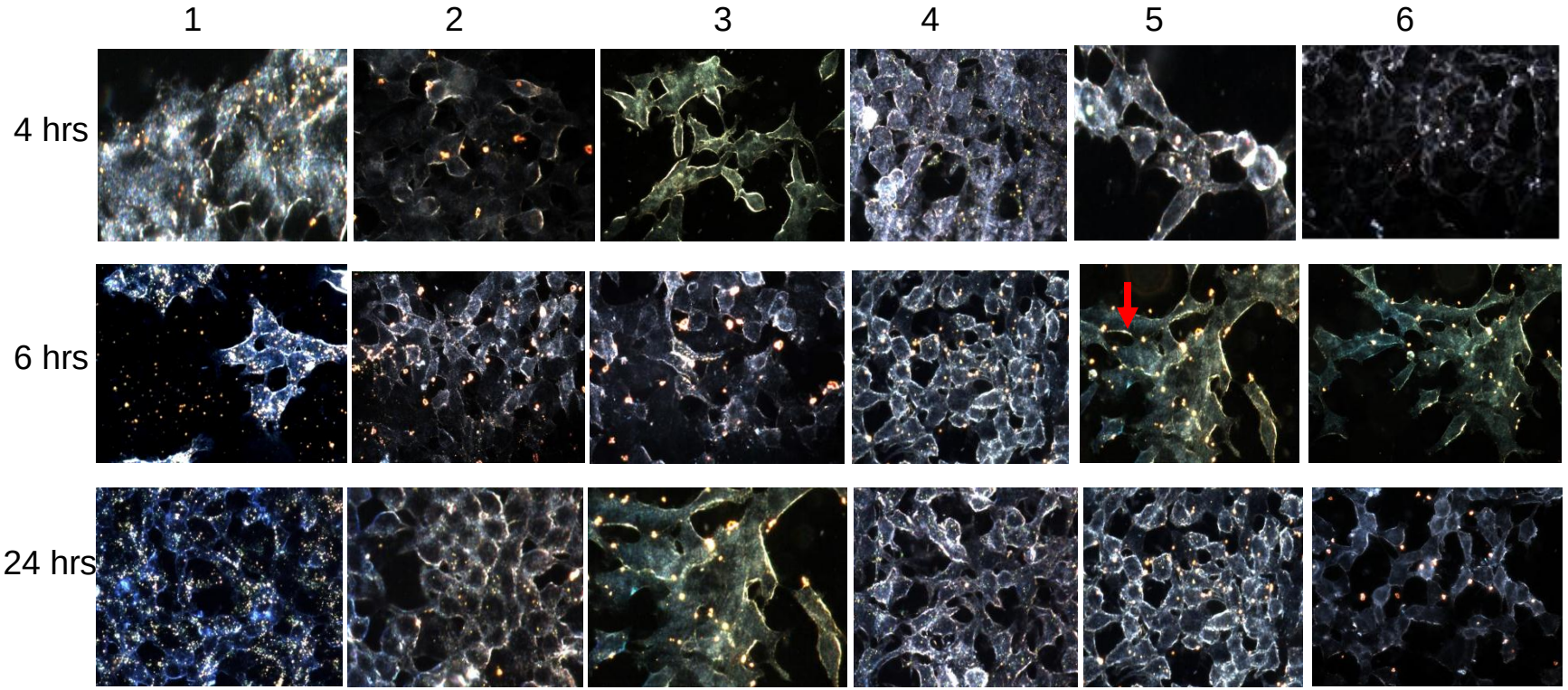
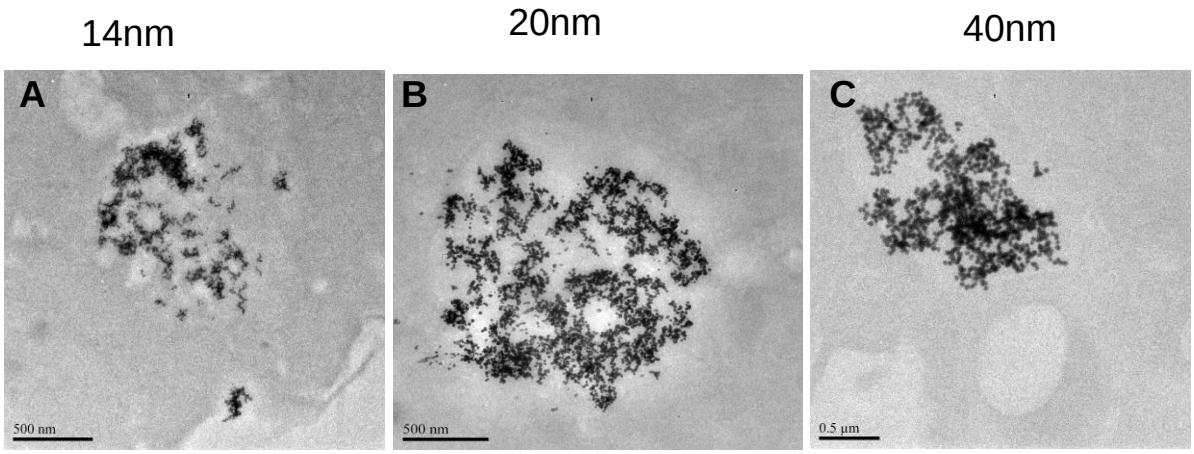
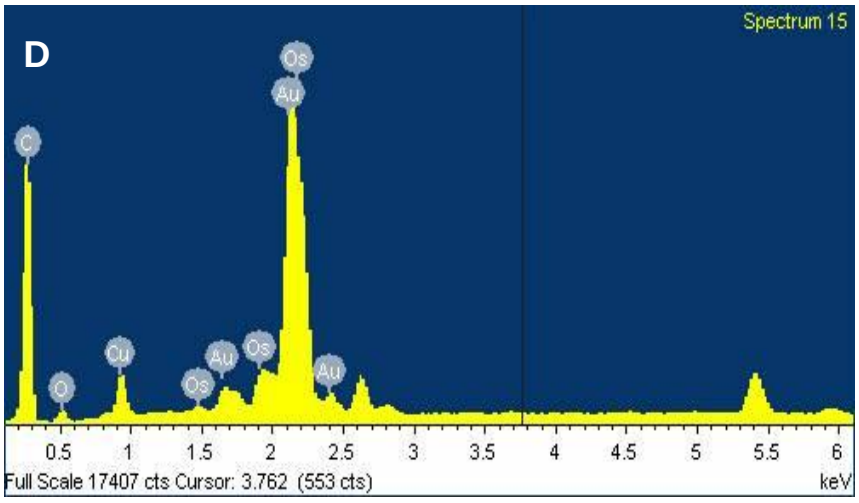


Figure 3.6: HEK 293 cells incubated with (1) azide-PEG, (2) NTA-PEG, (3) biotin-PEG, (4) carboxyl-PEG, (5) hydroxyl-PEG and (6) methoxy-PEG coated AuNPs for 4, 6 and 24 hrs

3.3.2 Intracellular localization and distribution of AuNPs in cells via TEM analysis

TEM imaging was used to confirm AuNPs uptake in cells, their intracellular distribution and localization in cellular compartments. The gold nanospheres were visible in cellular compartments without additional staining. Figure 3.7 shows TEM images of HepG2 incubated with citrate AuNPs for 24 hrs. The images confirmed uptake of AuNPs in cells and indicated that the nanoparticles tend to come together inside cells to form polydisperse particles with distinguishable spherical morphology and aggregation. Furthermore, the AuNPs were confined in large vesicles within cells (Figure 3.7A and 3.7B) and in the cell cytoplasm (Figure 3.7C). AuNPs on the cell membrane were also seen, possibly during entry into the cells (Figure 3.7A) (Mu *et al.,* 2012). Intracellular AuNPs were confirmed by EDX analysis and revealed a significant Au peak at 2.3keV in cell samples that were exposed to the AuNPs (Figure 3.7D). The Au Peak at 2.3keV was reported in other studies investigating uptake of AuNPs using TEM (Ng *et al.,* 2011). In agreement with dark field images, a large number of the citrate AuNPs were detected on TEM images of cells.





Element	Weight (%)	Atomic mass (%)
C K	12.23	51.65
O K	0.40	1.26
Cu K	45.38	36.23
Os L	5.22	1.39
Au L	**36.78**	**9.47**

Figure 3.7: HepG2 cells incubated with AuNPs for 24 hrs (A-C). TEM images of citrate stabilized AuNPs and (D) EDX analysis confirming the elemental Au in cell sections. Cu was from the copper grids used for preparation of cell samples. Os peak was the result of the osmium tetroxide used for staining the cells.

The uptake of PEG-coated AuNPs in HepG2 cells was also confirmed by TEM analysis (Figure 3.8).

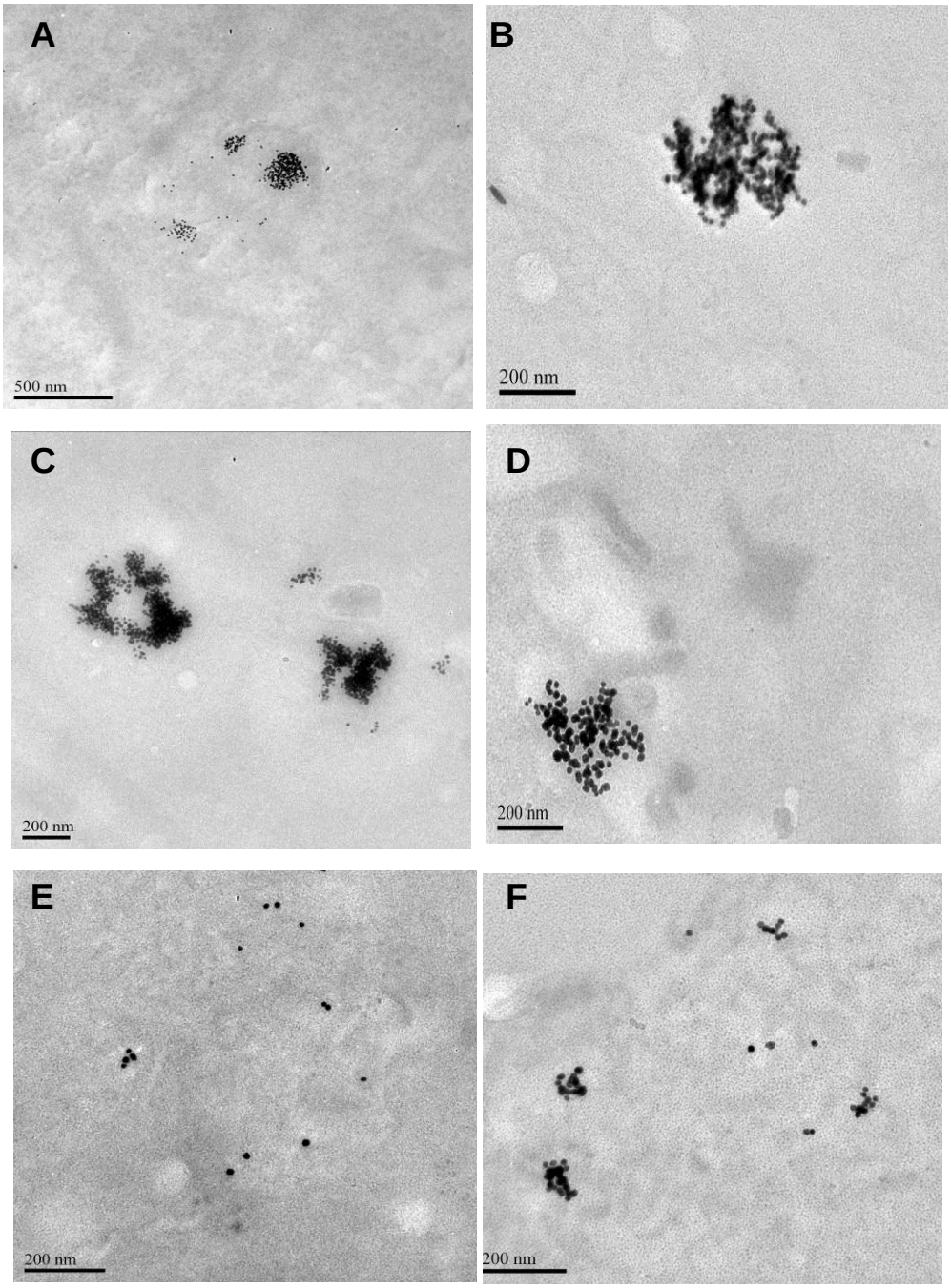


Figure 3.8: TEM images of HepG2 cells treated with (A) azide-PEG, (B) NTA-PEG, (C) biotin-PEG, (D) carboxyl-PEG; (E) hydroxyl-PEG and (F) methoxy-PEG AuNPs for 24 hrs.

The images show internalized PEG AuNPs in the cell cytoplasm (Figure 3.8A, 3.8B, 3.8C, 3.8E and 3.8F). The AuNPs were distributed in cells as single and aggregated nanoparticles of different sizes. Nonetheless, the spherical morphology of the AuNPs was retained on the

nanoparticles that have clumped. The majority of the single particles were dispersed in the cytoplasm, while clusters of AuNPs were confined in cellular vesicles (Figure 3.8A- 3.8C). Similar to cells that were incubated with citrate AuNPs, TEM images revealed PEG-AuNPs on the cell plasma membrane during entry into the cells (Figure 3.8D). These observations were confirmed in the literature for carboxyl- PEG-thioactic acid (TA)-AuNPs with kidney COS-1 cells (Oh *et al.,* 2011) and for methoxy-PEG AuNPs with U937 cells (Oh *et al.,* 2014a).

There was no evidence of localization of AuNPs in major organelles such as the nucleus or mitochondria in any of the sections of cells that were treated with the either the citrate stabilized or PEG-coated AuNPs (Figure 3.9). The lack of localization of AuNPs in these cellular compartments was reported for 14nm, 50nm and 74nm citrate stabilized AuNPs in breast cancer (MCF-7) cells (Chithrani *et al.,* 2009) and have been attributed to the size of the nanoparticles. Size and surface chemistry are two fundamental parameters that determine fate of nanoparticles in cellular organelles, where nanoparticles with smaller hydrodynamic size (< 5nm) are more likely to gain access to the nuclear membrane (Gu *et al.,* 2009; Dam *et al.,* 2012; Huang *et al.,* 2012; Fraga *et al.,* 2013; Lui *et al.,* 2013). Thus, the sizes of the AuNPs studied and the functional groups present on nanoparticle surface did not allow localization into the mitochondria or nucleus of the two cell lines

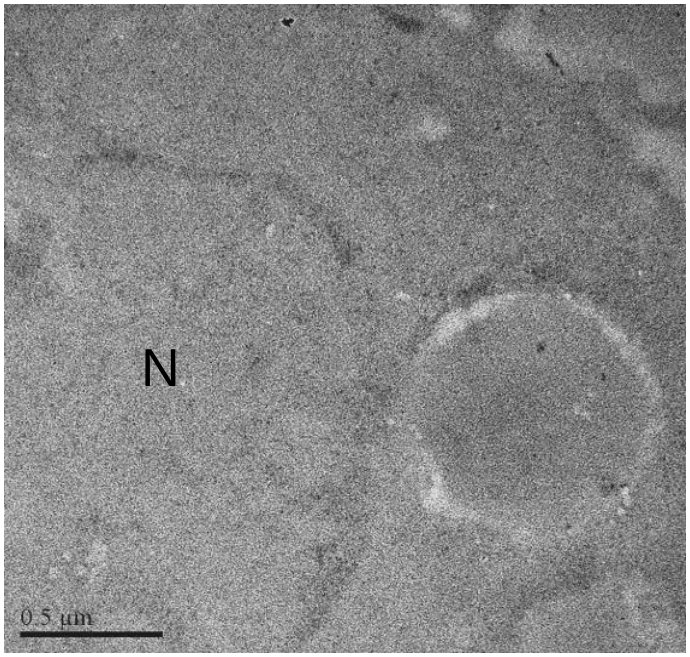


Figure 3.9: TEM image showing nuclear region of HepG2 cells free of AuNPs.

TEM images of HEK 293 cells incubated with citrate AuNPs are shown in Figure 3.10. The images confirmed uptake of the AuNPs by cells and indicated localization of the nanoparticles in cell cytoplasm (Figure 3.10A) and in cellular vesicles (Figure 3.10B and 3.10C). In Figure 3.10A, the nanoparticles are evenly dispersed in the cell cytoplasm, forming groups of different sizes. Closer inspection of Figure 3.10C revealed that AuNPs enter the cell as a group, which is then deposited in the vesicles where they form clusters of different sizes. Individual particles were also seen in the cell vesicles. In Figure 3.10C, a large group of the nanoparticles was seen in a vesicle located closer to the cell membrane, indicating the AuNPs were internalized as a group. Nonetheless, in all three figures, the nanoparticles showed a noticeable spherical morphology (Figure 3.10B and 3.10C).

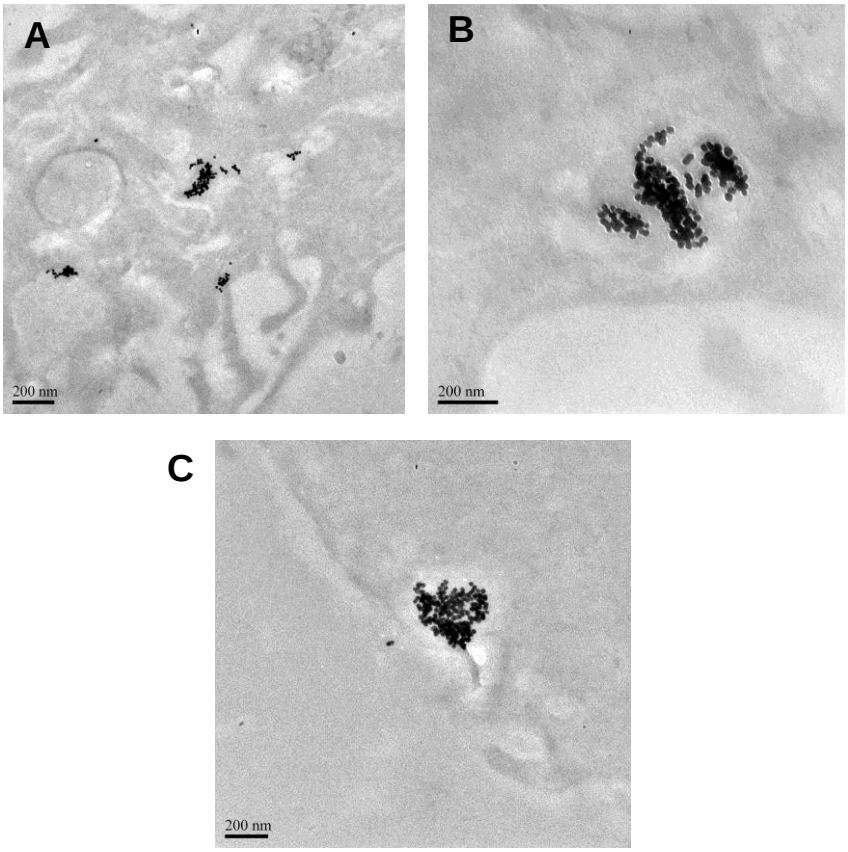


Figure 3.10: HEK 293 cells incubated with AuNPs for 24 hrs. Cells were treated with (A) 14nm, (B) 20nm and (C) 40nm citrate stabilized AuNPs.

TEM images of HEK 293 cells after incubation with PEG-coated AuNPs are shown in Figure 3.11. The images show accumulation of AuNPs in intracellular vesicles of different sizes (Figure 3.11B, 3.11C, 3.11D and 3.11E). Similar to citrate AuNPs, single and clusters of PEG-coated AuNPs were observed in the vesicles. The vesicles were located close to the cell periphery, thus are more likely to be the recycling vesicles of the endosomes and lysomes, indicating that endocytosis may be the main mechanism by which these AuNPs enters the cells (Chithrani *et al.,* 2009). Localization of AuNPs in vesicles have been reported in many other studies, including Lui *et al* (2013) who reported localization of citrate capped and surface modified AuNPs in the secondary lysosomes of HepG2 cells as small or large aggregates.

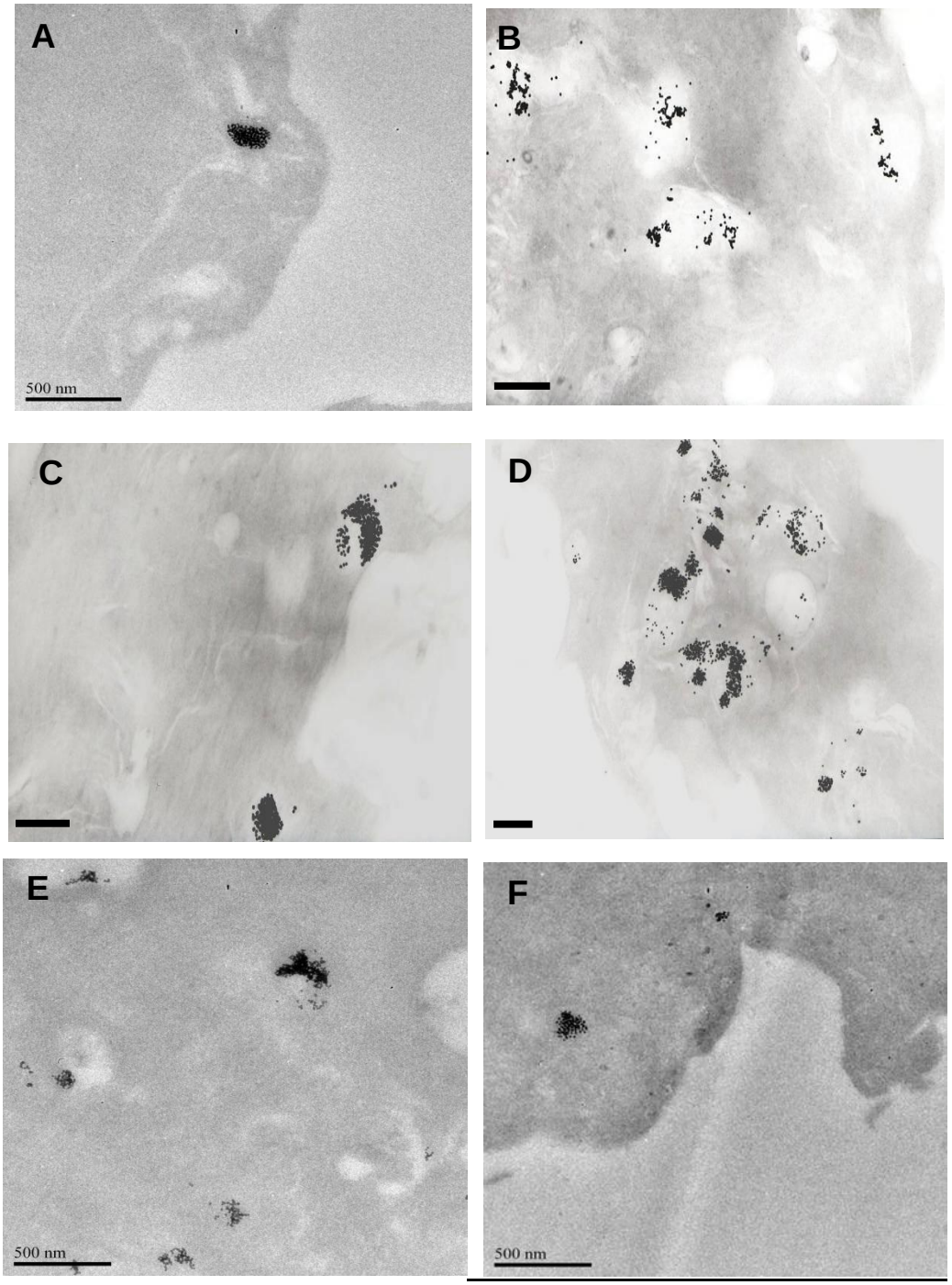


Figure 3.11: TEM images of HEK293 cells incubated with (A) azide-PEG, (B) NTA-PEG, (C) biotin-PEG, (D) carboxyl-PEG, (E) hydroxyl-PEG and (F) methoxy-PEG AuNPs for 24 hrs. (Scale 500nm)

The exocytosis of the 14nm citrate AuNPs and the 14nm carboxyl-PEG-AuNPs were investigated. TEM images showing citrate stabilized AuNPs in cells 3 and 4 weeks after incubation are shown in Figure 3.12. The images revealed that AuNPs remain in cellular vesicles (Figure 3.12A), where they are eventually secreted to the cell exterior (Figure 3.12B). The removal of the vesicle containing the AuNPs was evident as one form of excreting AuNPs from the cells (Chithrani and Chen, 2007; Sakhtianchi *et al.,* 2013).

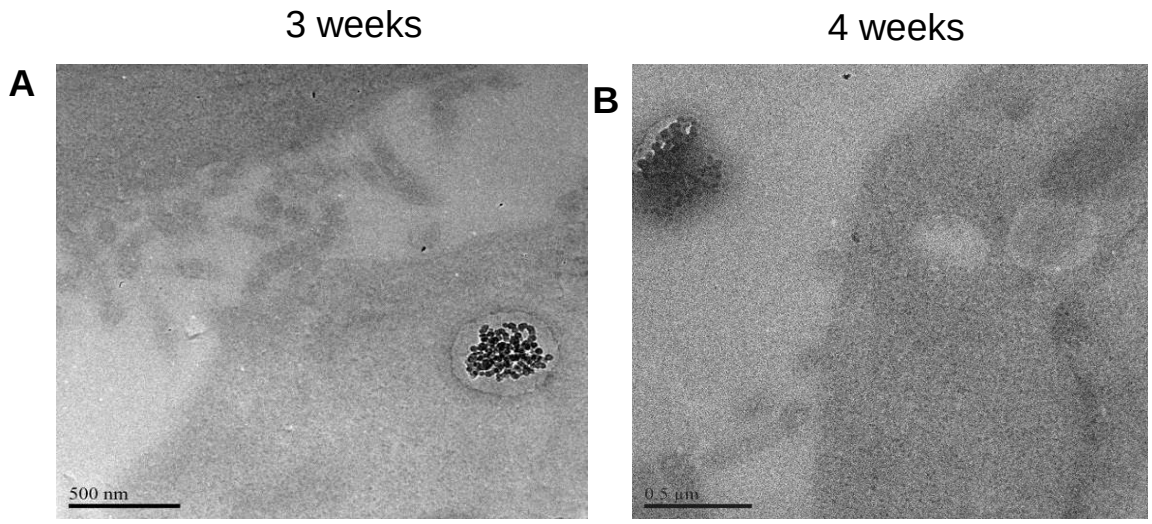


Figure 3.12: TEM image of HepG2 cells incubated with 14 nm citrate AuNPs for 3 and 4 weeks.

TEM images of 40nm citrate AuNPs incubated with cells for 1 (A), and 2 (B) weeks are shown in Figure 3.13. The AuNPs were excreted from cells as early as 1 week after incubation (Figure 3.13A). Nonetheless, the AuNPs remained in the cell two weeks after incubation (Figure 3.13B). These particles were found distributed along the vesicle membranes, leaving the interior of the vesicles empty.

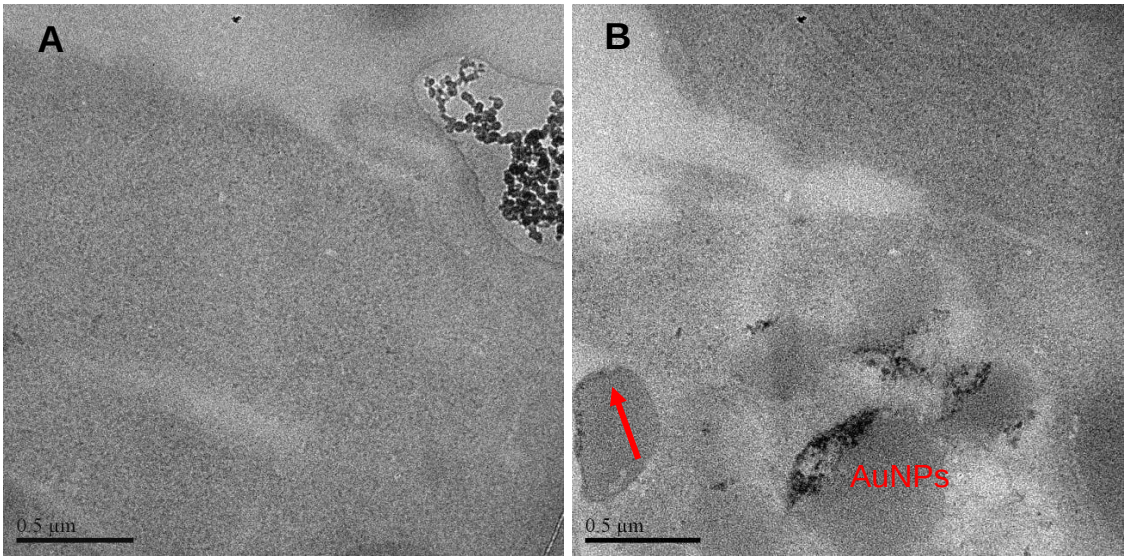


Figure 3.13: HepG2 cells incubated with 40nm citrate stabilized AuNPs. (A) Excreted vesicles with AuNPs were seen as early as 1 week after incubation. (B) Intracellular AuNPs were located in endo-lysosomal vesicle two weeks after incubation.

TEM images of the 14nm carboxyl-PEG AuNPs showed that these nanoparticles were retained in the cells for up to 3 weeks (Figure 3.14). The images showed that vesicles about to be removed from cells move toward the cell plasma membrane, where as shown in Figure 3.14C they are eventually excreted from the cells. The image in Figure 3.14D shows that some of the AuNPs were excreted from the cells without the vesicles. Nanoparticles escaping or that are leaked from loaded vesicles can travel through the cytoplasm, where they are eventually secreted by non- vesicle related secretion (Sakhtianchi *et al.,* 2013; Oh and Park, 2014b).

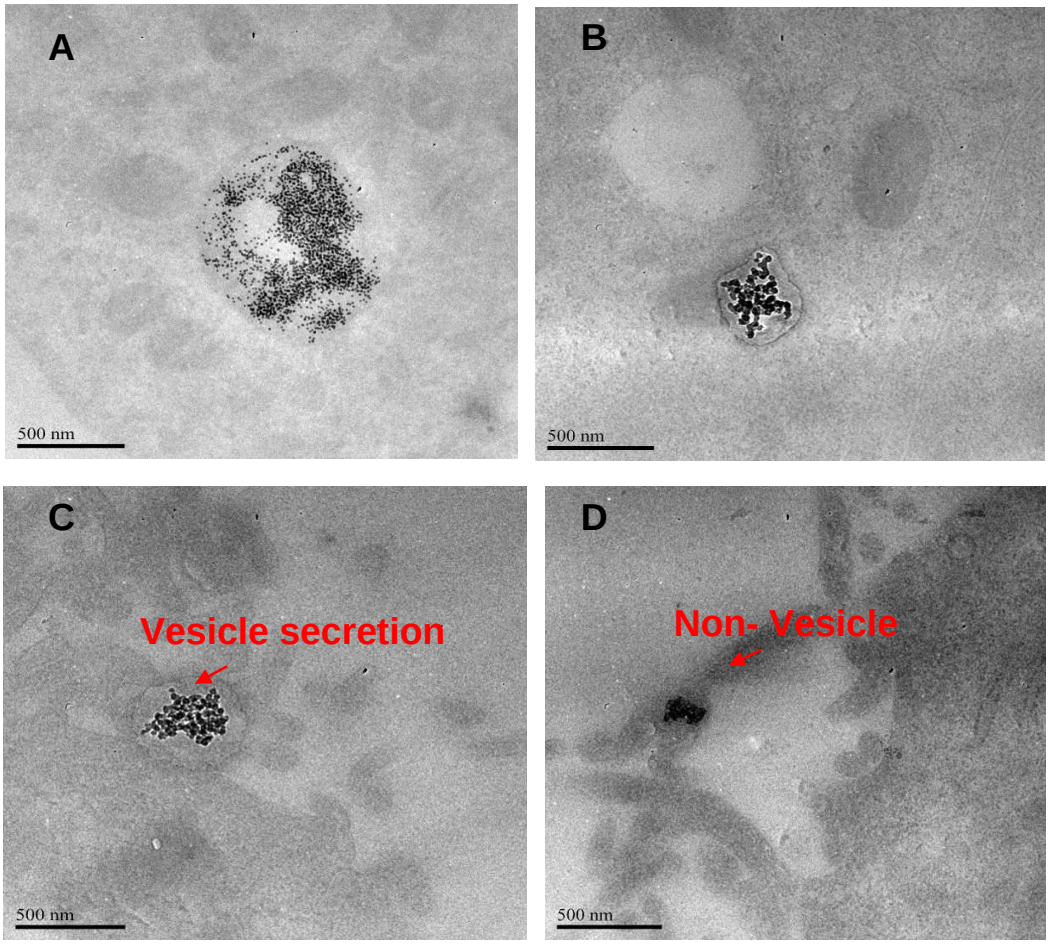


Figure 3.14: TEM sections of cells exposed to 14nm carboxyl-PEG-coated AuNPs (A) 1 week, (B) 2 weeks, (C) 3 week and (D) 4 weeks.

3.3.3 Quantitative analysis of intracellular gold nanoparticle concentrations with ICP- MS

ICP-MS technique was used to quantify the concentrations of 14, 20 and 40nm citrate stabilized and PEG functionalized AuNPs in the two cell types. The results represent Au content in a million cells that was exposed to a 1nM concentration of AuNPs. The concentrations (in µg/L) of AuNPs in the cell pellet, as indicated in the table in **Appendix 2** after 1, 4 and 24 hrs incubation are shown in Figure 3.15 and 3.16. Figure 3.15 and 3.16 showed cellular uptake of AuNPs as early as 1 hr after incubation, with the concentrations of 14nm and 40nm AuNPs increasing when the incubation time is increased (figure 3.15).

Figure 3.15 shows intracellular AuNPs in HepG2 cells. The median concentration of 14 and 20nm citrate AuNPs after incubation were not statistically significant from each other ($p>0.05$). On the other hand, the Wilcoxon rank-sum test showed a statistically significance difference between concentration of 40nm citrate AuNPs incubated with HepG2 cells for 1 and 24 hrs and on cells incubated with the 40nm AuNPs for 4 and 24 hrs. The concentration of 20nm citrate AuNPs in cells decreased as the incubation time was increased. For this AuNPs, the cells may have been saturated with the particles 4 hrs after incubation, at which point exocytosis of the AuNPs was most likely to occur. This observation may be dependent on size and surface chemistry of the AuNPs. A similar study by Chithrani *et al.* (2006) investigating the uptake of 14, 30, 50, 74 and 100nm citrate AuNPs in mammalian cells reported an increase in the uptake of 14, 50 and 74nm AuNPs in the first two hours of incubation with cells. Nonetheless, as the incubation time was increased the uptake rate was shown to decrease as cellular uptake reached a plateau after 4-7 hrs of incubation (Chithrani *et al.,* 2006).

The PEG-coated AuNPs showed the least uptake in HepG2 cells when compared to the citrate AuNPs, even after 24 hrs incubation. The data was in consistent with dark field microscopy images that revealed a high number of 14, 20 and the 40nm citrate AuNPs associated with cells than the PEG-coated AuNPs.

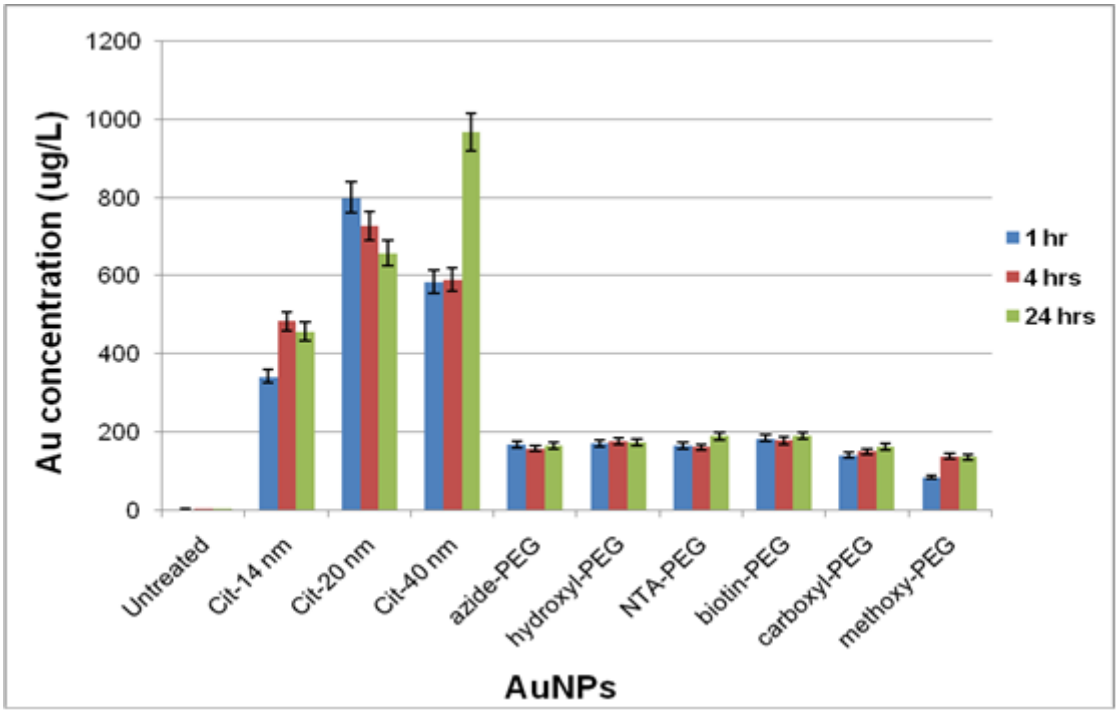


Figure 3.15: Quantification by ICP-MS showing the concentrations (in µg/L) of Au in HepG2 cells after 1, 4 and 24 hrs incubation with citrate stabilized and PEG-coated gold nanoparticles.

Figure 3.16 shows intracellular concentration of citrate stabilized AuNPs and PEG-coated AuNPs in HEK 293 cells. The figure indicates a high uptake of the 20nm citrate AuNPs in HEK 293 cells when compared to 14 and 40nm citrate AuNPs. There was an increase in the concentration of AuNPs as the incubation time was increased for the citrate AuNPs. Similar to HepG2 cells, uptake of PEG-coated AuNPs was low in HEK 293, even after 24 hrs of incubation. Statistical analysis revealed no significant difference in the concentrations of the PEG-coated AuNPs in cells.

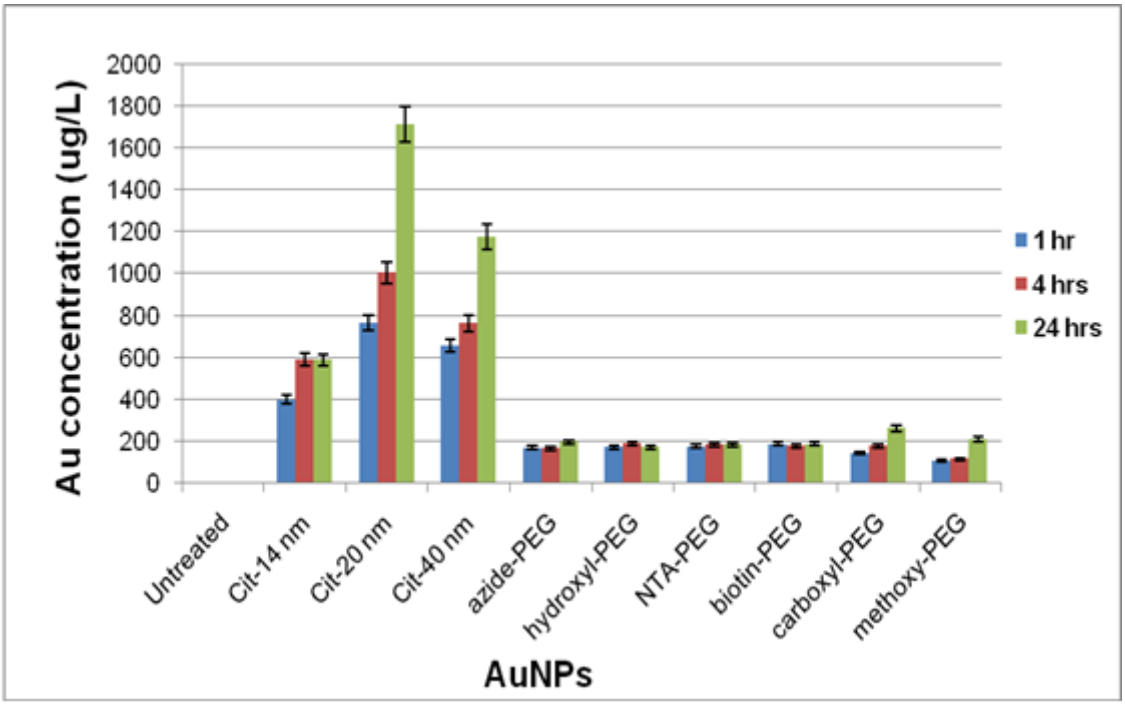


Figure 3.16: Quantification by ICP-MS showing the concentration (in µg/L) of Au element HEK 293 cells 1, 4 and 24 hrs incubation with citrate stabilized and PEG-coated AuNPs at 1nM concentration.

The high uptake concentration of citrate AuNPs in cells has previously been correlated to the binding of serum onto the citrate ions, increasing the adhesion of the AuNPs with cells (Chithrani *et al.,* 2009). The minimal uptake of PEG-coated AuNPs in cells has been attributed to the hydrophilicity of the PEG molecule, which has been shown to hinder the adhesion of nanoparticles to the cell membrane (Nativo *et al.,* 2008; Kettler *et al.,* 2014). In addition, the negatively charged groups such as the carboxyl group and neutral functional groups like the hydroxyl and the methoxy groups were expected to repel the negatively charged cell membrane (Frohlic, 2012, Saha *et al.,* 2013; Shang *et al.,* 2014; Kettler *et al.,* 2014).

Table 3.3 indicates differences in the median and IQR (interquartile range) of AuNPs concentrations in HepG2 and HEK 293 cells. The concentration of intracellular AuNPs in the

two cell lines were not statistically different ($p>0.05$). Further, a non-significant difference of the mean concentration in cells treated with PEG-coated AuNPs was seen. The results indicated a higher uptake of AuNPs in HEK 293 cells than in HepG2 cells. The differences in response of cells in nanoparticle uptake have in shown in literature, where normal cells were shown to transport more nanoparticles across the cell membrane, compared to the malignant cells (Ventakataraman *et al.,* 2005).

Table 3.3: Concentrations of AuNPs in HepG2 and HEK 293 cells.

AuNPs	**HepG2** **Median (IQR)**	**HEK 293** **Median (IQR)**	**p-value**
Cit- 14nm	362.1 (76.2-485.5)	342.1 (102.1-749.4)	0.6272
Cit- 20nm	948.2 (289-1085)	1041 (232.5-1429)	0.3538
Cit- 40nm	170.4 (776-1516)	658.2 (148.6-1083)	0.5660
Azide-PEG-AuNPs	71.9 (28-388)	91.8 (56.9-395.2)	0.5078
Hydroxyl-PEG-AuNPs	79.1 (7.8-423.1)	95.6 (20.7-411.2)	0.7573
NTA-PEG-AuNPs	80.2 (6.4-393)	71.8 (14.8-458.1)	0.8253
Biotin-PEG-AuNPs	90.4 (4.6-435.7)	98.7 (7.8-411.9)	0.6911
Carboxyl-PEG-AuNPs	74.3 (53.3-350.9)	91.2 (52.1-339.6)	0.6272
Methoxy-PEG-AuNPs	60 (43-195.4)	88.8 (47.7-236.5)	0.5660

Table 3.4 demonstrates the concentrations of AuNPs over 1, 4 and 24 hours interval in HepG2 and HEK 293 cells. There was no statistically significant difference in median concentrations of AuNPs. The median concentrations of AuNPs in HEK 293 were higher when compared to HepG2 after 4 hrs incubation period. The table indicates that during the 1 hr incubation, the median concentrations of 14nm citrate AuNPs, 20nm citrate AuNPs, NTA-PEG AuNPs, and carboxyl-PEG AuNPs were high in HepG2 cells when compared to the HEK 293 cells. Nonetheless, there was no statistically significant difference. The methoxy-

PEG AuNPs showed the least uptake in both cell types, which may be attributed to the weak interaction of the neutral surface charge on the methoxy functional group with the cell plasma membrane.

Table 3.4: Comparisons of median concentration of AuNPs in HepG2 and HEK 293 cells following incubation for 1, 4 and 24 hrs. IQR = Interquartile ranges.

Duration of incubation	AuNPs	Hep G2 Median (IQR)	HEK 293 Median (IQR)	p-value
1 hr	Cit- 14nm	434.6 (105.8-485.5)	342.1(101.9-749.4)	0.8273
	Cit- 20nm	948.2 (289.2-1162)	630 (232.5-1429)	0.8273
	Cit- 40nm	190.4 (48.5-1516)	736.4 (148.6-1083)	0.8273
	Azide-PEG-AuNPs	92.2 (19.4-393.3)	98.1 (10.8-407.1)	0.8273
	Hydroxyl-PEG-AuNPs	83.2 (7.2-423.1)	95.6 (2.7-421.7)	0.8273
	NTA-PEG-AuNPs	97.8 (5.1-393)	59.2 (1.1-462.9)	0.8273
	Biotin-PEG-AuNPs	98.4 (3.1-450.8)	95.7 (0.7-471)	0.8273
	Carboxyl-PEG-AuNPs	62.8 (7.1-350.9)	51.1(45.1-339.6	0.8273
	Methoxy-PEG-AuNPs	43 (11.9-195.3)	47.7 (39.34-237.5)	0.5127
4 hrs	Cit- 14nm	326.1 (49.5-1074)	709 (102.1-953.6)	0.8273
	Cit- 20nm	954.9 (142-1085)	1346 (180.9-1488)	0.2752
	Cit- 40nm	170.4 (52.3-1545)	658.2 (116.4-151)2	0.8273
	Azide-PEG-AuNPs	62.2 (16.3-388)	73.8 (24.2-395.2)	0.5172
	Hydroxyl-PEG-AuNPs	78.4 (5.4-445.2)	101.9 (7.4-459.3)	0.5172
	NTA-PEG-AuNPs	60.7 (4.6-414.5)	72.5 (4.3-474.9)	0.8273
	Biotin-PEG-AuNPs	90.4 (3.4-435.7)	118.8 (3.5-411.9)	0.8273
	Carboxyl-PEG-AuNPs	80.3 (11.5-353.8)	91.6 (52.1-382.6)	0.5127
	Methoxy-PEG-AuNPs	60 (54.1-296.9)	69 (36.58-236.5)	0.8273
24 hrs	Cit- 14nm	76.2 (18.5-1277)	230.4 (49.2-1481)	0.5127
	Cit- 20nm	488.9 (107.7-1378)	1041 (166.9-3923)	0.5127
	Cit- 40nm	125.7 (77.6-2699)	357.3 (52.1-3095)	0.8273
	Azide-PEG-AuNPs	71.9 (28-392.1)	91.8 (56.9-438.8)	0.5127
	Hydroxyl-PEG-AuNPs	79.1 (7.8-435.7)	85.9 (20.7-411.2)	0.8273
	NTA-PEG-AuNPs	80.2 (6.4-476.1)	71.8 (14.8-458.1)	0.8273
	Biotin-PEG-AuNPs	81 (4.6-457.2)	98.7 (7.8-454.3)	0.8273
	Carboxyl-PEG-AuNPs	74.3 (53.3-356.4)	324.7 (73-387.4)	0.5127
	Methoxy-PEG-AuNPs	70.1 (34.4-301.5)	192.4 (88.8-350.4)	0.2752

3.4 Summary and Conclusion

This chapter described the uptake of 14, 20 and 40nm citrate stabilized AuNPs and PEG coated AuNPs presenting different functional groups on two major cell lines, representing accumulation sites of the AuNPs *in vivo*. Dark field imaging and TEM analysis was used to assess uptake and intracellular localization of the AuNPs. Following this, ICP-MS analysis was to confirm the uptake of AuNPs in cells by providing a quantitative analysis on Au concentration in the cell pellet. The results indicated the uptake of AuNPs in both cells type, where a higher degree of uptake citrate AuNPs was seen in both cell types than in cells incubated with the PEG coated AuNPs. Furthermore, gold concentration by ICP-MS revealed that the citrate stabilized AuNPs had the highest uptake in both cell types.

Uptake was shown to be dependent on size for the citrate stabilized AuNPs, where the 40nm citrate AuNPs showed a higher uptake concentration compared to the 14 and 20nm AuNPs. Uptake of citrate AuNPs varied in the two cell lines. Nonetheless, there was no statistical difference in the concentrations of citrate AuNPs and PEG coated AuNPs in the two cells. A time dependent uptake of the 40 nm citrate AuNPs and carboxyl-PEG AuNPs in HepG2 and 14, 20 and 40nm citrate AuNPs and azide-PEG, carboxyl-PEG and methoxy-PEG AuNPs in HEK 293 cells was seen.

The findings indicated predominant localization of the gold nanospheres in the recycling vesicles of the endosomes and lysosomes, with a few individual or single nanoparticles accumulating in the cell cytoplasm. There was no evidence of nuclear or mitochondrial accumulation in cells treated with AuNPs, indicating that size and surface coating play a major role in determining the fate of nanoparticles in cellular compartments (Krpetic, 2011). TEM images suggest that the uptake of the AuNPs in HEK 293 and HepG2 cells to be via an

endocytosis, as indicated by some of the absorbed nanoparticles on the cell surface during uptake.

By incubating the nanoparticles with the cells for extended times, the exocytosis of the AuNPs was studied. The results showed that AuNPs remain in the cells for up to 3 weeks, after which they were removed from cells. TEM images have indicated that the exocytosis of citrate AuNPs and PEG coated AuNPs to be similar, as observed in HepG2 cells where vesicles containing the nanoparticles were excreted to the medium during exocytosis. These observations emphasize the importance of AuNPs size and surface chemistry (or charge) in cellular uptake, cell localization as well as in the fate of AuNPs in cells. Nonetheless, the effect of the functional groups in cellular uptake and on the fate of AuNPs in cells needs further investigating. However, further *in vivo* studies need to be conducted to confirm these *in vitro* observations as clearance of nanoparticles from cells prevents unintended toxicity associated with particles that have prolonged intracellular retention.

3.5 References

Ammann A. 2007. Inductively coupled plasma mass spectroscopy (ICP-MS): a versatile tool. *Journal of Mass Spectrometry*. 42: 419- 427.

AshaRani PV, Low Kah Mun G, Hande MP, Valiyaveettil S. 2009. Cytotoxicity and genotoxicity of silver nanoparticles in human cells. *ACS Nano,* 3:279–290.

Brandenberger C, Clift MJD, Vanhecke D, Muhfeld C, Stone V, and Rothen-Rutishauser B. 2010. Intracellular imaging of nanoparticles: Is it an elemental mistake to believe what you see? *Particle and Fibre Toxicology*, 7 (15): 1-6.

Brown A, and Hondow N. 2013. Electron microscopy of nanoparticles in cells. *Frontiers of Nanoscience*, Chapter 4, Vol 5.

Chithrani BD and Chen WCW. 2007. Elucidating the mechanism of cellular uptake and removal of protein –coated gold nanoparticles of different sizes and shapes. *Nanoletters* 7, 6) 1542-1555

Chithrani BD, Steward A, Allen C, and Jaffary DA. 2009. Intracellular uptake, transport, and processing of nanostructures in cancer cells. *Nanomedicine: Nanotechnology, Biology, and Medicine,* 5: 8–127.

Dam DHM, Lee JH, Sisco PN, Co DT, Zhang M, Wasielewski MR and Odom TW. 2012. Direct observation of nanoparticles-cancer cell nucleus interaction. *ACS Nano*, 6 (4): 3318-3326.

Fraga S, Faria H, Soares ME, and Carmo H. 2013. Influence of the surface coating on the cytotoxicity, genotoxicity and uptake of gold nanoparticles in human HepG2 cells. *Journal of Applied Toxicology.* DOI 10.1002/jat.2865.

Freese C, Uboldi C, Gibson MI, Unger RE, Weksler BB, Romero IA, and Kirkpatrick CJ. 2012. Uptake and cytotoxicity of citrate- coated gold nanospheres: Comparative studies on human endothelial and epithelial cells. *Particle and Fibre Toxicology*, 9 (23): 1-11.

Frohlic E. 2012. The role of surface charge in cellular uptake and cytotoxicity of medical nanoparticles. *International Journal of Nanomedicine*, 7: 5577- 5591.

Gu Y-J, Heng J, Lin C-C, Lam YW, and Wong W-T. 2009. Nuclear penetration of surface functionalized gold nanoparticles. *Toxicology and Applied Pharmacology*, 237: 196- 204.

Huang K, Ma H, Lui J, Huo S, Kumar A, Wei T, Zhang X, and Liang X-J. (2012). Size-Dependent localization and penetration of ultrasmall gold nanoparticles in cancer cells, multicellular spheroids, and tumors in vivo. *ACS Nano*, 6 (5): 4483- 4493.

Kettler K, Veltman K, Van De Meent D, Van Wzel A and Hendriks AJ. Cellular Uptake of Nanoparticles as determined by particle properties, experimental conditions and cell type. *Environmental Toxicology and Chemistry.* 2014; 33 (3): 481- 492.

Krpetic S, Saleemi S, Prior IA, See V, Qureshi R, and Brust. 2011. Negotiation of Intracellular Membrane Barriers by TAT-Modified Gold Nanoparticles. *ACS Nano,* 5 (6): 5195- 5201.

Liu X, Huang N, Li H, Jin Q and Ji J. 2013. Surface and size effects on cell interaction of gold nanoparticles with both phagocytic and non-phagocytic cells. *Langmuir*, 29: 9138- 9148.

Lu S, Xia D, Huang G, Jing H, Wang Y, and Gu H. 2010. Concentration effect of gold nanoparticles on proliferation of keratinocyte. *Colloids and Surfaces B: Biointerphases*, 81: 406- 411.

Mayhew TM, Muhfeld C, Vanhecke D, and Ochs M. 2009. A review of recent methods for efficiently quantifying immune-gold and other nanoparticles using TEM sections through cells, tissues and organs. *Annals of Anatomy*, 19: 153-170.

Mu Q, Hondow NS, Krzeminski L, Brown AP, and Routledge MN. 2012. Mechanism of cellular uptake of genotoxic silica nanoparticles*. Particle and Fibre Toxicology*, 9 (29): 1- 11.

Muhfeld C, Rothen-Rutishauser B, Vanhecke D, and Ochs M. 2007. Visualization and quantitative analysis of nanoparticles in the respiratory tract by transmission electron microscopy. *Particle and Fibre Toxicology*, 4 (11): 1-17.

Nativo P, Prior IA, and Brust M. 2008. Uptake and Intracellular fate of surface –modified gold nanoparticles. *ACS Nano*, 2 (8):1639-1644.

Ng CT, Perumalsamy R, Watt F, and Yuan YL. 2010. Localizing cellular uptake of nanomaterials in vitro by transmission electron microscopy. *Microscopy: Science, technology and education*. *Formatted*. 1: 316-320.

Oh E, Delehanty JB, and Medintz IL. 2011. Cellular Uptake and fate of PEGylated gold nanoparticles is dependent on both cell-penetrating peptides and particle size*. ACS Nano*, 5 (8): 6434- 6448.

Oh E, Delehanty JB, Sapsford KE, Susumu K, Goswami R, Blanco-Canosa JB, Dawson PE, Granek J, and Medintz IL. 2011. Cellular Uptake and Fate of PEGylated Gold nanoparticles Is Dependent on Both Cell-Penetration Peptides and Particle Size. *ACS Nano*, 5 (8): 6434-6448.

Oh N and Park J. 2014a. Surface chemistry of Gold nanoparticles mediates their exocytosis in macrophages. *ACS Nano*, 8 (6) 6232-6241.

Oh N and Park J. 2014b. Endocytosis and exocytosis of nanoparticles in mammalian cells. *International Journal of Nanomedicine*, 9 (Suppl I) 51-63.

Rocha A, Zhou Y, Kundu S and Liang H. 2011. *In vivo* observation of gold nanoparticles in the central nervous system of *Blaberus discoidalis*. *Journal of Nanobiotechnology*, 9:5.

Saha K, Kim ST, Yan B, Oscar R, and Rotello VM. 2013. Surface functionality of nanoparticles determines cellular uptake mechanisms in mammalian cells. *Small*, 9 (2): 300-305.

Sakhtianchi R, Minchin RF, Lee KB, Alkilany AM, Serpooshan V, and Mahmoudi M. 2013. Exocytosis of nanoparticles from cells: Role in cellular retention and toxicity. *Advances in Colloid and Interface Science,* 201-202*:* 316-320.

Shang L, Nienhaus K, and Nienhaus GU. 2014. Engineered nanoparticles interacting with cells: size matters. *Journal of Nanobiotechnology*, 12 (5): 1-11.

Skebo JE, Grabinski CM and Hussain SM. 2007. Assessment of metal nanoparticle agglomeration, uptake, and interaction using high-illuminating system. *International Journal of Toxicology*, 29: 135-141.

Venkataraman AJS, Subramaniam C, Kumar RR, Priya S, Kumar TR, Omkumar RV, Annie John A, Pradeep T. 2005. Growth of Gold Nanoparticles in Human Cells. *Langmuir,* 21: 1562-11567.

Zhang Q, Hitchings VM, Schrand AM, Hussains B, and Goering PL. 2010. Uptake of gold nanoparticles in murine macrophage cells without cytotoxicity or production of pro-inflammatory mediators. *Nanotoxicology Informa Health Care*, 1-12. DOI: 10.3109/17435390.2010.512401.

Zhu Z-J, Tang R, Yeh Y-C, Miranda OR and Vachet RW. 2012. Determination of the intracellular stability of gold nanoparticles monolayers using mass spectrometry. *Analytical Chemistry*, 84: 4321-4326.

CHAPTER 4

IN VITRO ASSESSMENT OF CYTOTOXICITY OF GOLD NANOPARTICLES IN HUMAN LIVER AND KIDNEY CELLS

4.1 Introduction

Assessment of *in vitro* cytotoxicity provides the first step for the safety evaluation of nanomaterials. As discussed, the unique chemical and physical properties of nanoparticles influence the interaction and the subsequent cellular response to nanoparticles. In this chapter, the cytotoxicity of the 14, 20 and 40nm citrate stabilized and 14nm PEGylated AuNPs was assessed in HepG2 and HEK 293 cells using real time impedance technology.

The popular methods that are commonly used to evaluate *in vitro* cytotoxicity of nanomaterials, includes the 3-(4,5-dimethylthiazol-2-yl)-2,5-diphenyltetrazolium bromide (MTT) assay that measures the colorimetric product of the tetrazolium salt reduced by the mitochondria (Pan *et al.,* 2007; Chen *et al.,* 2009), the lactate dehydrogenase (LDH) assay, based on the extracellular secretion of lactate dehydrogenase as a marker of plasma membrane integrity (Uboldi *et al.,* 2009; Freese *et al.,* 2012), and also the adenosine triphosphate (ATP) assay, which measures intracellular ATP levels as a marker of metabolically active cells (Choi *et al.,* 2012; Vijayakumar *et al.,* 2012). Due to the absorption and fluorescence quenching properties of metal nanoparticles that interfere with the outcome of these assays, alternative systems that do not interfere with toxicity endpoint have been preferred for cytotoxicity measurement (Kroll 2009; Kroll 2012; Vetten *et al.,* 2013).

The impedance real time cell analyzer (RTCA) system provide a non-invasive and label free way to continuously monitor cell viability (Ürcan *et al.,* 2010). This technology allows long term real-time monitoring of cellular events, such as proliferation, adhesion, spreading, cell death and cellular response to a given treatment (Atienzar *et al.,* 2011). The impedance technology employs electrical current to quantify fluctuations in electrical impedance as cells grow and spread on a gold microelectrode array covered plate (Figure 4.1).

The spreading of cells on the microarray plate results in an increase in electrical impedance. A change in electrical impedance as a result of cell growth is displayed as a parameter termed cell-index (CI) (Moodley *et al.,* 2011). Thus, a higher CI values reflect greater cell proliferation and cell viability. Conversely, if the cells die, a decrease in adhesion will reduce the CI level. Hence, the CI monitors adhesion, spreading, proliferation and viability in a population of cells (Rahim and Üren, 2011).

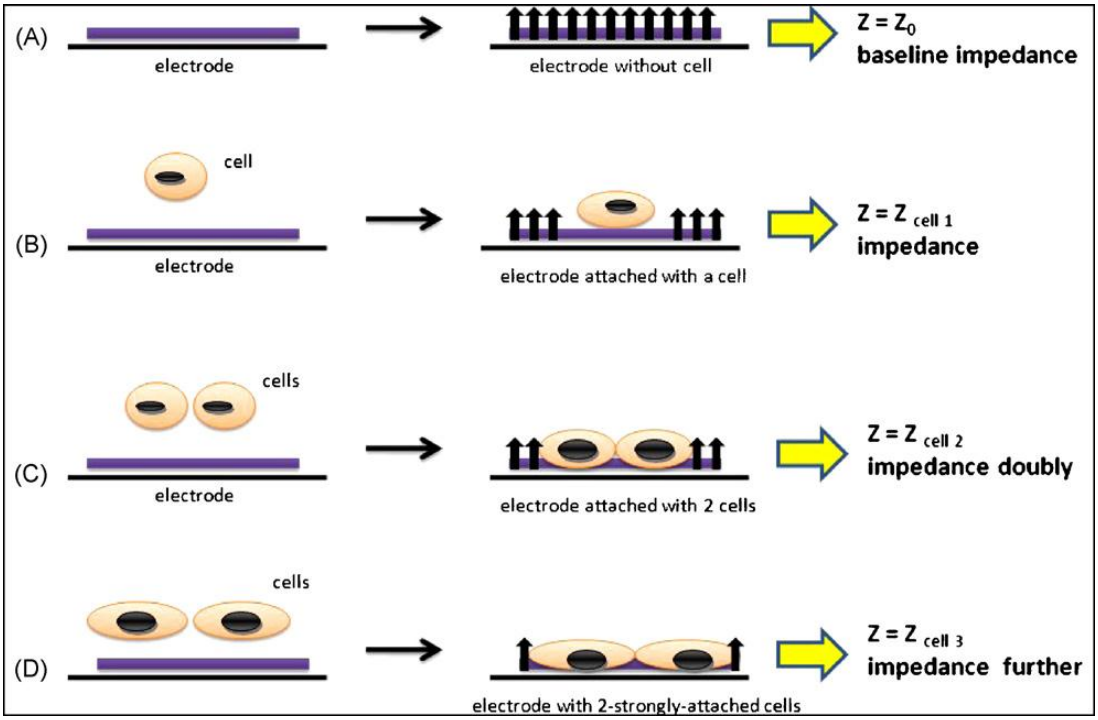


Fig. 4.1: Schematic diagram of impedance measurement. (A) There are no cells on an electrode (B-D) Impedance: Cells attaching to the electrode surface (Adapted from Urcan et al., 2010).

4.2 Experimental methods

4.2.1 Cell culturing for cytotoxicity studies

HepG2 and HEK 293 cells were maintained in EMEM and RPMI-1640 medium with L-glutamine supplemented with 10% fetal bovine serum, 1% penicillin/streptomycin solution at 37°C in a humidified 5% CO_2/95% air atmosphere. Cells were detached from the culture flask by a brief treatment with 1X trypsin-EDTA solution, as previously described. The viability of cells was determined with the trypan blue exclusion assay. Cells were counted with a countess cell counter. The cells were tested for mycoplasma contamination before being used for toxicity studies.

4.2.2 Testing of different cell densities for determining the optimal growth curve for HepG2 cells

Cell lines display a unique growth curves when they form a confluent monolayer on a substrates. Thus, the growth curve of a cell line over a certain periods of time must be established under optimal conditions. The growth curve represents cell viability and cell number in a population of cells at each growth phase. Impedance measurement of cells therefore requires that the unique growth curve of each cell line be determined prior to cytotoxicity measurements (Keogh, 2010; Smout *et al*., 2010; Rahim and Ren, 2011; Ke *et al.,* 2011). Thus in the preliminary experiments, different cell densities and culturing conditions were tested to identify the optimal growth curve of the selected cell lines.

The human live HepG2 cells were resuspended in cell culture medium and adjusted to densities of 2 500; 5 000; 10 000; 40 000 and 80 000 cells/well. The proliferation growth curve of the cells was monitored via the incorporated sensor electrode arrays of the E-Plate 96. The optimal cell seeding density and growth curve was selected according to the criteria set by the manufacturer, stating that the cells should be at the exponential phase of growth with a cell index of 1 or above for toxicity testing of compounds

4.2.3 Testing of different coating conditions for HepG2 cells

Different coating conditions were tested to improve attachment of HepG2 cells to the surface of the E-plate. The following coating substrates were tested: poly-L-lysine (purchased from Sigma, South Africa) and rat tail collagen, type 1 (purchased from BD biosciences, Germany). The E-plates were coated by following the recommendations illustrated by the manufacturer, with various concentrations ranging from 50µg/mL-200µg/mL of the coating material being tested. Cells were cultured at a concentration of 10 000 cells/well in poly-L-

lysine or rat tail collagen, type 1 coated plate. The proliferation growth curve of the cells was then monitored through the incorporated sensor electrode arrays of the E-Plate 96. The best combination of coating substrate and cell seeding density, with the cell index of 1 or above was selected for toxicity measurements of AuNPs.

4.2.4 Testing of different cell seeding densities for determining the optimal growth curve for HEK 293 cells

To find the optimal growth curve of the human liver HEK 293 cells, cells were suspended in culture medium and adjusted to densities of 50 000; 20 000; 10 000; 5 000 and 2 500 cells/well. Similarly, the proliferation curve of the cells was monitored through the incorporated sensor electrode arrays of the E-Plate 96. The optimal cell seeding density and growth curve was selected according to the criteria set by the manufacturer.

4.2.5 Cytotoxicity of AuNPs using real-time impedance measurement

For cytotoxicity testing, HepG2 and HEK 293 cells were seeded at a cell density of 10 000 and 50 000 cells/well respectively, based on the experimental results obtained in section 4.2.4 of the methodology. The E-plate for seeding HepG2 cells was coated with 150µg/mL poly-L-lysine to improve cell adhesion. To prepare the E-plates for HepG2 experiments, a 100µL of the Poly-L-lysine solution (freshly prepared and sterilized by filtration) was added to each well of the E-plate and was left overnight in the biosafety cabinet. Following the coating step, the plates were washed by rinsing twice with 1X PBS solution. The plate was left to dry overnight in a biosafety cabinet and were used immediately or kept at 4°C until needed. HEK 293 cells were seeded on non-coated sterile E-plate at the desired concentration.

To continue with the cytotoxicity experiment, the background reading was performed before addition of the cells to the plate, that is, in the presence of 50µL culture medium. The appropriate number of cells in 100µL of culture medium was then added to the plates to the desired cell seeding density. The E-plates containing the cells were incubated at room temperature for 30 min in a laminar flow cabinet and placed on the plate reader in the incubator for continuous recording of impedance. The introduction of the AuNPs to the cells was done 24 hrs post-plating. Untreated cells were used as the negative control wells and were supplemented with culture medium (without nanoparticles) during the treatment stage. After treatment, impedance was recorded at 1 min intervals for 2 hrs, 10 min interval for 6 hrs and 30 min intervals for the remaining time of the experiment (96 hrs for HepG2 cells and 56 hrs for HEK 293 cells). Results were expressed as means and standard deviation (*SD*). All experiments were performed in triplicate (n=3).

4.2.6 Instrumentation and software used for cytotoxicity measurement

4.2.6.1 XCELLigence RTCA system

Cytotoxicity studies were conducted using the xCELLigence RTCA single plate (SP) instrument from ACEA Biosciences with RTCA software (version 1.2) as published by Vetten *et al.* (2013). The system was used according to the instructions of the supplier. Parameters such as: average value, maximum and minimum values, standard deviation (SD), cell index (CI), and graphics are obtained with the RTCA associated software. The data is expressed in CI units.

4.2.7 Statistical analysis for cytotoxicity studies

The slope for each curve of the normalized CI for the time period between treatment point and the highest CI value, i.e. confluency, of the untreated cells was calculated. The calculated slopes were exported to the spreadsheet. The two sample *F test (Fischer's test*) and the two sample *student's t test* were used to compare if the differences between treated and untreated slopes were significant. Differences were considered statistically significant if the $p<0.05$. A p value >0.05 was considered non-significant.

4.3 Results and Discussion

Different cell densities were tested to find the optimal growth curve for HepG2 cells. The attachment of HepG2 cells on non-coated E-plates showed a lower cell index values for all tested seeding densities (Figure 4.2).

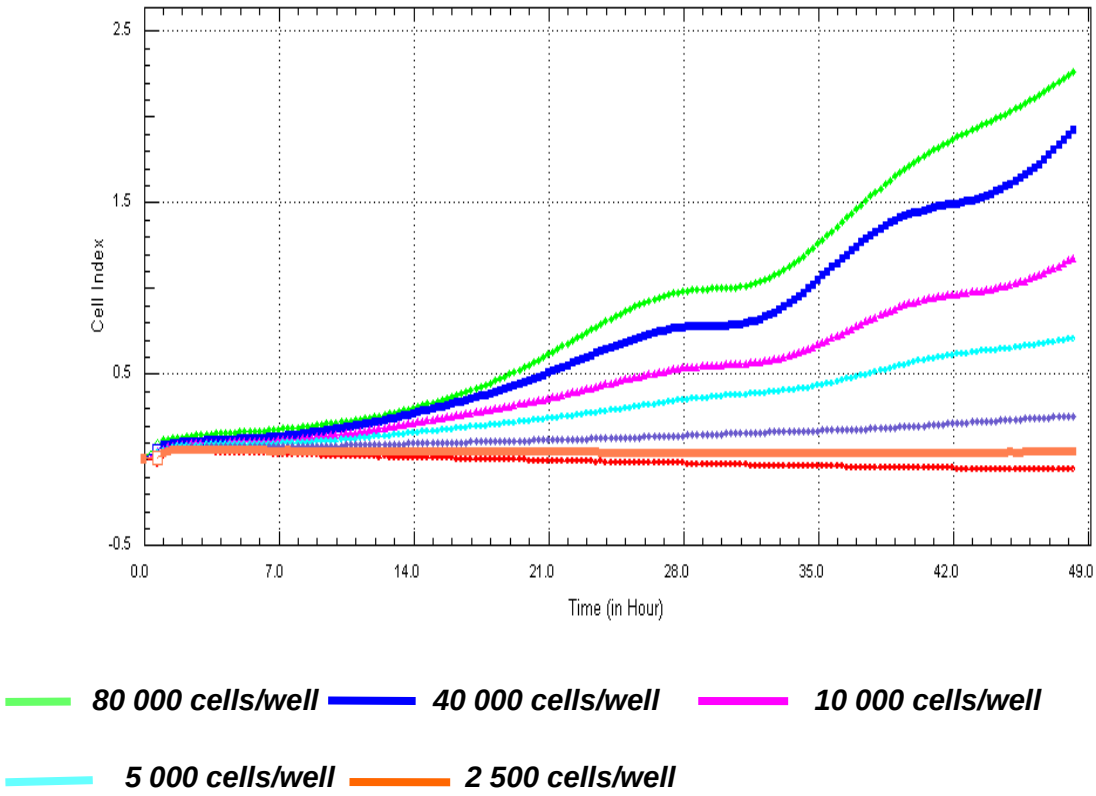


Figure 4.2: HepG2 cells seeded at different densities on non-coated E- plates.

The cell index values were below 0.5 in wells containing 2 500 and 5 000 cells and the CI was 1 in cells containing 10 000, 40 000 and 80 000 cells 24 hrs after seeding the cells. However, the cell number at this density could not be used for cytotoxicity studies, as the cells did not adhere to the normal growth curve. Therefore, the E-Plate wells were coated to promote cell adhesion. In a separate experiment, different coating substrates were tested to determine the substrate that would offer the optimal growth condition for HepG2 cells. There was an improvement in cell attachment on plates coated with rat tail collagen type 1; however it was not satisfactory for cytotoxicity studies (Figure 4.3).

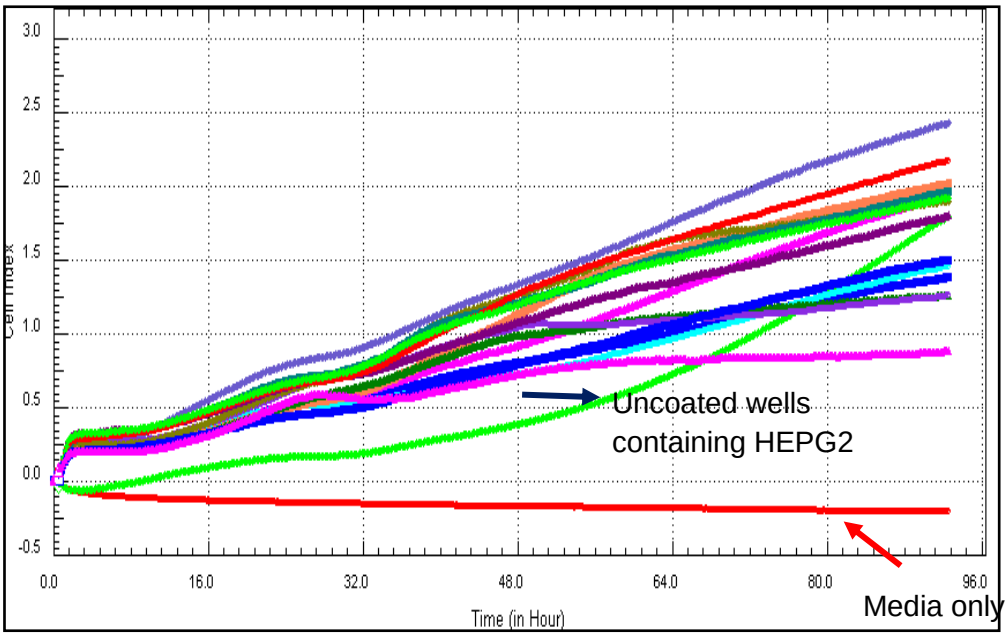


Figure 4.3: Growth curves of HepG2 cells seeded on collagen coated E-plate. The plates were coated with 50; 80, 100, 150, 200µg/mL of collagen for 24 hrs prior to cell seeding. HepG2 cells were seeded at 10 000 total cells/well. The green plot represents wells not coated with collagen containing HepG2 cells at 10 000cells/well; red plot is the control or media only well (indicated with red arrow).

Poly-L-lysine coating offered the best coating conditions, and improved attachment of HepG2 cells to the E-plate (Figure 4.4). Coating the plate with poly-L-lysine solution at concentration of 50µg/mL did not improve attachment of the cells to the wells. Nonetheless, a CI of 1 and above was attainable 24 hrs after incubation of cells on E-plates that were coated with 100, 150 and 200µg/mL poly-L-lysine solution. The wells that were coated with 100µg/mL showed a higher CI when compared to wells that were coated with 150 and 200µg/mL poly-L-lysine after 24 hrs. These growth curves as illustrated in Figure 4.4 were all suitable for use in cytotoxicity assessment studies. An optimal growth curve for cytotoxicity testing was selected based on the length of the exponential growth phase of the cell. At 100µg/mL coating concentration, the cells reached a stationery phase 48 hrs after seeding compared to wells that were coated with 150ug/mL poly-L-lysine, where the stationery phase

of growth was reached 64 hrs after incubation. The CI value in these wells increased throughout the exponential phase of growth. This concentration was taken as the optimum poly-L-lysine coating concentration and was used further in the following studies.

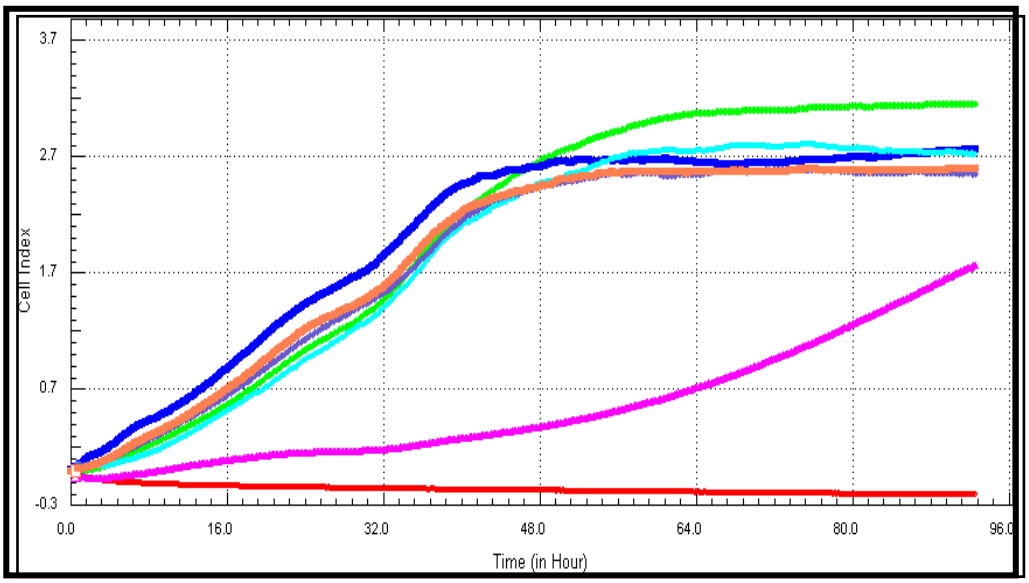


Figure 4.4: HepG2 cells seeded on Poly-L-lysine coated E plates. The cells were seeded at a concentration of 10 000 cells/well. The plate was coated with 100µL of 50, 100, 150 and 200µg/mL of Poly-L-lysine solution for 24 hrs before seeding with cells.

4.3.1 Real time impedance measurement of cytotoxicity of gold nanoparticles in HepG2 cells

Figure 4.5 shows the unique growth curve for HepG2 cells after seeding with 10 000 cells/well in a poly-L-lysine coated plate. The curve shows the exponential phase of growth, where the cells are rapidly proliferating. The stationery phase is reached 64 hrs after seeding. At this phase, the cells eventually stop growing as they run out of nutrients. The stationery growth phase is shown on the curve as a plateau.

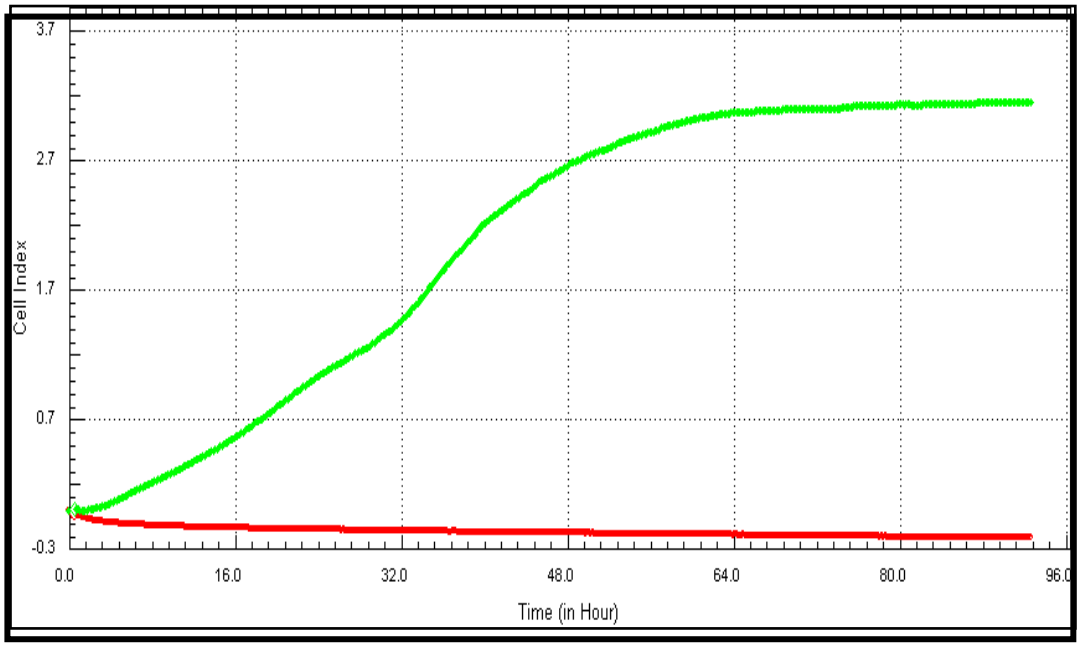


Figure 4.5: Growth curve of HepG2 cells seeded at 10000 cells/well in a Poly-L-lysine (150 µg/mL) coated E- plates.

The cytotoxicity effect of the AuNPs in HepG2 cells was presented as the normalized CI over time, measured over a period of 96 hrs or more. Figure 4.6 shows the proliferation curves of HepG2 cells treated with different concentrations of the 14nm citrate stabilized AuNPs.

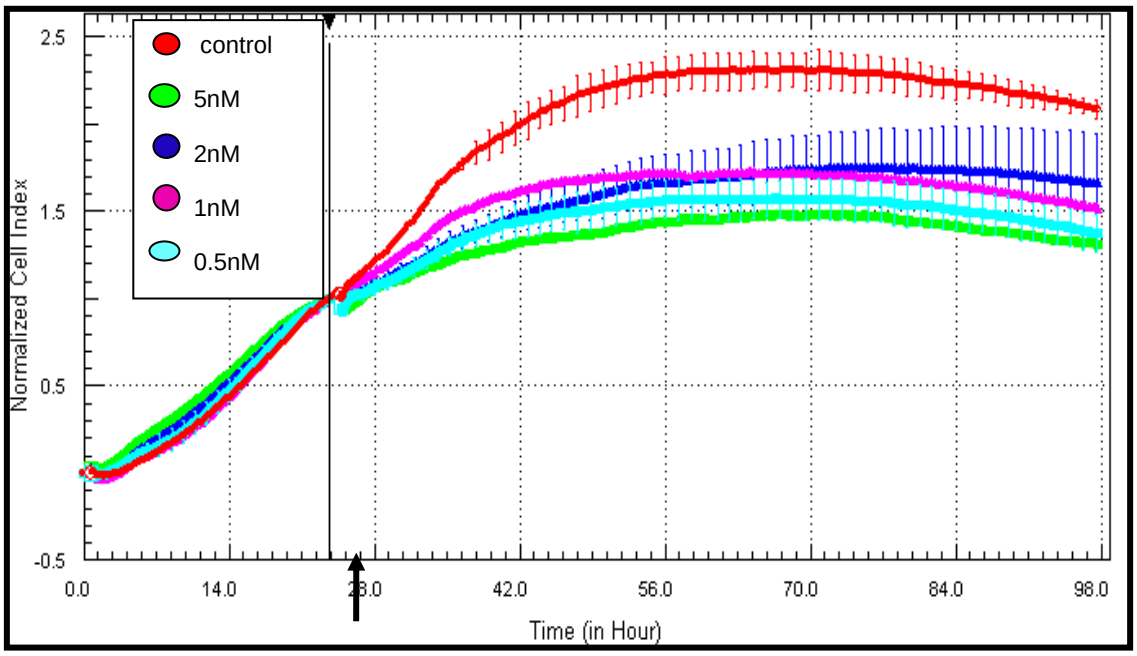


Figure 4.6: Impedance monitoring of proliferation and viability of HepG2 cells following incubation with 14nm citrate stabilized AuNPs at concentrations of 5, 2, 1; and 0.5nM.

Figure 4.6 demonstrates that treatment with 14nm citrate stabilized AuNPs significantly reduced the viability of cells ($p<0.01$), indicating that the AuNPs were cytotoxic to cells at the tested concentrations. A decrease in the CI was evident a few hours after the addition of the nanoparticles. As shown in the previous chapter, uptake of these AuNPs can occur as early as 1-4 hrs after incubation. After 4 hrs of treatment with AuNPs, the CI decreased at all tested concentrations. The decrease in CI value was evident for the duration of the experiment. A similar pattern of cell growth for 5nM and 0.5nM concentrations may be attributed to the uptake of these AuNPs. At 5nM concentration, the AuNPs form larger aggregates that are unable to enter the cells, indication that a small fraction of these nanoparticles will be taken up in the cells.

The presence of sodium citrate residues on the citrate stabilized AuNPs surfaces have been correlated to toxicity of these AuNPs (Uboldi *et al.,* 2009). In the literature, a number of studies were conducted to assess the cytotoxicity of citrate stabilized AuNPs of similar size. For example, the cytotoxicity of 10nm and 11nm Cit- AuNPs at different concentrations to human dermal endothelial (HDMEC) and human cerebral endothelial (hCMEC/D3) cells exposed for 48 hrs was reported (Freese *et al.,* 2012). On the other hand, non-cytotoxic effect, assessed by viability and membrane integrity, of 18nm Cit- AuNPs to K562 leukemia cell line (Connor *et al.,* 2005) and of 20nm citrate-stabilized AuNPs to HepG2 cells, assessed by cell viability and proliferation (Fraga *et al.,* 2013) were reported. All these studies reported in the literature have implemented the absorbance-based XTT assay and other assay systems that rely on photometric measurements (Connor *et al.,* 2005; Freese *et al.,* 2012). This study has employed the non invasive impedance real time technology system to monitor cytotoxicity and thus give a more appropriate indication of response of the cells to these nanoparticles.

The 20nm citrate stabilized AuNPs showed a statistically significant change in the viability of the cells at the tested concentrations, implying that the nanoparticles induced cytotoxic effect on cells (Figure 4.7) ($p<0.01$). This effect was pronounced for cells that were exposed to 5, 2, and 0.5nM concentrations of AuNPs. Freese *et al.* (2012) reported the cytotoxicity effect of 25nm citrate AuNPs, after assessing viability and proliferation of human dermal endothelial (HDMEC) and human cerebral endothelial (hCMEC/D3) cells exposed to different concentrations of the citrate AuNPs (Freese *et al.,* 2012). Nonetheless, non-cytotoxic responses to the 20nm citrate AuNPs were reported in others studies using the traditional cytotoxicity assays (Liu *et al.,* 2013). Fraga *et al.* (2013) reported a non-cytotoxic effect of 20nm citrate AuNPs to HepG2 cells after assessing the mitochondrial activity and the plasma membrane integrity of treated cells with the MTT and the LDH assay (Fraga *et al.,* 2013). Citrate stabilized AuNPs were also found to be non-cytotoxic up to concentrations

of 300μM to human dermal fibroblast cells after assessing the viability of cells with the MTT assay (Qu and Lu, 2009)

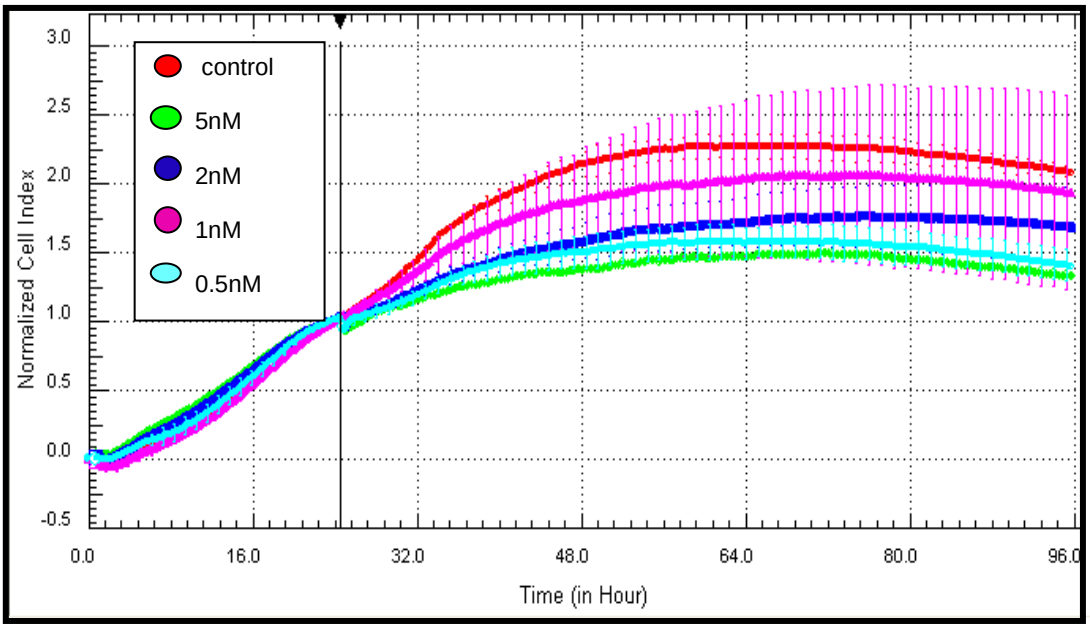


Figure 4.7: Impedance monitoring of proliferation and viability of HepG2 cells following incubation with 20nm citrate stabilized AuNPs at concentrations of 5, 2, 1; and 0.5nM.

Figure 4.8 shows that the 40nm citrate AuNPs did not show cytotoxic effect on cells at all tested concentrations ($p>0.05$), indicating a size dependent effect on cells. The proliferation curve shows that after treatment with the 40nm citrate AuNPs, the treated cells remained similar to that of untreated cells for the duration of the experiment. An increase in the viability of the treated cells compared to the untreated cells was seen 24 hrs after treatment with the AuNPs. This effect has been reported with citrate stabilized AuNPs in other cell lines (Shukla *et al.,* 2005; Freese *et al.,* 2011), and indicate that the AuNPs may stimulate growth of the cells. For example, Arnida *et al.* (2010) showed that 50 and 90nm spherical citrate AuNPs induced the proliferation of human prostate carcinoma PC-3 cells after assessing viability

and proliferation of cells for 88 hrs (Arnida *et al.,* 2010). The authors of this study indicated that the AuNPs were able to stimulate the proliferation of the cells, due to the ability of the AuNPs to reduce the amount of harmful reactive oxygen in cells (Arnida *et al.,* 2010). In a recent study, 40nm citrate stabilized AuNPs were shown to promote the proliferation of human lung cancer A549 cells during cytotoxicity measurements (Liu *et al.,* 2013).

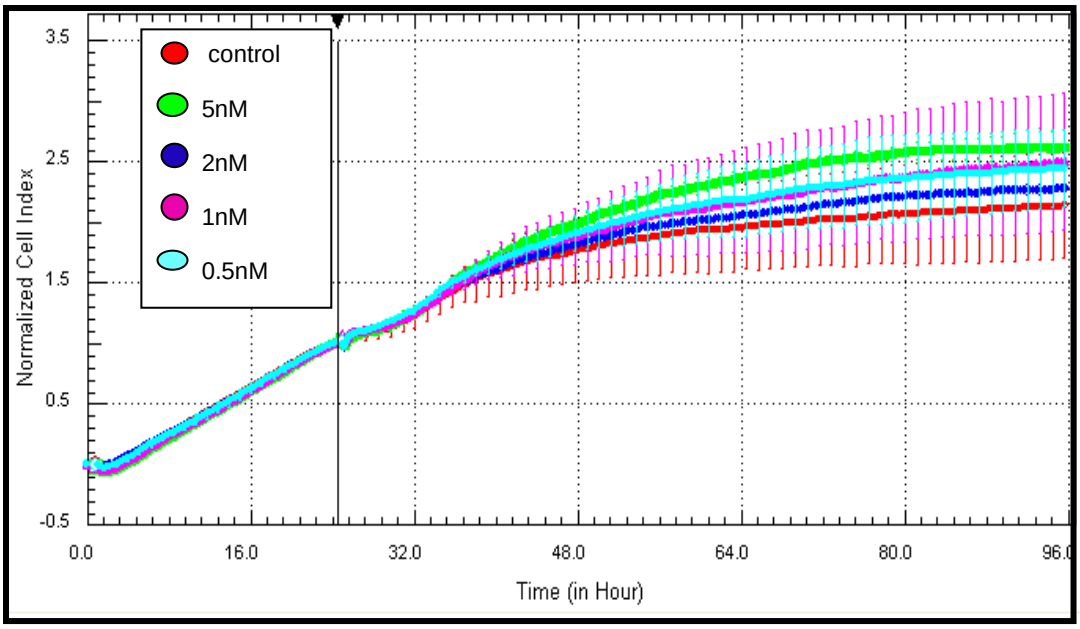


Figure 4.8: Impedance monitoring of proliferation and viability of HepG2 cells following incubation with 40nm citrate stabilized AuNPs at concentrations of 5, 2, 1; and 0.5nM.

Figure 4.9 shows the cytotoxicity of HepG2 cells treated with the azide-PEG coated AuNPs. At all tested concentrations, the AuNPs did not show cytotoxic effects on cells ($p>0.05$). The proliferation profile shows that after treatment with the AuNPs the proliferation of the treated cells was similar to that of untreated cells. At 24 hrs post treatment, the viability of the treated cell increased and was higher than that of the untreated cells. This increase in the cell viability was evident for the duration of the experiment. PEG-coated nanoparticles have been shown not to induce toxicity in many of the cell lines that have been used for

cytotoxicity studies of AuNPs, as a result of the reduced interaction with cells during uptake (Niidome *et al.,* 2006; Lee *et al.,* 2008; Gu *et al*., 2009; Rayavarapu *et al.,* 2010).

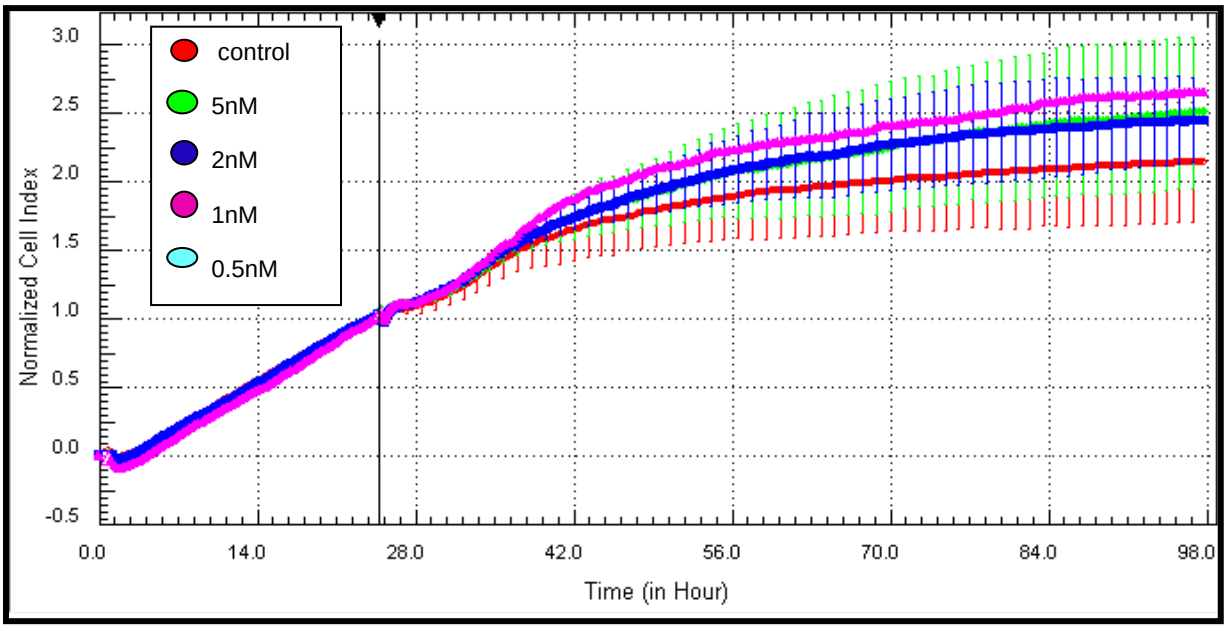


Figure 4.9: Impedance monitoring of proliferation and viability of HepG2 cells following incubation with azide-PEG coated AuNPs at concentrations of 5, 2, 1; and 0.5nM.

The NTA-PEG coated AuNPs showed a non-cytotoxic effect in cells at all tested concentrations ($p>0.05$) (Figure 4.10). Similar to the azide-PEG coated AuNPs, a few hours after treatment (24 hrs post treatment), the viability of the treated cell increased and was higher than that of the untreated cells. The increase in the cell viability was evident for the duration of the experiment.

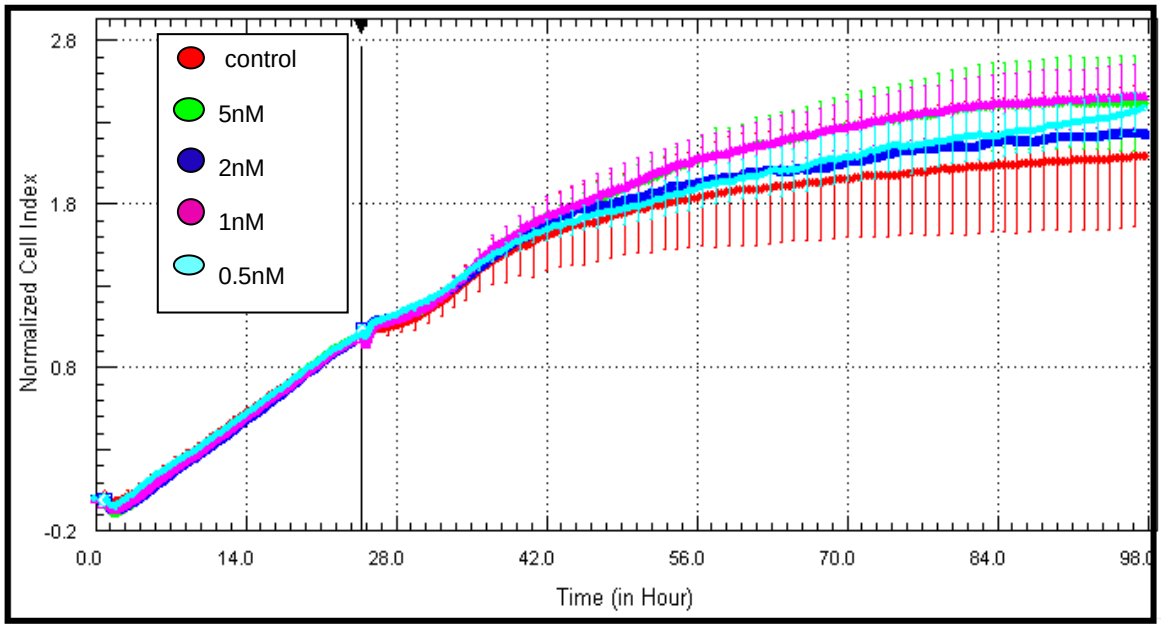


Figure 4.10: Impedance monitoring of proliferation and viability of HepG2 cells following incubation with NTA-PEG coated AuNPs at concentrations of 5, 2, 1; and 0.5nM.

Figure 4.11 demonstrate a concentration dependent effect of carboxyl-PEG coated AuNPs. At high concentrations the viability of HepG2 cells was significantly reduced as the CI was zero. The decrease in viability of cells was seen immediately after the addition of the AuNPs ($p<0.01$) and 2nM ($p<0.01$). The viability of cells treated with 5 and 2nM carboxyl-PEG AuNPs continued to decrease for the duration of the experiment. A CI value of zero means no viable cells are attached to the microelectrodes, indicating dead cells. The adverse effect of the carboxyl-PEG AuNPs on the cells may be the result of the reaction of the terminal end groups on the carboxyl functional group with cellular constituents. Nonetheless, the carboxyl-PEG coated AuNPs did not induce any cytotoxic effect to cells at lower concentrations of 0.5nM ($p=0.5$) and 1nM AuNPs ($p=0.3$), as the proliferation curves of treated cells followed that of untreated cells. The CI of treated cells at lower concentrations was similar to that of untreated cells.

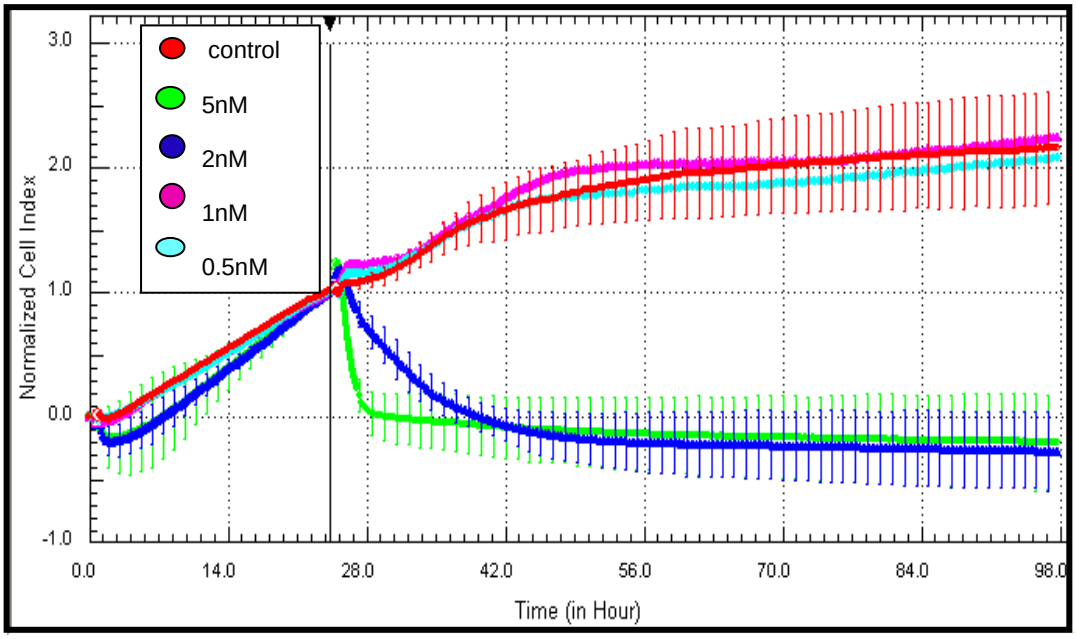


Figure 4.11: Impedance monitoring of proliferation and viability of HepG2 cells following incubation with carboxyl-PEG coated AuNPs at concentrations of 5, 2, 1; and 0.5nM.

Figure 4.12 shows the proliferation curves of HepG2 cells treated with biotin-PEG AuNPs. The figure shows a non-cytotoxic response of the AuNPs at all tested concentrations, for the duration of the experiment ($p>0.05$). Similarly, an increase in cell viability of the treated cells was seen, 24 hrs after treatment with the nanoparticles. In the literature, biotin-PEG coated AuNPs were found to be non-cytotoxic to human leukemia K562 cells at concentrations up to 250µM, even after three days of incubation (Connor *et al.,* 2005). Evenmore, viability of the K562 leukemia cells was shown to increase over time when measured by the MTT assay. As mentioned, the increase in the cell viability may be the result of the reduced interaction of the PEG-coated AuNPs with cells during uptake (Niidome *et al.,* 2006).

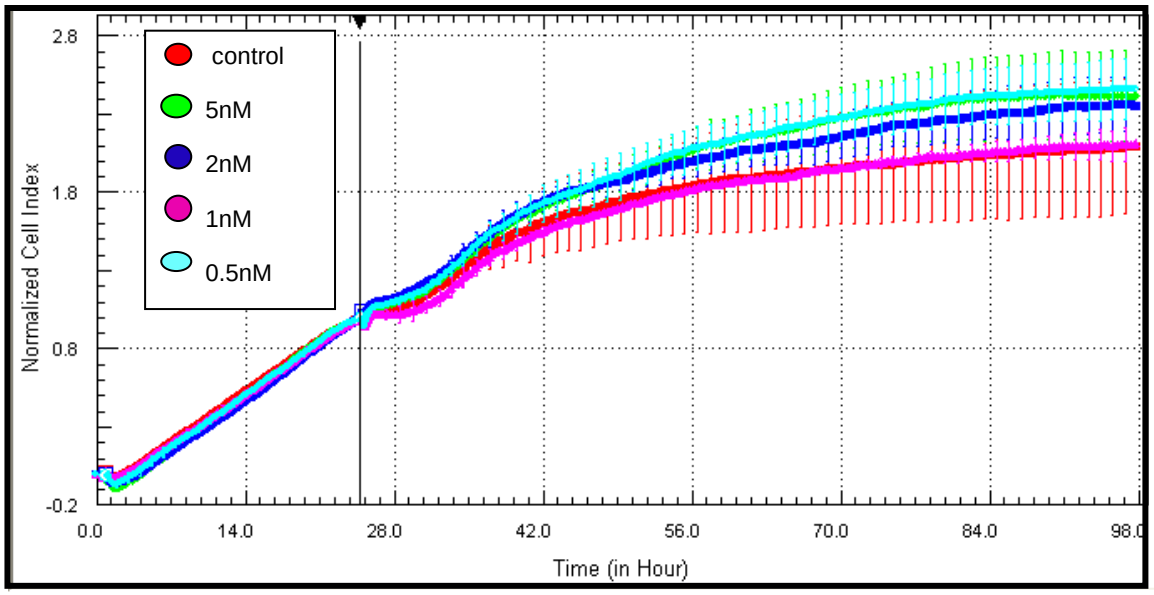


Figure 4.12: Impedance monitoring of proliferation and viability of HepG2 cells following incubation with biotin-PEG coated AuNPs at concentrations of 5, 2, 1; and 0.5nM

Figure 4.13 shows the proliferation curves of cells after the addition of hydroxyl-PEG AuNPs. A non-cytotoxic response of the AuNPs was seen for all tested concentrations in the treated cells, for the duration of the experiment ($p>0.05$). The figure shows that after treatment with the AuNPs the curve of the treated cells followed that of untreated cells. The observation was evident 24 hrs after treatment with the particles, following which the viability of the treated cells increased and was higher than that of untreated cells.

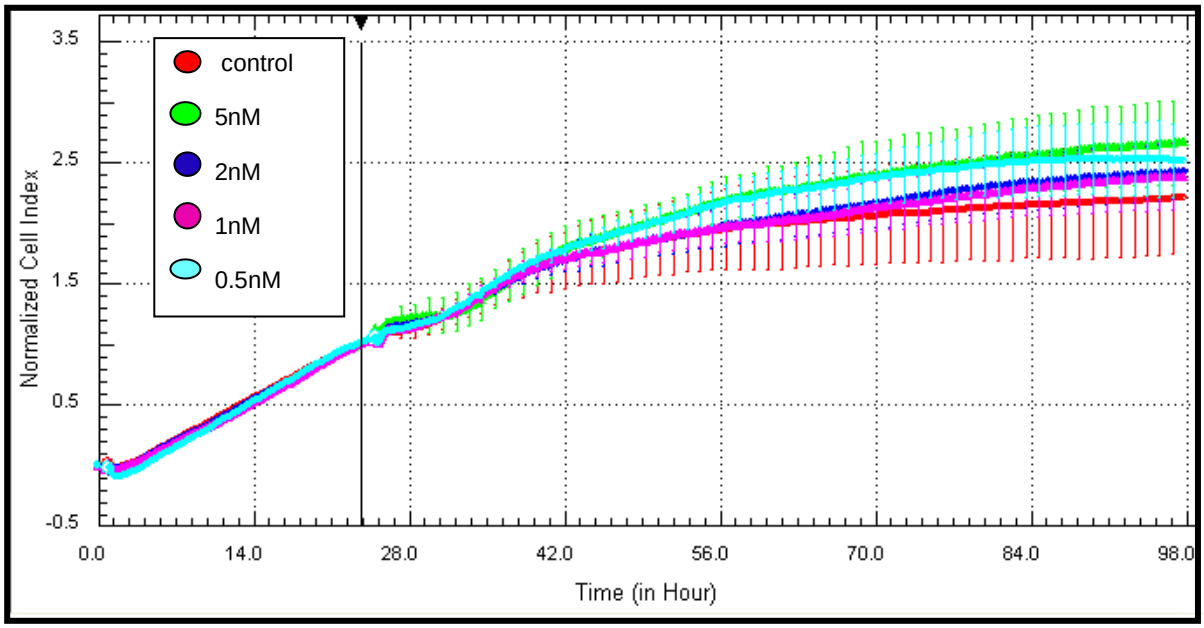


Figure 4.13: Impedance monitoring of proliferation and viability of HepG2 cells following incubation with hydroxyl-PEG coated AuNPs at concentrations of 5, 2, 1; and 0.5nM.

The methoxy-PEG coated AuNPs decreased the viability of cells at 2, 1 and 0.5nM concentrations ($p<0.05$) (Figure 4.14). Cytotoxicity with the AuNPs was seen immediately after addition to the cells. Our results however, observed no effect on the viability of cells that was treated with the methoxy-PEG AuNPs at 5nM concentrations ($p>0.05$). This may be attributed to the lack of entry of the AuNPs into cells, possibly due to aggregated particles at this concentration. In the literature, a non-cytotoxic effect of 15nm methoxy-PEG thiol functionalized AuNPs in human breast carcinoma MDA-MB-231 cells was reported, after assessing cell viability and proliferation with MTT assay (Shenoy *et al.,* 2006). In the study, no change in viability and proliferation of cells was reported after treatment with 200µg/mL for AuNPs. In addition, the viability of cells was increased compared to untreated cells (Shenoy *et al.,* 2006).

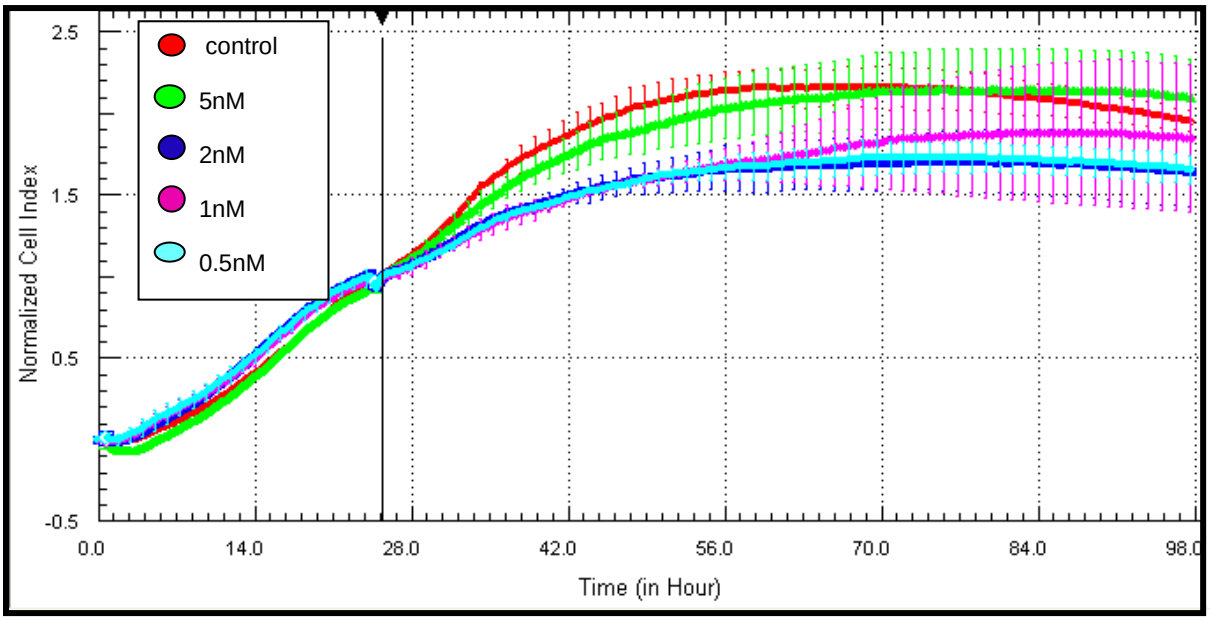


Figure 4.14: Impedance monitoring of proliferation and viability of HepG2 cells following incubation with methoxy-PEG coated AuNPs at concentrations of 5, 2, 1; and 0.5nM.

4.3.2 Real time impedance measurement of cytotoxicity of gold nanoparticles in HEK 293 cells

The optimal density for seeding cells for cytotoxicity studies in HEK 293 cells was obtained at a cell concentration of 50 000 cells/well. Figure 4.15 shows the unique growth curve for HEK cells. The figure shows that the cells reached the exponential phase 24 hrs after culture. The stationery growth phase was reached at 40 hrs after culture, with the growth curve reaching a plateau 56 hrs after culture. Thus for cytotoxicity measurement of the AuNPs, the cells were treated at 24 hrs and were monitored for 36 hrs.

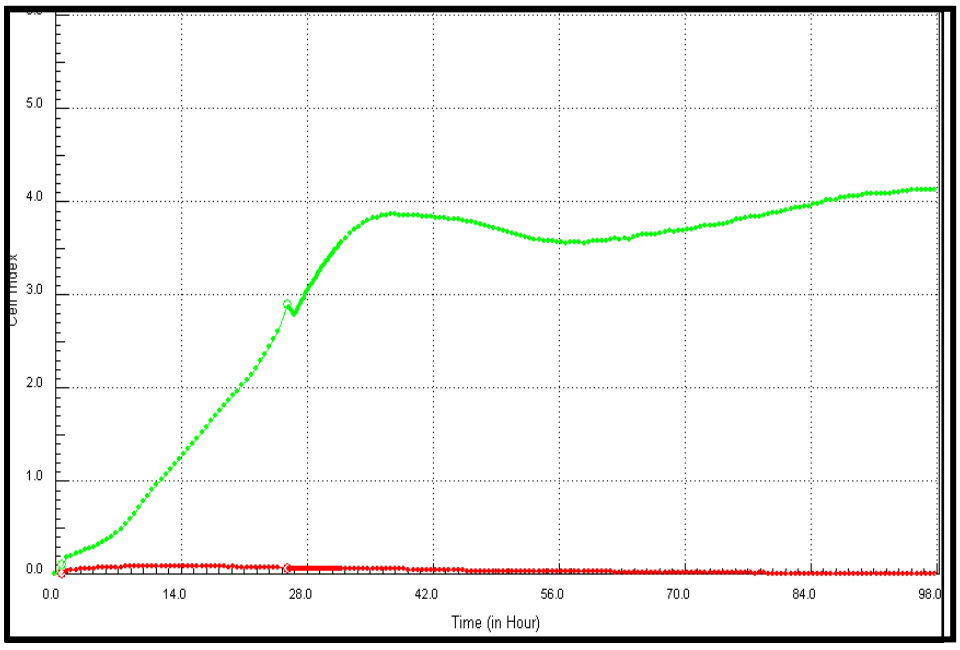


Figure 4.15: HEK 293 cells growth curve at a cell density of 50 000 cells/well.

As in the previous section, the CI was used as a measure of cytotoxicity, indicating cell viability and proliferation. The CI value and the proliferation curve of the untreated cells were used as the negative control, and were compared to the treated cells. Figure 4.16 shows the

proliferation curve of HEK 293 cells treated with 14nm citrate stabilized AuNPs. A decrease in the viability of cells was seen at the selected concentration ($p<0.05$), indicating cytotoxicity of the AuNPs. The decrease in cell viability was evident 8 hrs after treatment of cells with the AuNPs and continued for the duration of the experiment.

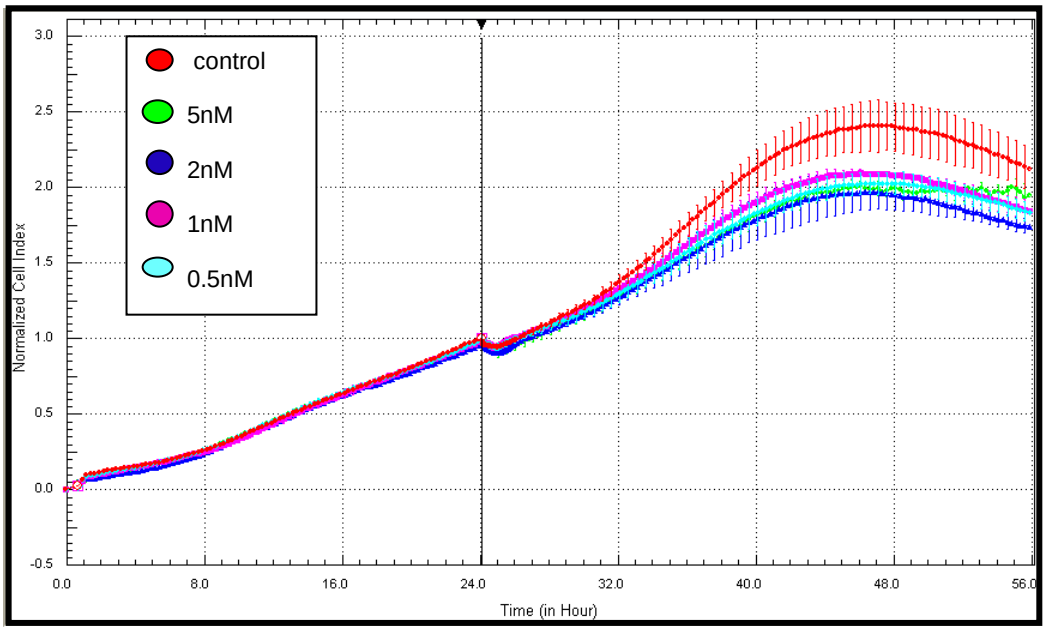


Figure 4.16: Impedance monitoring of proliferation and viability of HEK 293 cells following incubation with 14nm citrate stabilized AuNPs.

In contrast to HepG2 cells, the 20nm citrate stabilized AuNPs did not induce cytotoxic effect on HEK 293 cells at the tested concentrations($p>0.05$)(Figure 4.17). The proliferation of the treated cells was similar to that of untreated cells. In the literature, non-cytotoxicity responses were reported on cells treated with citrate AuNPs of this size range (Kim *et al.,* 2009; Chen *et al.,* 2009)

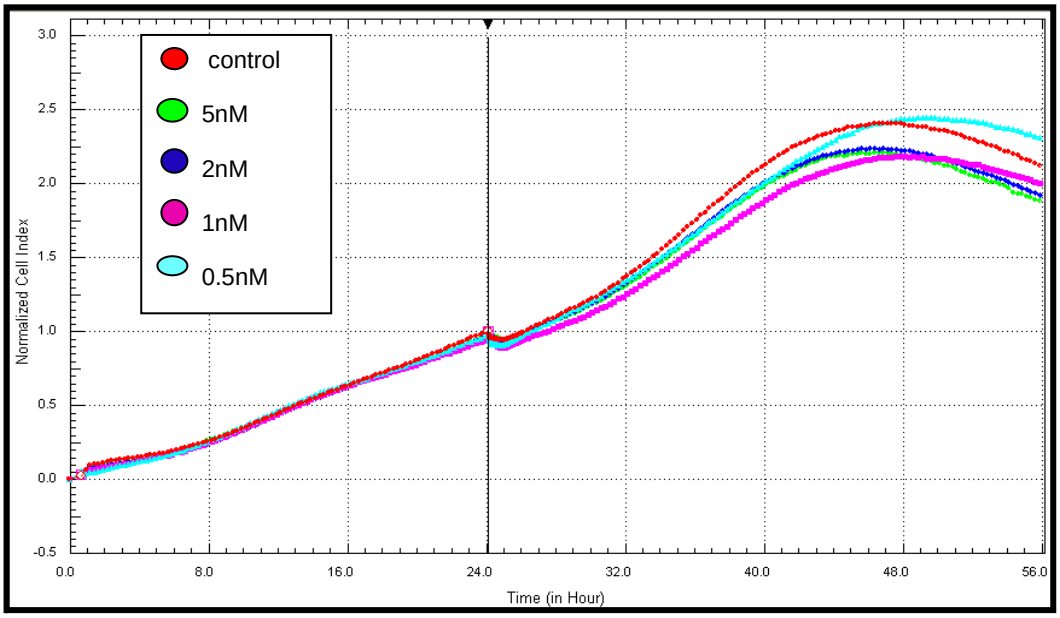


Figure 4.17: Impedance monitoring of proliferation and viability of HEK 293 cells following incubation with 20nm citrate stabilized AuNPs.

Figure 4.18 shows the proliferation curve of HEK 293 cells after treatment with 40nm citrate stabilized AuNPs. A non-cytotoxic response to cells was seen at the tested concentrations ($p>0.05$). The CI of cells treated with 5nM concentration showed a sudden increase after the addition of the nanoparticles. This observation could be the result of nanoparticles not entering the cells due to their larger size, but attaching to the cell surface to induce this effect.

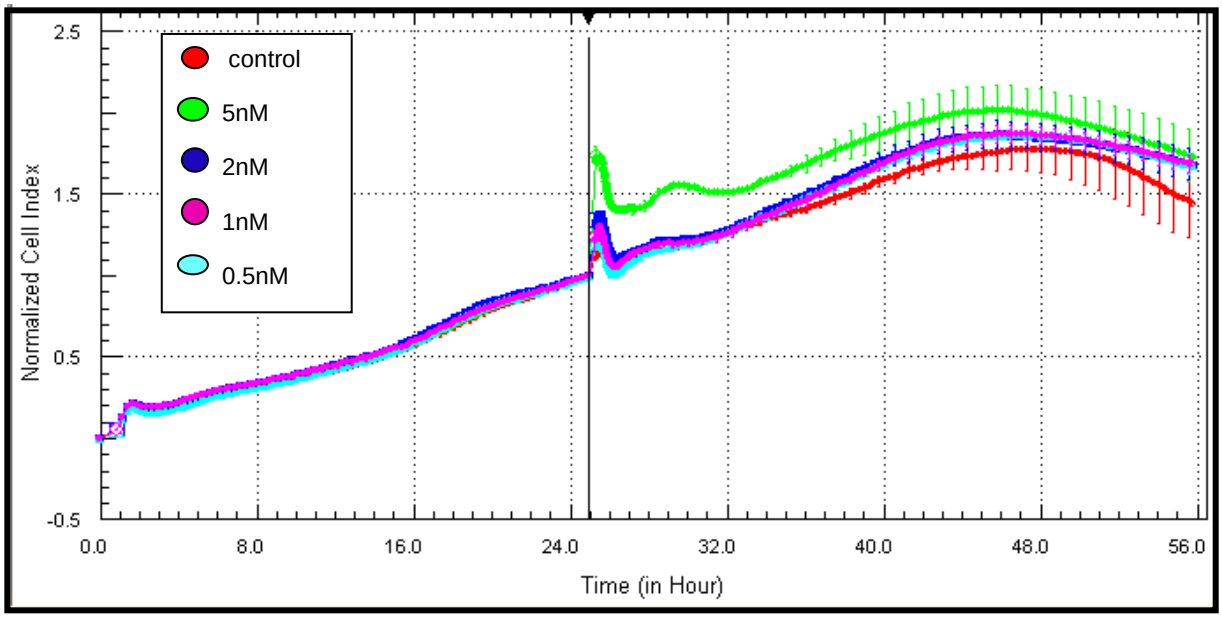


Figure 4.18: Impedance monitoring of proliferation and viability of HEK 293 cells following incubation with 40nm citrate stabilized AuNPs.

The cytotoxicty profile of HEK 293 cells treated with the azide-PEG coated AuNPs is shown in Figure 4.19. The curves demonstates a non-cytotoxic response of the nanoparticles at the tested concentrations ($p>0.05$). The CI and the proliferation of the treated cells was not affected by the particles, as they were similar to the control cells. Non-cytotoxic effect of the AuNPs was evident from the time of treatment and continued for 20 hrs after treatment (40 hrs as shown on the curve). However, at 42 hrs, the cells reached the stationery phase where a decrease in the viabilty of treated cells was seen. In the stationery phase, cells are depleted of nutrients and are affected in their growth. Hence, measurements at this point are not significant as the cells are metabolically inactive and unable to maintain adequate growth.

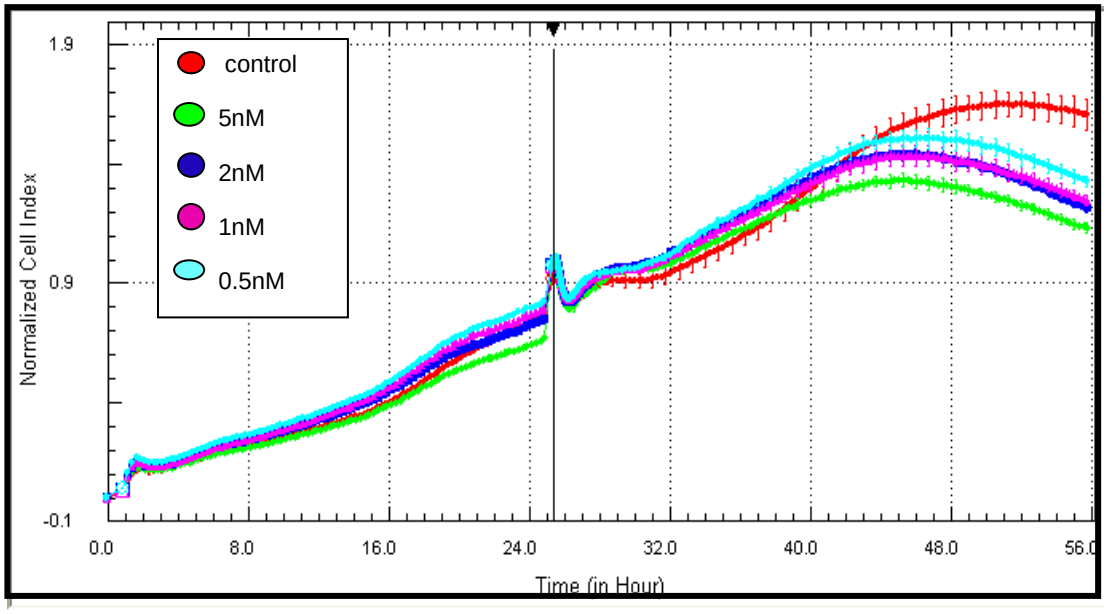


Figure 4.19: Impedance monitoring of proliferation and viability of HEK 293 cells following incubation with azide-PEG gold nanoparticles at concentrations of 5, 2, 1; and 0.5nM.

Figures 4.20A and 4.20B shows the proliferation curves of HEK 293 cells treated with NTA-PEG coated AuNPs at a concentration range of 5nM to 0.01nM. In Figure 4.20A the AuNPs were shown to be cytotoxic to cells at the tested concentrations of 5, 2, 1 and 0.5nM. The viability of the treated cells was statistically significant to the viability of untreated cells ($p=0.003$; $p<0.01$). In the figure, a concentration-dependent response of the cells was seen a few hours after addition of the AuNPs. Cells treated with higher concentration induced the most adverse effect on cells. In addition to viability, the proliferation of the cells was also affected by treatment with the AuNPs. The cytotoxicity effects in treated cells continued for the duration of the experiment.

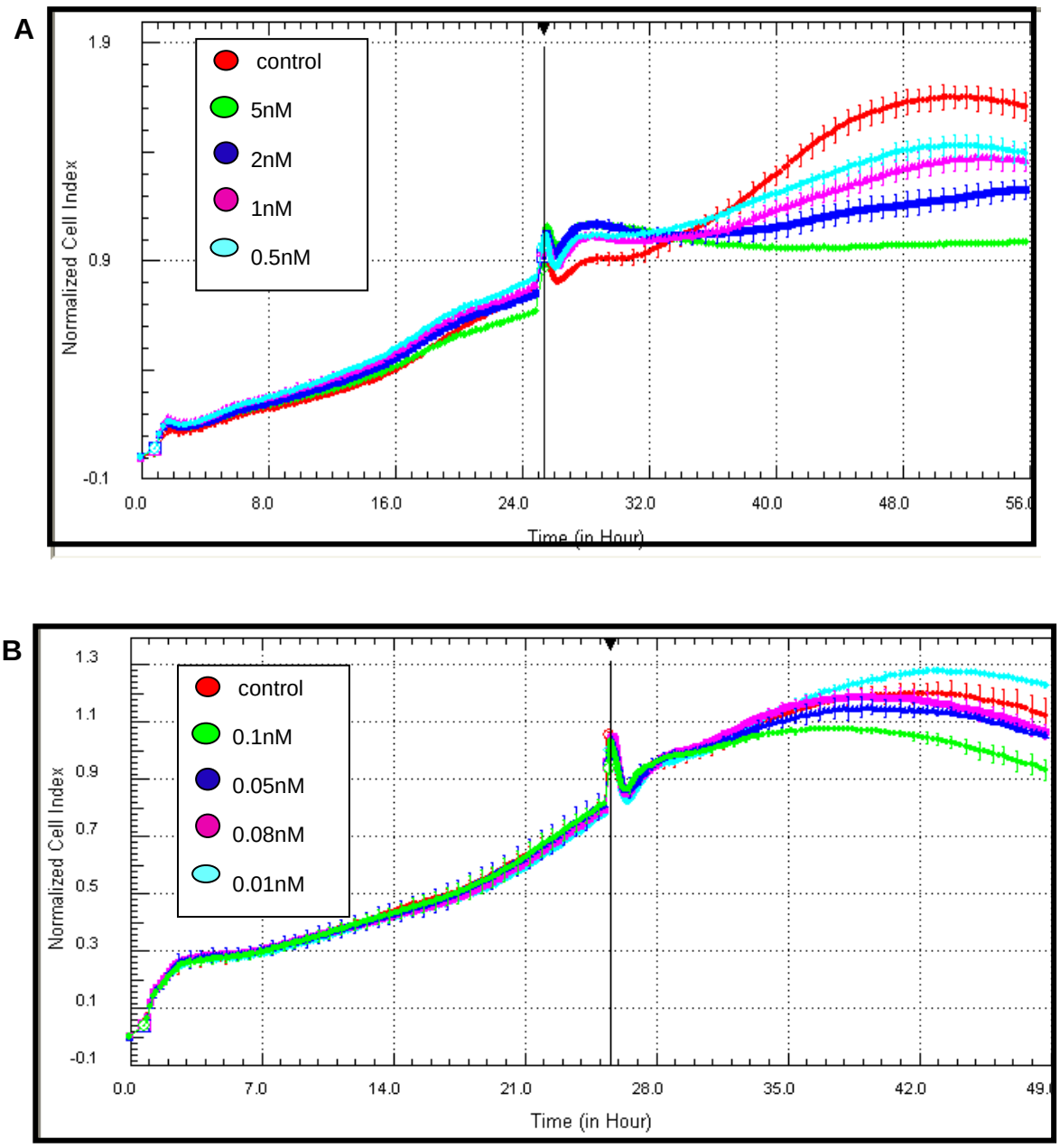


Figure 4.20: Impedance monitoring of proliferation and viability of HEK 293 cells following incubation with NTA-PEG AuNPs at concentrations of 5, 2, 1; and 0.5nM (A). (B) shows CI at concentrations 0.01, 0.08, 0.05 and 0.1nM.

At lower concentrations, non-cytotoxic effect of NTA-PEG AuNPs on cells was seen. Figure 4.20B shows the proliferation curve of cells after treatment with 0.1, 0.05, 0.08 and 0.01nM NTA-PEG coated AuNPs. At lower concentrations, the proliferation curve of the treated cells

was similar to that of untreated cells. In addition, an increase in the CI of the cells was seen with the lowest treated concentration.

The proliferation curves of cells treated with the carboxyl-PEG coated AuNPs are shown in Figure 4.21. A cytotoxic response was seen with cells at the selected concentrations ($p<0.01$ for 5, 2, 1nM; $p<0.05$ for 0.5nM), in a concentration dependent manner. The viability and the proliferation of the treated cells were affected by the AuNPs, as the CI was reduced immediately after addition of the AuNPs and remained low throughout the exposure test. The adverse effect on cells was more pronounced at high concentration of AuNPs.

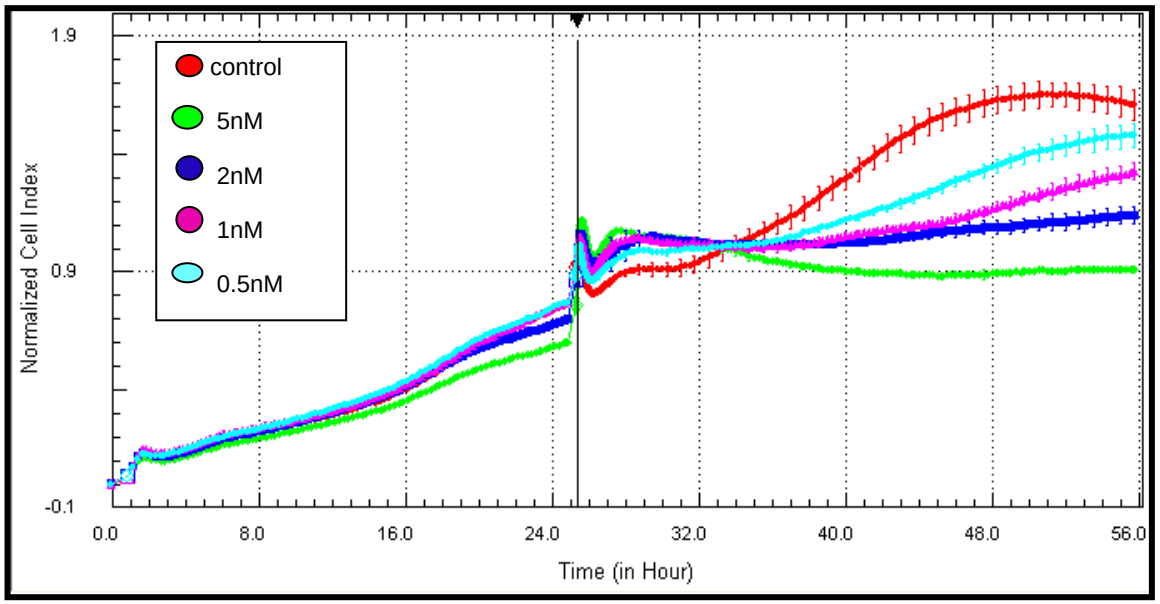


Figure 4.21: Impedance monitoring of proliferation and viability of HEK 293 cells following incubation with carboxyl-PEG gold nanoparticles at concentrations of 5, 2, 1; and 0.5nM.

Figure 4.22 shows proliferation of HEK 293 cells after treatment with the biotin-PEG AuNPs. Similar to the carboxyl-PEG AuNPs, a concentration dependent cytotoxic response was seen after treatment with AuNPs at concentrations 5, 2, 1; and 0.5nM (Figure 4.22A) ($p<0.01$ for 5, 2, 1nM; $p<0.05$ for 0.5nM). The CI and the proliferation of the cells were affected by

treatment with AuNPs which lasted for the duration of the experiment. Similarly, the adverse effect on cells was more pronounced at high concentration of AuNPs. Impedance measurement of cell growth at lower concentrations of the biotin-PEG AuNPs shown in Figure 4.22B indicated a non-cytotoxic effect on cells, as the proliferation curve of the treated cells was similar as that of untreated cells 20 hrs after exposure (Figure 4.22B). The CI of treated cells was not statistically different to that of untreated cells ($p>0.05$).

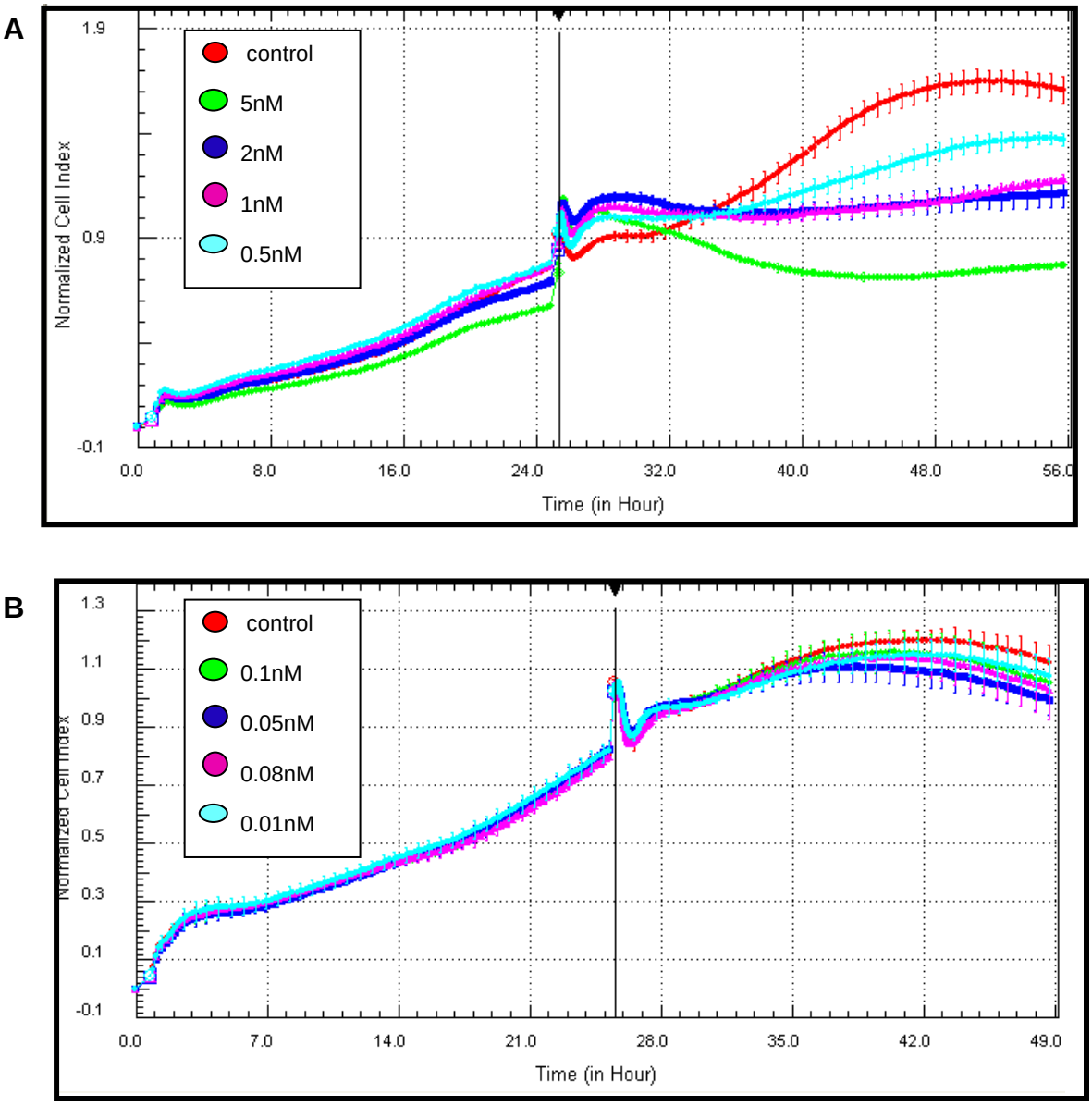


Figure 4.22: Impedance monitoring of proliferation and viability of HEK 293 cells following incubation with biotin-PEG AuNPs at concentrations of 5, 2, 1; and 0.5nM (A). (B) shows CI at concentrations 0.01, 0.08, 0.05 and 0.1nM.

The hydroxyl-PEG coated AuNPs induced cytotoxicity in HEK 293 cells after treatment with 5, 2, 1; and 0.5nM ($p<0.01$), indicated in Figure 4.23A. The proliferation curve and the CI of the treated cells were significantly affected by the treatment with AuNPs. Figure 4.23B shows that treatment of cells with lower concentrations of hydroxyl-PEG AuNPs showed a non-cytotoxic response, as the curves of the treated cells was similar to that of untreated cells.

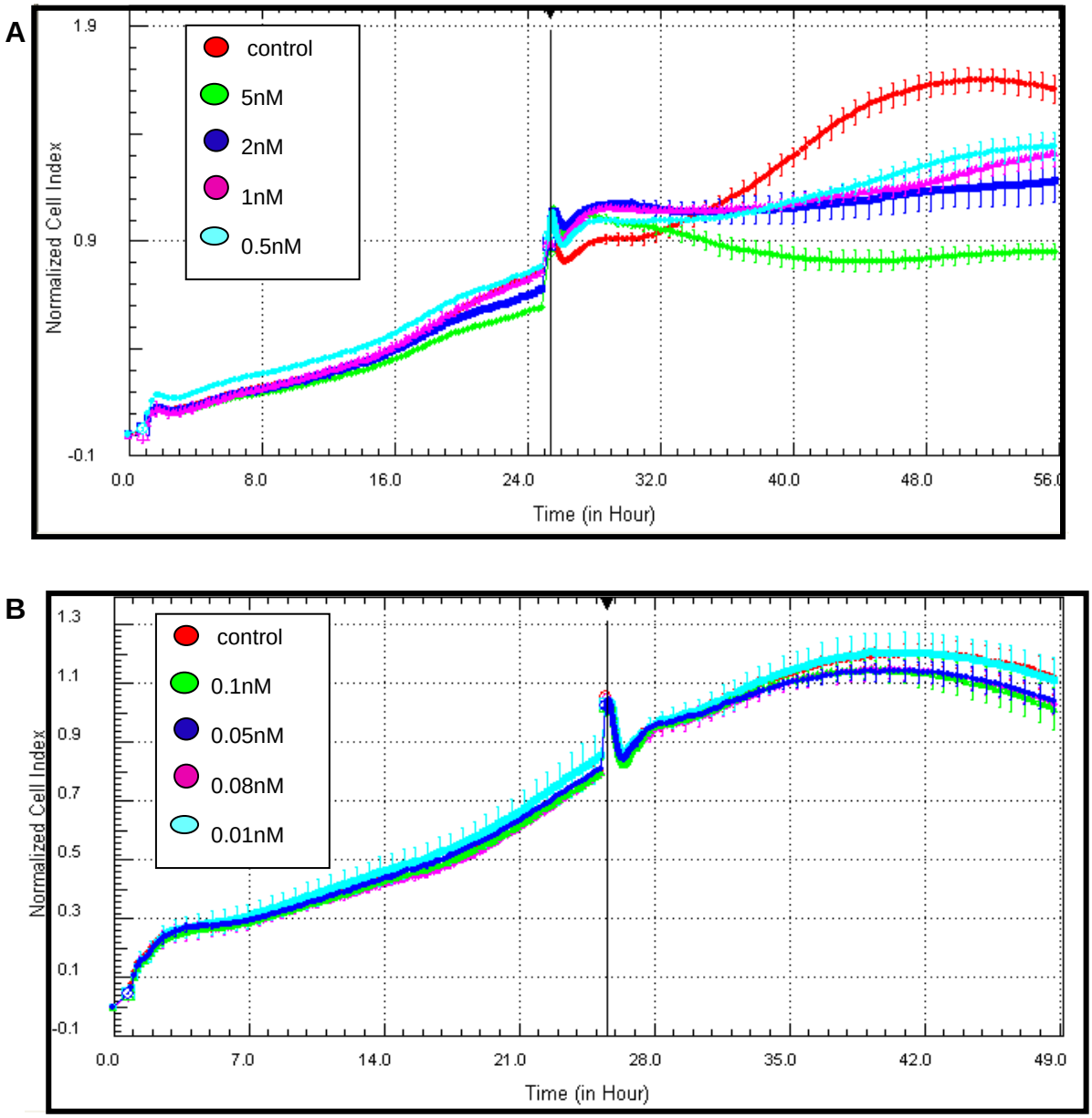


Figure 4.23: Impedance monitoring of proliferation and viability of HEK 293 cells following incubation with hydroxyl-PEG gold nanoparticles at concentrations of 5, 2, 1; and 0.5nM (A). (B) shows CI at concentrations 0.01, 0.08, 0.05 and 0.1nM.

The proliferation curves of HEK 293 cells treated with methoxy-PEG coated AuNPs are shown in Figure 4.24. A decrease in viability of cells was seen 8 hrs after treatment with high concentration of the AuNPs ($p<0.01$), indicating cytotoxicity of the AuNPs at this

concentration. At low concentrations (2, 1 and 0.5nM), the CI and proliferation curve of the treated cells was similar to that of untreated cells, indicating a non-cytotoxic response.

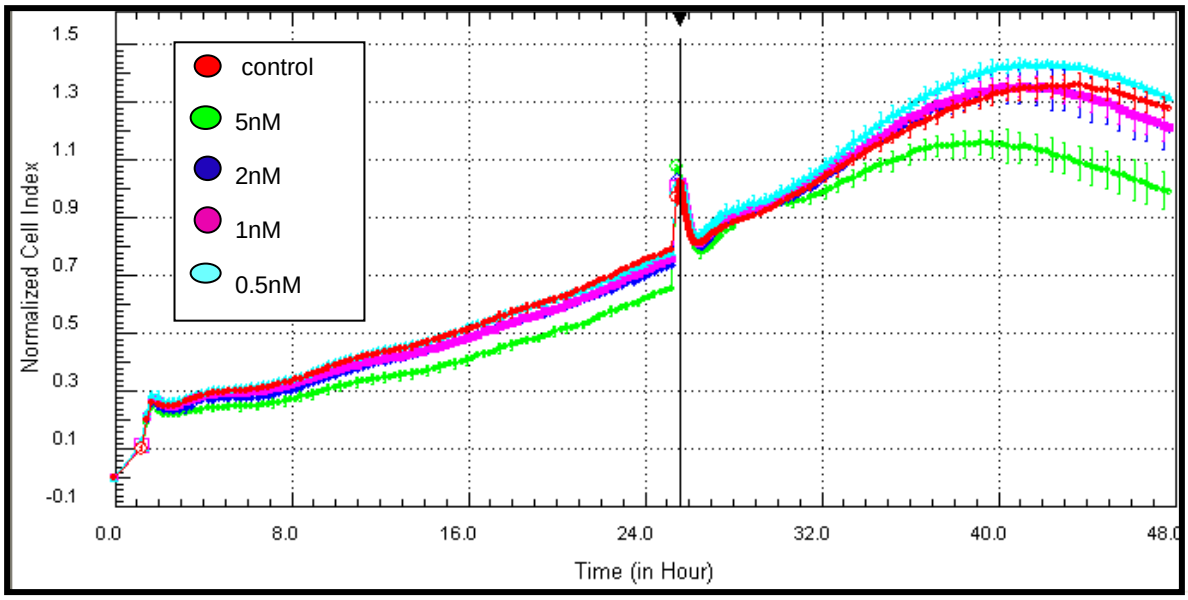


Figure 4.24: Impedance monitoring of proliferation and viability of HEK 293 cells following incubation with methoxy-PEG gold nanoparticles of 5, 2, 1; and 0.5nM.

4.4 Summary and Conclusions

The cytotoxicity of 14, 20 and 40nm citrate stabilized and PEG functionalized AuNPs was assessed in human liver carcinoma and embryonic kidney cultured cells. Through the use of label free impedance measurement, the viability and proliferation state of cells treated with different concentrations of the AuNPs was monitored in real time. Real time cytotoxicity measurement of 14 and 20nm citrate AuNPs in HepG2 cells indicated cytotoxic effect on cells, with a significant decrease in cell viability over time. On the other hand, the 40 nm citrate AuNPs did not induce cytotoxicity in cells. Treatment of HepG2 cells with azide-PEG, biotin-PEG, hydroxyl-PEG, NTA-PEG did not induce an adverse effect on cells for the duration of the test, while the carboxyl-PEG AuNPs induced a concentration dependent effect on cells. High concentrations of carboxyl-PEG AuNPs decreased the viability of HepG2 cells to a CI of 0, indicating no cell survival at this concentration. The proliferation curve of HepG2 cells treated with carboxyl-PEG AuNPs was also affected at 5 and 2nM tested concentrations.

The cytotoxicity profiles of 14nm citrate AuNPs in HEK 293 cells indicated cytotoxic effect on cells, while the 20 and the 40nm citrate AuNPs were non-cytotoxic to cells. The azide-PEG AuNPs were non-cytotoxic to HEK 293 cells at the tested concentrations. However, treatment of the cell lines with biotin-PEG, hydroxyl-PEG, and NTA-PEG induced cytotoxicity at concentrations of 5, 2, 1 and 0.5nM. At lower concentrations, biotin-PEG, hydroxyl-PEG, NTA-PEG and carboxyl-PEG AuNPs were non-cytotoxic to HEK 293 cells. The methoxy-PEG AuNPs were cytotoxic to cells at 5 nM concentration and non-cytotoxic at 2, 1 and 0.5nM concentrations.

In summary, the following observations were made:

I. HEK 293 cells were more sensitive to the AuNPs. The differences in cell response may be attributed to the different cell metabolism of the two cell types, HEK 293 cells (non-cancer cells) and Hep G2 cells (cancer cells). Cytotoxicity of AuNPs to HEK 293 cells was dependent on the concentration of the nanoparticles.

II. Cell response to the AuNPs was dependent on surface chemistry. In HepG2 cells, the citrate AuNPs induced cytotoxicity by decreasing the CI of cells. On the other hand, PEG-coated AuNPs stimulated proliferation of cells, regardless of the functional group on the nanoparticle surface. The PEG-coated AuNPs induced cytotoxicity in HEK 293 cells by reducing viability and affecting proliferation of cells, regardless of the functional group on the AuNPs surface, while the citrate AuNPs induced cytotoxicity in HEK 293 cells by decreasing the cell viability.

III. Size dependent cytotoxic response for the citrate stabilized AuNPs. Cytotoxicity assessment of 14, 20 and 40nm citrate stabilized AuNPs on cells, indicated that the 14nm citrate AuNPs results in undesirable adverse effects in both cell types. An increased uptake of the 14nm citrate AuNPs in both cells result in large quantities of the nanoparticles in cellular compartments to induce cytotoxicity effect. In contrast, the 40nm citrate stabilized AuNPs, did not induce adverse effects in both cells lines, as a result of their lower uptake and due to the larger diameter.

4.5 References

Arnida, Malugin A, and Ghandehari H. 2010 Cellular uptake and toxicity of gold nanoparticles in prostate cancer cells: a comparative study of rods and spheres. *J Appl Toxicol,* 30 (3):212–217.

Atienza JM, Yu N, Kirstein SL, Xi B, Wang X, Xu X, and Abassi YA. 2006. Dynamic and label-free cell-based assays using the real-time cell electronic sensing system. *Assay Drug Dev Technol,* 4:597-607.

Chen PC, Mwakwari SC, and Oyelere AK. 2008. Gold nanoparticles: from medicine to nanosensing. *Nanotechnology Science and Application*, 1: 45-66.

Choi SY, Jeong S, Jang SH, Park J, Park JH, Ock KS, Lee SY, and Joo SW: 2012. *In vitro* toxicity of serum protein-adsorbed citrate-reduced gold nanoparticles in human lung adenocarcinoma cells. *Toxicology in Vitro*, 26:229–237.

Connor EE, Mwamuka J, Gole A, Murphy CJ, and Wyatt MD. 2005. Gold nanoparticles are taken up by human cells but do not cause acute cytotoxicity. *Small*, 1:325–327.

Fraga S, Faria H, Soares ME, and Carmo H. 2013. Influence of the surface coating on the cytotoxicity, genotoxicity and uptake of gold nanoparticles in human HepG2 cells. *Journal of Applied Toxicology.* DOI 10.1002/jat.2865.

Freese C, Uboldi C, Gibson MI, Unger RE, Weksler BB, Romero IA, and Kirkpatrick CJ. 2012. Uptake and cytotoxicity of citrate- coated gold nanospheres: Comparative studies on human endothelial and epithelial cells. *Particle and Fibre Toxicology*, 9 (23): 1-11.

Gu YJ, Cheng J, Lin C, Lam YW, Cheng SH, and Wong WT. 2009. Nuclear penetration of surface functionalized gold nanoparticles. *Toxicology and Applied Pharmacology*, 237; 196-204.

Ke N, Wang X, Xu X, Abassi YA. 2011. The xCELLigence system for real-time and label-free monitoring of cell viability. *Methods Mol Biol*, 740:33–43.

Keogh RJ. 2010. New technology for investigating trophoblast function. *Placenta*, 31: 347–50.

Kroll A, Pillukat M H, Hahn D, Schnekenburger J. 2009 Current *in vitro* methods in nanoparticle risk assessment: limitations and challenges. *Eur J Pharm Biopharm,* 72:370–377.

Kroll A, Pillukat MH, Hahn D, Schnekenburger J. 2012. Interference of engineered nanoparticles with *in vitro* toxicity assays. *Arch Toxicol,* 2012.

Lee JS, Green JJ, Love KT, Sunshine J, Langer R, and Anderson DG. 2009. Gold, poly (β-amino ester) nanoparticles for small interfering RNA delivery. *Nano Lett*, 9: 2402–2406.

Liu X, Huang N, Li H, Jin Q, and Ji J. 2013. Surface and size effects on cell interaction of gold nanoparticles with both phagocytic and non-phagocytic cells. *Langmuir*, 29: 9138- 9148.

Moodley K, Angel CE, Glass M, and Graham ES. 2011. Real-time profiling of NK cell killing of human astrocytes using xCELLigence technology. *J. Neurosci. Methods*, 200:173–180.

Niidome T, Yamagata M, Okamoto Y, Akiyama Y, Takahashi H, and Niidome Y. 2006. PEG-modified gold nanorods with a stealth character for *in vivo* applications. *Journal of Controlled Release*, 114: 343- 347.

Pan Y, Neuss S, Leifert A, Fischler M, Wen F, Simon U, Schmid G, Brandau W, and Jansen Denchet W. 2007. Size- dependent cytotoxicity of gold nanoparticles. *Nanoparticle Toxicity*, 3 (11): 1941- 1949.

Qu Y, and Lu X. 2009. Aqueous synthesis of gold nanoparticles and their cytotoxicity in human dermal fibroblasts-fetal. *Biomedicine Materials*, 4: 025007.

Rahim S and Urën A. 2011. A real time electrical impedance based technique to measure invasion of epithelial cell monolayer by cancer cells. *Journal of Visualized Experiments*, 50.

Rayavarapu RG, Petersen W, Hartsuiker L, Chin P, Janssen H, van Leeuwen FWB, Otto C, Manohar S, and Leeuwen TG. 2010. *In vitro* toxicity studies of polymer-coated gold nanorods. *Nanotechnology,* 21: 145-149.

Shenoy D, Fu W, Li J, Crasto C, Jones G, DiMarzio C, Sridhar S, and Amiji M. 2006. Surface Functionalization of Gold nanoparticles using hetero- bifunctional poly (ethylene glycol) spacer for intracellular tracking and delivery. *International Journal of Nanomedicine*, 1(1): 51-57.

Shukla R, Bansal V, Chaudhary M, Basu A, Bhonde RR, and Sastry M. 2006. Biocompatibility of gold nanoparticles and their endocytotic fate inside the cellular compartment: a microscopic overview. *Langmuir*, 21: 10644.

Smout MJ, Kotze AC, McCarthy JS, and Loukas A. 2010. A novel high throughput assay for anthelmintic drug screening and resistance diagnosis by real-time monitoring of parasite motility. *PLoS Negl Trop Dis* 2:4:e885.

Uboldi C, Bonacchi D, Lorenzi G, Hermanns MI, Pohl C, Baldi G, and Kirkpatrick C. 2009. Gold nanoparticles induce cytotoxicity in the alveolar type-II cell lines A549 and NCIH44I. *Particle and Fibre Toxicology,* doi: 10.1186/1743-8977-1186-1118.

Urcan E, Haertel U, Styllou M, Hickel RB, Harry Scherthan H, and Reichl FX. 2010. Real-time xCELLigence impedance analysis of the cytotoxicity of dental composite components on human gingival fibroblasts. *Dental Material*, 26: 51- 58.

Vetten MA, Tlotleng N, Rascher DT, Skepu A, Keter FK, and Gulumian M. 2013. Label free in vitro toxicity and uptake assessment of citrate stabilized gold nanoparticles in three cell lines. *Particle and Fibre Toxicology,* 10 (50): 1-15.

Vijayakumar S and Ganesan S. 2012. *In vitro* cytotoxicity assay on gold nanoparticles with different stabilizing agents. *Journal of Nanomatererials*. 2012: 1-9.

CHAPTER 5

MECHANISMS OF GOLD NANOPARTICLES TOXICITY

5.1 Introduction

The exact mechanisms by which AuNPs affect cells remain unclear. However, studies on ultrafine nanoparticles and ENPs have established that nanoparticles can induce damage to the cell by the (i) release of inflammatory cytokines, (ii) DNA damage and (iii) production of reactive oxygen species (ROS) (Buzea *et al.,* 2007; Fu *et al.,* 2014). A schematic diagram of the possible toxicity pathways induced by nanoparticles in cells is shown in Figure 5.1. In this chapter, the induction of pro-inflammatory cytokines and chromosomal DNA damage as possible mechanisms of AuNPs toxicity in HepG2 and HEK 293 cells are investigated. Furthermore, the generation of free radicals in biological solutions containing AuNPs was studied.

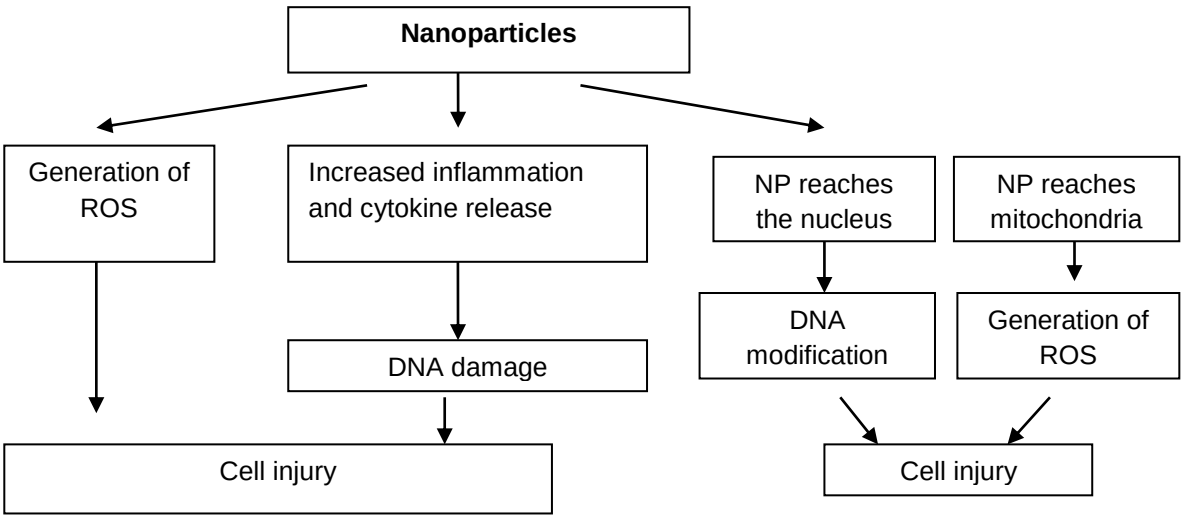


Figure 5.1: Proposed mechanisms by which nanomaterials can induce cellular toxicity (Buzea et al., 2007)

5.1.1 Pro-inflammatory release in response to cell-nanoparticle interaction

Exposures of cells to external stimuli or foreign substances have been shown to induce the release of pro-inflammatory cytokines to the surrounding medium (Jeng and Swanson, 2006; Nel *et al.,* 2006). In the study, the secretion of interleukin (IL)-6 and tumor necrosis factor (TNF) used as mediators for cell communication, immune response and cell division was assessed in growth medium after treatment of cells with AuNPs. The concentration of IL-6 and TNF-α was measured with the flow cytometer.

5.1.2 DNA damage as a mechanism of nanoparticle toxicity

The ability of nanoparticles to cause DNA damage indirectly via oxidative stress or directly by nanoparticles interacting with nucleus has been studied. Cytokine release has also been shown to promote DNA damage through strand breaks and chromosomal fragmentation (Singh *et al.,* 2009). Even though a drawback of possible interaction of nanoparticles with DNA exists with other genotoxicity test methods, the chromosome aberration have been tested to be reliable for assessing DNA damage of intact cells (George *et al.,* 2016). Therefore, DNA damage in cells was assessed in this study using chromosome aberration test.

5.1.3 Free radical generation

A number of nanomaterials, including AuNPs have been found to catalyze the generation of free radicals in the presence of hydrogen peroxide (H_2O_2), making the safety of these materials a concern (Halliwel *et al.,* 2000). To understand the biological effect of

nanoparticles and their safety, it is significant to examine reactions between AuNPs and biological components that are present in cells. Thus, this study examined the production of hydroxyl radicals by AuNPs in cell free systems consisting of hydrogen peroxide as a biological constituent present in cells (Halliwel *et al.,* 2000; Halliwel and Whiteman, 2004). The reactions of hydrogen peroxide and AuNPs stabilized with citrate and polyethylene glycol were assessed in acidic and alkaline buffer solutions to mimic biologically relevant conditions. The acidic recycling vesicles of the endosomes and lysosomes were AuNPs are localized within cells were represented by a buffering solution with a pH range of 3.6-4.6. On the other hand, a buffer with a pH range of 6.5-7.0 represented cytoplasmic conditions within the cells.

The generation of hydroxyl radicals was assessed using electron spin resonance (ESR) technique for identifying and quantifying short-lived free radical species (Jeong *et al.,* 2016). Briefly, ESR uses a spin trapping agent to identify free radicals in a sample. The absorption of a free radical species is measured in a magnetic field in the microwave frequency region (Hawkins and Davies, 2014; He *et al.,* 2014). Therefore, the absorption signal and the intensity depends on the type of the free radical generated, thus the absence of a molecule with unpaired electrons in a test sample will result in no signal from the instrument.

5.2 Experimental Procedures

5.2.1 Determination of pro-inflammatory cytokines after gold nanoparticle exposure

The induction of cytokines in cells was assessed using the flow cytometer. The cell supernatants were processed according to the manufacturers' instructions using the BD Cytometric Bead Array (CBA) Human Th1/Th2/Th17 Cytokine Kit, from BD Biosciences. Briefly, the cells were grown to 50% confluency in a 12-well plate. The AuNPs were added to

the cells to a final concentration of 1nM and the plates were incubated for a further 4 and 24hrs. Following incubation, the supernatant was removed from the plate, centrifuged at 13 000 X g for 30min to pellet excess AuNPs. The centrifugation step was carried out to reduce non-specific attachment of AuNPs not taken up by cells but remained in the culture medium with the cytometric beads used in the assay. The supernatant was analyzed immediately or kept at -70°C until required for analysis.

The supernatant was analyzed on a flow cytometer (BD FACS brand cytometer equipped with a 488nm argon laser). Three hundred events were collected for each capture bead. The results were exported to the BD FCAP Array software and were presented as means plus standard deviations. Two independent experiments were run on same samples. The concentrations (pg/mL) of IL-6 and TNF-α were calculated from a standard curve, produced using known concentrations of the cytokines standard supplied in the manufacturer's kit (**Appendix 3**). Post-hoc pairwise comparisons using Tukey-kramer and Tukey's HSD test was used to assess differences in the concentrations of IL-6 and TNF-α in supernatants of treated cells and the negative control groups. The Wilcoxon rank sum (Mann-Whitney) test was used to compare concentrations of IL-6 and TNF-α between the two cell types for each AuNPs after 4hrs and after 24hrs of incubation. A p value of <0.05 was considered statistically significant.

5.2.2 Chromosome aberration test for genotoxicity testing

Cells were cultured in a $25cm^2$ tissue-culture flasks as described above. After reaching 50% confluency, the cells were treated with 1nM AuNPs for 24 hrs. After incubation, the culture medium was removed and substituted with fresh medium containing Colcemid at a concentration of 0.1µg/ml to arrest metaphase cells. The flasks were further incubated for

2hrs. Following incubation with Colcemid, the cells were removed from the flasks by trypsinization as previously described. The cells were placed in a potassium chloride (KCl) hypotonic solution for 20 min and fixed in a 3:1 methanol/glacial acetic acid solution. Metaphase cells were spread on clean microscope glass slides and stained with 5% $^{v}/_{v}$ Giemsa stain. The slides were left to air-dry at room temperature and were assessed for structural chromosomal aberrations (SCA) using light microscope operated at 100X magnification. Untreated cells were used as the negative control. Cells treated with a genotoxic agent ethylmethanesulfonate (EMS) at 5mM (purchase from Sigma®) were used as positive control.

The percentage of cells with chromosome aberrations per 50 cells was scored. The genotoxic effect of AuNPs was analysed by comparing the number of chromosomal aberrations observed in treated cells with the negative control samples. Post-hoc pairwise comparisons using Tukey-kramer and Tukey's HSD test was used to compare statistical differences of aberration (%) in treated cells and the negative control groups. The Wilcoxon rank sum (Mann-Whitney) test was used to compare aberration (%) between the two cell types for each AuNPs after incubation. A p value of <0.05 was considered statistically significant.

5.2.3 Free radical generation using electron spin resonance

5.2.3.1 Preparation of reagents and reaction medium

Assay vials for ESR studies were washed in nitric acid solution before use. Briefly, the assay vials were soaked in 2L deionized water containing 500g sodium hydroxide (NaOH) pellets and ethanol. Following this, the vials were soaked in 25% $^{v}/_{v}$ nitric acid for 48hrs, rinsed with deionized water and dried in an inverted position overnight in an oven. Potassium chloride

(KCl) was used to prepare the buffer stock solutions, and employed as the reaction medium. A buffer 0.4M of KCl (pH 3.6), pH 4.6 and pH 6.5 were prepared as reaction medium. Before use, each buffer was treated with 1g/L of Chelex® 100 molecular biology grade resin to remove trace metals. The Chelex® 100 treated buffer solutions were left to stir overnight and sterilized by filtration through a 0.45µm filter. The pH of the solutions was determined before use and was re-adjusted to the desired pH using 100mM hydrochloric acid.

The spin trap 5, 5 dimethyl N-oxide pyrroline (DMPO), purchased from Sigma-Aldrich® (South Africa) was used to trap the hydroxyl radical. A stock solution of 1M DMPO was prepared, charcoal deactivated and filtered into clean nitric acid washed amber vials and stored at -20°C until used. A working solution of the DMPO was prepared by diluting 50µL of the stock solution into 5mL deionised water. The DMPO solution was filtered with nylon MS® syringe filters with 0.45µm pore size before use. A working solution of 8nM hydrogen peroxide solution was prepared by diluting 30µL of 30% H_2O_2 solution into 5mL deionized water. Ferrous iron (Fe^{2+}) was prepared by dissolving 280mg of iron chloride ($FeCl_2$) salt in 1mL of 0.5% EDTA solution. A working solution of Fe (II) was prepared by diluting 30µL stock solution into 5mL deionized water, which was filtered and sterilized before use. AuNPs solutions were prepared fresh to desired concentrations in water. The AuNPs were prepared in water as phenolic compounds in the cell culture medium have been shown to generate significant levels of hydrogen peroxide (Halliwell *et al.,* 2000; Halliwell and Whiteman, 2004).

5.2.3.2 Preparation of 4-hydroxyl Tempol (4-OH Tempol) ESR standard

The spin label, Tempol was used to calibrate the ESR. Briefly the calibration solution was prepared by dissolving 48±1mg of 4-hydroxy Tempol in 25mL deionized water. The absorbance of Tempol solution was measured at 429nm before preparing the working

solutions. A 50µM working stock Tempol solution was used to make the serial dilutions for the standard curve as illustrated in Figure 5.2.

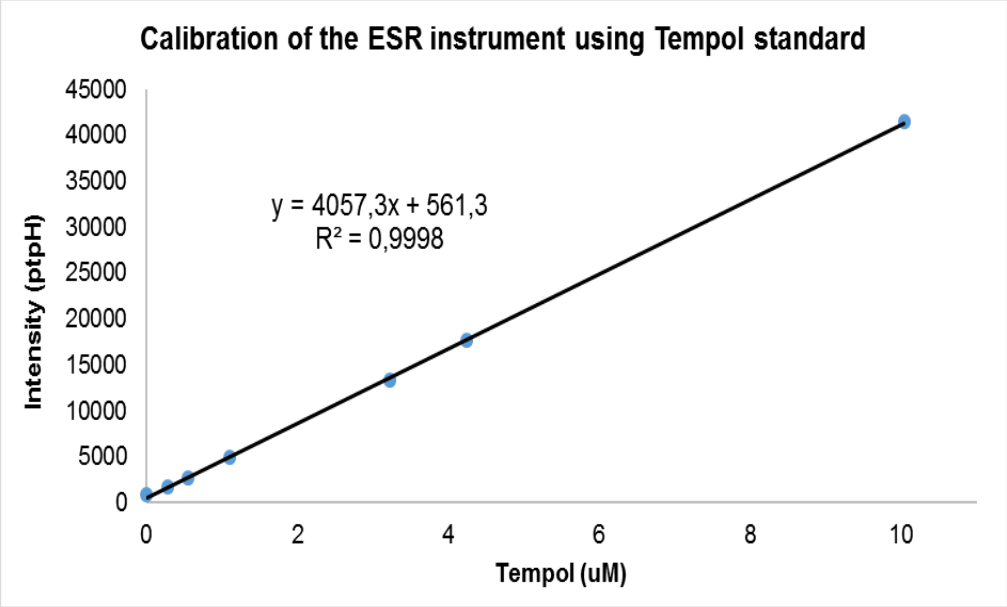


Figure 5.2: Calibration of the ESR instrument using the spin probe 4-hydroxyl Tempol

5.2.3.3 Measurement of free radicals using ESR

ESR measurements of free radicals were carried out in a Bruker EMX model ESR spectrophotometer (Bruker Corporation, Bruker South Africa (PTY) Ltd) consisting of peristaltic pump tubing, aqua flow sample cell, Teflon tubing and an auto sampler. The calibration settings of the instrument remained unchanged for the whole duration of the experiments. All reactions were carried out in amber vials placed in a heating block with incubation temperature of 37°C. The ESR was left to warm up for about 1 hr before performing the reactions. The reaction mixture was injected into the sample cavity to obtain an intensity reading for each reaction. Each sample was scanned in triplicate at 0, 1.5 and 3 minutes. An average of the peak-to-peak height of the three readings was taken to represent

the amount of radicals produced. The DMPO/•OH is a short lived radical and last for no more than 2 minutes, thus the ESR signal obtained 0- 2 minutes were interpreted as results.

For analysis, the instrument was set at 3G field modulation; 100G scan range, and 15.94mW microwave power for acquiring scans. The intensity of the ESR signal was obtained on the ESR spectrum of the hydroxyl radical spin adduct with DMPO (DMPO/·OH). The final reaction medium for the positive baseline or control consisted of 0.4M buffer solution, 100mM DMPO, 300µM H_2O_2, and 70µM Fe^{2+} solution to initiate ·OH production. A negative control reaction consisted of 0.4M buffer solution, 100mM DMPO and 300µM H_2O_2. To measure the decomposition of hydrogen peroxide in the presence of AuNPs in a 'Fenton-like reaction', H_2O_2 solution (300µM) was mixed with DMPO (100mM) in buffers of different pH ranges and the reaction was initiated by the addition of AuNPs solution to prepare a concentration of 0.5 and 2nM AuNPs in the reaction medium. The ability of AuNPs to promote (as a pro-oxidant) or reduce (as a anti-oxidant) the production of free radicals, in a system generating free radicals was measured in a reaction containing both Fe^{2+} and AuNPs. A concentration of AuNPs at which the DMPO/•OH signal was increased in the presence of Fe^{2+} was selected to initiate a reaction of hydrogen peroxide and AuNPs in a 'Fenton-like reaction' for measurement of the DMPO/•OH signal.

5.3 Results and Discussion

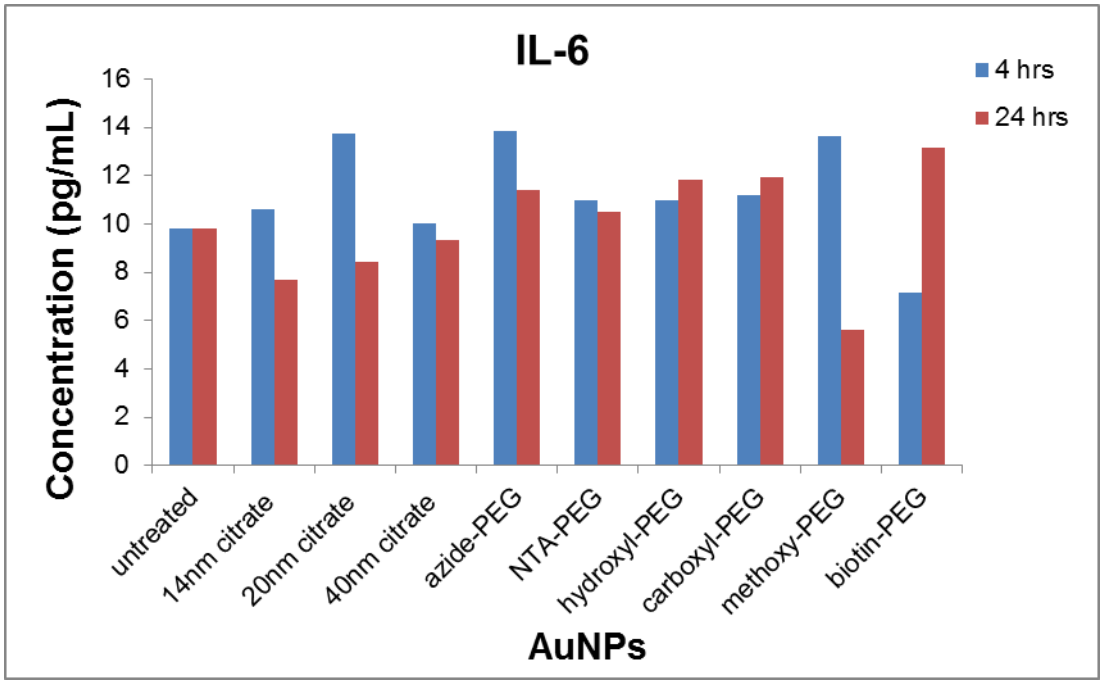
5.3.1 Determination of pro- inflammatory cytokines following gold nanoparticle exposure

Figures 5.3 show the concentrations of IL-6 (A) and TNF-α (B) in HepG2 cells after treatment with AuNPs. The graph indicates an increase in the concentration of IL-6 and TNF-α 4 hrs after incubation with 14nm, 20nm and 40nm citrate AuNPs, 14nm azide-PEG,

14nm NTA-PEG and the 14nm methoxy-PEG AuNPs. However, the secreted IL-6 and TNF-α in the supernatant of the treated cells was not statistically significant to the untreated cells. IL-6 and TNF-α in culture medium of cells treated with these AuNPs decreased when the incubation time was increased (after 24 hrs).

On the other hand, a time dependent increase in IL-6 and TNF-α concentration was seen in supernatant of cells treated with 14nm hydroxyl-PEG, 14nm carboxyl-PEG and 14nm biotin-PEG AuNPs. These were not statistically different from the untreated cells ($p>0.05$). A similar study reported a non-significant effect on inflammatory cytokine release after exposure of human alveolar epithelial A459 co-culture system to 15nm citrate AuNPs for 24 hrs (Brandenberger *et al.,* 2010). In the study, pre-stimulation of AuNPs-treated cells with lipopolysaccharide (LPS) was shown to significantly induce cytokine secretion in A459 co-culture cells.

A



B

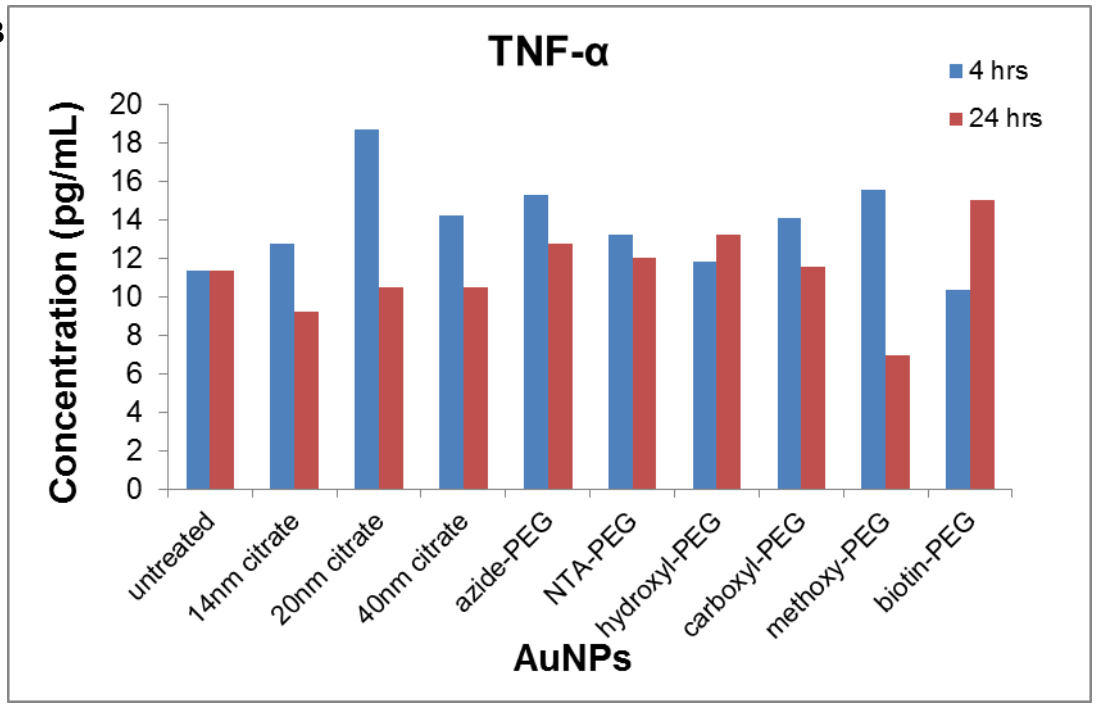


Figure 5.3: Concentration of (A) IL-6 and (B) TNF-α in culture medium of HepG2 cells exposed to AuNPs for 4 and 24 hrs.

The concentrations of secreted IL-6 (A) and TNF-α (B) in culture medium of HEK 293 cells after treatment with AuNPs is shown in Figure 5.4. A time dependent response in IL-6 was seen in cell culture medium of cells treated with 14, 20 and 40nm citrate AuNPs, 14nm azide-PEG, 14nm NTA-PEG, 14nm hydroxyl-PEG, 14nm methoxy-PEG and 14nm biotin-PEG AuNPs (Figure 6A). Nonetheless, statistical analysis revealed a non-significant difference in IL-6 concentration of these samples when compared to untreated cells ($p>0.05$). In addition, the concentrations of IL-6 after 4 and 24 hrs incubation in these samples was not significantly different from each other ($p>0.05$). A time dependent increase in the concentration of TNF-α was seen in cell supernatant of 40nm citrate stabilized AuNPs, 14nm methoxy-PEG and 14nm biotin-PEG treated samples (Figure 4B). Similar to HepG2 cells, a decrease in the concentration of TNF-α, with increasing incubation time was evident in supernatant of cell samples treated with 14nm and 20nm citrate AuNPs, as well as in 14nm azide-PEG and 14nm carboxyl-PEG AuNPs. There was, however, no significant difference in the concentration of TNF-α in these samples after 4 and 24 hrs incubation.

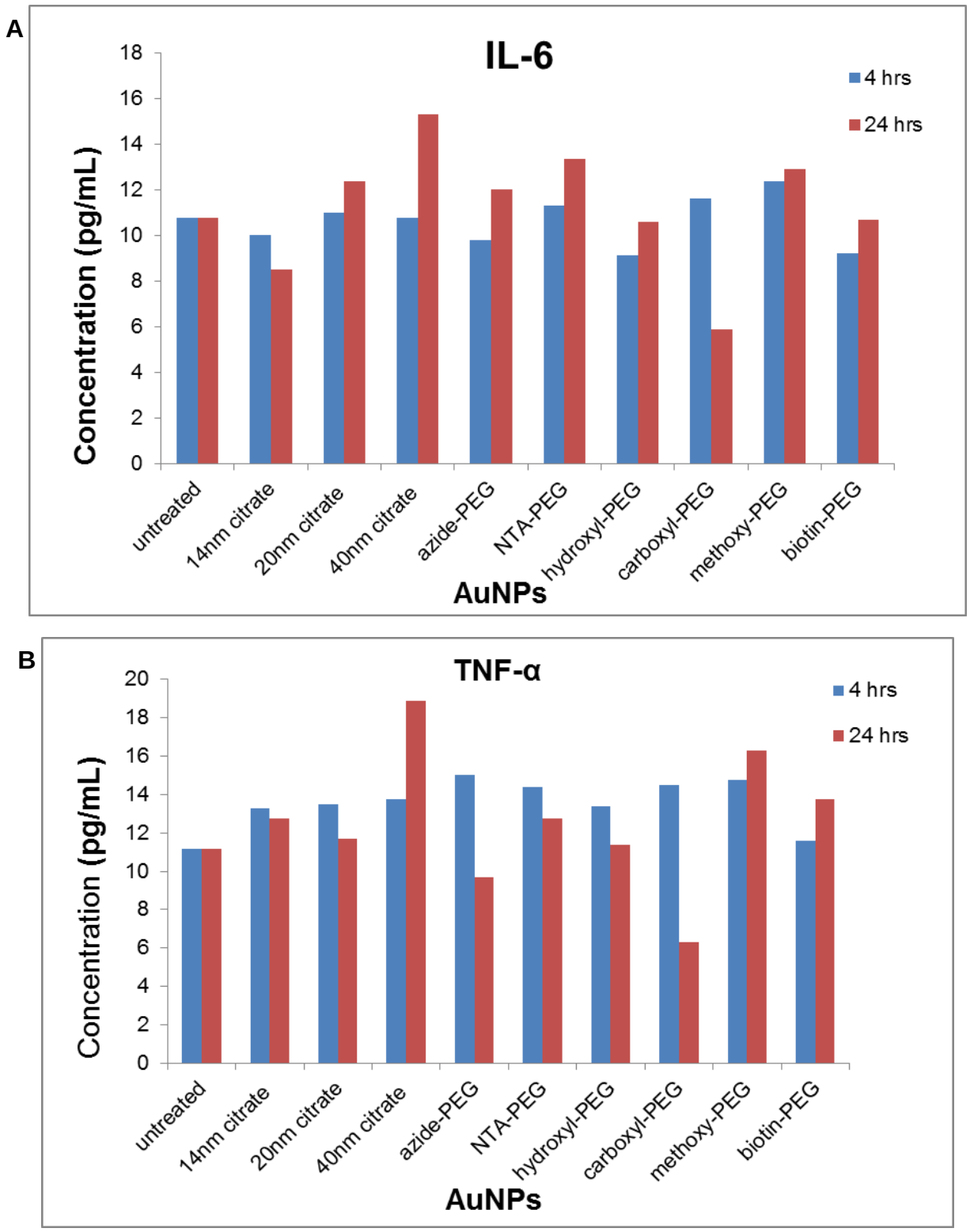


Figure 5.4: Concentration of (A) IL-6 and (B) TNF-α in cell culture medium of HEK 293 cells exposed to AuNPs for 4 and 24 hrs.

The Wilcoxon rank sum (Mann-Whitney) test further revealed a non-significant difference in the concentrations of IL-6 and TNF-α released in HepG2 and HEK 293 cells treated with AuNPs after 4 and 24 hrs incubation ($p>0.05$). Table 5.1 shows a comparison of the concentration of IL-6 and TNF-α in HepG2 and in HEK 293 cells.

Table 5.1: Comparison of concentrations (pg/mL) of IL-6 and TNF-α released in HepG2 and HEK 293 cells after treatment with AuNPs

AuNPs	**IL-6**		**TNF-α**		**p-value**	
	HepG2	**HEK 293**	**HepG2**	**HEK 293**	**IL-6**	**TNF-α**
Untreated	9.8± 0.02	10.8± 0.01	11.3± 0.01	11.1± 0.01	0.12	0.08
14nm citrate	9.10± 2.12	9.25± 1.06	10.95± 2.47	12.95± 1.00	1.00	0.22
20nm citrate	11.05± 3.75	11.65± 1.00	14.6± 5.59	12.6± 1.27	1.00	1.00
40nm citrate	9.65± 1.00	13.05± 3.18	12.35± 2.61	16.25± 3.60	0.12	0.44
azide-PEG	12.60± 1.70	10.95± 1.63	14.00± 1.83	12.35± 3.88	0.43	0.44
hydroxyl-PEG	11.4± 1.00	9.85± 1.10	12.5± 1.00	12.3± 1.41	0.12	1.00
NTA-PEG	10.75± 1.00	12.3± 1.41	12.6± 1.00	13.00± 1.00	0.12	0.44
biotin-PEG	10.10± 4.24	9.95± 1.07	12.65± 3.32	12.65± 1.48	1.00	1.00
carboxyl-PEG	11.5± 1.00	8.75± 4.03	12.85± 1.77	10.40± 5.57	0.44	1.00
methoxy-PEG	9.6± 5.46	12.6± 1.00	11.30± 5.74	15.25± 1.01	1.00	0.44

5.3.2 Chromosome aberration test for genotoxicity testing

Chromosome aberrations in the form of breaks, dicentric chromosome, rings, and fragmentation were assessed in cells after treatment with AuNPs. The number of aberrations in treated cells was compared to untreated cells to determine the level of DNA damage. Figure 5.5 shows the number of aberrations (expressed as % aberration) in HepG2 cells 24 hrs after treatment with citrate stabilized and PEG coated AuNPs. The graph indicates that cells treated with 14nm citrate AuNPs have the highest percentage of aberrations when compared to cells treated with other AuNPs. The number of aberrations in these groups was also significantly different to untreated control groups ($p< 0.05$), indicating the possible genotoxic effect of the 14nm citrate stabilized AuNPs in HepG2 cells.

Positive results on the genotoxicity of AuNPs have been reported. Li *et al.* (2008) reported a 4 fold increase in chromosomal aberrations when MRC-5 lung fibroblasts cells were treated with different concentrations of 20nm citrate AuNPs at 1nM concentration for 72 hrs. In the study, the mutagenicity of DNA bases by measuring the quantity of 8hydroxy-deoxyguanosine (8OHdG) in MRC-5 human fetal lung fibroblast cell line. Also, the genotoxicity of citrate AuNPs in HepG2 cells have been demonstrated after incubation of cells with 1-5µM concentration of spherical AuNPs for 24 hrs (Paino *et al.,* 2012).

The graph in Figure 5.5 indicates an increase in percent aberration after treatment of cells with 14, 20 and 40nm citrate AuNPs, as well as in cells treated with 14nm azide-PEG, NTA-PEG, carboxyl-PEG, biotin-PEG, hydroxyl-PEG and methoxy-PEG coated AuNPs. Even so, when compared to the negative control groups, the percentage of aberrations in cells treated with 20 and 40nm citrate AuNPs as well as the PEG coated MPCs and MMPCs was not statistically significant ($p>0.05$). The results indicate the size dependent effect of citrate

AuNPs, where the 14nm citrate was genotoxic to cells compared to the 20 and 40nm citrate AuNPs. In Figure 5.5, the 20nm citrate AuNPs showed a high percent aberration when compared to 40nm citrate AuNPs. The PEG MPCs (14nm carboxyl-PEG, hydroxyl-PEG and methoxy-PEG AuNPs) showed an increased percentage in aberration compared to the PEG MMPCs (azide-PEG, NTA-PEG and biotin-PEG AuNPs). However, the difference in effect of the PEG MPCs and PEG MMPCs was not statistically significant.

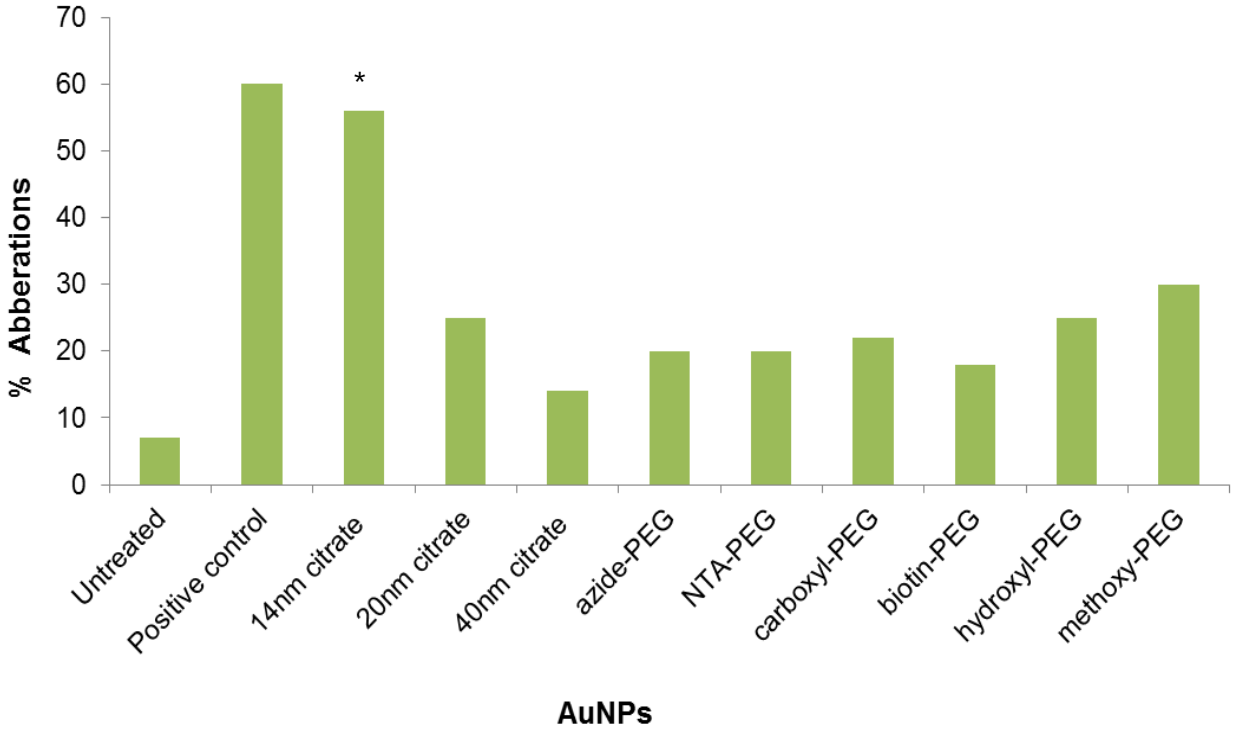


Figure 5.5: Percent chromosome abberation in HepG2 cells incubated with AuNPs for 24 hrs.

In Figure 5.6, the citrate AuNPs (14nm and 20nm), azide-PEG, NTA-PEG, carboxyl-PEG, biotin-PEG, hydroxyl-PEG and the methoxy-PEG AuNPs indicated a significant difference in percent aberrations when compared to the negative control groups ($p<0.05$), indicating the DNA damaging effect of these AuNPs to HEK 293 cells. Compared to the 14 and 20nm citrate AuNPs, the 40nm citrate AuNPs showed the least effect in cells, indicating that size

may be a compounding factor in determining genotoxicity of cells, with smaller nanoparticulate sizes posing a higher risk.

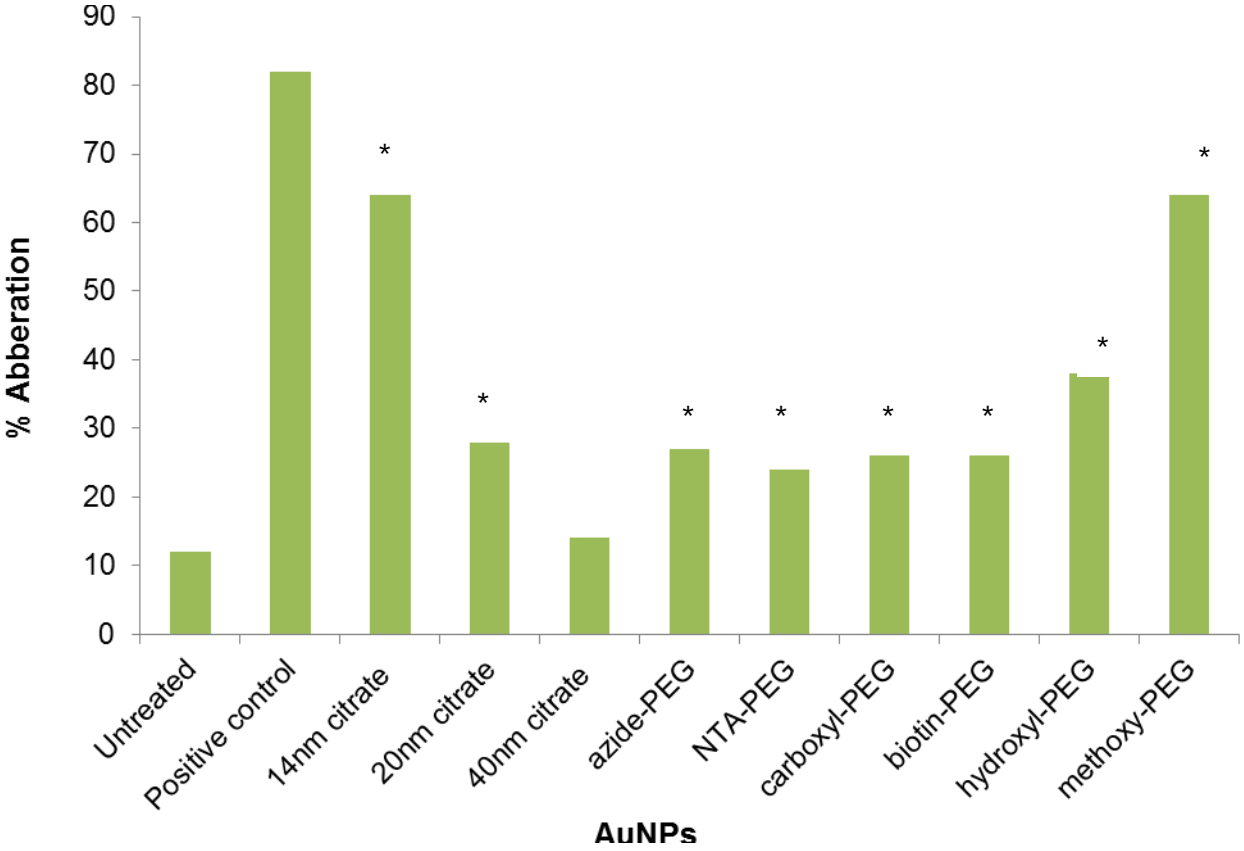


*Figure 5.6: Percent chromosome abberation in HEK 293 cells incubated with AuNPs for 24 hrs. *p<0.05.*

5.3.3 Free radical generation using electron spin resonance

The ability of AuNPs to promote hydroxyl radical generation in the Fenton-like reaction was detected over a wide range of buffer solution with pH 3.6; 4.6 and 6.5, simulating physiological conditions in lysosomes, endosomes and cell cytoplasm. A typical ESR scan of a buffer solution is shown in **Appendix 4**. A Fenton reaction, where the decomposition of hydrogen peroxide was catalyzed in the presence of ferrous iron was used in the study as

the positive baseline (referred to as the F60). The negative baseline was measured in a reaction of hydrogen peroxide without ferrous iron (referred to as the F0).

Figure 5.7 shows the ESR signal intensity of DMPO/•OH radical in the positive and the negative baseline (pH 3.6) over time. The ESR spectra showing a peak-to peak ratio of the DMPO/•OH adduct in Fenton reaction at pH 3.6 is shown in Figure 5.7C. The ESR spectrum of the negative baseline with no peaks is shown in Figure 5.7B.

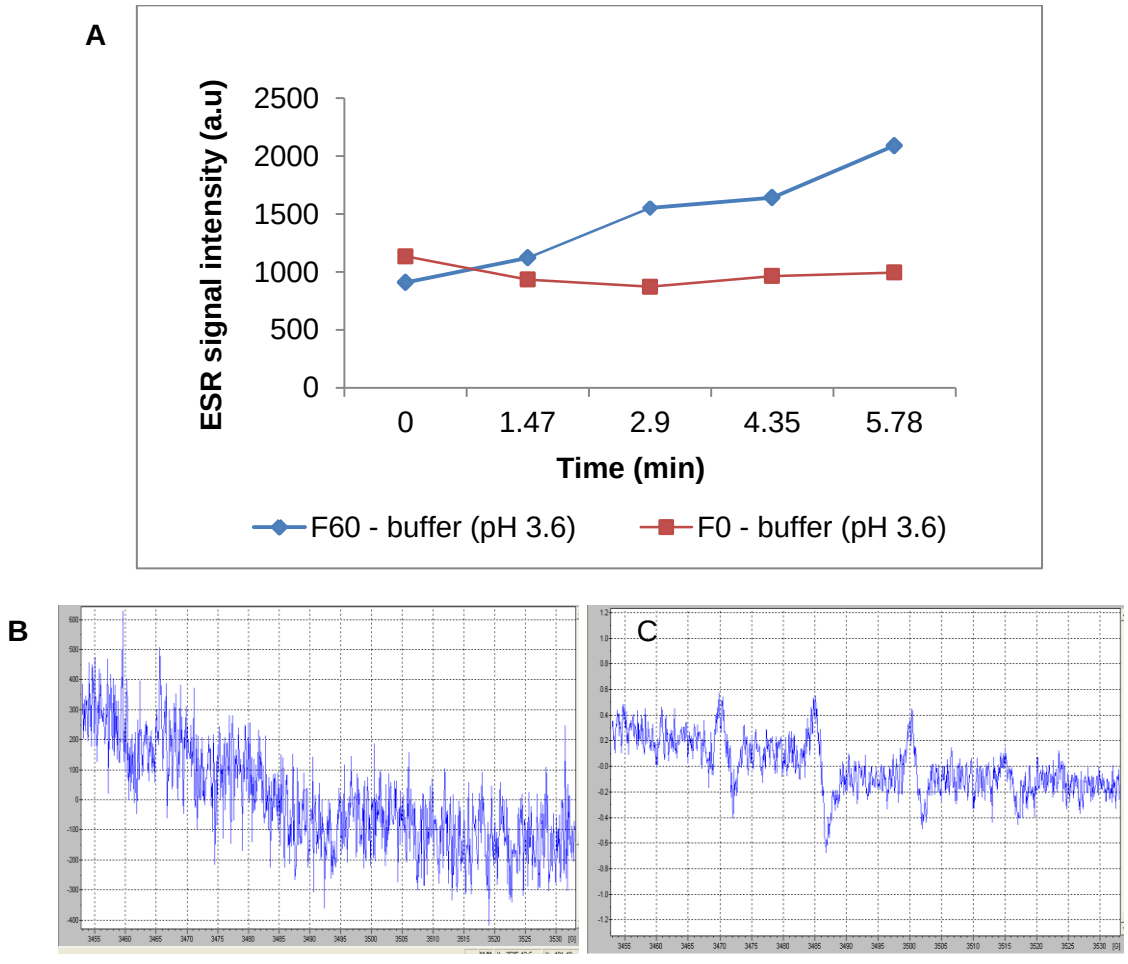
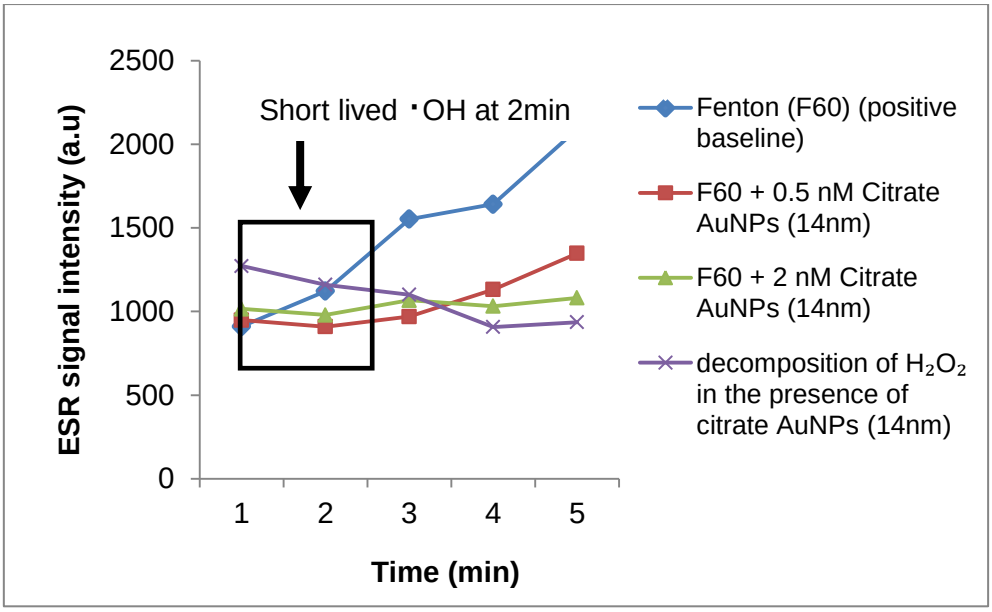


Figure 5.7: ESR signal intensity of H_2O_2 decomposition in the presence of Fe^{2+}(F60). (F0) represent the negative baseline without Fe^{2+}. The ESR spectra of the reactions F0 (b) and F60 (c) are shown.

The ESR signal intensity in a reaction of hydrogen peroxide, ferrous iron and 14nm citrate AuNPs is shown in Figure 5.8. In Figure 5.8A, different concentrations of citrate AuNPs were added to the reaction medium (pH 3.6) containing Fe^{2+} and hydrogen peroxide to determine the effect of AuNPs concentration on the generation of hydroxyl radicals. In the presence of AuNPs and Fe^{2+}, the signal intensity of DMPO/·OH obtained in the first 2 minutes of the reaction was low when compared to the positive baseline. In these reactions, the DMPO/•OH signal intensity was similar to the negative baseline. On the other hand, in a reaction where the AuNPs were added without Fe^{2+}, the DMPO/•OH signal intensity increased. The DMPO/•OH radical is a short lived radical, thus the intensity recorded in the first 2 min of the reaction indicated the presence of the hydroxyl radical.

A reaction showing the catalytic activity of citrate AuNPs in the presence of hydrogen peroxide is indicated. At the start of the reaction, a short lived DMPO/•OH adduct was observed, indicating the ability of these AuNPs to catalyze the decomposition of hydrogen peroxide to generate hydroxyl radicals. The ESR spectra showing the peak-to-peak signal of the DMPO/•OH adduct in a reaction of hydrogen peroxide and AuNPs is shown in Figure 5.8B. Similar to related studies, the stability of the DMPO/•OH adduct was determined to have a half-life of about 2 minutes, thereby declining with time (Bačić *et al.,* 2008).

A



B

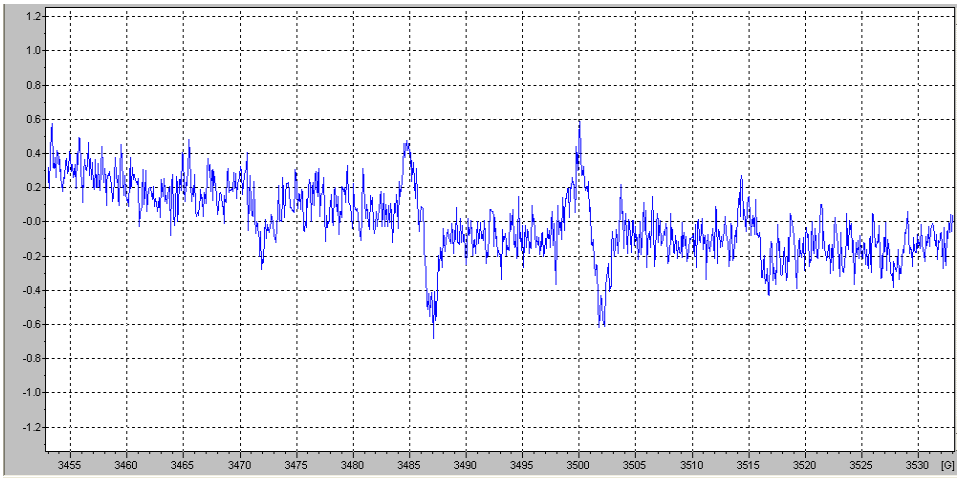


Figure 5.8: ESR signal intensity in the reaction of hydrogen peroxide and 14nm citrate stabilized AuNPs. F60 represented a positive baseline in reaction medium containing hydrogen peroxide and Fe^{2+}. AuNPs were added at different concentrations to the F60 reaction (red and green plot). AuNPs (in the absence of Fe^{2+}) were used to catalyze the decomposition of hydrogen peroxide (purple plot). The ESR scan shows the DMPO/•OH obtained in the reaction of H_2O_2 and citrate AuNPs (pH 3.6) at about 2 minutes after initiating the reaction.

The reaction between hydrogen peroxide and 20nm citrate AuNPs at pH 3.6 is shown in Figure 5.9. The spectra showing the DMPO/•OH signal intensity of the Fenton. The signal intensity of the DMPO/•OH adduct decreased in reactions containing AuNPs and Fe^{2+}. In

addition, different concentration of the AuNPs did not affect the DMPO/•OH signal. At the tested concentration, the signal intensity was similar to that of the negative baseline. Figure 5.9 also indicates that in the absence of Fe^{2+}, these AuNPs alone do not play a role in the generation of hydroxyl radicals by catalyzing the decomposition of hydrogen peroxide. The signal intensity of DMPO/·OH adduct in the reaction of AuNPs and hydrogen peroxide was similar to the negative baseline.

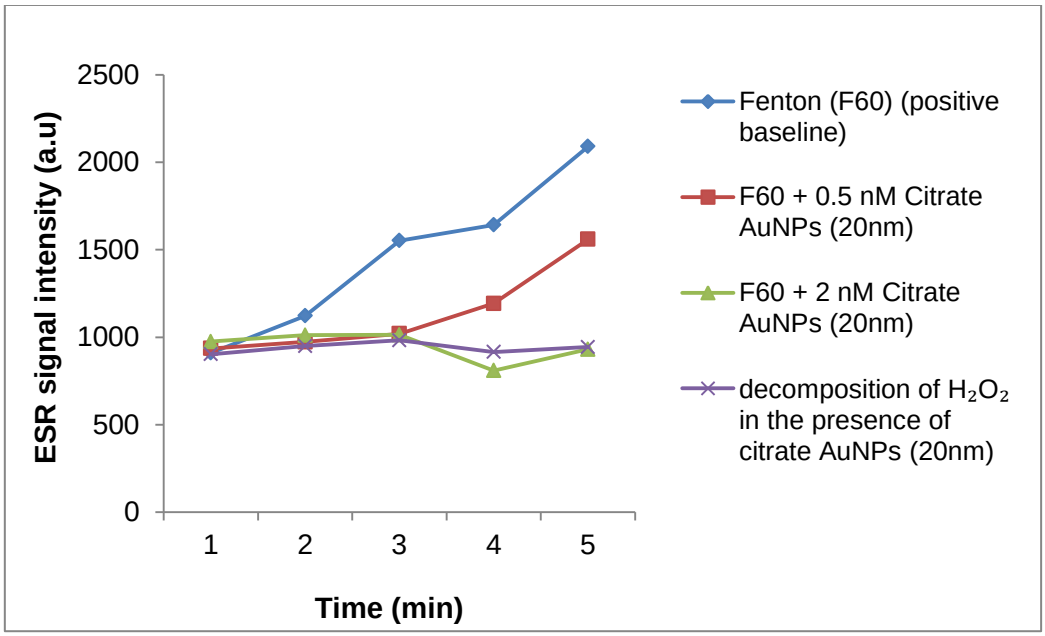


Figure 5.9: ESR signal intensity in the reaction of hydrogen peroxide and 20nm citrate stabilized AuNPs. AuNPs were added at different concentration in the presence of hydrogen peroxide and Fe^{2+}. AuNPs (in the absence of Fe^{2+}) were used to catalyze the decomposition of hydrogen peroxide at pH 3.6.

Similarly, the 40nm citrate AuNPs did not affect the generation of hydroxyl radicals in the Fenton reaction (Figure 5.10). The effect these AuNPs on the DMPO/•OH signal intensity was dependent on concentrations, with high concentrations decreasing the intensity of hydroxyl radicals. In addition, these AuNPs did not have an effect in the decomposition of

hydrogen peroxide as the intensity of DMPO/·OH adduct was similar to the negative baseline.

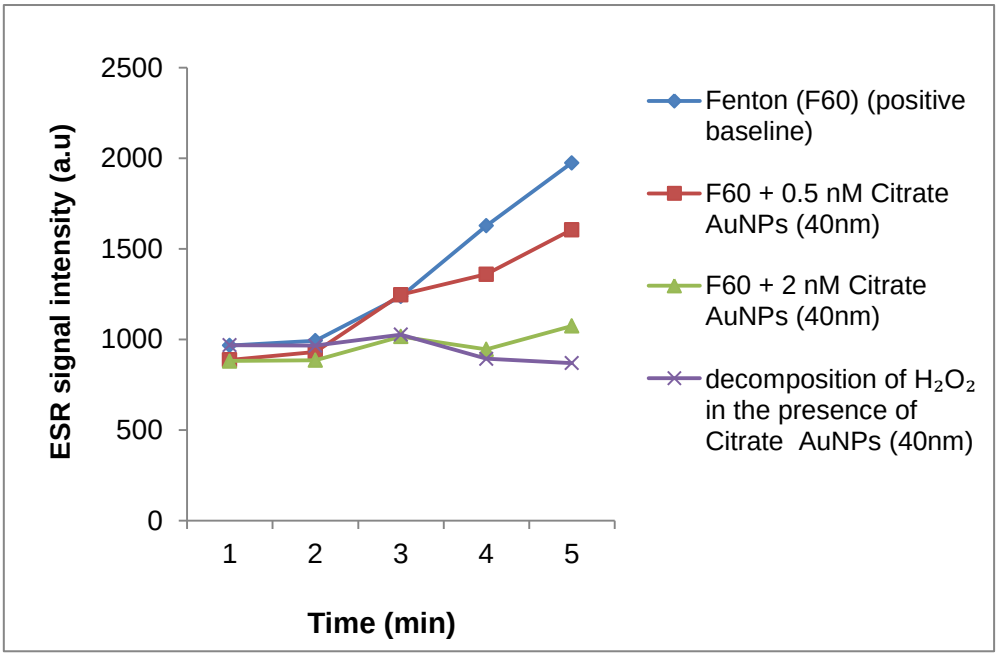


Figure 5.10: ESR signal intensity in the reaction of hydrogen peroxide and 40nm citrate stabilized AuNPs. AuNPs were added at different concentration in the presence of hydrogen peroxide and Fe^{2+}. AuNPs (in the absence of Fe^{2+}) were used to catalyze the decomposition of hydrogen peroxide at pH 3.6.

The signal intensity of the DMPO/•OH in the presence of hydrogen peroxide and azide-PEG coated AuNPs is shown in Figure 5.11, which indicates a decrease in the DMPO/•OH intensity in reactions of Fe^{2+} and AuNPs. The addition of different concentrations of these AuNPs did not influence the generation of hydroxyl radical. In addition, in the absence of Fe^{2+}, the azide-PEG AuNPs did not generate hydroxyl radicals in the presence of hydrogen peroxide. Similarly, signal intensity of DMPO/·OH was similar to the negative baseline.

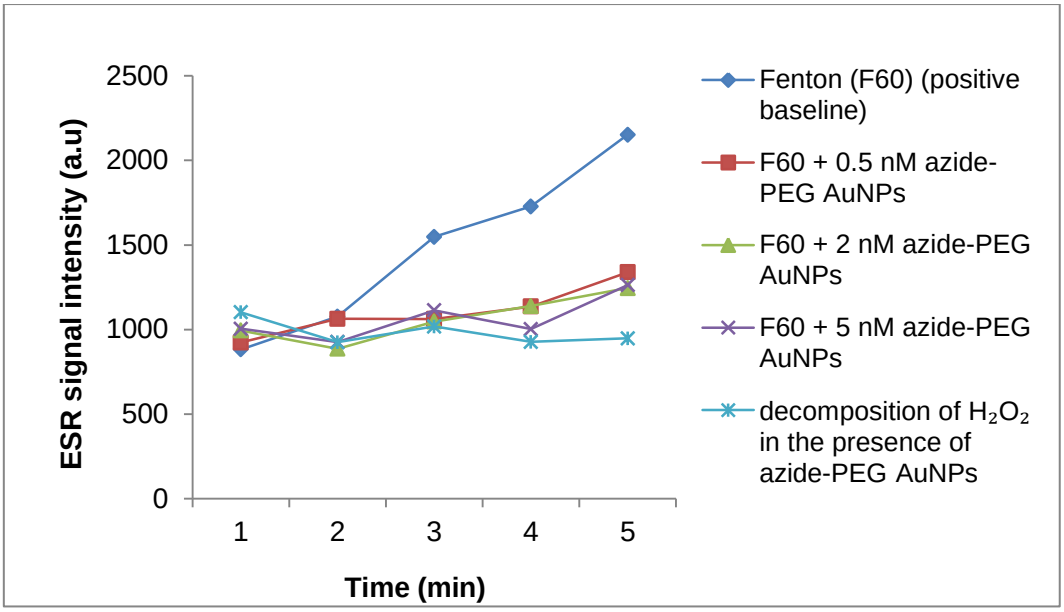


Figure 5.11: ESR signal intensity in the reaction of hydrogen peroxide and azide-PEG AuNPs. The azide-PEG AuNPs were added at different concentration. AuNPs were assessed for their ability used to catalyze the decomposition of hydrogen peroxide in the absence of Fe^{2+}.

Figure 5.12 shows the signal intensity of DMPO/·OH after the addition of different concentrations of NTA-PEG AuNPs in the reaction containing Fe^{2+}. The NTA-PEG AuNPs did not promote the generation of hydroxyl radical generation when added to the reaction containing Fe^{2+}. The NTA-PEG AuNPs were able to catalyze the decomposition of hydrogen peroxide to generate hydroxyl radicals.

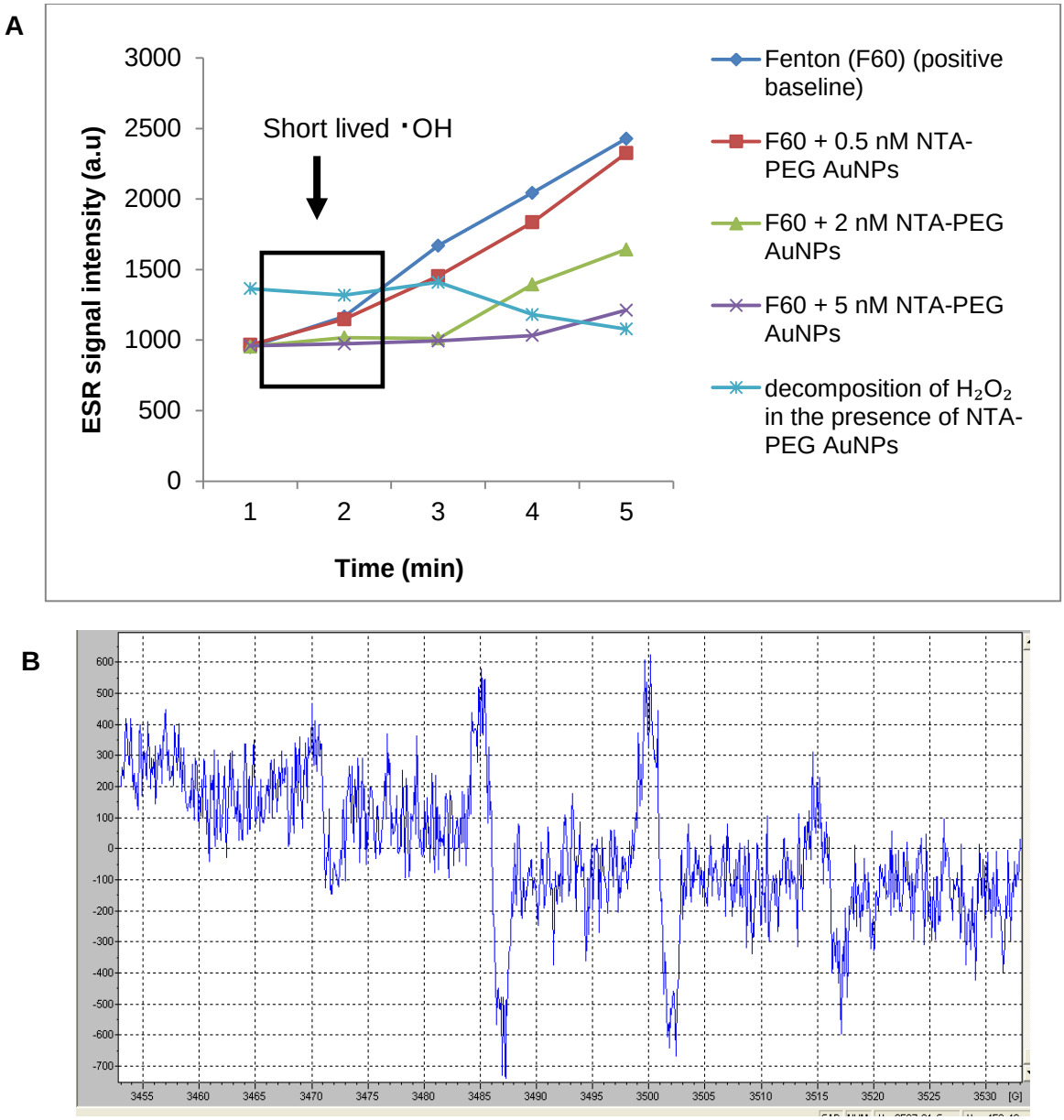


Figure 5.12: ESR signal intensity in the reaction of hydrogen peroxide and NTA-PEG AuNPs. AuNPs were assessed for their ability used to catalyze the decomposition of hydrogen peroxide in the absence of Fe^{2+}. The *ESR scan shows the DMPO/•OH obtained in the reaction of H_2O_2 and NTA-PEG AuNPs (pH 3.6).*

The reactions between hydrogen peroxide and carboxyl-PEG AuNPs is shown in Figure 5.13. Similar to NTA-PEG AuNPs, a short lived DMPO/•OH peak was seen when carboxyl-PEG AuNPs were added in the reaction medium containing hydrogen peroxide, indicating the ability of these AuNPs to catalyse the formation of hydroxyl radicals (Figure 5.13). The

reaction is also shown by an increase in the DMPO/·OH signal intensity as indicated in Figure 5.13A. Similarly, the DMPO/·OH adduct intensity was evident for about 2 minutes, declining with increasing reaction time. In reactions of $Fe^{2+}$and AuNPs, the DMPO/•OH signal was similar to the positive baseline. At high concentrations, the intensity of the DMPO/•OH signal was reduced.

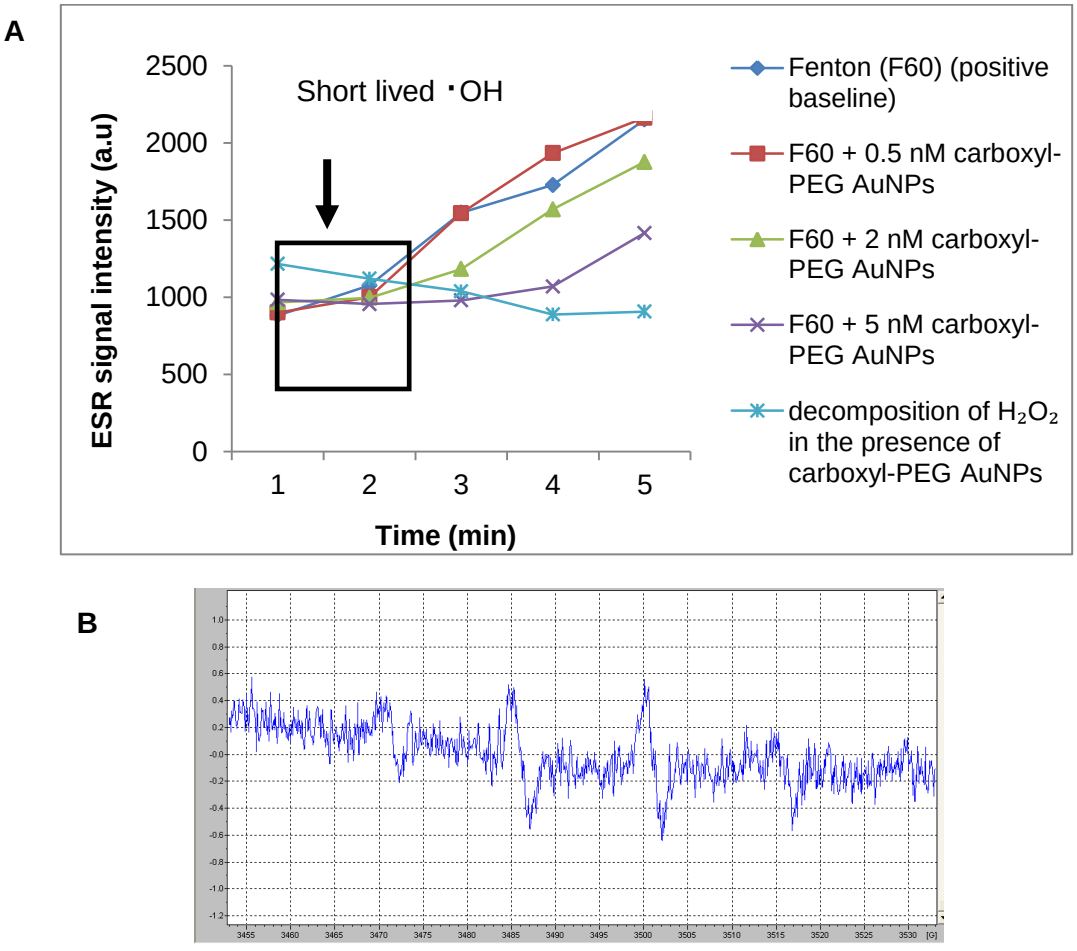


Figure 5.13: ESR signal intensity in the reaction of hydrogen peroxide and carboxyl-PEG AuNPs. The carboxyl-PEG AuNPs were added at different concentration was assessed for their ability used to catalyze the decomposition of hydrogen peroxide in the absence of Fe^{2+}. The ESR scan shows the DMPO/•OH obtained in the reaction of H_2O_2 and carboxyl-PEG AuNPs (pH 3.6).

The reaction between biotin-PEG AuNPs and hydrogen peroxide in the absence of Fe^{2+} shows that the biotin-PEG AuNPs alone do not catalyze the decomposition of hydrogen peroxide to generate hydroxyl radicals (Figure 5.14). The signal intensity of this reaction was similar to the negative baseline.

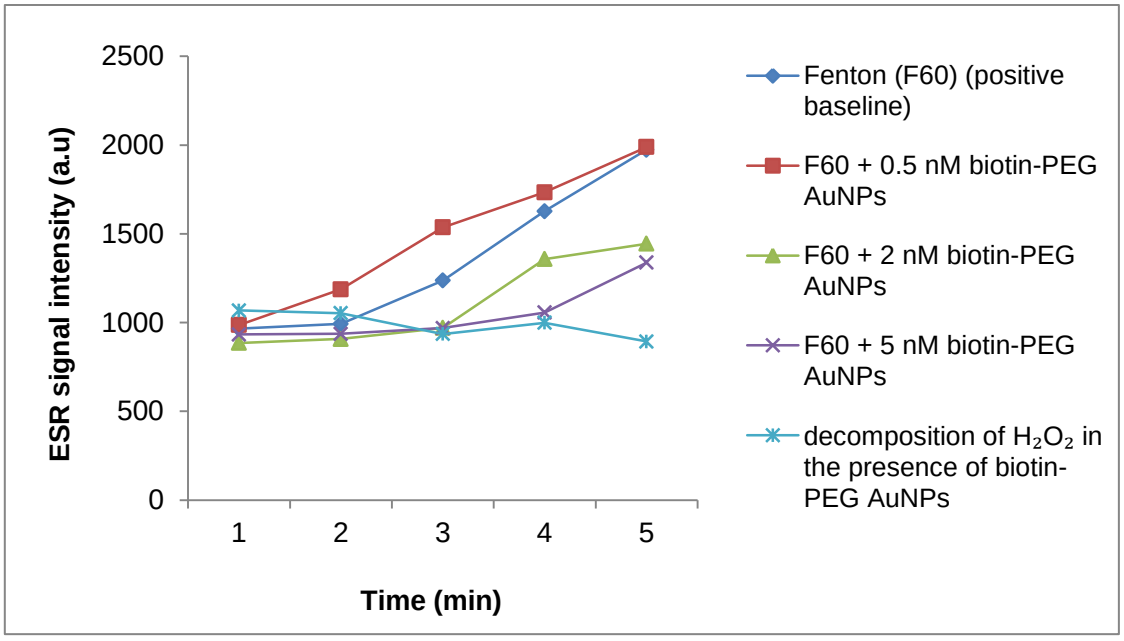


Figure 5.14: ESR signal intensity in the reaction of hydrogen peroxide and biotin-PEG AuNPs. The biotin-PEG AuNPs were added at different concentration). AuNPs were assessed for their ability used to catalyze the decomposition of hydrogen peroxide in the absence of Fe^{2}.

Similar to the biotin-PEG coated AuNPs, low concentrations of hydroxyl-PEG AuNPs slightly increased the intensity of the DMPO/·OH adduct in a reaction of hydrogen peroxide and Fe^{2+} (Figure 5.15). The results may indicate that the hydroxyl-PEG coated AuNPs may influence the generation of hydroxyl radicals. At high concentrations, the intensity of the DMPO/•OH adduct was decreased, indicating a concentration dependent effect. In the absence of Fe^{2+},

the hydroxyl-PEG AuNPs did not catalyze the decomposition of hydrogen peroxide as the intensity of the DMPO/·OH was similar to that of the negative control.

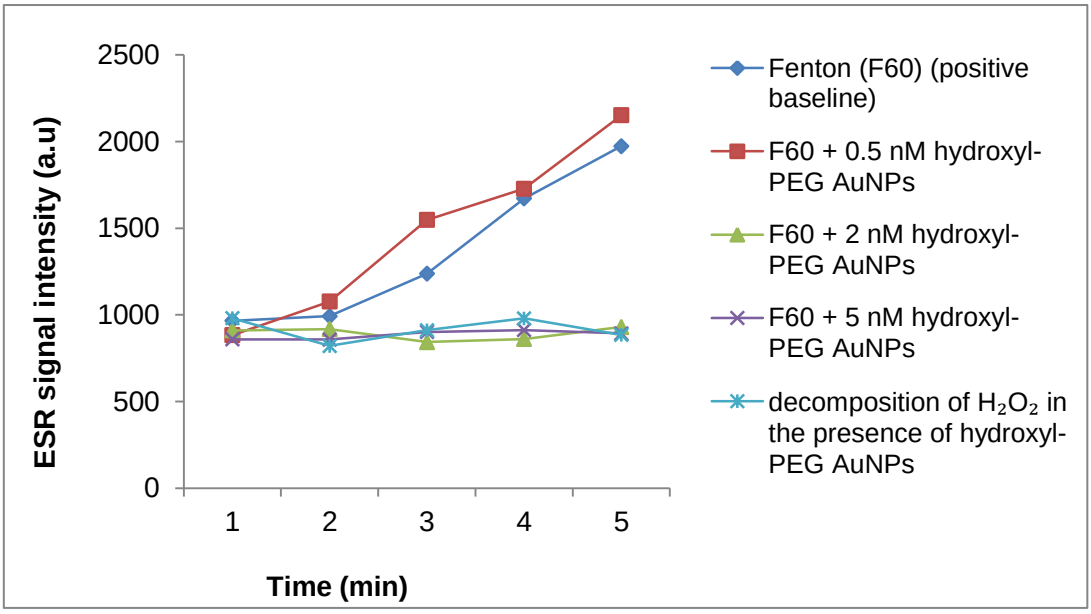


Figure 5.15: ESR signal intensity in the reaction of hydrogen peroxide and hydroxyl-PEG AuNPs. The hydroxyl-PEG AuNPs were added at different concentration. AuNPs were assessed for their ability used to catalyze the decomposition of hydrogen peroxide in the absence of Fe^{2+}.

The ESR signal intensity of the DMPO/·OH adduct in the presence of methoxy-PEG AuNPs is shown in Figure 5.16. These AuNPs did not promote the generation of hydroxyl radicals in Fenton reaction. The intensity of the DMPO/·OH signal was significantly reduced at 2 and 5 nM concentrations. The Figure also indicates that the methoxy-PEG AuNPs did not catalyze the decomposition of hydrogen peroxide to generate hydroxyl radicals.

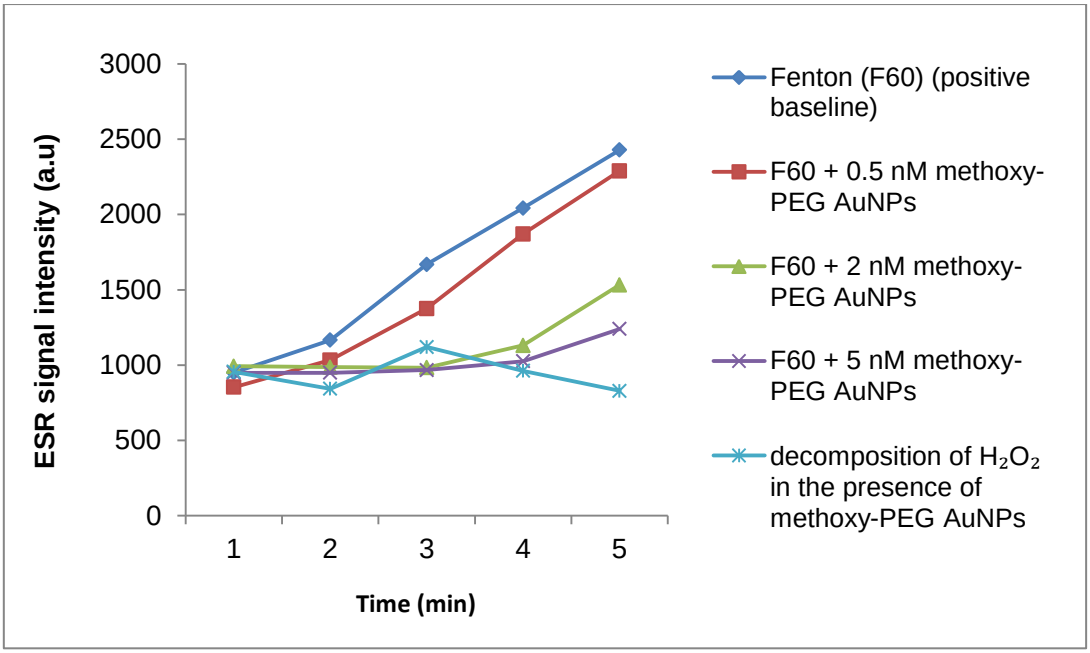


Figure 5.16: ESR signal intensity in the reaction of hydrogen peroxide and methoxy-PEG AuNPs. The hydroxyl-PEG AuNPs were added at different concentration. AuNPs were assessed for their ability used to catalyze the decomposition of hydrogen peroxide in the absence of Fe^{2+}.

A summary of ESR intensity showing the catalytic activity of AuNPs is shown in Figure 5.17. The figure indicates that three of the tested nanoparticles, citrate (14nm), NTA-PEG and carboxyl-PEG show the ability to decompose hydrogen peroxide into hydroxyl radicals at pH 3.6. The nanoparticle ligands (20nm and 40nm citrate AuNPs), biotin-PEG, azide-PEG, methoxy-PEG, and the hydroxyl-PEG AuNPs do not exhibit this characteristic.

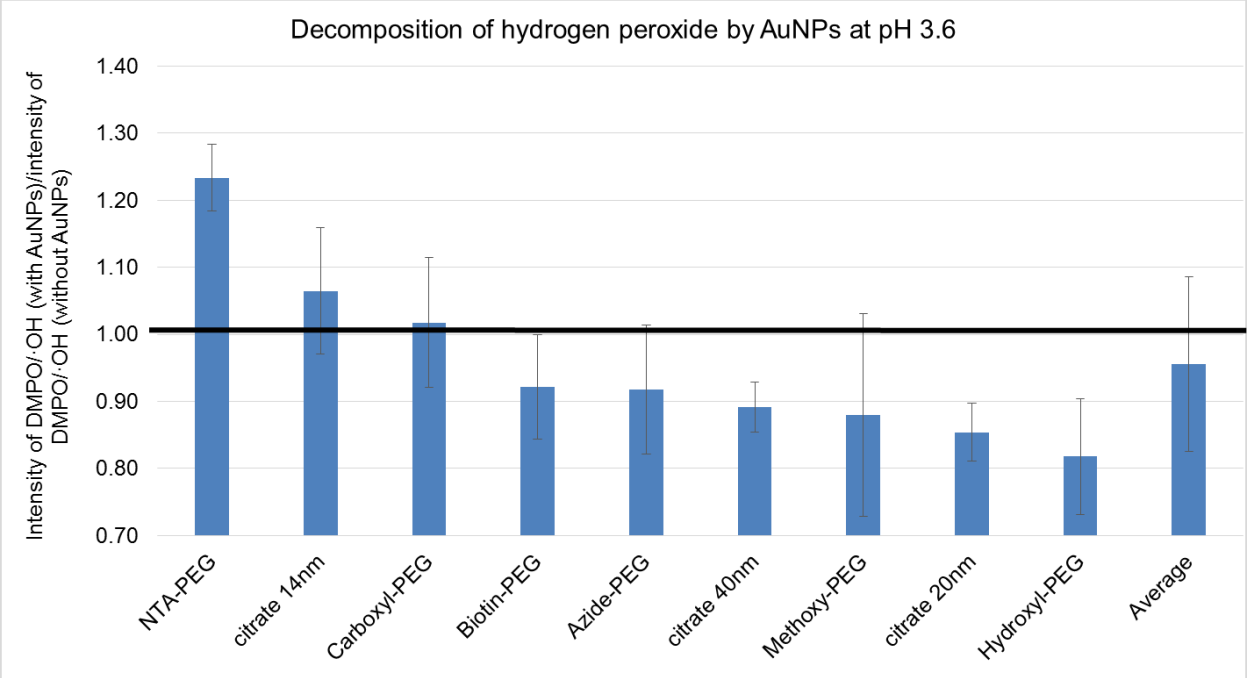


Figure 5.17: Decomposition of hydrogen peroxide by AuNPs at pH 3.6. The data represents each particle displacement ratio from the negative baseline

The negative and the positive baseline in a reaction medium with pH 4.6 are shown in **Appendix 4 and Appendix 5**. Figure 5.18 shows the signal intensity of the DMPO/·OH adduct in the presence of citrate AuNPs (A-C). At this pH solution, the AuNPs did not promote the generation of hydroxyl radicals in the Fenton reaction neither did they show catalytic activity in the decomposition of H_2O_2 to hydroxyl radicals. In addition, the DMPO/·OH signal intensity was greatly reduced compared to reactions that were conducted at lower pH solutions. This observation was similar to studies that assessed the catalytic activity of citrate and PEG modified AuNPs in different buffer solutions, where the catalytic activity of AuNPs was evident in solutions of lower pH (He *et al.,* 2013). The ESR signal intensity of DMPO/•OH radical in the positive and the negative baseline (pH 4.6) over time.

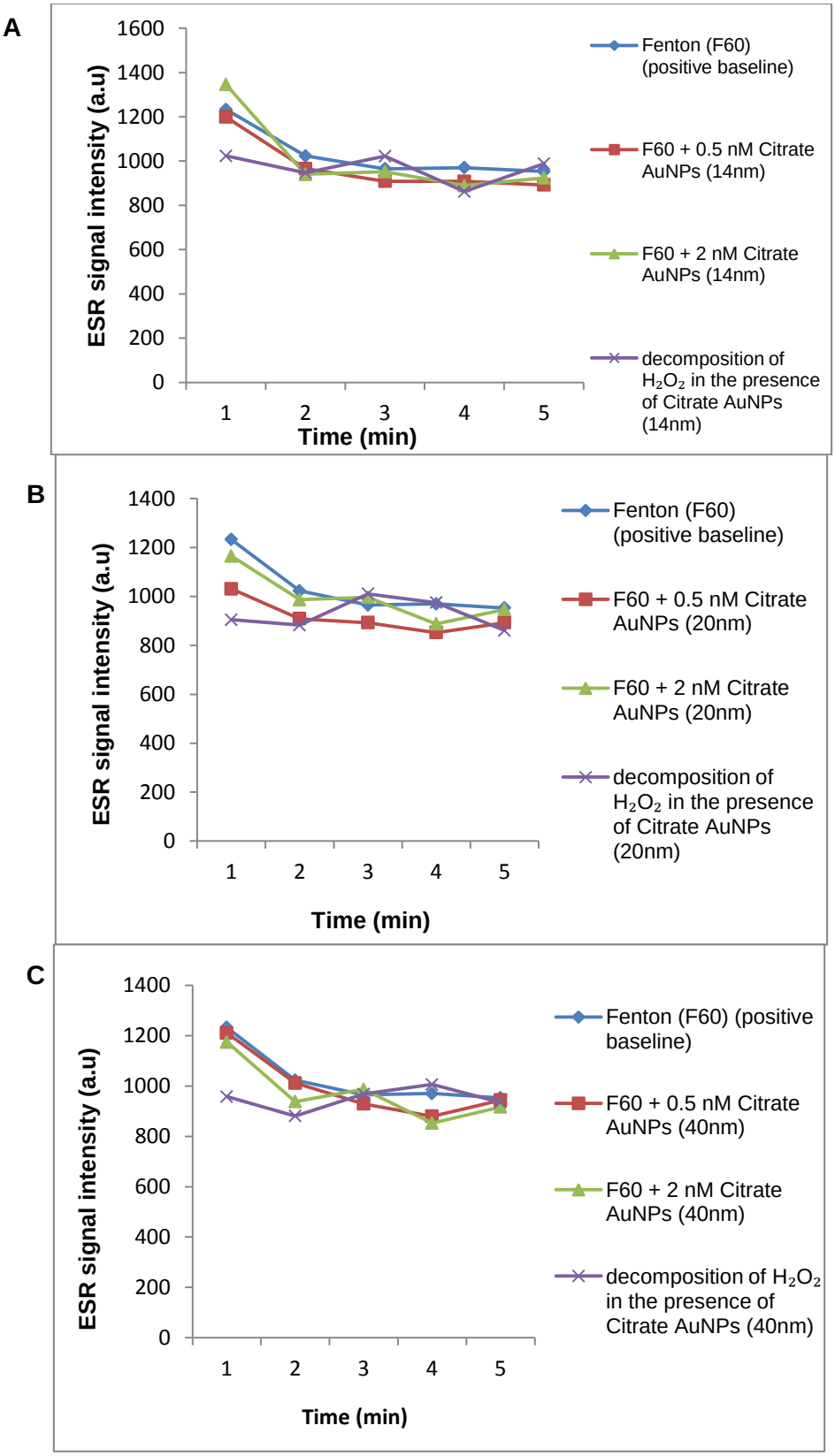


Figure 5.18: ESR signal intensity showing the effect of (A) 14nm, (B) 20nm and (C) 40nm citrate stabilized AuNPs on the generation of ·OH at pH 4.6.

Figure 5.19 shows the ESR signal intensity of the DMPO/•OH adduct in the presence of (A) azide-PEG, (B) NTA-PEG and (C) carboxyl-PEG AuNPs in pH solution of 4.6. In a reaction containing azide-PEG and NTA-PEG AuNPs (without Fe^{2+}), the intensity of DMPO/•OH decreased. The carboxyl-PEG AuNPs did not promote the generation of hydroxyl radicals in Fenton reaction neither did they show catalytic activity in the decomposition of hydrogen peroxide (Figure 5.19C). The intensity of the DMPO/•OH signal was significantly reduced in the presence of carboxyl-PEG AuNPs at the tested concentrations.

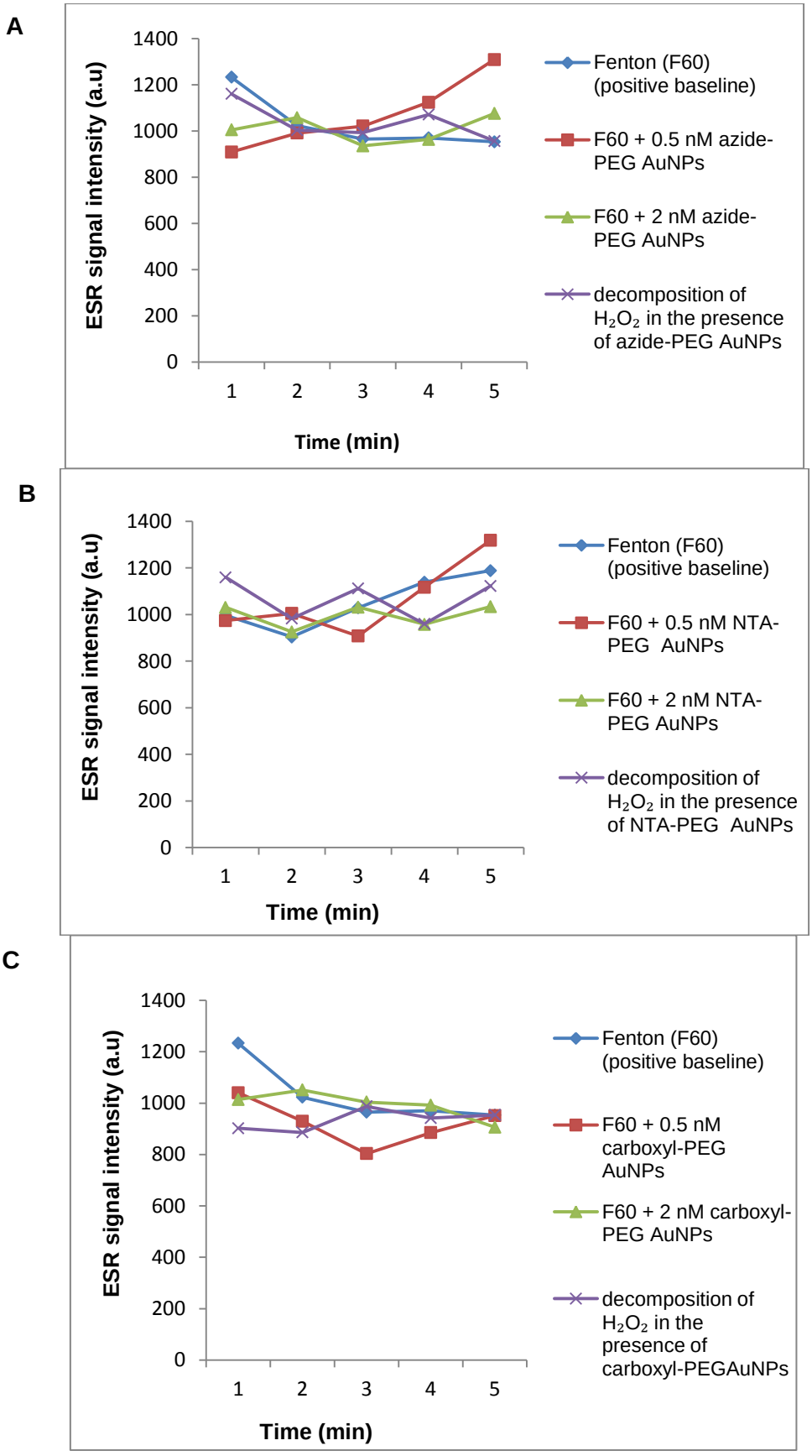


Figure 5.19: ESR signal intensity showing the effect of (A) azide-PEG, (B) NTA-PEG and (C) carboxyl-PEG AuNPs on the generation of •OH at pH 4.6.

Figure 5.20 shows the ESR signal intensity of the DMPO/•OH adduct in the presence of (A) biotin-PEG and (B) hydroxyl-PEG AuNPs in a reaction medium with pH 4.6. The AuNPs did not promote the generation of hydroxyl radicals in the presence of Fe^{2+}. The figure also indicates that the AuNPs did not catalyze the decomposition of hydrogen peroxide to generate hydroxyl radicals.

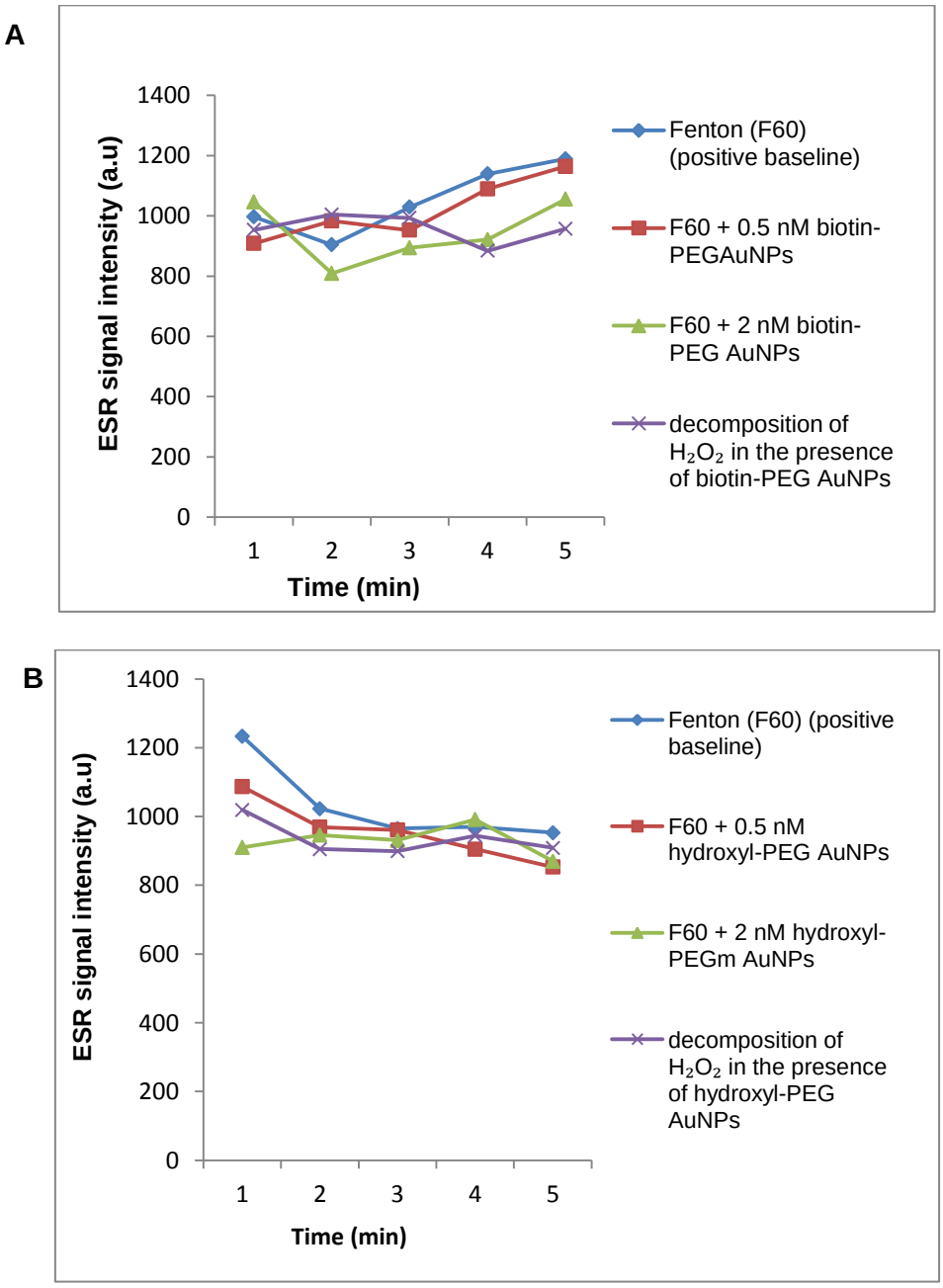


Figure 5.20: ESR signal intensity showing the effect of biotin-PEG (A) and hydroxyl-PEG (B) AuNPs on the generation of •OH at pH 4.6.

The ESR signal intensity of the DMPO/•OH adduct in the presence of methoxy-PEG AuNPs is shown in Figure 5.21. Similarly, the AuNPs did not promote the generation of hydroxyl radicals in Fenton reaction neither did they catalyze the decomposition of hydrogen peroxide to generate hydroxyl radicals.

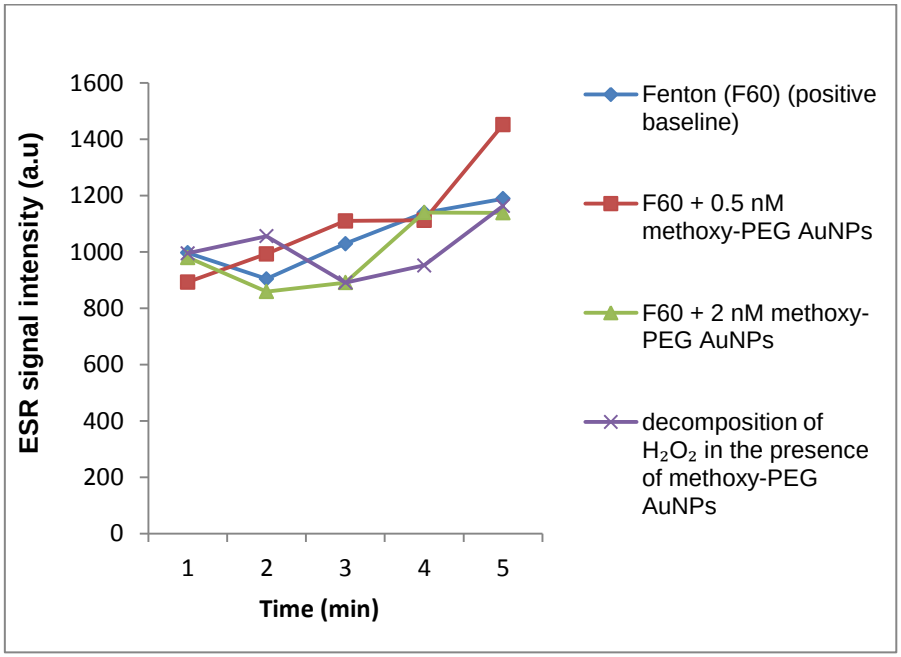


Figure 5.21: ESR signal intensity showing the effect of methoxy-PEG AuNPs on the generation of ·OH at pH 4.6.

In reaction medium with high pH, the intensity of the DMPO/•OH in the reaction of hydrogen peroxide, Fe^{2+} and AuNPs was lower than readings obtained in medium with pH 3.6 and pH 4.6. At pH 6.5 the intensity of DMPO/•OH in a reaction of Fe_{2+} and H_2O_2 was less than 1000 (Table 5.2).

Table 5.2: Intensity of DMPO/•OH in reaction medium pH 6.5.

Time	H_2O_2, Fe^{2+} and AuNPs			H_2O_2 and AuNPs		
	0.02	**1.45**	**2.88**	**0.02**	**1.45**	**2.88**
14nm citrate AuNPs	950	956	974	1008	921	888
20nm citrate AuNPs	1030	935	1019	901	963	895
40nm citrate AuNPs	1020	1055	829	944	910	1034
azide-PEG AuNPs	935	968	929	988	987	947
NTA-PEG AuNPs	905	998	860	1011	891	964
carboxyl-PEG AuNPs	987	903	962	924	897	975
biotin-PEG AuNPs	968	1018	1019	1003	910	923
hydroxyl-PEG AuNPs	892	1025	924	1020	880	912
methoxy-PEG AuNPs	956	963	917	973	912	978

5.4. Summary and Conclusion

The secretion of cytokines and structural chromosomal aberrations were investigated as mechanisms for AuNPs toxicity in cells. The concentration of TNF-α and IL-6 in cells were assessed as a result of their role in inflammatory responses and proliferation processes within cells. The results indicated a non-significant difference in the concentrations of IL-6 and TNF-α secreted in HepG2 and HEK 293 cells after treatment with AuNPs. From the results and existing studies, the effect of AuNPs on pro-inflammatory cytokine production can be shown to depend on nanoparticle size, functionalization as well as on the type of cells (Dykman and Khlebtsov, 2016).

Chromosomes of cells showed aberrations in HepG2 and HEK 293 cells treated with 14nm citrate AuNPs. This was statistically significant to the untreated control groups in both cell lines. In addition, the citrate AuNPs (20nm), azide-PEG, NTA-PEG, carboxyl-PEG, biotin-PEG, hydroxyl-PEG and the methoxy-PEG AuNPs showed a high percentage of aberrations in HEK 293 cells. The results suggest that genotoxicity of AuNPs is dependent on the cell type. Even though the results may indicate the possible damaging effect of these AuNPs to HepG2 and HEK 293 cells, additional genotoxicity testing may be required to confirm adverse effects of the AuNPs. Nonetheless, HEK 293 showed to be the most sensitive cell type. In both cell types, response was depended on size and surface chemistry.

A low percentage of aberrations obtained in cells treated with citrate AuNPs (20nm and 40nm) in HepG2 cells and 40nm citrate AuNPs in HEK 293 is indicative that genotoxicity effect of AuNPs depends on particle size. In addition, minimal effect of azide-PEG, NTA-PEG, carboxyl-PEG, biotin-PEG and hydroxyl-PEG as compared to the methoxy-PEG coated AuNPs may indicate that genotoxicity is dependent surface functional group.

The effect of AuNPs in free radical generation was assessed with ESR spectrophotomer in reaction solutions with pH 3.6, 4.6 and 6.5. The pH of the medium at which the reactions were initiated was significant to mimic intracellular compartments were AuNPs taken up by cells have been shown to localize. ESR spectra in a reaction of citrate AuNPs (14nm), NTA-PEG AuNPs and carboxyl-PEG AuNPs at pH 3.6 showed the catalytic activity of these AuNPs in the decomposition of hydrogen peroxide to generate hydroxyl radicals. This was confirmed by four line spectra characteristic of the DMPO/•OH adduct.

The short lived radical in the ESR spectra at pH 3.6 was observed 1-2 minute after the addition of AuNPs to a reaction medium containing H_2O_2. The ability of these AuNPs to generate free radicals may be the result of the toxicity effects observed in our previous findings (Vetten *et al.,* 2013; Tlotleng *et al.,* 2016). In the studies, the citrate AuNPs (14nm) was found to induce toxicity in embryonic kidney cells (HEK 293) and in bronchial epithelial cell line BEAS-2B (Vetten *et al.,* 2013). The carboxyl-PEG AuNPs showed toxicity effects in HEK 293 cells and in hepatocyte carcinoma cell line (HepG2) (Tlotleng *et al.,* 2016). Rushton *et al.* (2010) demonstrated the possibility of predicting nanoparticle toxicity with ESR based assays in a cell free system. The results showed the ability of copper nanoparticles, titanium dioxide (TiO_2) and AuNPs to contribute to the generation of hydroxyl radicals (Rushton *et al.,* 2010).

The signal intensity of the DMPO/•OH obtained at pH 3.6 was greater than the intensity observed obtained at pH 4.6 and 7.2, indicating that hydroxyl generation by AuNPs may depend on the pH of the surrounding medium. These results indicate that AuNPs deposited in the acidic compartments of the endosomes and lysosomes as indicated in uptake studies are more likely to generate hydroxyl radical, inducing oxidative stress.

The results obtained in this study were similar to results of a study by He *et al.* (2012 and 2013), where the catalytic activities of AuNPs and AgNPs in the decomposition of hydrogen peroxide was shown to be dependent on pH. In the study, the influence of AuNPs concentration and AuNPs size on the generation of •OH was investigated (He *et al.,* 2013). The generation of •OH by tannic acid-coated AuNPs with sizes ranging from 10-100nm was found to be greater in solution with pH 1.2 compared to reactions conducted in solutions with pH 4.6. The effect of pH in hydroxyl generation by nanoparticles were suggested to result from the pH-dependent redox behavior of hydrogen peroxide and the ability of the nanoparticles to facilitate electron transfer (He *et al.,* 2014)

Our results indicated that particle size may also influence the DMPO/•OH signal, where the 20nm and 40 nm citrate AuNPs did not show catalytic activity in hydroxyl generation. The attraction of these nanoparticles to each other as observed in TEM images may results in increased size of these particles in reaction medium, which may be the reason for the size dependence hydroxyl radical generation by these nanoparticles. The influence of AuNPs size on hydroxyl radical generation was also reported by He *et al. (*2013) where a decline in the DMPO/•OH signal was seen with increased particle size (He *et al.,* 2013). The reason for the results by He *et al.* (2013) was not clear.

In reactions containing Fe^{2+}, both 14nm citrate AuNPs, NTA-PEG and carboxyl-PEG AuNPs did not influence or promote •OH generation as confirmed by a decrease in the intensity of the DMPO/•OH. In these reactions, the addition of different concentration of nanoparticles was noted to result in a decline and a loss of ESR signal in a dose dependent manner. This observation was similar to other studies where the effect of concentration of AuNPs on intensity during ROS generation was investigated (Zhang *et al.,* 2003). In the study, the interaction between nitroxyl radicals and gold nanoparticles of various sizes was shown. Increasing the concentration of nanoparticles resulted in a loss of ESR signal (Zhang *et al.,* 2003). The loss of ESR signal was the result of an electronic interaction between the generated radicals and the surface of nanoparticles (Zhang *et al.,* 2003).

Surface coatings on AuNPs have been shown to influence signal intensity of free radicals in reactions catalyzed by nanoparticles. The catalytic activity of NTA-PEG AuNPs and carboxyl-PEG AuNPs in the generation of hydroxyl radicals as opposed to the azide-PEG, hydroxyl-PEG AuNPs, biotin-PEG and methoxy-PEG AuNPs suggest that functional groups may play role in promoting free radical generation.

In reaction medium with high pH, a decrease in the signal intensity of DMPO/•OH in reaction of Fe^{2+} and AuNPs was observed. This was evident for citrate AuNPs and PEG-coated AuNPs at all tested concentrations, and also for the control reactions. The pH of the reaction medium has been shown to influence the mechanism of free radical generation (He *et al.,* 2012; Yin *et al.,* 2012). In conclusion, the results indicated that the ability of AuNPs to generate hydroxyl radical may depend on the pH of the medium, particle size, the functional group on the nanoparticle surface as well as on the nanoparticles concentration. There are critical determinants that can affect the generation of ROS.

5.5 References

Bačić G, Spasojevic I, Secerov B, and Mojovic M. 2008. Spin-trapping of oxygen free radicals in chemical and biological systems: New traps, radicals and possibilities. *Spectrochimia Acta Part A*, 69: 1357-1366.

Brandenberger C, Rothen- Rutishauser B., Muhfeld C, Schmid O, Ferron GA, and Maier KL. 2010. Effects and uptake of gold nanoparticles deposited at the air- liquid interface of a human epithelial airway model. *Toxicology and Applied Pharmacology*, 242: 56- 65.

Buzea C, Pacheco Blandina I, and Robbie K. 2007. Nanomaterials and nanoparticles: Sources and toxicity. *Biointerphases,* 2 (4): 170- 172.

Dykman LA and Khlebtsov NG. 2016. Immunological properties of gold nanoparticles. *Chemical Science,* 00-13.

Fu PP, Xia Q, Hwang H-M, Ray PC, and Yu H. 2014. Mechanism of nanotoxicity: Generation of reactive oxygen species. *Journal of Food and Drug Analysis*, 22 (1): 64-75.

George JM, Magogotya M, Vetten MA, Buys AV, and Gulumian M. 2016. An investigation of the genotoxicity and interference of gold nanoparticles in commonly used in vitro mutagenicity and genotoxicity assays. *Toxicological Sciences,* 1-18.

Halliwell B, and Whiteman M. 2004. Measuring reactive oxygen species and oxidative damage in vivo and in cell culture: how should you do it and what do the results mean?. *British Journal of Pharmacology*, 142: 231-255.

Halliwell B, Clement MV, and Ramalingam J. 2000. Hydrogen peroxide. Ubiquitous in cell culture and *in vivo? Clinical Review*, 50: 251-257.

Hawkins CL and Davies MJ. 2014. Detection and characterisation of radicals in biological materials using EPR methodology. Biochimia et Biophysica Acta, 1840: 708-721.

He W, Liu Y, Wamer WG, and Yin J-J. 2014. Electron spins resonance spectroscopy for the study of nanomaterial-mediated generation of reactive oxygen species. *Journal of food and drug analysis*, 22: 49-63.

He W, Zhou Y-T, Wamer WG, Hu X, Wu X, Zheng Z, Boudreau MD, and Yin J-J. 2013. Intrinsic catalytic activity of Au nanoparticles with respect to hydrogen peroxide decomposition and superoxide scavenging. *Biomaterials*, 34: 765-773.

He W, Zhou Yu-T, Wamer W, Boudreau MD, and Yin JJ. 2012. Mechanisms of the pH dependent generation of hydroxyl radicals and oxygen induced by Ag nanoparticles. *Biomaterials*, 33 (30): 7547-7555.

Jeng HA, and Swanson J. 2006. Toxicity of metal oxide nanoparticles in mammalian cells. *J Environ Sci Health Hazard Subst Environ Eng*, 41 (12): 2699-711.

Jeong MS, Yu K-M, Chung H-H, Park SJ, Lee AY, Song MR, Cho M-H, and Kim JS. 2016. Methodological considerations of electron spin resonance spin trapping techniques for measuring reactive oxygen species generated from metal oxide nanomaterials. *Scientific report,* 6: 26347, 1-10.

Li JJ, Zou L., Hartono D, Ong CN, Bay B H, and Yung LL. 2008. Gold nanoparticles induce oxidative damage in lung fibroblasts in vitro. *Advanced Materials*, 20: 138- 142.

Nel A, Xia T, Madler L, and Li N. 2006. Toxic Potential of Materials at the nanolevel. *Science*, 311: 622- 627.

Paino IMM, Marangonia VP, Oliveira RCS, Antunes LMG, Zucolotto V. 2011 Cyto and genotoxicity of gold nanoparticles in human hepatocellular carcinoma and peripheral blood mononuclear cells. *Toxicology Letters*, 215: 119-125.

Rushton EK, Jingkun Jiang J, Leonard SS, Eberly S, Castranova V, Biswas P, Elder A, Han X, Gelein R, Finkelstein J, and Oberdörster G. 2010. Concept of Assessing Nanoparticle

Hazards Considering Nanoparticle Dosemetric and Chemical/Biological Response metrics, *Journal of Toxicology and Environmental Health Part A*, 73 (5), 445 – 461.

Singh N, Manshian B, Jenkins G J, Griffiths SM, Williams PM, Mafffeis TG, Wright CJ, and Doak SH. 2009. NanoGenetoxicology: the DNA damaging potential of engineered nanomaterials. *Biomaterials*, 30: 3891- 3814.

Tlotleng N, Vetten MA, Keter FK, Skepu A, Tshikhudo R, and Gulumian M. 2016 Cytotoxicity, intracellular localization and exocytosis of citrate capped and PEG functionalized gold nanoparticles in human hepatocyte and kidney cell. *Cell Biol Toxicol*, 32 (4): 305-21.

Vetten MA, Tlotleng N, Rascher DT, Skepu A, Keter FK and Gulumian M. 2013. Label free in vitro toxicity and uptake assessment of citrate stabilized gold nanoparticles in three cell lines. *Particle and Fibre Toxicology*, 10 (50): 1-15.

Wang S, Chen W, Liu A-L, Hong L, Deng H-H, and Lin X-H. 2012. Comparison of the Peroxidase-Like Activity of Unmodified, Amino-Modified, and Citrate-Capped Gold Nanoparticles. *ChemPhysChem*, 13: 1199-1204.

Yen HJ, Hsu SH, Tsai CL. 2009. Cytotoxicity and immunological response of gold and silver nanoparticles of different sizes. *Small,* 5 (13): 1553-61.

Yin J-J, Fu PP, Lutterodt H, Zhou Y-T, Antholine WE, and Wamer W. 2012. Dual Role of Selected Antioxidants Found in Dietary Supplements: Crossover between Anti- and Pro-Oxidant Activities in the Presence of Copper. *American Chemical Society*, 60: 2554-2561.

Zhang Z, Beg A, Levanon H, Fessenden R W, and Meisel D. 2003. On the interaction of Free Radicals with Gold Nanoparticles, *J. AM. CHEM. SOC*.125: 7959- 7963.

CHAPTER 6

CONCLUSIONS AND FUTURE OUTLOOK

The present study provides an in-depth toxicity assessment of various gold nanoparticle systems developed in South Africa. Due to the anticipated demand of these systems in therapeutic and diagnostic applications, their cellular interactions, toxicity effects and exocytosis mechanisms were examined. The physico-chemical properties of the AuNPs were evaluated in cell growth medium, to determine the stability and dispersity of AuNPs prior exposure to cells. Nanoparticle parameters influencing interaction with cells such as size, aggregation, surface chemistry were thoroughly assessed. Representative cell models of major accumulating sites for AuNPs were chosen for *in vitro* toxicity studies. The internalization, localization and sub-cellular distribution of the AuNPs was investigated. Furthermore, exocytosis of AuNPs from cells was assessed.

Dose-response of cells to AuNPs was evaluated, where the effect of AuNPs on the cell viability and proliferation was evaluated using real time impedance technology. Further toxicity studies were undertaken by assessing the induction of pro-inflammatory cytokines IL-6 and TNF-α as major regulators in cell growth and differentiation, as well as in inducing DNA damage and apoptosis. Genotoxicity studies were conducted through the assessment of structural chromosomal aberration. Finally the generation of free radicals by AuNPs in physiological buffers with pH mimicking endosomal, lysosomal and cytoplasmic conditions was assessed by ESR technique. The ability of AuNPs to scavenge free radicals was also investigated.

The conclusions that were evident from the study are listed by subject below, in terms of the characterizations undertaken:

1. The stability of AuNPs in cell growth medium was influenced by media components. Even so, the hydrodynamic sizes and morphology of AuNPs was not changed in culture medium as determined by TEM and UV-vis spectrophotometer. Furthermore, zeta potential measurement indicated the strong negative charge on the AuNPs surface, which aid in preventing AuNPs aggregation. FTIR analysis confirmed the presence of functional groups on AuNPs surfaces.

2. Dark field imaging and TEM indicated that all citrate and PEG coated AuNPs were internalized by cells. However, ICP-MS analysis revealed a higher quantity of citrate AuNPs in both cell types than the PEG coated AuNPs. The PEG coated AuNPs showed a reduced uptake in both cell types, regardless of the functional groups. TEM imaging indicated that AuNPs enter the cell by endocytosis as polydisperse and individual nanoparticles, where they accumulate in endosomes, lysosomes and in cytoplasm compartments within the cell. Accumulation of the AuNPs in cell compartment was not dependent on functional groups or on the size of the particles. Exocytosis studies indicated that AuNPs remain in the cell for up to 3-4 weeks, and are thereafter removed by vesicle secretion of diffusion of AuNPs from the cell plasma membrane.

3. Cytotoxicity studies revealed that AuNPs may influence cell proliferation and viability. Cellular response to citrate and PEG coated AuNPs varied in the two cell types. In both cell types, the 14nm citrate AuNPs indicated toxicity effect, while the 40nm citrate AuNPs was non-cytotoxic to both cell types. However, the HEK 293 cells were the most sensitive to AuNPs. The results indicated that cellular toxicity of these AuNPs therefore depends on a combination of concentration, size and functional group of the nanoparticle surface.

4. Further analysis of cellular toxicity revealed a non-significant secretion of IL-6 and TNF-α in both cell types. Structural aberrations in treated cells were non-significant when compared to positive controls. Statistical analysis revealed that in both cell lines, the 14nm citrate stabilized AuNPs induced a noticeable effect of aberrations. The citrate AuNPs (20nm), azide-PEG, NTA-PEG, carboxyl-PEG, biotin-PEG, hydroxyl-PEG and the methoxy-PEG AuNPs showed a high percentage of aberrations in HEK 293 cells.

5. ESR spectrophotometry indicated the catalytic properties of the citrate stabilized AuNPs (14nm), carboxyl-PEG AuNPs and the NTA-PEG AuNPs at pH 3.6. These AuNPs were reactive in promoting the generation of hydroxyl radicals during the decomposition of hydrogen peroxide. This characteristic may be attributed to the carboxylic group on the carboxyl and the NTA functional group. However, hydroxyl radical generation by AuNPs decreased with increasing pH of the reaction medium, indicating that AuNPs localized in cell cytoplasm may not induce free radical generation. Generation of the reactive hydroxyl radicals may be one of the possible mechanisms of cellular toxicity by AuNPs, which are deposited in the lysosomes and endosomes.

In conclusion, the results presented in this study give an indication on the fate of AuNPs on long term exposure to cells. The results indicated the ability of AuNPs to induce toxicity in cells through generation of free radicals and cellular DNA damage, which cause adverse effect on cell proliferation and viability as well as induce oxidative damage to lipids and proteins. The catalytic activity of NTA-PEG AuNPs and carboxyl-PEG AuNPs in the generation of hydroxyl radicals as opposed to the azide-PEG, hydroxyl-PEG AuNPs, biotin-PEG and methoxy-PEG AuNPs suggests that functional groups and chemical reactions that occur on the nanoparticle surface play role in cellular toxicity. However, since toxicity studies were conducted *in vitro*, where major defense system of the cells are not present; the overall

effect detected might be significant or non-significant in *in vivo* models. Thus, the recommendations below are necessary for future studies.

Recommendations for future studies

1. Assess toxicity effects of the gold nanoparticle systems on cellular models that will be representative of the *in vivo* environment, such as in primary cell cultures or in an appropriate animal model.

2. Assess the mechanisms of AuNPs-assisted decomposition of hydrogen peroxide in acidic environment.

3. Investigate lysosomal dysfunction as a possible mechanism of AuNPs toxicity.

4. Investigate different endpoints for oxidative stress by AuNPs in cells.

5. Elaborate on the role of AuNPs in ROS mediated cellular toxicity, by assessing chemical reactions that occurs on nanoparticle surfaces upon interaction with cells.

6. Investigate the stability of citrate stabilized and functionalized AuNPs in cells. In this view, an understanding on whether the observed toxicity effects is the result of stable AuNPs, the degraded functional groups or Au core interacting with cell components will be clarified. Future studies on the biodegradability of AuNPs can attempt to further classify these nanoparticles in a nanotoxicological classification system (NCS). However, the result in this study indicate that AuNPs may be placed in either class III (size < 100nm, nanoparticles are endocytocised by cells and are biodegradable) or class IV (size is <00nm, nanoparticles are endocytocised by cells and are non-biodegradable) of the NCS.

APPENDICES

Appendix 1

Publication Abstracts

Melissa A Vetten, Nonhlanhla Tlotleng, Delia Tanner Rascher, Amanda Skepu, Frankline K Keter, Kailen Boodhia, Leigh-Anne Koekemoer, Charlene Andraos, Robert Tshikhudo and Mary Gulumian. Label-free in vitro toxicity and uptake assessment of citrate stabilized gold nanoparticles in three cell lines. *Particle and Fibre Toxicology,* 2013, 10: 50.

Background: Reliable in vitro toxicity testing is needed prior to the commencement of in vivo testing necessary for hazard identification and risk assessment of nanoparticles. In this study, the cytotoxicity and uptake of 14nm and 20nm citrate-stabilized gold nanoparticles (AuNPs) in the bronchial epithelial cell line BEAS-2B, the Chinese hamster ovary CHO cell line, and the human embryonic kidney cell line HEK 293 were investigated.

Methods: Cytotoxicity of the AuNPs was assessed via traditional XTT-, LDH-, and ATP-based assays, followed by cell impedance studies. Dark-field imaging and hyperspectral imaging was used to confirm the uptake of AuNPs into the cells.

Results: Interference of the AuNPs with the XTT- and ATP-based assays was overcome through the use of cell impedance technology. AuNPs were shown to be relatively non-toxic using this methodology, with the CHO cells being the most sensitive cell type with 20nm AuNPs having the highest toxicity. Uptake of both AuNPs was observed in all cell lines in a time- and cell type-dependent manner.

Conclusions: Using the cell impedance and dark-field hyperspectral imaging technologies, it was possible to study the toxicity of the AuNPs in the different cell lines and show that these cells could internalize the AuNPs with their subsequent intracellular aggregation. It was also possible to show that this toxicity would not correlate with the level of uptake but it would correlate with cell-type and the size of the AuNPs. Therefore, these two label-free methodologies used in this study are seen to be suitable for in vitro studies on the effects of AuNPs, and could present themselves as appropriate and valuable methodologies for future nanoparticle toxicity and uptake studies.

Nonhlanhla Tlotleng, Melissa A Vetten, Pam Sharp, Frankline Keter, Amanda Skepu Robert Tshikhudo and Mary Gulumian. Cytotoxicity, intracellular localization and exocytosis of citrate

capped and PEG coated gold nanoparticles in human hepatocytes and kidney cells. *Cell biology and Toxicology*, 2016, 32 (4): 305-21.

Surface modified gold nanoparticles (AuNPs) are nanomaterials that hold promise in drug delivery applications. In this study, the cytotoxicity, uptake, intracellular localization, and the exocytosis of citrate-stabilized (Cit-AuNPs) and polyethylene glycol (PEG)-modified gold nanoparticles with the carboxyl (COOH) terminal functional group were assessed in human embryonic kidney (HEK 293) and the human caucasian hepatocytes carcinoma (Hep G2) cell systems, representing two major accumulation sites for AuNPs. The zeta (ζ)-potential measurements confirmed the negative surface charge of the AuNPs in water and in cell growth medium. The transmission electron microscopy confirmed the size and morphology of the AuNPs. Both types of AuNPs were shown to induce cytotoxic effects in cells. The Hep G2 cells were more sensitive cell type, with the COOH-PEG-AuNPs inducing the highest toxicity at higher concentrations. Dark field microscopy and TEM images revealed that the AuNPs were internalized in cells, mostly as agglomerates. TEM micrographs further revealed that the AuNPs were confined as agglomerates inside vesicle-like compartments, likely to be endosomal and lysosomal structures as well as in the cytosol, mostly as individual particles. The AuNPs were shown to remain in cellular compartments for up to three weeks but thereafter; clearance of the gold nanoparticles from the cells by exocytosis was evident. The results presented in this study may therefore give an indication on the fate of AuNPs on long term exposure to cells, and may also assist in safety evaluation of AuNPs.

Key words: Cytotoxicity, exocytosis, gold nanoparticles, subcellular localization, transmission electron microscopy, uptake.

Mary Gulumian, Melissa A Vetten, Kailen Boodhia, and Nonhlanhla Tlotleng. Toxicity assessment and intracellular uptake of gold nanoparticles: Effect of ligands, functional groups and cell type. *Toxicology Letters*, 2016, 259.S186. http://dx.doi.org/10.1016/j.toxlet.2016.07.444

Introduction: For their unique electronic and optical properties, and also for the ease of their surface modification through functionalization, gold nanoparticles (AuNPs) have been identified as a possible material for delivery of therapeutic agents.

Objective: In this study, the cytotoxicity, mechanisms of uptake, intracellular localization, and the exocytosis of citrate-stabilized and ligand derivatised AuNPs were assessed in human embryonic kidney (HEK 293), human Caucasian hepatocytes carcinoma (HepG2), bronchial epithelial (BEAS-2B), Chinese Hamster Ovary (CHO) cell systems, and in U937 monocyte-derived macrophages. The surface modified AuNPs have included Poly(ethylene glycol) (PEG) modified biotin, nitriloacetic acid [NTA], COOH, hydroxyl (OH), and methoxy (OCH3) functional groups as well as pro-apoptotic peptide, glucose-regulated protein 78 (GRP-78) binding peptide and trans-activating transcriptional peptide (TAT).

Materials and methods: The cytotoxicity was assessed using the xCELLigence real-time cell analyzer (RTCA) with RTCA software, version 1.2. The intracellular uptake was determined using the CytoViva® 150 Unit integrated onto the Olympus BX43 microscope and the intracellular localization and exocytosis was determined using a JOEL-JEM 1010 electron microscope, operated at 120 kV.

Results: Cell specific toxicity could be observed with all the AuNPs where HepG2 cells were found to be a more sensitive cell type. Functional group dependent uptake was also observed where those carrying POH, PBTN, PNTA, or PAZ AuNPs no uptake could be observed. The mechanisms of uptake were found to be caveolin mediated endocytosis and that these AuNPs were able to be cleared from cells through exocytosis

Appendix 2

Quantitative analysis of Intracellular gold nanoparticles using ICP MS techniques

Quantification of AuNPs in HepG2 cells					
1hr					
Media		Buffer (wash)		Cell pellet	
Sample ID	Au concentration (µg/L)	Sample ID	Au concentration (µg/L)	Sample ID	Au concentration (µg/L) in 10^6 cells
14nm Cit	434.6	14nm Cit	105.8	14nm Cit	485.5
20nm Cit	1162	20nm Cit	289.5	20nm Cit	948.2
40nm Cit	190.4	40nm Cit	48.5	40nm Cit	1516
14nm PAZ	393.3	14nm PAZ	92.27	14nm PAZ	19.42
14nm POH	423.1	14nm POH	83.27	14nm POH	7.256
14nm PNTA	393	14nm PNTA	97.84	14nm PNTA	5.143
14nm PBTN	450.8	14nm PBTN	98.43	14nm PBTN	3.159
14nm PCOOH	350.9	14nm PCOOH	62.81	14nm PCOOH	7.115
14nm $POCH_3$	195.4	14nm $POCH_3$	43.05	14nm $POCH_3$	11.9
N/C	4.684	N/C	0.7579	N/C	0.5871

4hr					
Media		Buffer (wash)		Cell pellet	
Sample ID	Au concentration (µg/L)	Sample ID	Au concentration (µg/L)	Sample ID	Au concentration (µg/L) in 10^6 cells
14nm Cit	326.1	14nm Cit	49.58	14nm Cit	1074
20nm Cit	1085	20nm Cit	142	20nm Cit	954.9
40nm Cit	170.4	40nm Cit	52.35	40nm Cit	1545
14nm PAZ	388	14nm PAZ	65.2	14nm PAZ	16.31
14nm POH	445.2	14nm POH	78.43	14nm POH	5.448
14nm PNTA	414.5	14nm PNTA	60.77	14nm PNTA	4.697
14nm PBTN	435.7	14nm PBTN	90.45	14nm PBTN	3.464
14nm PCOOH	353.8	14nm PCOOH	80.31	14nm PCOOH	11.5
14nm $POCH_3$	296.9	14nm $POCH_3$	60.01	14nm $POCH_3$	54.18
N/C	6.007	N/C	1.016	N/C	1.217

24hr					
Media		Buffer (wash)		Cell pellet	
Sample ID	Au concentration (µg/L)	Sample ID	Au concentration (µg/L)	Sample ID	Au concentration (µg/L) in 10^6 cells
14nm	76.22	14nm Cit	18.55	14nm Cit	1277

Cit					
20nm Cit	488.9	**20nm Cit**	107.7	**20nm Cit**	1378
40nm Cit	125.7	**40nm Cit**	77.64	**40nm Cit**	2699
14nm PAZ	392.1	**14nm PAZ**	71.98	**14nm PAZ**	28.02
14nm POH	435.7	**14nm POH**	79.1	**14nm POH**	7.849
14nm PNTA	478.1	**14nm PNTA**	80.29	**14nm PNTA**	6.409
14nm PBTN	457.2	**14nm PBTN**	81.06	**14nm PBTN**	4.61
14nm PCOOH	356.4	**14nm PCOOH**	74.39	**14nm PCOOH**	53.35
14nm $POCH_3$	301.5	**14nm $POCH_3$**	70.13	**14nm $POCH_3$**	34.46
N/C	6.032	**N/C**	1	**N/C**	1.57

Quantification of AuNPs in HEK 293 cells

1hr

Media		**Buffer (wash)**		**Cell pellet**	
Sample ID	**Au concentration (µg/L)**	**Sample ID**	**Au concentration (µg/L)**	**Sample ID**	**Au concentration (µg/L) in 10^6 cells**
14nm Cit	749.4	**14nm Cit**	101.9	**14nm Cit**	342.1
20nm Cit	1429	**20nm Cit**	232.5	**20nm Cit**	630
40nm Cit	736.4	**40nm Cit**	148.6	**40nm Cit**	1083
14nm PAZ	407.1	**14nm PAZ**	98.1	**14nm PAZ**	10.86
14nm POH	421.7	**14nm POH**	95.63	**14nm POH**	2.755
14nm PNTA	462.9	**14nm PNTA**	59.27	**14nm PNTA**	1.196
14nm PBTN	471	**14nm PBTN**	95.78	**14nm PBTN**	0.7234
14nm PCOOH	339.6	**14nm PCOOH**	51.11	**14nm PCOOH**	45.09
14nm $POCH_3$	237.5	**14nm $POCH_3$**	47.75	**14nm $POCH_3$**	39.34
N/C	3.43	**N/C**	0.2238	**N/C**	0.06081

4hr

Media		**Buffer (wash)**		**Cell pellet**	
Sample ID	**Au concentration (µg/L)**	**Sample ID**	**Au concentration (µg/L)**	**Sample ID**	**Au concentration (µg/L) in 10^6 cells**
14nm Cit	709	**14nm Cit**	102.1	**14nm Cit**	953.6
20nm Cit	1346	**20nm Cit**	180.9	**20nm Cit**	1488
40nm Cit	658.2	**40nm Cit**	116.4	**40nm Cit**	1512
14nm PAZ	395.2	**14nm PAZ**	73.83	**14nm PAZ**	24.21

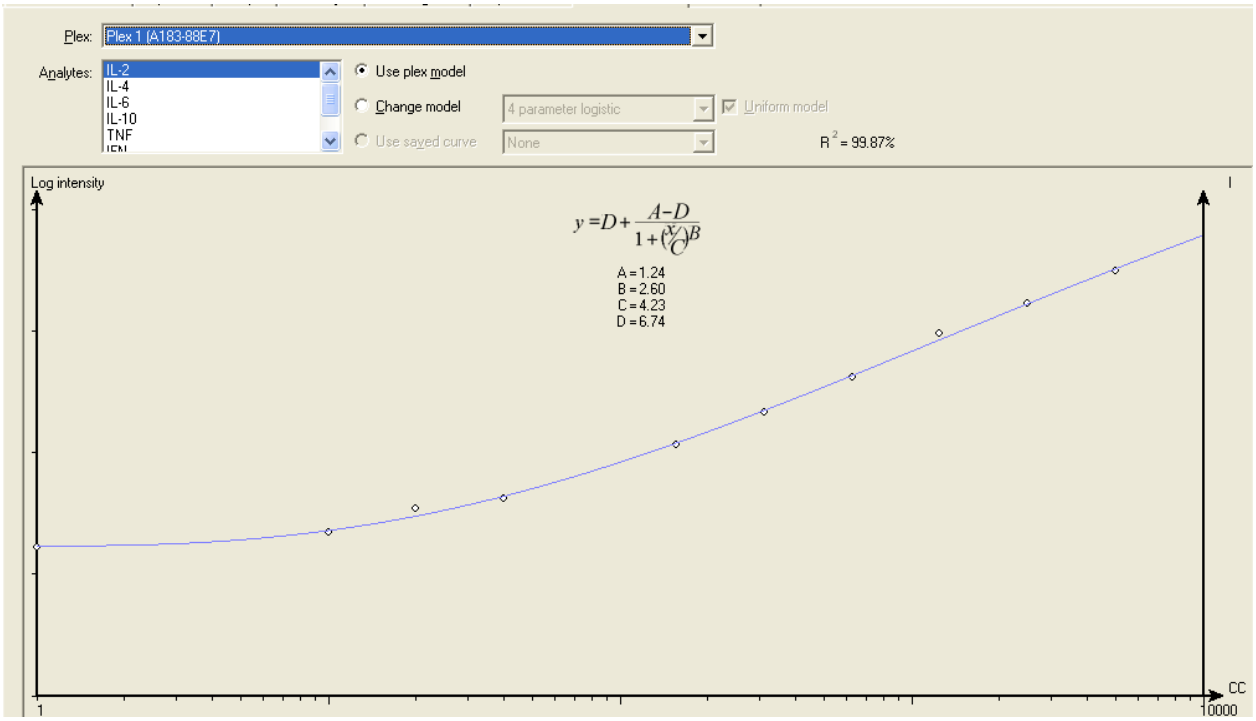
14nm POH	459.3	**14nm POH**	101.9	**14nm POH**	7.485
14nm PNTA	474.9	**14nm PNTA**	72.58	**14nm PNTA**	4.342
14nm PBTN	411.9	**14nm PBTN**	118.8	**14nm PBTN**	3.534
14nm PCOOH	382.6	**14nm PCOOH**	52.1	**14nm PCOOH**	91.61
14nm $POCH_3$	236.5	**14nm $POCH_3$**	69.02	**14nm $POCH_3$**	36.58
N/C	4.614	**N/C**	0.2662	**N/C**	0.8936

24hr

Media		**Buffer (wash)**		**Cell pellet**	
Sample ID	**Au concentration (µg/L)**	**Sample ID**	**Au concentration (µg/L)**	**Sample ID**	**Au concentration (µg/L) in 10^6 cells**
14nm Cit	230.4	**14nm Cit**	49.23	**14nm Cit**	1481
20nm Cit	1041	**20nm Cit**	166.9	**20nm Cit**	3932
40nm Cit	375.3	**40nm Cit**	52.15	**40nm Cit**	3095
14nm PAZ	438.8	**14nm PAZ**	91.85	**14nm PAZ**	56.96
14nm POH	411.2	**14nm POH**	85.97	**14nm POH**	20.73
14nm PNTA	458.1	**14nm PNTA**	71.8	**14nm PNTA**	14.88
14nm PBTN	454.3	**14nm PBTN**	98.73	**14nm PBTN**	7.866
14nm PCOOH	324.7	**14nm PCOOH**	73.08	**14nm PCOOH**	387.4
14nm $POCH_3$	350.4	**14nm $POCH_3$**	88.86	**14nm $POCH_3$**	192.4
N/C	6.481	**N/C**	1.163	**N/C**	4.451

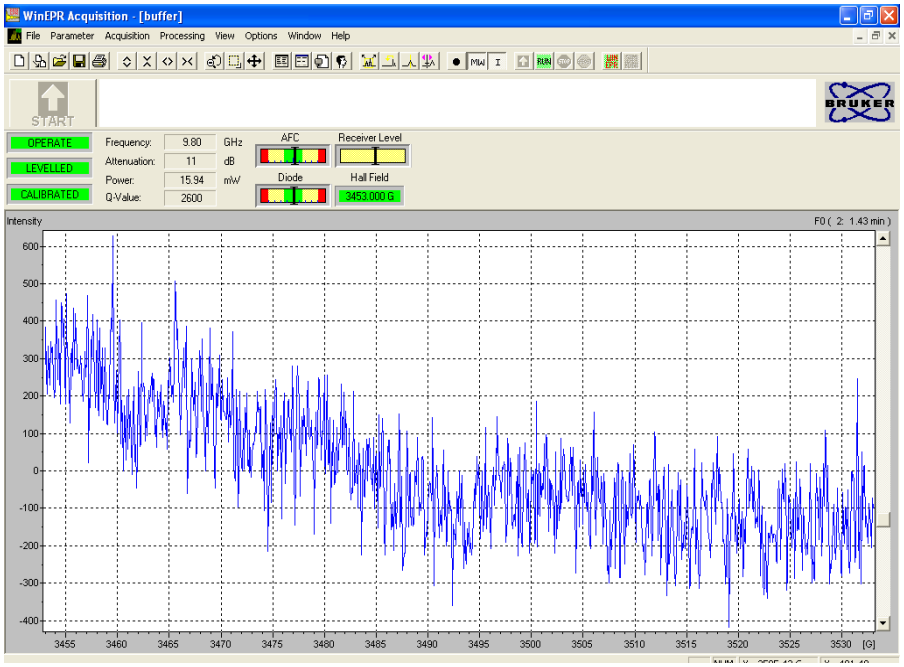
Appendix 3

Standard curve for cytokine detection in cultured cells



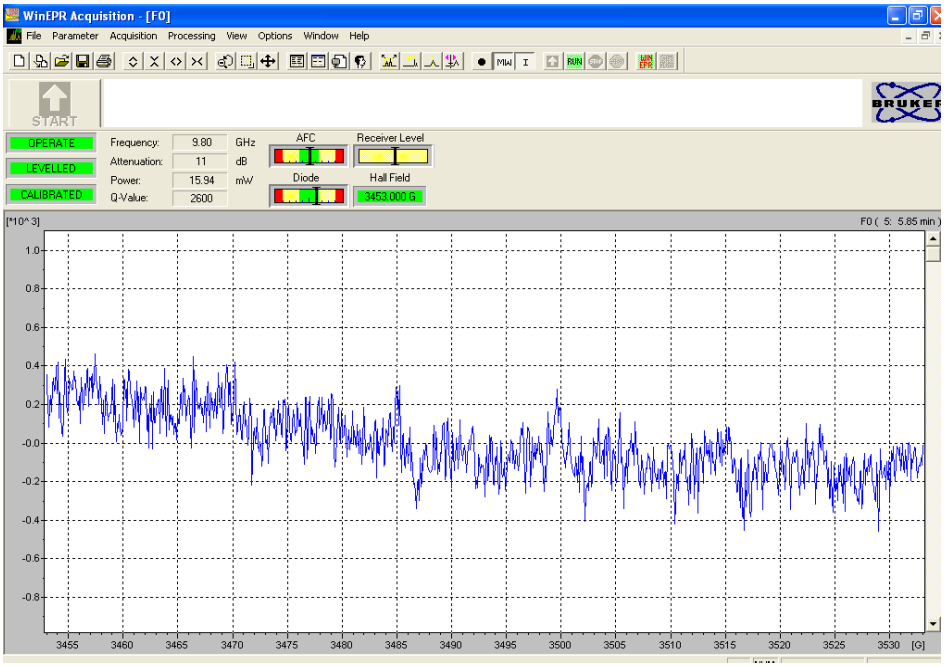
Appendix 4

ESR signal intensity of typical buffer solution at pH 3.6.



Appendix 5

ESR signal intentisity showing the weak DMPO/·OH obtained in the negative baseline containing DMPO and hydrogen peroxide at pH 4.65.



Appendix 6

ESR signal intentisity of DMPO/·OH obtained in the positive baseline during the decomposition of hydrogen peroxide in the presence of ferric iron in pH 4.65.

